# Formulation of aqueous core capsules for the triggered release of proteins

Geoffrey Brun

Université Paris VI – Pierre et Marie Curie

École doctorale 388
Chimie Physique et Chimie Analytique de Paris-Centre

*École Normale Supérieure – Département de Chimie*
*Pôle de Chimie-Biophysique*

# Formulation de capsules à cœur aqueux pour la délivrance stimulable de protéines

*Formulation of aqueous core capsules for the triggered release of proteins*

Par Geoffrey BRUN

Thèse de doctorat de physico-chimie

Dirigée par Christophe TRIBET

Présentée et soutenue publiquement le 18 décembre 2015, devant un jury composé de :

| | |
|---|---|
| Mme. BLOCH-GALLEGO Évelyne | Membre invité |
| M. HOURDET Dominique | Examinateur |
| Mme. LADAVIÈRE Catherine | Rapporteur |
| M. LUND Reidar | Examinateur |
| Mme. MARIE Emmanuelle | Examinateur |
| M. SIX Jean-Luc | Rapporteur |
| M. TRIBET Christophe | Directeur de thèse |

# Contents


**Introduction** 1

**1. Sensitivity of cells to uneven distributions of peptides and proteins** 5
- 1.1. Representative proteins of interest . . . 5
- 1.2. Characteristic scales: concentrations, time and lengths . . . 7
- 1.3. Summary and conclusion . . . 12

**I. Light-controlled release, a review** 15

**Introduction** 17

**2. Light-sensitive liposomes** 19
- 2.1. Light-induced increase of permeability . . . 21
- 2.2. Light-triggered pore formation . . . 30
- 2.3. Membrane disruption . . . 33
- 2.4. Encapsulation yield and preparation conditions . . . 34
- 2.5. Summary on light-sensitive vesicles . . . 37

**3. Micro- and nanometer-sized hydrogels** 39
- 3.1. Photodegradable hydrogels . . . 40
- 3.2. Light-triggered gel collapse . . . 46
- 3.3. Encapsulation yield and loading constraints . . . 49

**4. Aqueous core—polymer shell capsules** 51
- 4.1. Layer-by-layer assemblies . . . 51
- 4.2. Polymersomes . . . 56
- 4.3. Capsules made of solid polymers . . . 62
- 4.4. Hybrid membranes . . . 66
- 4.5. Role of the stimulation wavelength . . . 67

**Summary** 69

**II. Light-sensitive liposomes** **71**

**Introduction** **73**

**5. Surfactant sensitized vesicles** **75**
Introduction . . . 75
5.1. Liposome solubilization by the azoTAB surfactant . . . 77
Conclusion . . . 86

**6. Azobenzene-based polymer sensitizer** **87**
Introduction . . . 87
6.1. Experimental conditions . . . 90
6.2. Interpretation of typical photo-triggered release patterns . . . 91
6.3. Data analysis . . . 95
Conclusion . . . 103

**III. Temperature-sensitive capsules made by the reverse emulsion method** **105**

**Introduction** **107**

**7. PolyNIPAM-based millimeter sized capsules** **111**
7.1. Adaptation of published protocols . . . 111
7.2. PolyNIPAM-based capsules . . . 115
7.3. Effect of mixed membrane composition . . . 125

**8. PolyNIPAM-based nanocapsules** **131**
8.1. Description of the synthesis of nanometer sized capsules . . . 131
8.2. PolyNIPAM nanocapsules characterization . . . 137

**9. UCST polymer-based millimeter-sized capsules** **143**
9.1. Characterization of the UCST polymer . . . 143
9.2. Adaptation of the capsule preparation procedure to the UCST polymers . . . 147
9.3. Characterization of capsules made from UCST polymers and ovalbumin . . . 151

**Conclusions & perspectives** **159**
Liposomes . . . 162
Polymer capsules . . . 163

**IV. Appendices** **165**

**A. Role of molecular gradients on biological systems** **171**

**B. Currently used gradient generators** **179**

**C. Materials & Methods** **193**

**D. Experimental techniques** **203**

**E. Preparation and characterization of liposomes** **209**

**F. Preparation and characterization of polymer capsules** **215**

**G. Quantitative and real-time FRAP measurements** **227**

**Bibliography** **235**

**Abbreviations & acronyms** **263**

# Introduction

# Introduction

From isolated cells up to whole organs, dynamic responses to changes occurring in their environment are a vital issue. For this purpose, perception of chemical cues is one of the most fundamental, and subtle, mechanisms that cells from all kingdoms have developed. Though rooted in simple molecular events – basically specific binding of molecules to receptors on the cell outer membrane – complex signal inputs can be interpreted by cells. They can take various shapes, like concentration thresholds or gradients of molecular cues. Diverse fields of biomedical research are actively studying the cellular mechanisms that govern the response to concentration patterns of external molecules, including embryogenesis (morphogen gradients and gradients of guidance cues [1]), neurobiology (e.g. neuron excitation/inhibition), immunology (inflammatory responses mediated by cytokines), etc. (for more details, see appendix A, p. 171). Results on the control of signaling gradients and cross-talks between signaling pathways find important echoes in actual biomedical research (e.g. on cancers), in tissue engineering and developments of techniques for organ healing.

Modern experimental studies of the cell response to external molecules have reached a high degree of control of the spatial and temporal variations of concentrations. Depending on the considered system, the nature of signaling molecules and the range of relevant times and length scales totally differ. A vast variety of experimental devices have been implemented accordingly to the variety of contexts. In brief, experiments seeking to observe fast responses ($\ll 1$ hour) on a local scale (e.g. micrometer resolution) are essentially carried out using micropipette injections [2–5]. In the opposite case of long incubation/observation times (hours – days) and large length scales, well-controlled gradients of concentrations are produced based on ad hoc positioning of one or several slow-releasing source(s) and sink(s) distributed in the cell-culture medium. Microfluidic devices designed in the last 10 years have achieved impressive successes in this field, with unprecedented degree of control of concentration gradients generated over 100 µm to 1 mm (see references [5, 6] and section *1.2 Characteristic scales: concentrations, time and lengths*, p. 7). The control of exposure to bioactive peptides and proteins remains however a challenge because these molecules are fragile, sometimes available in limited amounts, and in practice may diffuse freely only on very short distances. In particular, communications between mammalian cells involve proteins that can:

- be prone to denaturation or aggregation;
- adsorb on the walls of devices and interact with the gels used for cell culture (interplay with the extracellular matrix).

These constraints motivate the quest for alternatives to conventional (diffusion-based) gradient-forming devices. New means/tools for protein delivery should accordingly provide closer mimicry of a localized secretion of activating agents and protect proteins against degradation until it is delivered. The purpose of this thesis is to explore possibilities of designing artificial cargoes, that ideally should be versatile (compatible with most peptides and proteins), easy to manipulate in conventional cell culture systems, and should enable quantitative control of uneven spatial and temporal delivery. In this context, we will identify the possible systems that can "trap" proteins of interest into cargoes, and achieve on-demand and remote-controlled release.

# 1. Overview of (mammalian) cell sensitivity to uneven spatial distributions of external peptides or proteins

This chapter briefly derives the specifications delivery systems must follow. The aim is to provide sound basis to comments in the bibliographic listing (next chapter) about feasible approaches. The main specificities rely on characteristic and relevant conditions of use (length scales, time scales, environment), and the need for compatibility with protein handling and release. With regard to the biological context, we focus on the more demanding conditions of recent experimental assessments, which basically address the question of sensitivity of eukaryotic cells and/or tissues to gradients – for instance, we do not consider studies of bacterial chemotaxis that are nicely performed in conventional, gradient-forming devices. Three main fields dominate the studies of mammalian cell responses in the literature of controlled heterogeneous distribution of biomolecular cues:

1. experiments on cell polarization, growth and/or migration related to embryogenesis and development;
2. polarization and migration of leukocytes related to immunology;
3. migration of cancer cells motivated by works on metastasis.

The typical properties of the corresponding molecular cues and conditions of cell responses are summarized below, as important framework for the design of new relevant experimental tools.

## 1.1. Representative proteins of interest

A limited collection of activating molecules regularly appears in model studies, as prototypical representatives of a vaster range of the peptides and proteins that are secreted in vivo. They belong to diverse families – basically cytokines, growth factors, peptide components of the extracellular matrix or formed upon degradation of pathogens (figure 1.1). Progress in cell engineering enables to produce these model proteins and peptide factors under forms that are overexpressed by secreting cells and/or can be purified in solutions.

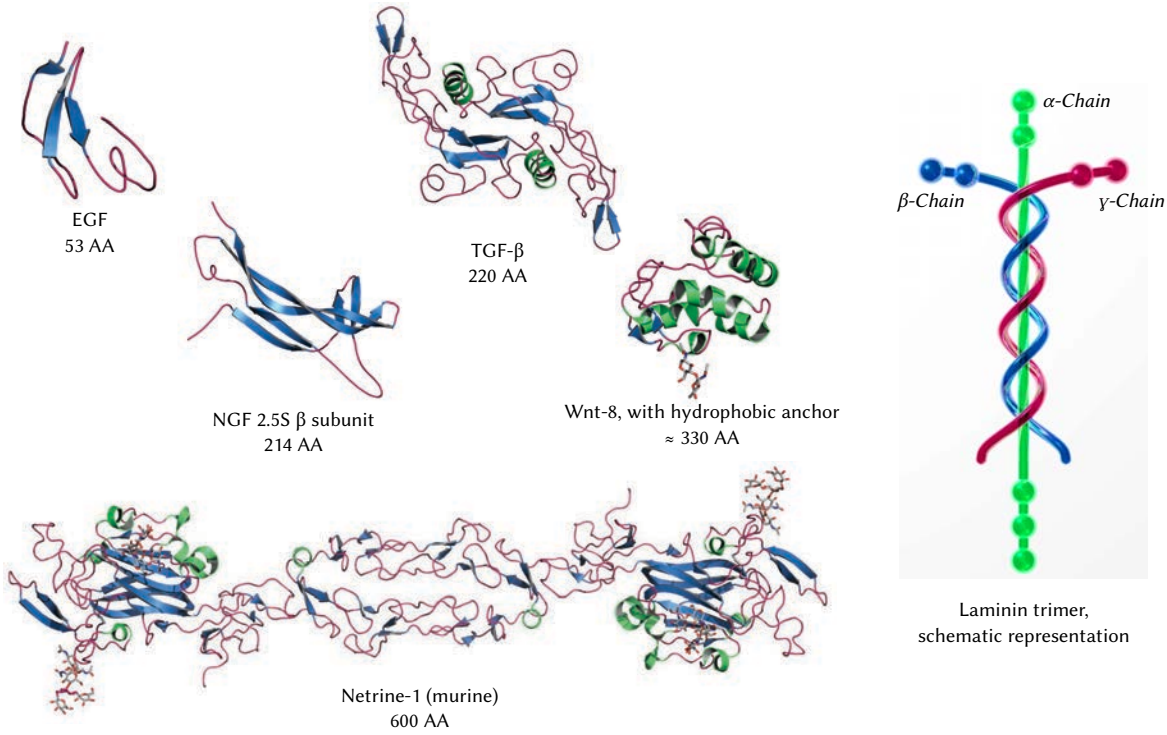


**Figure 1.1.** *The diversity of sizes and structures of proteins involved in cell guidance or communication. "AA" means "amino acids", the crystal structure may show part of the whole proteins. EGF, epidermal growth factor (6.4 kDa, pdb 1EGF), small soluble and rigid, activate transcriptions in cell and cell growth; Wnt proteins (35 kDa, pdb 4F0A) involved in signaling pathways use either nearby cell-cell communication; NGF, nerve growth factor (53 kDa as dimer, pdb 1BET), small secreted protein important for the growth, maintenance, and survival of certain target neurons; TGF, transforming growth factor (26 kDa, pdb 1KLA), family of bone morphogenetic proteins, typically non-covalent dimer of about 220 amino acids; Netrin-1 (≈ 70 kDa under the monomer form, pdb 4OVE) a class of proteins of involved in axon guidance; laminin are heterotrimer glycoproteins (400–1,000 kg/mol) strongly interacting with the extracellular matrix.*

It is obvious from figure 1.1 that no characteristic size emerge among these proteins. Their size ranges from the smallest *N*-formylated oligopeptides (e.g. *N*-formyl-methionine-leucine-phenylalanine, fMLP, released by bacteria) to high-molecular weight complex multidomain glycoproteins that may polymerize in even larger networks (e.g. laminin ∼ 400–1,000 kDa). The solubility and free diffusion of some cues may even be an issue, and immobilization on surfaces can be preferred for both avoiding uncontrolled adsorptions, and implementing relevant biological configurations (e.g. studies of mechanical coupling with the substrate). For instance, laminin was used in so-called "substrate-bound" gradient [5] that were prepared by printing, or controlled diffusion-adhesion processes of laminin solutions. Present systems manage with the deposition on the top of flat substrates (usually covered with cationic biomolecules to trigger strong adsorption), prior to cell seeding. *In situ attachment (permanent, or transient) of cues interacting with the matrix (laminin, netrin,*

*epidermal growth factors, etc. [7]) is clearly a challenge, in particular with a control in the three dimensions of the samples (i.e. 3D-controlled release).*

Presentation of smaller domains, under the form of soluble recombinant proteins, may be sufficient to study cell responses. Accordingly, the usual range of molar masses goes from < 500 g/mol up to 400 kg/mol, with many examples of proteins having 200–400 aminoacids (20–50 kg/mol). This point to one important constraint for the design of generic cargoes: the "open" form shall *be compatible with the release and fast (free) diffusion of relatively large molecules (10–20 nm), but the closed form shall also trap/hide relatively small ones (< 1 nm).*

A second general feature is the possible need for specific interaction of the proteins with their environment. The presence of hydrophobic moieties can for instance reflect the importance of binding to lipid bilayers, and a trend to form clusters in solutions. This is the case of Wnt proteins (35 kDa) involved in signaling pathways of either nearby cell-cell communication (paracrine) or for same-cell communication (autocrine). The Wnt proteins are secreted glycoproteins that are lipid-modified (e.g. palmitoylation) on a conserved pattern of cysteine residues. Palmitoylation initiates targeting of the Wnt protein to the plasma membrane for secretion and it allows the Wnt protein to bind its receptor. The requirement for the binding onto lipid membranes hampers its delivery in simple aqueous solutions, which may explain that most experiments on exposure to Wnt were carried out using secreting cells [8–10]. *The use of complex solutions, containing lipid membrane mimics, shall thus not be overlooked.*

As they are strongly regulated in vivo, these proteins may not always be stable under their active form, and for instance they can be highly sensitive to proteases present in the extracellular medium. This is the case for the tumor necrosis factors (TNF) which are primarily produced by macrophages – but it is produced also by a broad variety of cell types to promote inflammatory responses – as a 233-amino acid-long transmembrane protein arranged in stable homotrimers, and released via proteolytic cleavage by the metalloprotease as a homotrimeric cytokine (sTNF). The soluble 51 kDa trimeric sTNF tends to dissociate at concentrations below the nanomolar range, thereby losing its bioactivity. Mild handling conditions (physiological pH, ionic strength, T, etc) are of primary importance to preserve the activity. As an example, thermally treated cues (deactivation upon heating solutions at 70 ℃ for a few minutes) can be used in blank experiments [11].

## 1.2. Characteristic scales: concentrations, time and lengths

Co-cultures (cell-based biomolecule sources embedded in gels such as explants or transfected cell lines) are predominantly used by biologists to create and assess conditions of inter-cell stimulation and communication. It is certainly highly relevant in biology. However, no clear characteristic scales can be inferred from these experiments, due to high variability and difficulties to quantitatively characterize the environment (unknown level of biomolecule

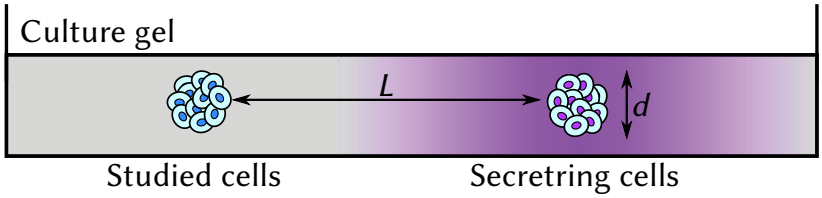


**Figure 1.2.** *1D gradient generated in a culture gel by the coculture method. The gradient is represented in purple, and is established around the cluster of generated cells. The typical distance between the studied cells and the secreting cells $L$ is 1 mm; the size of both clusters $d$ is in the 100 µm – 1 mm range. Collagen is often used as the culture medium, at a concentration of 2–3 g/L [12, 13].*

secreted by the cells, poor repeatability of inter-cellular distances and limited possibilities to control inter-cellular gaps shorter than 100 micrometers). Measurements of concentrations (e.g. using fluorescent fusion proteins) is technically very challenging due to effective elicitation of cell responses at nanomolar concentrations of cues.

Characteristic features of efficient cell stimulations are thus deduced from experiments practiced in artificial devices, based on either micropipette injection or spontaneous diffusion of soluble cues between source compartment(s) and sink(s) (see figures 1.3 and 1.4, and appendix B, p. 179 for technical details). We summarize here the typical features of the distribution/delivery of cues that can be obtained in these conventional devices. Simply reproducing these features with an alternative tool would be of low interest. In addition, we identify the challenges and complexities that are worth to address and motivate alternative approaches.

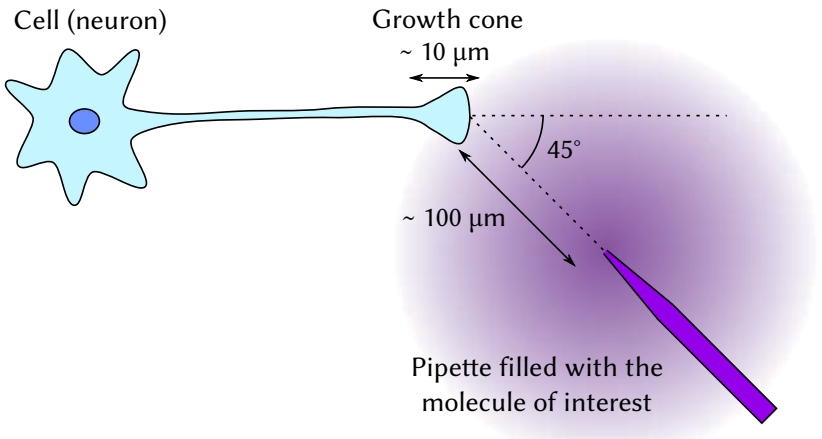


**Figure 1.3.** *A pipette is used to create a local source of a molecule of interest in a culture medium. The gradient is represented in purple. The scale of the targeted cell (leukocyte) or part of cell (the growth cone of a neuron) is typically 10 µm. The pipette is located 100 µm away from the cell. The concentration of the molecule is assumed to be 1/1000 of the one in the pipette.*

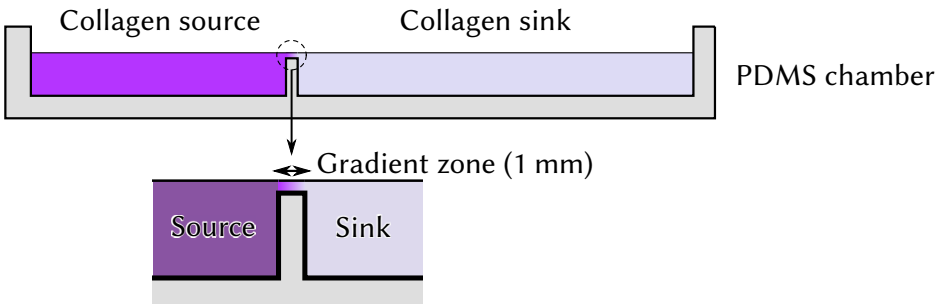


**Figure 1.4.** *A gradient of molecules is established in the collagen junction between two chambers filled with collagen. One of the chambers contains the molecule and acts as a source, while the other one does not contain the molecule initially, and acts as a sink.*

### 1.2.1. Characteristic times of exposure to cues

Diffusion-based gradients are not established immediately. The characteristic diffusion time can be estimated from Fick equations: $\tau \sim L^2/D$, where $\tau$ is the characteristic diffusion time, $L$ is the characteristic diffusion length and $D$ the diffusivity of the cues. For a protein which does not bind to the culture substrate (gel or surface), diffusivity is faster and of the order of 100 µm²/s. At distances as long as one millimeter away from the source, $\tau \sim 10^4$ s: a few hours are needed to reach the target, and this time drop down to about one minute at distances of a few tens of micrometers. This kind of experiment is therefore limited to relatively "slow" stimulations. Microfluidic devices can be designed to flush gradients of concentrations that are perpendicular to the fluidic channel, which enables to modulate a flow directly applied to the cells.

Fast gradient modulation in time is therefore possible, at time scales only limited by the flow rate. However, the shear stress induced to the cells in those conditions has been reported to alter their behavior [14, 15]; the observed effects ranges from modification of the cytoskeleton, shape distortion, to detachment of cells from the culture plate. The fastest system – used to study the chemotaxis of leukocytes to fast-switching linear gradients – is able to modify the steepness of the gradients in the timescale of 5 seconds [16].

The fastest microfluidic switches to date can establish a linear variation of concentration over a region of 200 micrometers, within 10 seconds for small molecules (GABA, 101 g/mol), but 15 minutes for large proteins (netrin-1) [17]. In a device reported in reference [18], a linear gradient is obtained in a channel 200 µm wide, in 2 minutes for 70 kg/mol dextran. Similar devices shown in figure 1.5 were used to study neuron chemotaxis in netrin gradients [19] and the effect of Wnt3a on melanoma cells [20]. Fast transverse variation of concentration at zero shear has also been achieved via diffusion through a thin membrane flowed on one side with an aqueous solution (so called "dynamic gradients" by Melosh et al. [21], as described in appendix B, p. 179). The authors claim that gradients are established in the timescale of 45 seconds.

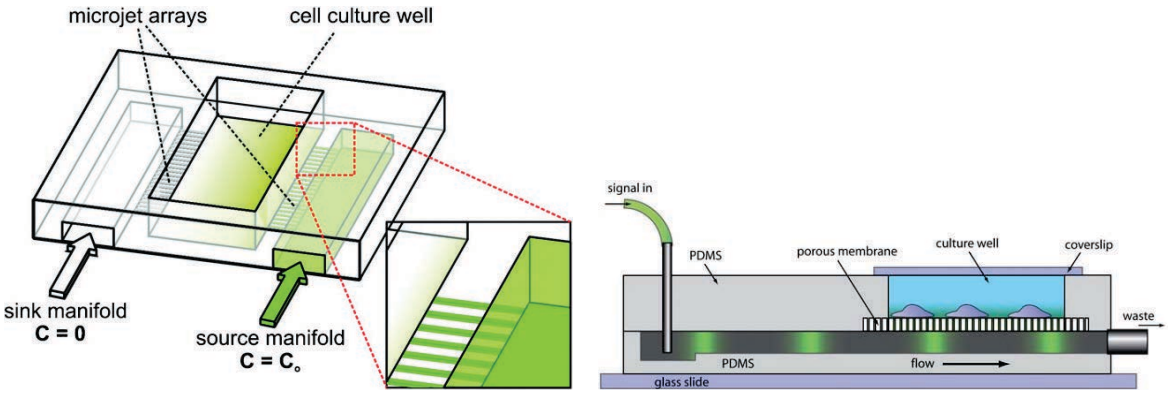


(a) (b)

**Figure 1.5.** *Microfluidic devices used to rapidly modulate changes of concentrations and gradients in 2D cell cultures in liquid media, (a) at low flow near the neurons [19] or (b) zero flow [21].*

## 1.2.2. Characteristic spatial range of gradients

At timescales longer than $\tau$, a gradient of concentration establishes and stationary state may be reached. The gradient feature is usually expressed by its relative slope over a characteristic length. The relative slope, noted $s$, is calculated as $s\ (\text{in } \%) = 100 \cdot \Delta C/C$, where $\Delta C$ is the difference of concentration between two ends of the cell, or over a test segment of the cell (e.g. one neurite), and $C$ is the mean value of the concentration along the cell. The characteristic length is in the range of 10 µm, and often assumed to be exactly 10 µm (see figure 1.6).

Reproducible gradients of high steepness and localized around a microsource can be obtained using pipette microinjections (in typically one minute to 10 minutes [4], but it is considered stable for one hour [23, 24]). By this method, the average concentration of cues around the cell is controlled by the concentration in the pipette, and pulsed injections stabilize gradient steepness in the range of 10–30 % [4, 11, 25]. This system has been applied on various kinds of cells, ranging from neurons cultured in 3D collagen gel [2] to leukocytes [26] or cancerous cells [27] in 2D culture conditions. The same diversity is found for the released molecules, ranging from proteins [2, 28] to peptides [26]. Cells may respond at short time scales by spatial redistribution of their membrane receptors (< 30 s), of organelles and/or cytoskeleton (minutes), shape distortion (e.g. angular redirection of growth cone in neurites, < 60 minutes). But faster events cannot be captured, such as recruitment/activation of signaling proteins on the activated regions.

Quantification of micropipette observation may also be an issue. Authors derives the concentration pattern based on theoretical models that have been the subject of vivid discussions and criticisms [4–6]. The assumed linear relationship between the released molecule from the pipette and the pulse duration and frequency is not always true. The gradient is also often considered 2D, neglecting the vertical component, which was shown experimentally to matter (confocal imaging, using labeled dextran).

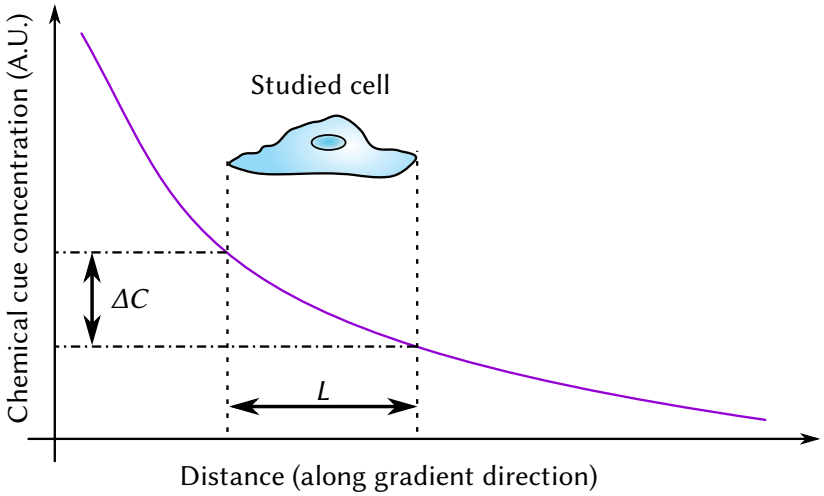


**Figure 1.6.** *A cell in a gradient of a molecule of interest. The relative gradient steepness, $s$ in percentage, is defined as $s = 100 \cdot \Delta C/C$, where $C$ is the mean concentration on the cell level [22].*

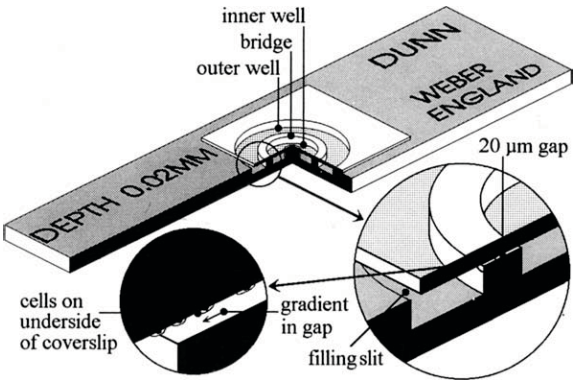


**Figure 1.7.** *Schematic view of the Dunn chamber, widely-used for cell culture. Reprinted from [29].*

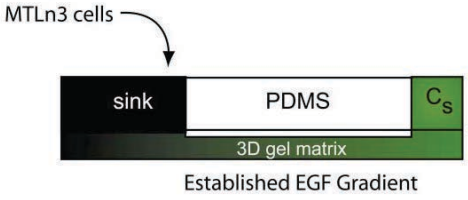


**Figure 1.8.** *Gradient generated from a sink and a source through a channel. Reprinted from [30].*

These remarks suggest that pipette-based stimulation is preferred for qualitative tests. The technique suffers from others drawbacks, the main one being that it is invasive in gels (breakage of the matrix) and not easy to adjust in real time to cell movements (risk of mechanical damage on cells). Another constraint is that concentration in the pipette must be about 1000 time higher than the concentration activating the cells – usually in the nanomolar range. Namely, efficient concentration in the pipette were experimentally measured at about 10 micromolar NGF [2] or 0.1 micromolar netrin [11] on neurons, 1 micromolar fMLP or interleukins on leucocytes [26], 50 micromolar EGF to induce locomotion of cancer MTL cell lines [27]. Such concentrations on the order of 1 mg/mL (or below) are reasonably reached in available samples (e.g. commercial or home-purified solutions), though using hundred of microliters can become rapidly expensive – the typical price of recombinant netrin-1 is $\sim 400\,€$ for 50 micrograms.

Smoother and more robust gradients with slopes $< 10\,\%$, generally 1–5 %, are formed by diffusion between a source compartment and a sink one in various geometries of microchambers, as shown in figures 1.7 and 1.8, and in annexe B, p. 179. Cells fairly respond to smooth gradients, and even shallow ones (0.1 %). This is the case of neutrophils exposed to cytokines such as fMLP [30–33], neural explants exposed to NGF around 1–3 nM [34–37], cancer cell line exposed to growth factors (MTL) [30, 38, 39]. Access to long duration and accurate control on concentration patterns suggested that cell responses can be highly subtle. For instance, locomotion was not activated on neutrophils in stable stationary gradients lacking fluctuations [40], or the direction of motion could be reversed upon slow decrease of the concentration of chemokines [41]. Similarly many open questions are debated in the field of morphogenetic control of neurons in embryos. Important parameters of control include concentrations of guidance cues (and their gradients), time of exposure to guidance molecules, degree of interaction with extracellular matrix (that may modulate the cross-talk with e.g. mechano-transduction pathways). The studies of signaling events have thus to encompass the response to delivery of controlled amounts of guidance molecules, with micrometer resolution at the spot of release, while enabling to manage with the local mechanical rigidity and force applied on the cells in hydrogel (ideally 3D) substrates. Part of these goals are reachable in microchambers, until modulation at long distances ($> 100$ micrometer) of the test cell is sufficient. But binding of cues in gel substrates, cell migrations, and importance of short activation or dual activation (by activators and inhibitors) motivate to broaden the toolbox of cell biologists. A mild (non-invasive) local release can nicely complete the presently available systems.

## 1.3. Summary and conclusion

Quantitative assessments of cell responses to soluble protein cues rely nowadays on delivery systems based on micropipette and/or gradient-forming devices. Interestingly, the order of magnitude of concentration conditions that cells can interpret has been determined. Representative cases show that cells, in particular neurons, can detect threshold concen-

trations below nM, and shallow gradients (0.1 %), but reaching steeper gradient (1–10 %) may also be required. The whole complexity and sensitivity of cells to its environment cannot however be explored with the available systems. First, cell-activation and control of local delivery of cues at (sub)second time scales is difficult due to experimental constraints on distances between cells and protein sources. This hampers observations in real time of important steps in the mechanisms of responses, such as the reorganization of receptors rapidly moving on the top of cell membranes. Second, at long time scales – from hours to days – cells may move or grow, requiring to modulate the concentration pattern, to keep constant the activation conditions. Third, studies of cells grown in gels with adhesion and motion allowed in the three dimensions of space would certainly avoid the artifacts likely to occur in 2D flat substrates, but is hardly accessible with conventional manipulations (e.g. pipettes break the gels). The history of samples may also matter (e.g. memory effect of cells, dual activation and/or activation by sequences of exposure to different molecules, etc.).

Next challenges in the field are accordingly the design of tools capable to mimic secretion as follows:

- release of adjustable aliquots of signaling proteins directly in contact to, or at micrometer distance from, the cell membrane (to achieve fast stimulation);
- non-invasive in situ modulation of position of the source and/or the release rate (to adjust conditions to cell motion or shape evolutions);
- versatile on/off switch of delivery (to study memory effects).

# Part I.

# Light-controlled release, a review

# Introduction

The aim of this thesis is to develop a system able to release arbitrary molecules in a 3D cell culture medium, with a control in space and time. As shown in the last part, systems targeting a transient (second scaled) release and confined (micrometer scale) are scarce in the toolbox proposed to biologists. The representative technique is based on micropipette manipulations, which causes damages to culture medium, and which may not be as quantitative as they are claimed[1]. Two constraints are therefore added to our system: it must preserve the integrity of the cell culture medium and release a known amount of molecule. We also want the system to use as few molecules as possible, as the availability of the released molecule can be problematic.

One technique, shown in references [43–45], relies on the in-situ release of the entrapped molecule from an artificial carrier. Here, hollow polystyrene beads or liposomes are reported. The principle of this technique is to entrap the molecule in a carrier, which remains tight under physiological or experimental conditions. These vehicles are dispersed in the cell culture medium; the molecule, entrapped, is never seen by the cells, thus inactive. Under an external stimulus, the vehicle becomes leaky or destroyed, and the entrapped molecule is released and becomes active.

Our system should target various molecules, including peptides or proteins, which must stay biologically active after their release. The activity of a protein can be hindered by several factors, like the pH, the ionic strength, the redox potential, an increased temperature, freeze/thaw cycles, freezer-drying, the presence of organic solvents or the presence of amphiphilic molecules [46–49]. This suggests that proteins must stay in a buffered aqueous medium of controlled temperature, from its encapsulation to its release.

Concerning the modalities of release, several are available: enzymatic degradation, pH, temperature, ionic strength, redox potential modulation, magnetic fields, light or sound waves are reported [50, 51]. Due to the previous remark on the protein activity, only a few can still be considered. The same can be done for the studied cells. Their “normal” behavior is subjected to the culture conditions; any deviation from the standard conditions of pH, salinity, temperature or redox potential may hinder its activity. This excludes de facto chemical stimulations, which are not relevant anyway: the diffusion of molecules in the culture medium means that even a local stimulation will extend quickly and create a large source of encapsulated molecules.

Cell sensitivity to shear stress also excludes any sound wave stimulation. The last two candidates are magnetic fields and light. Our aim is to develop a system that can be useful

[1] For details on the micropipette technique, see references [5, 6, 42]

in a standard biological experiment, with live imaging. They rely mostly on the observation of the culture medium with an epifluorescence microscope or a confocal microscope. The possibility to control light illumination of the sample in term of time and space, and the availability of illumination systems on standard biology equipments make the light an ideal stimulus.

So, we are looking for an encapsulating system for proteins, peptides and small molecules, able to release its content on a short timescale upon light illumination. From this point of view, the available light-sensitive systems can be classified in two set of binary classes: slow/fast release and "preserve protein activity" or not. Systems based on molecule entrapment in a dry polymer matrix are automatically excluded from the selected systems: the entrapment conditions (dried hydrophobic polymer) and the kinetics of release (in the timescale of the hour) are crippling. This includes the particles developed by A. Almutairi's team, based on poly(lactic acid)/poly(glycolic acid) heated by infra-red light [52] and the photolysable ones based on coumarins and orthonitrobenzenes [53–58]. To this, we may add a system based on a cinnamic acid-based 2+2 cyclization [59] and one based on photomanipulated permanent sources made of PLGA [60]. Three main classes of candidates remain: the lipids vesicles, the microgels and the polymer capsules; all three give the possibility to encapsulate the molecule in an aqueous medium and release it using light. They will all be reviewed in the next sections.

# 2. Light-sensitive liposomes

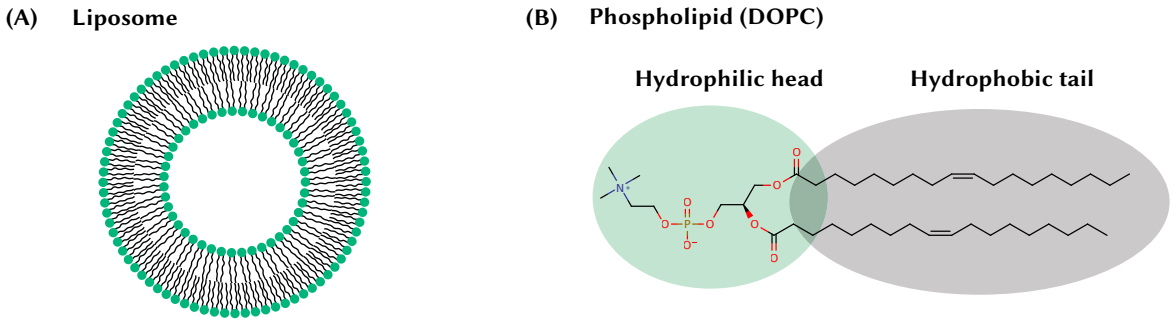


**Figure 2.1.** *A: a schematic view of a liposome slice, made from a lipid bilayer shaped as a sphere surrounding an aqueous core. B: an example of a phospholipid, here DOPC. The hydrophilic part of the molecule is highlighted in green, the hydrophobic one in grey.*

Since their discovery by Bangham et al. [61], liposomes have been of great help to build molecule delivery systems, with applications ranging from cosmetics to drug delivery [50, 62]. Liposomes are vesicles made from phospholipid bilayers and an aqueous core, as shown on figure 2.1. Vesicles of various composition and size can be formulated. Diameters range from 10 nm to 10 µm; unilamellar vesicles, with only one lipid bilayer constituting the membrane, as well as multilamellar vesicles, made of multiple stacked bilayers, can be prepared as almost monodisperse objects [63].

Hydrophilic molecules of interest, when entrapped inside the aqueous core of the vesicle, can escape either by passive diffusion through an intact membrane or by breaking the membrane; these events can be triggered by external stimuli. Membrane tightness can be modulated using several additives, like cholesterol [64, 65]. Other routes involve the loss of the membrane integrity; they rely on the creation of pores, the disruption of the membrane or the dissolution of the membrane and its dispersion as micelles. They are illustrated on figure 2.2.

Assembled in a bilayers, lipids can be viewed as a two dimensional system, in which lateral movements are possible. Each lipid is characterized by a phase transition temperature ($T_m$), corresponding to the transition from a gel – solid – state to a liquid state. In the gel state, lipids can be considered as frozen and immobile, while any lateral movement is allowed in the liquid state. Transition temperatures of natural lipids cover roughly the [– 50 °C, 100 °C] range. Thus, increasing the temperature leads to the disorganization of the lipids; less tightly packed, the permeability is increased. Packing can also be affected by specific molecules inserted in the bilayer.

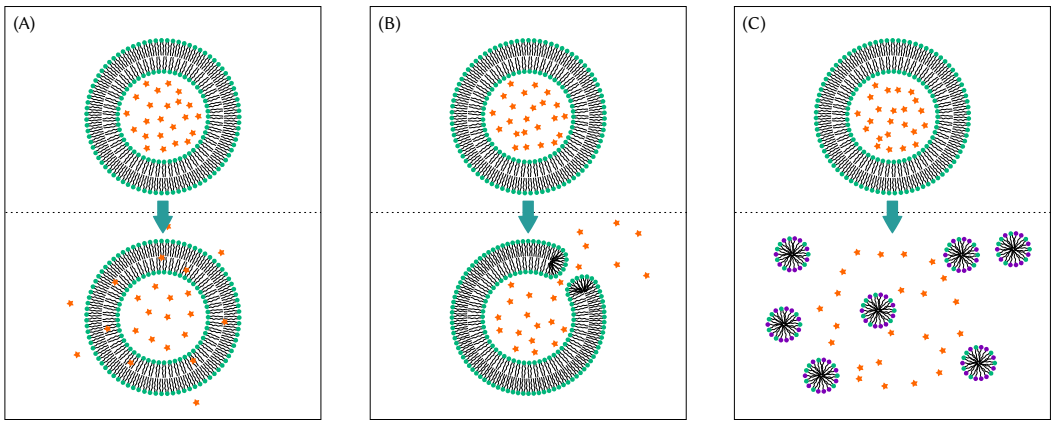


**Figure 2.2.** *Release of a drug entrapped in the aqueous core of a liposome. (A) the permeability of the lipid bilayer is increased, allowing molecules to escape the liposome by diffusion. (B) the encapsulated molecule escapes the liposome through a pore created in its membrane. (C) release of all the content of the liposome by breaking the membrane.*

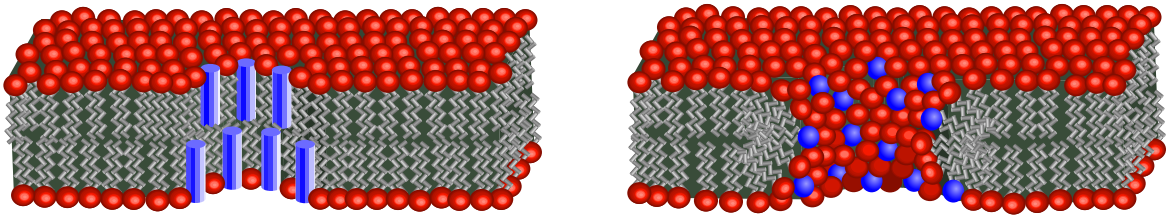

**Figure 2.3.** *Mechanisms of pore stabilization. On the left, the pore is stabilized with a molecule (blue cylinder) with a hydrophobic face in contact with the bilayer and an hydrophilic one in contact with the aqueous buffer; On the right, a surfactant (blue heads) with a small packing parameter permit this stabilization.*

In fluid state, pores spontaneously open and close in the lipid bilayer. In regular membranes, their lifetime is too short to allow the release of the entrapped content. Phospholipids are cylindrical-shaped molecules which assemble in bilayers in aqueous media, and take the shape of spheres. This organization in spherical objects leads to an inner tension referred to as the membrane tension; the smaller the radius of the vesicle, the higher the tension. This tension is responsible for the opening of the pores. When a pore opens, the inner part of the bilayer – hydrophobic – comes into contact with water. This unfavorable event is associated with an energy called the line tension, and is in favor to the closing of the pore. Adding cholesterol to the lipid bilayer is known to increase the line tension, thus reducing the lifetime of the pores, while adding surfactants has the reverse effect [66]. The stabilization of the pore with surfactants – or other amphiphilic molecules like polymers [67, 68] – relies on *masking* the hydrophobic layer, as shown on figure 2.3. Cylindrical bi-faced molecules (e.g. permeabilizing peptides [69]) lead to the left case, while conical surfactants and hydrophilic polymers grafted with hydrophobic anchors lead to the one of the right.

The last route leads to the complete dissolution of the bilayer. The phospholipids are

dispersed into micelles, either by a modification of their structure or by adding a surfactant inside the medium.

## 2.1. Light-induced increase of permeability

Optical control of the packing and the orientation of molecules inside the bilayer appears to be by far the most studied system. Basically, any molecule inserted in the bilayer affects the packing of lipids. Accordingly, phototriggered variations of the conformation and/or the degree of insertion of this molecule in the bilayer are expected to change the permeability of the liposomes.

### 2.1.1. Retinoic acid-based sensitizer

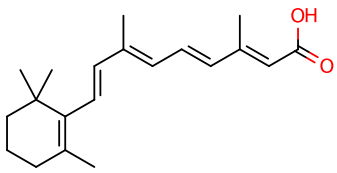


**Figure 2.4.** *Tretinoin, also know as all-trans retinoic acid.*

Retinoic acid (see figure 2.4) is a light-isomerizable molecule which has been used to increase liposome permeability [70]. One or both of the alkyl chain of a phospholipid is replaced by this molecule. Upon UV irradiation, the trans bonds of retinoic acid isomerises to cis, which perturb the packing of lipids in the bilayer, thus permeabilize it. They have been used to build liposomes 50 to 300 nm large, entrapping carboxyfluorescein, and releasing their content upon continuous UV light irradiation (360 nm, 50 W/m²). The kinetics of release were fast, as it was reported to be complete within 30 seconds at 25 ℃ (see figure 2.5). However, these liposomes were not tight: ≈ 20 % of the entrapped carboxyfluorescein is released in one hour at 25 ℃. Increasing the temperature to 37.5 ℃ makes this value rise to ≈ 60 %, which means that in a few hours at a physiological temperature, the capsules are empty. This probably explains why this system did not lead to further developments.

### 2.1.2. Azobenzene-based additives

Another light-isomerizable molecule is the azobenzene. Its thermodynamically stable isomer, the trans – apolar – one, can be converted into a cis – polar – one by UV irradiation. The reverse isomerization occurs with visible light irradiation or thermal relaxation (see figure 2.6). These light-sensitive groups have been included into the lipid bilayer; light irradiation causes the azobenzene to isomerize, perturbing the packing of the lipids and increasing the permeability of these objects.

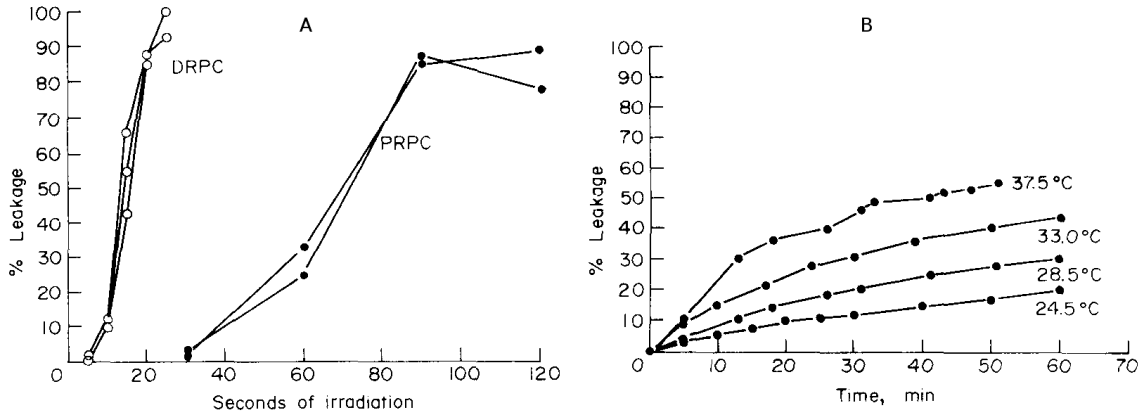


**Figure 2.5.** *Reprinted from reference [70]. A: leakage of carboxyfluorescein upon UV irradiation.* DRPC *stands for diretinoyl-glycerophosphocholine and* PRPC *for pamitoyl retinoyl-glycerophosphocholine. B: carboxyfluorescein leakage from DRPC liposomes in the dark.*

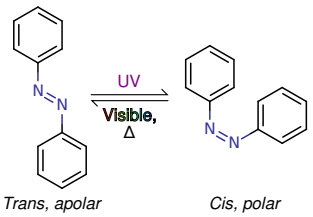


**Figure 2.6.** *Trans and cis isomers of the azobenzene moiety. This group isomerizes with light: UV light turns the trans (apolar) group in the cis (polar) one. Cis to trans reverse isomerization is obtained either by visible light irradiation or by thermal relaxation (Δ).*

## Azobenzene-modified lipids

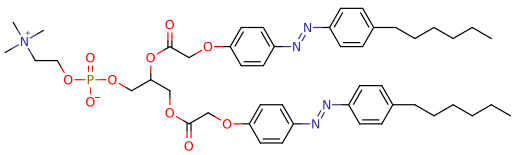

**Figure 2.7.** *Lipid "bis-azo", used in reference [71].*

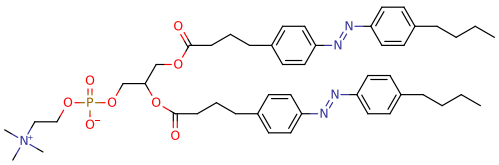

**Figure 2.8.** *Lipid "bis-azo", used in reference [72].*

As shown on figures 2.7 and 2.8, azobenzene groups have been introduced in phopholipids, replacing both of the hydrophobic tails. The one shown on figure 2.8 has been mixed with other natural lipids (DMPC, DPPC, DPEPC, DSPC) to make 400 nm size vesicles encapsulating carboxyfluorescein. The content of these vesicles was released using pulsed laser irradiation (355 nm, 15 mJ, 3 $mm^2$), and occurred in the timescale of 10 ms [72, 73]. Increasing the temperature of the sample below the phase transition temperature of the lipids increased the kinetics of release. In the case of DPPC/bis-azo liposomes, at least 3 % mol. of bis-azo were required for the UV irradiation to trigger a release [74].

The same group reported that adding cholesterol to the lipid bilayer decreased the amount of trans to cis isomerizations required to trigger the release [73, 75]. A continuous blue light

irradiation (470 nm, LED) was sufficient to trigger the release from DPPC/6 % mol. bis-azo liposomes, as shown on figure 2.10. The release was slower than with UV irradiation, and occurred in the timescale of 10 seconds. In fact, irradiating azobenzene with a visible light does not lead to 100 % trans isomers; irradiating an all trans sample lead to a cis:trans isomer mixture. The cis:trans ratio at steady state depends on the azobenzene and the wavelength used. In this case, the ratio obtained with the 470 nm irradiation is not reported. This set of experiments suggests that an unknown minimal amount of cis isomers are required for the release to occur.

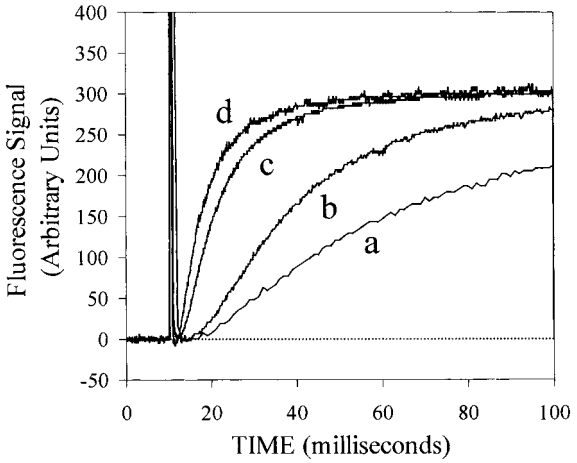


**Figure 2.9.** *Reprinted from reference [73]. Increase in fluorescence intensity due to calcein release, following exposure to a single 355 nm laser pulse, from liposomes of DPPC at 16 ℃ containing 6 % mol. Bis-Azo PC and (a) 0 % mol., (b) 5 %, (c) 10 % and (d) 15 % cholesterol.*

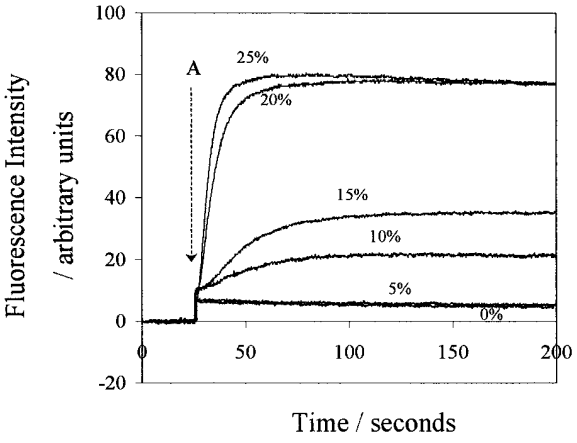


**Figure 2.10.** *Reprinted from reference [75]. Liposomes prepared from DPPC and 6 % mol. bis-azo. Kinetics of release as a function of the cholesterol content. A: start blue light irradiation (470 nm, LED, continuous)*

The permeability upon cis isomerization has been attributed to the H-aggregation of azobenzenes in the lipid bilayer [71, 76]. This phenomenon can occur only when the azobenzene lipids are next to each other. The lipids used in the previously reported experiments were mostly DPPC, whose phase transition temperature is 41 ℃. These experiments were conducted at 25 ℃, where the lipid bilayers are in gel state. Under such conditions, the diffusion of lipids in the bilayer is limited; for the azobenzene to aggregate, they have to be close to each other from the beginning. Adding cholesterol at concentration below 20–25 % mol. increase the fluidity of the bilayer, while increasing the packing of the lipids. The lipids are thus allowed to diffuse in the membrane and regroup themselves, which explains why in presence of cholesterol the required amount of cis isomers to trigger the release is lower. In the same references is also reported that the release can only occur when the lipid is in the gel state. Increasing the temperature above the lipid melting temperature disables the release. This confirms that leakage depends on the formation of defects between rigid lipid domains in the lipid bilayer. In general, these defects create small gaps, whose size

permits only the escape of small molecular weight molecules. This has been confirmed in reference [77], where doxorubicin (543.5 g/mol) escaped the liposome 20 times slower than acridine orange (265.4 g/mol).

### Azobenzene-based surfactants

Another method to destabilize the lipid bilayer relies on the incorporation of azobenzene-based surfactant inside it. The first reported system demonstrates the release of bromothymol blue from 30 nm sized liposomes made of DPPC, sensitized with the surfactant shown on figure 2.11. The release is triggered by the exposure of the liposome suspension for 5 minutes to UV light (366 nm) [78, 79]. The release constants, assuming a first-order release

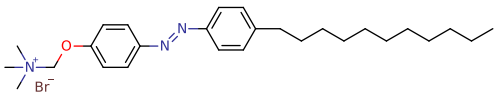

**Figure 2.11.** *Light-sensitive azobenzene-based surfactant used in references [78, 79].*

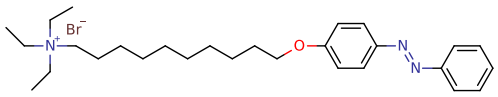

**Figure 2.12.** *Light-sensitive azobenzene-based surfactant used in references [80].*

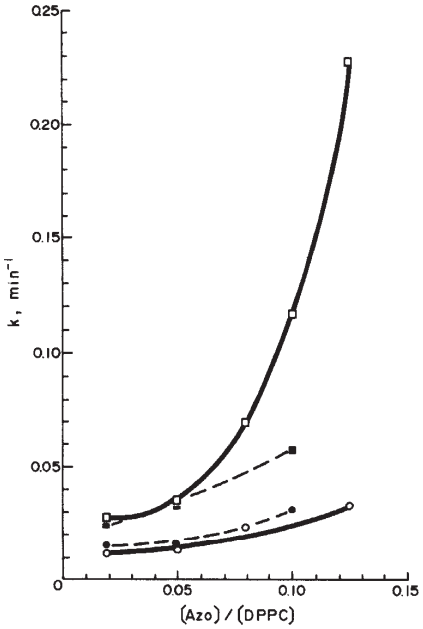


**Figure 2.13.** *Reprinted from reference [79] Rates of bromothymol blue (BTB) release ([BTB] = 8.3 μM) from DPPC liposomal membranes ([DPPC] = 0.17 mM) containing amphiphatic azobenzenes in trans- and cis-configurations at 25 ℃: ○ trans-$C_4$Azo; □ cis-$C_4$Azo; ● trans-$C_2$Azo; ■ cis-$C_2$Azo.*

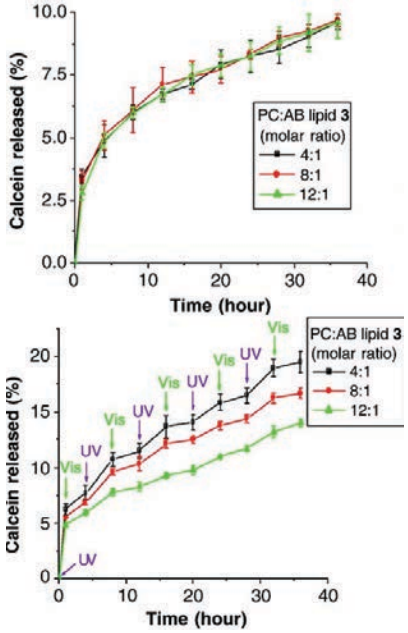


**Figure 2.14.** *Reprinted from reference [81]. Release of calcein. Top: sample kept in the dark. Bottom: periodical UV and visible light irradiation.*

rate, are shown on figure 2.13. According to the authors, the surfactants are inserted in the lipid bilayers; the release occurs under UV light irradiation, as the surfactant perturbs the packing of the lipids. However, when heated above the melting temperature, these liposomes remained light-sensitive. This suggests that the mechanism of release is not the same as the one observed with the azobenzene-modified phopholipids, as pointed out by the authors. They suggest that the entrapped molecules escape through channels in the bilayer, induced by the conformational change of the surfactant.

Azobenzene has also been incorporated in cholesterol-based surfactants, to sensitize liposomes loaded with calcein [81]. Here the lipid (egg PC):surfactant ratio equals 1:1. The release leak under UV irradiation (365 nm, power unknown) was slow: 40 hours were required to release only 25 % of the entrapped dye. This system suffers also from a constant release when kept in the dark (see figure 2.12). 8 % of the initial amount of entrapped calcein is released within 1 day.

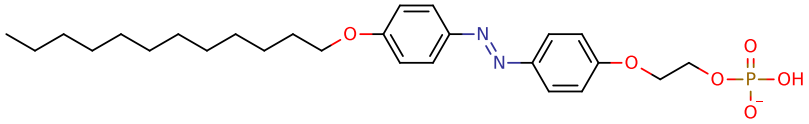


**Figure 2.15.** *Phosphate based surfactant, from reference [82].*

Phospholipid-less vesicles have also been sensitized with azobenzene-based surfactants. In reference [82], vesicles are made from dihexadecyl phosphate (24 mg) and an azobenzene-based surfactant (1–2 mg, cf. figure 2.15). 30 % of entrapped potassium ions are released after 35 minutes, upon UV light irradiation (360 nm). These vesicles suffer also from a high passive release rate: 10 % of the encapsulated potassium is released in 6 hours without stimulation; the light stimulation multiplied by 5 the release rate of potassium.

In reference [80], the vesicle is composed of cholesterol sulfate (75 % mol.) and an azobenzene-based surfactant (25 % mol., cf. figure 2.12). They have been proved to be less permeable than their phospholipid-based counterparts; the kinetics of release are still behind the ones of the *bis-azo* liposomes, suggesting that the mechanism of release do not rely on the perturbation at the interface of lipid domains. 80 % of entrapped sulforhodamine B is released in 300 s upon UV (365 nm) irradiation. The main advantage of this system over the previous one is the low passive release: ≈ 7 % within 30 days in the dark. This system reminds the ones shown in paragraph *2.1.2 Azobenzene-modified lipids*, p. 22. But the membrane made is described as fluid, which means that the mechanism of release is different. Yet, this may explain why the release upon UV irradiation is slow. The precise mechanism of release is not known; the authors only claim that the isomerization of the azobenzene disturbs globally the packing of the lipids initially tightly packed.

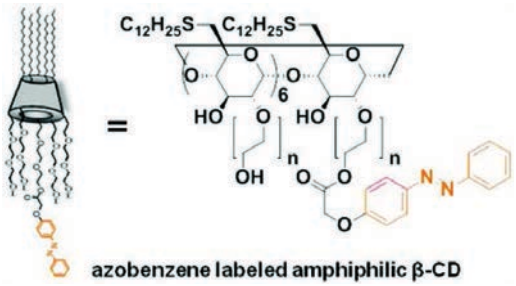


**Figure 2.16.** *Light-sensitive channels, made of azobenzene and cyclodextrine. Reprinted from reference [83].*

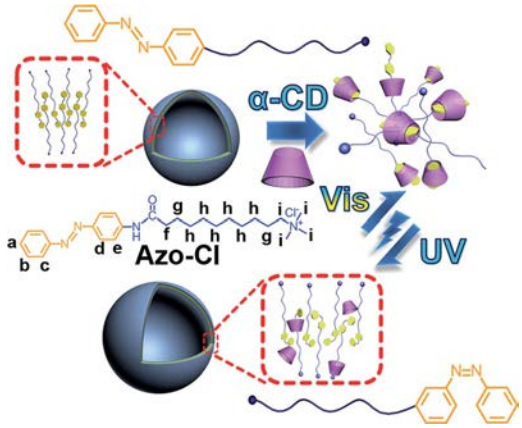


**Figure 2.17.** *Artificial bilayers made of azobenzene-based surfactant assemblies. The presence of cyclodextrines made these objects light-sensitive. Reprinted from reference [84].*

### Supramolecular associations

Cyclodextrine/azobenzene associations have also been used to build light-sensitive vesicles. On its trans isomer, the azobenzene molecule (the guest) is able to enter a cyclodextrine cycle (the host). On UV irradiation, the azobenzene turns into a cis isomer and escapes the cyclodextrine.

In reference [83] is reported an artificial light-sensitive channel, made of azobenzene/cyclodextrine association (see figure 2.16). 100 nm DOPE:DOPC:cholesterol (2:1:1 mol.) vesicles have been sensitized with these molecules (10–30 % mol.). The highest release rates were obtained with 30 % mol. of the channel: sulforhodamine B was released in the timescale of 2 hours upon UV light irradiation (350 nm). However, this is only 3 times faster than the release occurring in the dark. Moreover, this system is limited to the release of small molecules, as they have to pass through the channel.

The system presented in reference [84] is based on non-phospholipidic bilayers, made of an azobenzene-based surfactant and cyclodextrines (see figure 2.17). These vesicles are destroyed upon UV light irradiation (340 nm), and reassembled upon blue light irradiation (450 nm). The associated timescales are in the 10–50 s range. Neither the encapsulation nor the release has been characterized yet.

## 2.1.3. Spiropyrane based sensitizers

Spiropyrane is converted into a zwitterionic merocyanine upon UV irradiation, and can be transformed back to its initial form upon irradiation with visible light or by thermal relaxation (see figure 2.18). They have been integrated in surfactants (see figure 2.19) and have been proved to increase the permeability of lipid bilayers to ions. Here $K^+$ and a cobalt(II) complex have been encapsulated in bilayers made hexadecyl phosphate and this

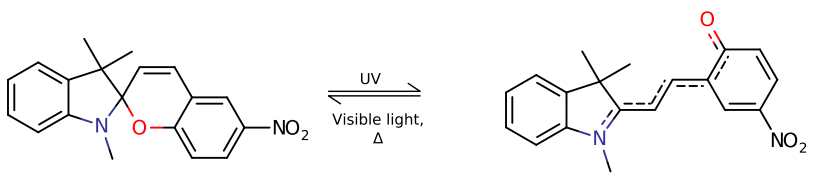


**Figure 2.18.** *Spiropyrane cycle opens upon UV illumination, going from a neutral form to a zwitterionic one. The reverse process occurs upon visible light irradiation or thermal relaxation.*

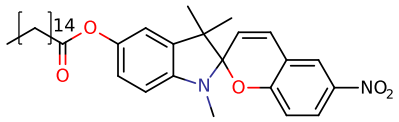


**Figure 2.19.** *Spiropyrane-based surfactant, from reference [85].*

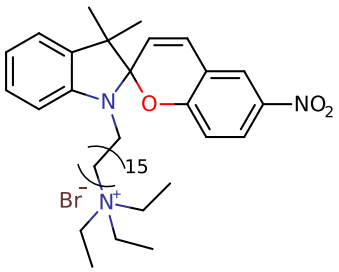


**Figure 2.20.** *Spiropyrane-based surfactant, from reference [86].*

surfactant at a ratio in the 0.5–2.0 % mol. range. In this system, the permeability of the membrane is increased when irradiated with visible light and decreased with UV light. The authors claim that the spiropyrane takes more space in the membrane than the merocyanine, thus perturbs it more. Irradiating the samples with visible light (> 400 nm) released both cobalt(II) complexes and potassium ions, in the timescale of several hours [85].

Another kind of surfactant has been reported in reference [86] (see figure 2.20). This surfactant has been added to DPPC SUV, at a 10–20 % mol. amount. Entrapped carboxyfluorescein was released within 2 minutes after 1 minute of UV irradiation (365 nm, 5.76 mW/cm²). The fast kinetics of release is explained by the abrupt change of behavior of the surfactant upon light isomerization. In its initial state, the quaternary ammonium head is the only hydrophilic part of the molecule, the spiropyrane-terminated alkyl chain is implanted in the lipid bilayer. Upon isomerization, the spiropyrane become hydrophilic and gains the surface, letting only an alkyl loop in the membrane. This disturbs the packing of the lipid bilayer, increasing its permeability without disrupting it [86].

### 2.1.4. Light-induced polymerization of lipids

Unsaturated lipids, as shown on figure 2.21, can be crosslinked under UV-light irradiation. Initially reported as a way to stabilize the bilayer and reduce the passive leakage from liposomes [89, 90], the photopolymerization of lipids has been used to trigger the release from the same objects. In reference [87], these lipids are mixed at 20 % mol. with a saturated lipid (DSPC, DAPC, DPPC) and a PEG-bearing lipid to build 200 nm sized liposomes

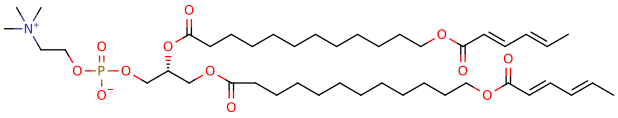

**Figure 2.21.** *Light-polymerizable phopholipid, from reference [87].*

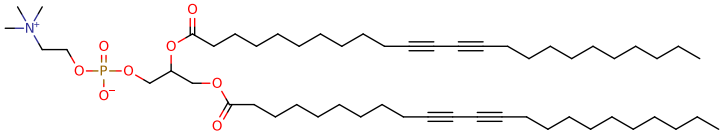

**Figure 2.22.** *Light-polymerizable phospholipid, from [88].*

encapsulating ANTS/DPX – a fluorophore/quencher couple. The release of the entrapped dye occurred in the timescale of 20 seconds upon UV (254 nm, 20–40 mW/cm²) irradiation.

An alkyne-bearing polymer was also used, which enabled to use visible light to trigger the polymerisation (see figure 2.22). UV light (254 nm) could be used to trigger the release, but it was also confirmed with a continuous blue laser irradiation (488+514 nm, 166 mW/cm²) for several minutes. In the UV irradiation conditions, entrapped calcein was release in the timescale of 10 minutes. High concentration of photopolymerizable polymer (> 20 % mol.), entrapped calcein is spontaneously released in the dark, at 4 ℃ within 24 hours. Blue irradiation has been proposed for the release of doxorubicin in cancerous cells, as blue light can increase the toxicity of this drug by photoactivation [88, 91].

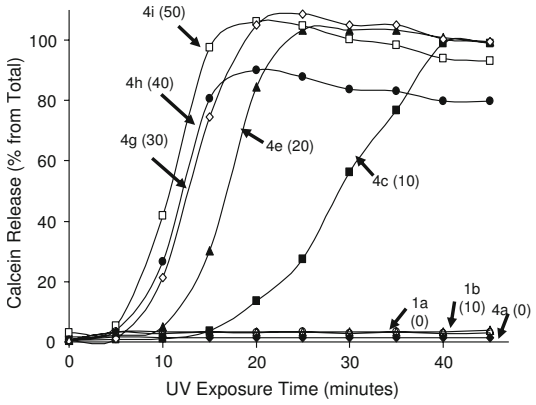


**Figure 2.23.** *Reprinted from reference [88]. Effect of various concentrations of $DC_{8,9}PC$ on kinetics and extents of UV-induced calcein release from liposomes. Liposomes containing varying concentrations of $DC_{8,9}PC$ were treated with UV for 0-–45 min and calcein release was measured. The mole % of $DC_{8,9}PC$ in the formulations are given in* parentheses. *The data are reproducible from at least three independent experiments.*

The permeabilization mechanism here is similar to the one reported for azobenzene-based phospholipids, and relies on a phase separation of the lipids. As before, the lipids have to be in the gel phase for the release to occur. This has been confirmed by mixing photopolymerizable lipids with DOPC, whose melting temperature is – 17 ℃. With this fluid membrane, no release occurs upon UV light irradiation [87].

### 2.1.5. Temperature-elevating systems

The permeability of lipid bilayer can be affected by the temperature. The properties of light-absorption of several dyes and nanoparticles have been used to convert locally the light into heat. The dye or the nanoparticle can be attached to the lipid, be entrapped inside the bilayer or inside the vesicle core, or even be dispersed outside the vesicle [92].

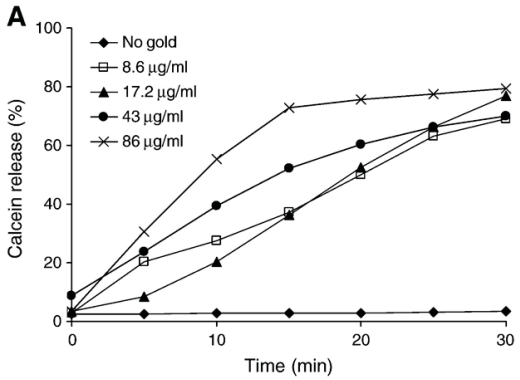


**Figure 2.24.** *Reprinted from reference [92]. UV light-induced calcein release from liposomes at constant temperature (37 ℃).*

Gold nanoparticles, covalently attached to the lipid bilayer, have been used to sensitize 200–500 nm sized liposomes made of DSPC/DPPC mixture. Entrapped calcein was released in the timescale of 10 minutes upon continuous UV (250 nm) light irradiation (see figure 2.24). The release is triggered as soon as the phase transition temperature is crossed. For DSPC/DPPC mixture, it is in the 34–48 ℃ range, depending on the lipid ratio [92].

As for dyes, temperature-sensitive liposomes – made of a mixture of DPPC and DPPG with a phase transition temperature of 41 ℃ – have been loaded with calcein and dispersed in an artificial blood stream [93]. The release occurred within 5 seconds upon yellow laser irradiation (588 nm, 200 ms, 20–80 mW/0.13 mm$^2$). The light is absorbed by the hemoglobin and turned locally into heat. When the phase transition temperature of the lipids is reached, the release occurs.

### 2.1.6. Summary

In such systems, the kinetics of release is driven by diffusion through the lipid bilayers or packing imperfections at the limits of lipid domains. The smaller and hydrophobic the

molecule, the faster the diffusion [85]. It should not be too hydrophobic though or it may become trapped inside the bilayer, as it was observed with doxorubicin [77]. The application potential to proteins is low, as there is no proof of release with such light-sensitive systems in the literature.

## 2.2. Light-triggered pore formation

### 2.2.1. Phase transition of phospholipids/lysolipids mixtures

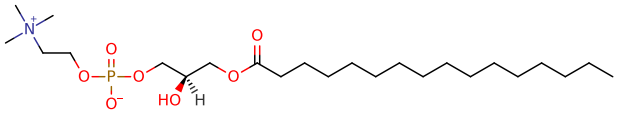

**Figure 2.25.** *Skeletal representation of 1-palmitoyl-2-hydroxy-sn-glycero-3-phosphocholine (16:0 Lyso PC), a lysolipid.*

The release from the vesicles can be significantly accelerated by creating pore in the membrane bilayer, which makes liposomes also permeable to nanometer-large molecules such as globular proteins. Pores can be created by heating vesicles made of specific lipids, as reported in reference [94]. This allowed to release BSA at 42 ℃ in the timescale of the minute from liposomes of 100 nm diameter, made of a 16:0 Lyso PC:PEG-DSPE:DPPC mixture, with a 10:4:90 mol. ratio. 16:0 Lyso PC is a lysolipid, which is a particular type of phospholipids lacking one of the two hydrophobic tails (cf. figure 2.25). Therefore, they do not have the typical cylindrical shape of a two-tailed phospholipid, but rather a conical one. Thus, they are able to stabilize pores – created by increasing the temperature – by reducing the line tension, as mentioned in the introduction of this chapter.

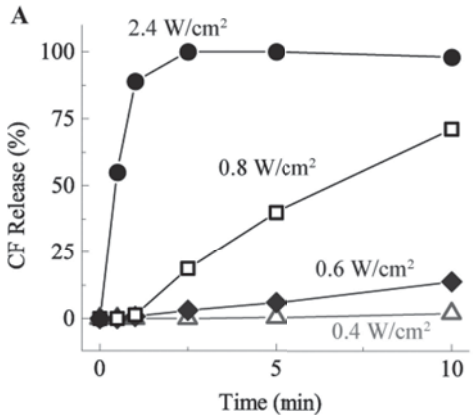


**Figure 2.26.** *Reprinted from reference [95]. Carboxyfluorescein release rate from lysolipids vesicles, sensitized with gold nanoshells.*

In references [95, 96], gold nanoshells have been used to convert the light into heat. Their absorption is partly due to the plasmon resonance effect, which allowed to use infrareds (800 nm, 2.4 mW/cm²) to trigger the release. Carboxyfluorescein was released in 1 minute from 200 nm liposomes made of DPPC:DSPE-PEG:MPPC – monopalmitoyl phosphatidylcholine, a lysolipid (see figure 2.26). A temperature of 41 ℃ is sufficient to release completely the encapsulated carboxyfluorescein. The same system has successfully been used to release locally doxorubicin in an in-vivo prostate cancer model.

## 2.2.2. Polymer stabilized pores

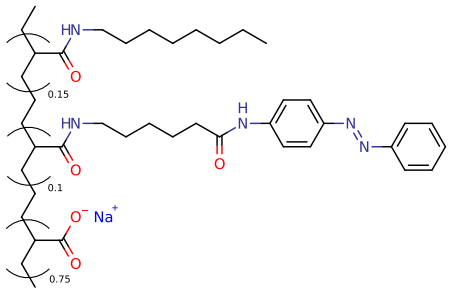


**Figure 2.27.** *Amphiphilic polymer, bearing hydrophilic side-groups (carboxylates), hydrophobic side-groups ($C_8$ alkyl chain) and azobenzenes. From reference [97].*

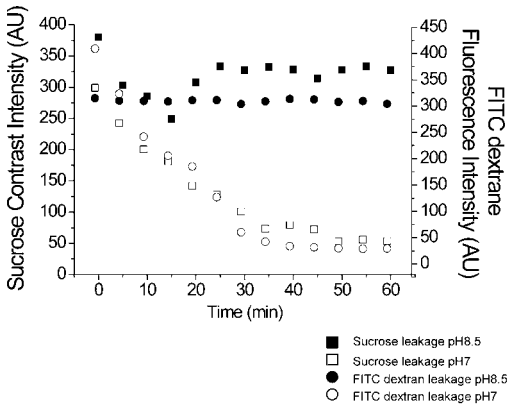


**Figure 2.28.** *Reprinted from reference [97]. Leakage profiles of polymer-sensitized GUV.*

Amphiphilic azobenzene-bearing polymers, as shown on figure 2.27, have been used to create or stabilize pore in the membrane of giant vesicles made of DOPC [97]. As reported before, DOPC is an unsaturated lipid whose melting temperature is – 17 ℃; the lipids in the lipid bilayer are in the liquid crystal state, where pore spontaneously opens. In its cis conformation, the azobenzene groups grafted on the polymer are hydrophilic and do not interact much with the lipid bilayer. Irradiating the polymer with visible light switches the azobenzene in their trans conformation; more hydrophobic, they will interact with the membrane. Grafted on a polymer chain, they are able to stabilize pores and maintain them on timescales sufficient for the encapsulated content to be released. The pores created by this polymer have been reported to be in the range of 10 nm. The release of encapsulated dextran (4 kg/mol) occurred in the timescale of 30 minutes upon visible light irradiation (see figure 2.28).

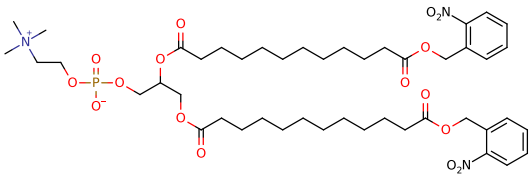

**Figure 2.29.** *Photolabile phospholipid: DLPC modified with an orthonitrobenzyl ester. From reference [98].*

### 2.2.3. Photolysable phospholipid

Light-induced lysis of lipids has also been used to trigger the release of molecules entrapped in liposomes. Liposomes have been made of DLPC modified with orthonitrobenzyl ester at the end of their alkyl chain (shown on figure 2.29). Irradiating the lipids with UV light (Hg lamp) cleaves the ester bond and leaves two carboxylic acid functions per chain. This molecule is able to stabilize pore in the lipid bilayer, as explained for the amphiphilic azobenzene-bearing polymer. Encapsulated ovalbumin (45 kg/mol) is released in the timescale of the 20 seconds. A prolonged irradiation of the liposomes leads to their destruction.

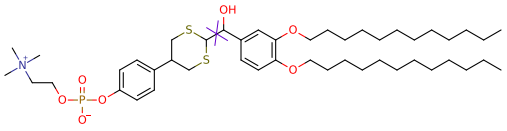

**Figure 2.30.** *Photolysable phopholipid, based on a dithiane group. Irradiation with UV light breaks the bond marked with a purple cross. From reference [99].*

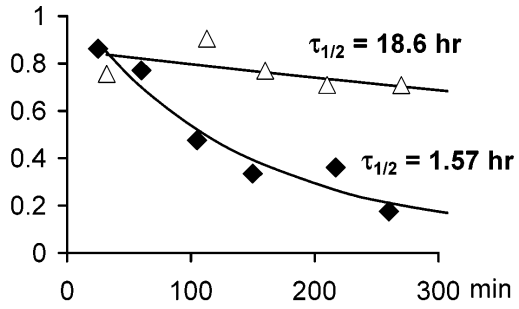


**Figure 2.31.** *Reprinted from reference [99]. Release of a fluor labeled probe from POPC:cholesterol:dithiane-lipid vesicles, followed by NMR. ◆: UV irradiated sample. △: sample kept in the dark.*

A dithiane-based light-sensitive lipid has also been developed. Irradiated with light, the aromatic part of the lipid is excited; an electron transfer to the dithiane group leads to the destruction of the lipids (see figure 2.30). The resulting aromatic aldehyde, connected to two hydrophobic tails, is apt to stabilize pores. Liposomes made from a mixture of this lipid, cholesterol and POPC have been reported to release their content upon UV light irradiation ($\lambda \geq 300$ nm), but are not destroyed in the process [99, 100]. This supports how hypothesis concerning the ability of the cleaved lipid to stabilize pores. A fluorinated pyridinium based probe is released in the timescale of one hour and half (see figure 2.31).

## 2.3. Membrane disruption

This mode of release is the most brutal one, as it relies on the complete disruption of the membrane. All the content of the vesicle is abruptly released, with no distinction of the molecular weight or the hydrophilicity of the encapsulated object.

### 2.3.1. Bare vesicles

The simplest reported method consists in using focused laser pulses of high power to break a vesicle. No light-sensitive molecule was required to induce the liposome rupture. As reported by Torre et al. [43, 44], several pulses of 1 µJ coming from a 355 nm laser focused on 1–10 µm vesicles are sufficient to break it; the vesicles were made of cholesterol:L-α-phosphatidylcholine:stearylamine 10:70:20 % mol. The release was estimated to occur in timescales lower than the second. This method was successfully used to release netrin-1 and semaphorin, and study their effect on a 2D culture of neurons. The mechanism leading to the vesicle breakage is not known; it may be based on a local heating of the medium, a cavitation caused by the high power laser pulse or a photodegradation of the lipids. While seducing, this technique suffers from several limitations. Only one liposome is manipulated at a time, and this manipulation requires a custom-made optical setup of optical tweezers, built from an infrared laser. The high power of both the breaking laser and the optical tweezers (1,024 nm, ∼ MW/cm²) are reported not to cause damages to the cells. Yet it seems rather difficult to achieve either high throughput experiments or long term release with this system, due to the single-liposome release.

### 2.3.2. Dye-sensitized vesicles

Finally, dyes have also been used to sensitize the membrane of giant vesicles (diameter ranging from 2 to 5 µm). Sulforhodamine encapsulated in the liposomes is able to release

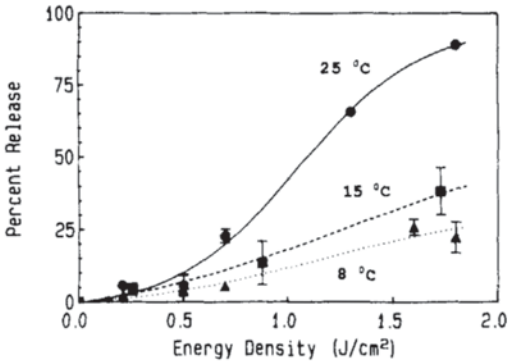


**Figure 2.32.** *Reprinted from reference [101]. Release of sulforhodamine from giant vesicles, upon pulsed light irradiation. Sulforhodamine initial concentration: 50 mmol/L.*

itself by pulsed light irradiation (532 nm, 0.5 J/cm²) [101]. This lead to the instant destruction of the vesicle, and has been shown to occur in less than 1 µs. Concentration of dye as high as 50 mmol/L are required for this effect to occur. Lower concentrations require higher light power. The benefit of using a dye is the reduction of light power required to break the vesicle, compared to bare ones. In the bare liposomes assay, 1 µJ were focused on ≈ 4 µm², which leads to 25 J/cm², while only 0.5 J/cm² (1/50) are required with the dye. The release here is caused by a local elevation of the temperature above the phase transition temperature of the lipid mixture (41 °C, mixture of L-α-phosphatidylcholine and dicetyl phosphate). In fact, to release the same amount of dye while decreasing the temperature, the power of the laser must be increased (see figure 2.32). The same effect was observed by adding cholesterol at concentration below 33 % mol., as it is known to increase the melting temperature. The exact temperature generated by the laser pulse is unknown.

The dye can also be stuck in the bilayer of giant vesicles, as it is the case with DiD (a lipid tracing dye) [102–104]. A single pulse from a 645 nm laser (3 ns, 560 nJ, area unknown) is sufficient to break a 400 nm sized vesicle. The mechanism involved in the vesicle breakage is also a photothermal one [103]. A high increase of temperature is reported with this dye. The highest release occurs when the lipids are in the gel state; the dye – segregated into raft domains, thus concentrated in restricted areas – is expected to increase locally the temperature between 100 and 200 °C above the one of the bulk. Due to the small size of the heat source, no temperature increase should be detected few micrometers away. This technique has been used to release a protein ($O^6$-alkylguanine-DNA alkyltransferase) inside CHO cells; the stimulation has been proved to preserve cell viability. However applied to the encapsulation of proteins in submicronic vesicles, the generated heat will elevate the temperature inside the vesicle and may denaturate encapsulated proteins.

## 2.4. Encapsulation yield and preparation conditions

Several methods for the encapsulation of molecules in liposomes have been proposed. Some are compatible with the manipulation of proteins, while others not due to the use of solvents or inadequate temperatures (see section 2.4.4 *Other procedures* below). One important parameter is the encapsulation yield. As mentioned in the introduction, the processed molecules may include proteins produced in low amounts (≤ 2 mg) and/or difficult to concentrate in aqueous solution (≥ g/L). Preparation procedures of large unilamellar vesicles will be reviewed with this constraint of a need for a high encapsulation yield in mind.

### 2.4.1. The film hydration method

The film hydration method relies on the hydration of a preformed lipid film with the solution to encapsulate. The film is made by the evaporation of a solution of lipids in organic solvents, like methanol or chloroform. While these solvents may be harmful, extensive drying of

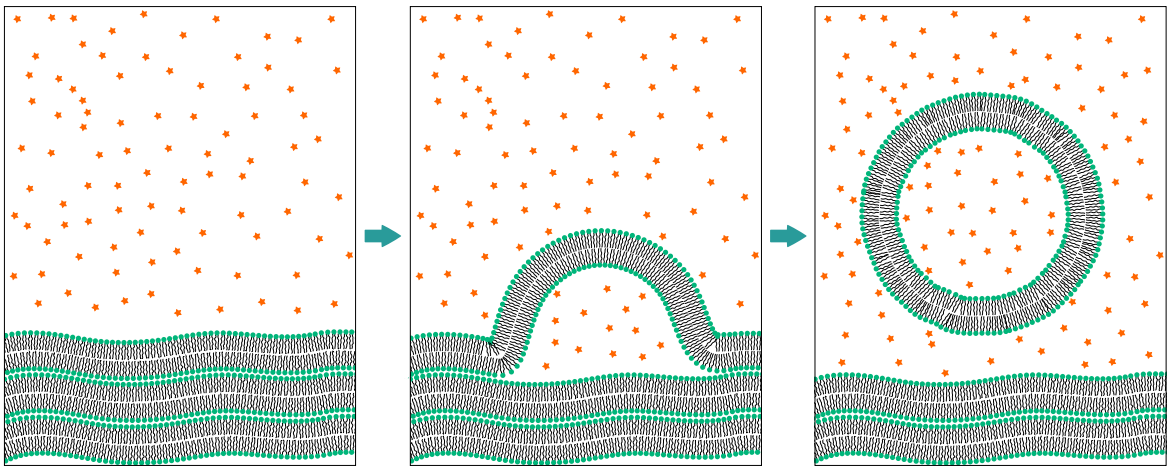

**Figure 2.33.** *Lisposome formation by the film hydration method. A film composed of stacked lipid bilayers is immersed in a solution containing the molecule to encapsulate. Spontaneously or mechanically, the film detaches to form vesicles, entrapping the surrounding solution.*

the film gets rid of all of them. The dried film is hydrated with a solution of the molecule to encapsulate. The concentration of the lipid is generally in the range of 1–10 g/L. The steps involved in film hydration may include suspension shearing, freeze/thaw cycles, sonication, heating and extrusion on a syringe filter [105–107]. The techniques relying on freeze/thawing, sonication and heating are not adapted to our application due to the risks of protein denaturation.

As illustrated on figure 2.33, not all the engaged solution is encapsulated in the vesicles, leading to a limited encapsulation yield. In a typical experiment, where 200 nm sized DOPC liposomes are prepared, with lipid concentration of 10 g/L, the encapsulation yield is at best 8 % (see appendix C.4.1, p. 200). This technique has however the main advantage of being compatible with mild handling conditions.

An encapsulation yield as high as 50 % can be reached under certain conditions. If the molecule to encapsulate can be made to have some affinity for the lipid membrane, up to half the initial amount of protein may stay in the liposome, while the other half will be attached onto the outer leaflet and removed during the liposome isolation step. This technique has been applied to the encapsulation of superoxide dismutase in liposomes made of DPPC:cholesterol [108] or trypsin in DPPC:cholesterol:dicetyl phosphate liposomes [109]. Depending on how the protein is retained on the interface, the encapsulation yield may depend on the pH or the ionic strength of the solution, e.g. in the case of electrostatic interactions.

### 2.4.2. Detergent dialysis method

Vesicles can also be prepared from an initial suspension of mixed micelles, composed of the phospholipid and a high-CMC surfactant. Removing the surfactant yields vesicles,

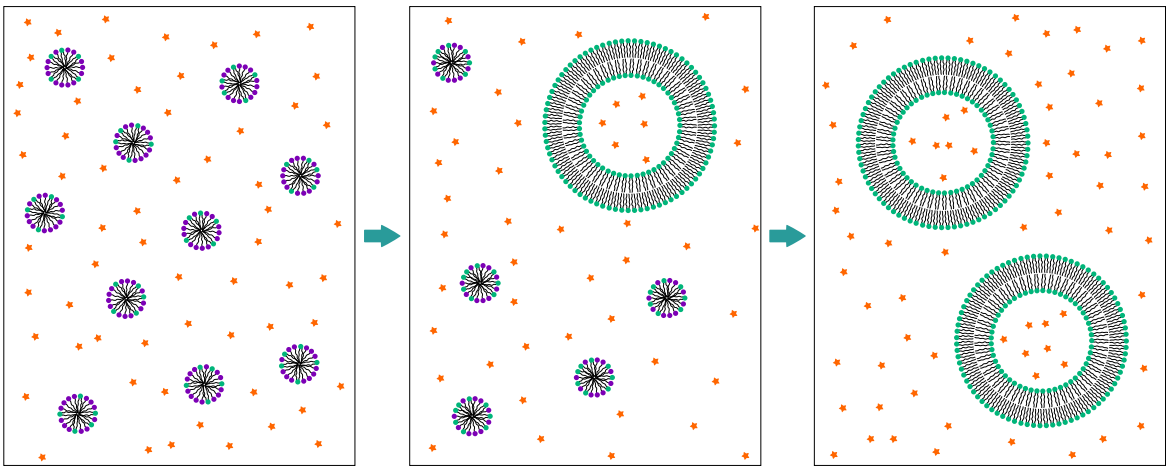

**Figure 2.34.** *Lisposome formation by the detergent dialysis method.*

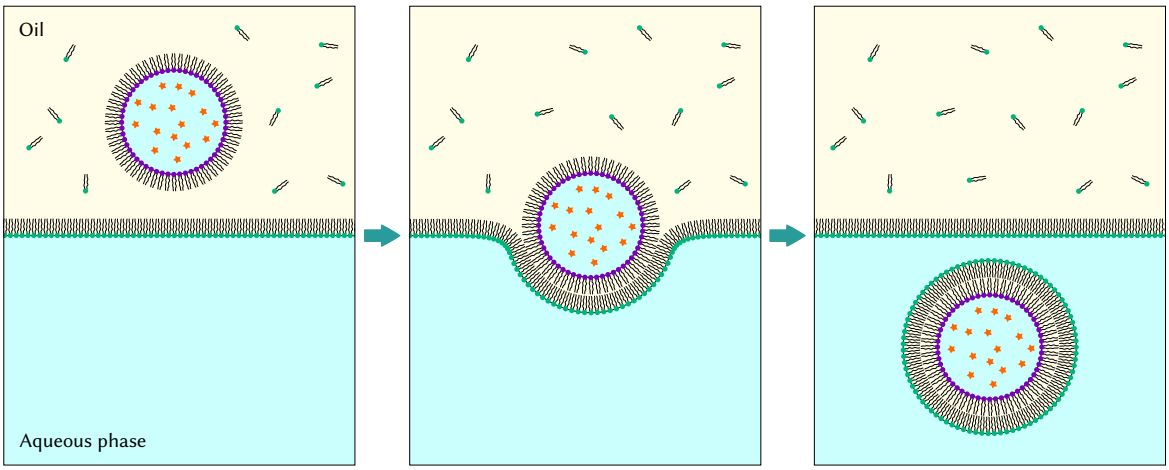


**Figure 2.35.** *Liposome preparation by the reverse emulsion method, as presented in reference [111].*

whose size depends on the rate of surfactant removal (see figure 2.34). Various surfactants have been used, from ionic ones (sodium cholate, CTAC), known to denaturate proteins, to gentler non-ionic ones (Triton X-100, octyl-β-D-glucopyranoside, C12E8) [110]. The surfactant is removed either by dialysis or using adsorbing beads.

The preparation conditions are compatible with protein manipulation, but this technique suffers from the same drawback as the film hydration method. The encapsulation yield is low and limited to the volume fraction during vesicle formation, which makes it less suitable for our application.

### 2.4.3. Reverse emulsion method

In this procedure, the aqueous solution to encapsulate is emulsified in an oil using phospholipids as stabilizers. Aqueous droplets are transferred from oil to water by centrifugation,

which allows to encapsulate most of the initial emulsified solution. This process is illustrated on figure 2.35. 60 % of encapsulation yield are reached with this technique [111]. Higher yields (98 %) are reported, using a surfactant as costabilizer during the emulsification phase [112]. Sonication, which may affect protein activity, can be replaced by a microfluidic-based emulsification procedure [113], but leads to larger vesicles. This technique may be used to process proteins.

### 2.4.4. Other procedures

The *solvent injection method* is a commonly reported method. It relies on the injection of a lipid solution in an organic solvent miscible to water (ethanol, ether) into the aqueous solution to entrap [114]. The *reverse phase evaporation method* is also a common preparation procedure. The lipid is dissolved in an organic solvent immiscible to water. This solution is emulsified into the aqueous phase to encapsulate. The liposomes are obtained after evaporating the organic solvent. High encapsulation yields of 65 % can be reached through this technique [115]. Less common techniques, relying on heating a solution of lipids in a mixture of water/glycerol to 60–120 °C, or using supercritical fluids with organic solvents are also reported [116].

All these techniques rely either on heating the protein solution or the use of organic solvents in the contact to the protein. None are not compatible with the encapsulation of proteins and will not be developed further. More details are available in references [63, 65, 107, 116, 117].

## 2.5. Summary on light-sensitive vesicles

### 2.5.1. Release mechanisms and associated timescales

In this chapter, we presented light-sensitive liposomes with various release properties. Concerning the release time, a broad range is covered and ranges from the microsecond to several hours. We are interested in *fast* releasing systems, with a characteristic time below the second. Only two systems amongst the reported ones reach this criterion: the first one is based on the permeabilization of the membrane and the other one on the disruption of the membrane.

The first system family relies on the increase of permeability of the lipid bilayer. It is possible to release small hydrophilic molecules, but nothing has been shown on the release of proteins. In fact, they may not be able to cross the membrane at all, due to their size, their ionization state and their hydrophilicity. Slightly hydrophobic molecules have been reported to stay stuck in the lipid bilayer. Therefore, this system is not adequate to the release of proteins. For these objects to escape, nanometer sized holes must be created in the lipid bilayer.

The second system family relies on a physical disruption of the membrane, which leads to release of the entrapped content regardless of its molecular weight. This method has successfully been applied to the release of active proteins in a cell culture medium. However, the *fast* release relies on high-power laser irradiation. Several configurations have been reported to this aim: either bare liposomes irradiated with pulsed UV light or liposomes sensitized with dyes or nanoparticles. The mechanism of release is not always specified, but the temperature elevation induced by the laser irradiation is predominant. Specific lipids formulations – in particular the ones containing lysolipids – have been developed to respond violently to a slight increase of temperature. In fact, the vesicles can be completely tight at 37 ℃, but made permeable and released their content above 41 ℃. The increase of temperature is thus neither harmful for the cells, if it ever reach them, nor to the encapsulated material. Coupled to a dye or light-absorbing nanoparticles, these vesicles can be used for a fast light-triggered release of proteins. One precaution should be taken when used dye-sensitized liposomes, in particular with the ones inserted inside the lipid bilayer. As cells and liposomes are similar by their membrane composition, the dyes can also attach to the cell membrane; depending on the dye concentration, this may perturb or even kill the cell.

### 2.5.2. Liposome size

As shown throughout this review, liposomes of various sizes can be obtained, roughly from 10 nm to 10 µm. In our case, the culture medium will limit the maximum size we can use. The collagen gel in which the cells are cultured has a mesh size in the range of 10 µm [118]. To ensure the free diffusion of the vesicles in the gel, their diameter must be significantly smaller than the size of the mesh: 1 µm is the upper limit.

### 2.5.3. Yield of encapsulation

The last point of this discussion is the yield of encapsulation for these systems. As mentioned before, proteins used for cell stimulation are often valuable/fragile products. The losses during encapsulation must be as small as possible, which is offered by the reverse emulsion technique. The encapsulation conditions must also preserve protein activity, and this is abided by the same technique.

To conclude, lipid vesicles are a serious candidate for drug encapsulation and release.

# 3. Micro- and nanometer-sized hydrogels

The second candidate for protein release in cell culture media are micro- or nanometric sized hydrogels, referred to as *nanogels* in this document. These systems are constituted of a hydrophilic polymer matrix entrapping an aqueous buffer and the molecules of interest. As the major constituting part of those gels is water, the conditions are adequate for the entrapment of peptides and proteins. Three main mechanisms of release are reported in the literature for the release of molecules: passive diffusion, gel destruction and gel collapse (see figure 3.1). Passive diffusion will not be considered here, as it opposes to triggered release. It must be avoided and can be if the mesh size of the gel network is smaller than the size of the entrapped proteins. Entrapped molecules can be released from this tight network by breaking the gel apart. Similarly, stimuli-induced gel collapse leads to the expulsion of the entrapped content. This is presumably due to a fracturing of the network during the shape/volume transitions.

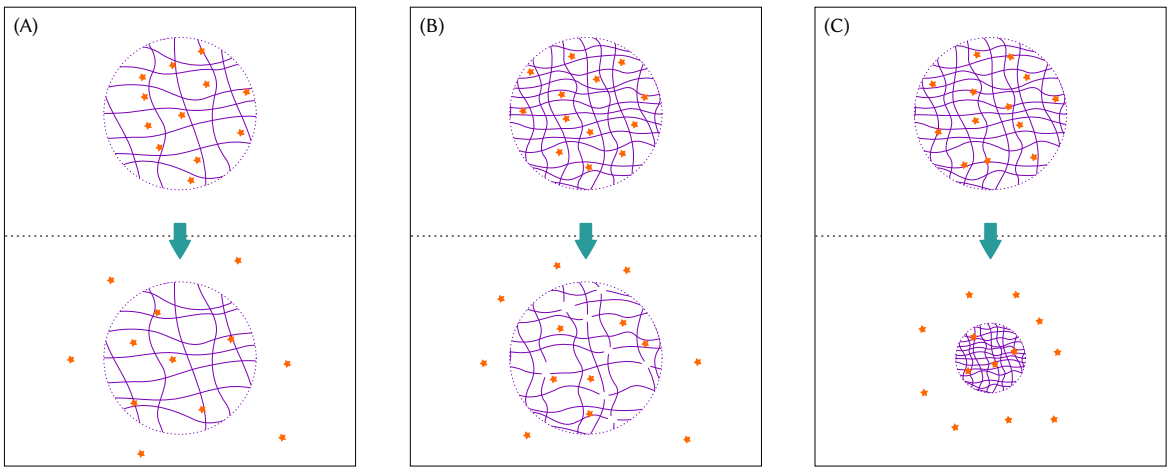


**Figure 3.1.** *Mechanisms of release from a hydrogel which will be developed in this part. (A): passive diffusion through the gel meshes. (B): release triggered by gel disruption. (C): gel collapse.*

The light-sensitive systems based on the creation of reactive oxygen species (ROS) or radicals have deliberately been excluded from the review below. Even generated locally, e.g. with light irradiation, they can diffuse and cause damages to the cells, either as oxygen species or secondary radicals. The targeted structures include the unsaturated phospholipids,

the proteins, enzyme cofactors and DNA. They may even lead to the death of the cell [119, 120].

## 3.1. Photodegradable hydrogels

### Photocleavable hydrogels

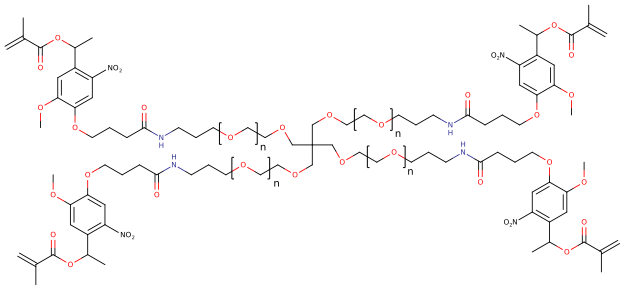

**Figure 3.2.** *Photodegradable crosslinker used to build light-degradable hydrogels (n = 28). From references [121, 122].*

PEG-based bulk hydrogels have been specifically designed to encapsulate proteins, as reported in reference [121]. The so-called *PARCEL* system was built from the monomer shown on figure 3.2; this acrylamide-derivative is polymerized by radical polymerization in water in the presence of the proteins of interest. Several proteases (chymotrypsin, elastase) have been successfully entrapped in the gel. In the gel, the proteases showed no activity towards external proteins, and low activity towards themselves. The activity was regained by releasing the proteins upon UV irradiation (365 nm, 20 mW/cm², see figure 3.3). Several monomers have been developed, all based on the same light-sensitive orthonitrophenyl moiety. The smaller ones have been proposed to prevent protein escape by diffusion [123]; polymerized, they give a gel whose mesh size is 3.6 nm (calculated). *NanoPARCEL* is a version of the gels synthesized as small particles in the 150 nm range, built only from the "linker" shown on figure 3.2. This allows their dispersion in culture media [122, 124]. The gels are prepared by radical polymerization between the acrylamide-based monomers and ammonium persulfate in an aqueous medium, under agitation; this was sufficient to obtain monodisperse nanogel suspensions. The size of the nanogels depends on the amount of initiator introduced. As before, various proteases were successfully entrapped in these gels – trypsin, chymotrypsin, thermolysin, papain, caspase and elastase – by adding them to the reaction mixture before the polymerization. They were released from the particles also by continuous UV light irradiation (365 nm, 20 mW/cm², 10 s), but no information on the efficiency of release nor on the gel hydrolysis have been given. The activity of the released protein, here caspase, is assessed by a biological test, as its release inside the cell leads to

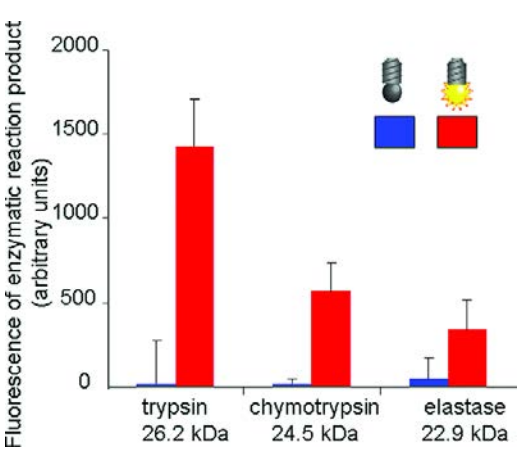


**Figure 3.3.** *Reprinted from reference [123]. Activity of gel-encapsulated enzymes, before (in blue) and after (in red) irradiation (365 nm, 20 mW/cm², 1–4.5 minutes).*

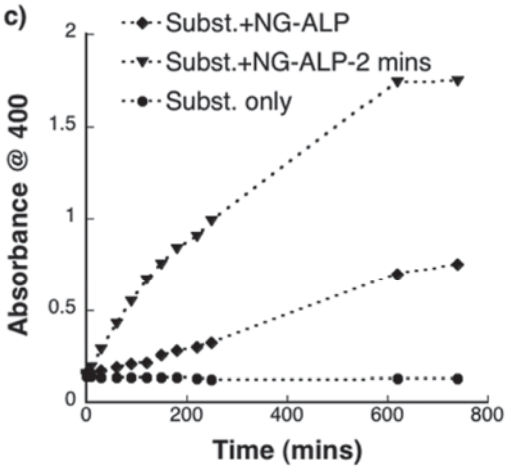


**Figure 3.4.** *Reprinted from reference [125]. Absorbance of para-nitrophenyl, a product of the degradation of para-nitrophenyl phosphate by the phosphatase entrapped in the nanogel. ●: substrate only (para-nitrophenyl phosphate); ◆: substrate + enzyme loaded nanogel, without irradiation; ▼: same as before, with 2 minutes UV light irradiation.*

the cell death. These particles are internalized in cells and irradiated with UV light, leading to the death of the cell within 10 minutes.

A similar system has been designed by Anseth et al. [125]. It differs from the previous one by the synthesis method, as the gels are prepared by radical polymerization in an inverse emulsion. Alkaline phosphatase has been encapsulated in these objects. While the encapsulation yield has not been characterized, it is suspected to be higher in this case than in the previous one, due to the preparation method. The release was triggered by UV light irradiation (365 nm, 10 mW/cm²) and monitored by following the activity of the released phosphatase on paranitrophenyl phosphate (see figure 3.4). The obtained curve is a superimposition of the kinetics of release and the kinetics of the enzymatic degradation of the para-nitrophenyl phosphate. The same absorbance curve plotted for the free enzyme attains a plateau in 200 seconds. For the released enzyme the plateau is obtained in 600 seconds, which means that the characteristic time of release is in the timescale of a few hundred of seconds.

In reference [126], hyaluronic acid is grafted with an orthonitrophenyl derivative. In aqueous media, the chains self-assemble into nanogels with an hydrophobic core made of the orthonitrophenyl moieties. Doxorubicin was entrapped in the hydrophobic core of the nanogels, in its basic (hydrophobic) form. Continuous UV light irradiation (365 nm, 1.5 mW/cm², 30 minutes) doubles the rate of doxorubicin release. The associated release time is in the timescale of the hour.

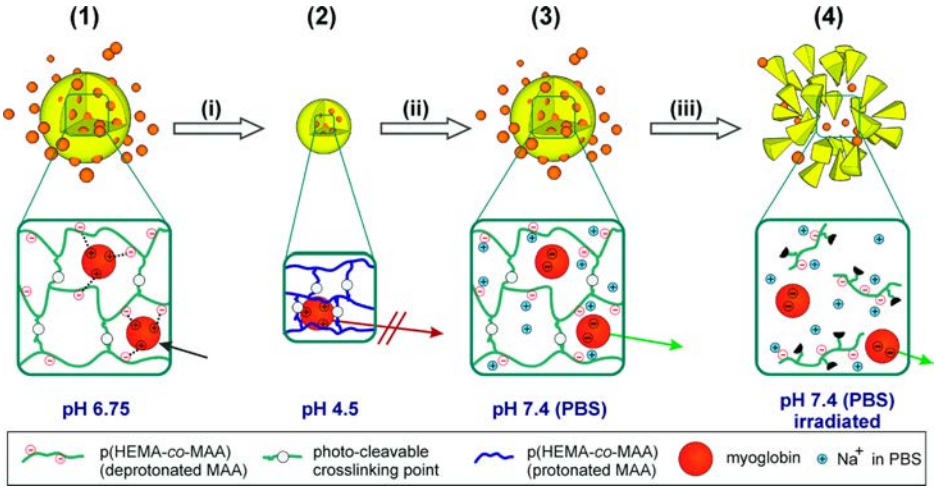


**Figure 3.5.** *Reprinted from reference [127]. Schematic illustration of the loading and release strategy for p(HEMA-co-MAA) microgels. (1–2) Loading of large cationic functional compounds into the anionic gel: (i) entrapment by pH-induced deswelling. (3) Diffusion controlled release: (ii) reswelling in PBS. (4) Degradation controlled release: (iii) irradiation in PBS.*

One protein – the myoglobin – has been entrapped in nanogels made of 2-hydroexyethyl methacrylate (HEMA) and metacrylic acid (MAA) copolymers, crosslinked with orthonitrobenzyl ester based molecules (see figure 3.5). The nanogels are prepared in reverse emulsion; the monomers in the aqueous phase are polymerized by radical polymerization. The protein, cationic, is retained in the gel by electrostatic interactions. A high loading efficiency is expected; a value of 53.2 % is reported. Loading occurs at pH 6.75, where the carboxylic acids of the gel are ionized. When the pH is lowered, these acid functions protonates and makes the gel to collapse, preventing the protein to escape. In a physiological buffer (pH, salinity), the protein is spontaneously release by a reswelling of the gel and a screening of the electrostatic interactions by the salts. 40 % of the loaded proteins are released in the timescale of 3 hours, but only 60 % are reached after 26 hours. The protein still in the gel can be released with UV irradiation to yield 100 % (1.5 hours or irradiation, $\lambda = 315–390$ nm) [127].

Dextran-polyacrylamide gels are also reported [128]. Acrylate based monomers – containing a light-sensitive orthonitrophenyl ester – are grafted on dextran chains. These chains are cross-linked by radical polymerization in reverse emulsion; the size of the obtained nanogel depends on the size of the initial emulsion. These gels are light and dextranase sensitive, but no encapsulation and release tests have been performed yet. With a turbidity-based measurement, it has been reported that these gels are destroyed in the timescale of one minute under continuous UV light irradiation (365 nm, 30 mW/cm$^2$).

Some other applications for these gels includes light-control of cell gel culture [129] and on-demand light-triggered cell-release [130].

All the examples reported in this section are based on the same photocleavable molecule (see figure 3.6), probably because it is commercially available and has decent light-sensitive

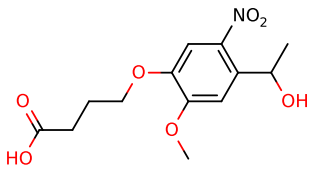


**Figure 3.6.** *Photocleavable orthonitrobenzyl-based group, developed and patented by C. P. Holmes (see reference [131]). This molecule is available from various commercial sources.*

properties[1]. The molar extinction coefficient ($\varepsilon$) of this molecule at 350 nm is 5,400 L/mol/cm in water:methanol 90:10 % vol and is reported to have an hydrolysis constant ($k$) of $3.3{\cdot}10^{-4}\,s^{-1}$ under UV light irradiation [137]. However, no mention of its quantum yield of photolysis ($\Phi$) could be found. It should be comparable to molecules of the same class though (methoxy substituted orthonitrophenyl esters); their quantum yield is often high, in the range of 0.2 [132]. This molecule is characterized by a low extinction coefficient, but is counterbalanced by a high quantum yield of photolysis – the photolysis efficiency of photocleavable molecules can be compared using the product $\varepsilon \cdot \Phi$ [138]; this value is proportional to the amount of release. For this molecule, $\varepsilon \cdot \Phi$ = 1,080 L/mol/cm; this is relatively low, molecules with a $\varepsilon \cdot \Phi$ 10 times higher are described [132]. This would allow the same result with a 10 times lower irradiation. However, this increase of photolysis efficiency is done at the expense of a 10 times higher molar extinction coefficient. This means that at a constant amount of photocleavable links, the gels will absorb more the light. For the only gel whose mesh size is reported – 3.6 nm, ref [123] – the concentration of photocleavable molecules in the bulk gel can be estimated from the structure of the gel: approximatively 2 nitrobenzyl ester can be counter per 3D gel mesh. This gives a concentration in the order of $2/((3.6 \cdot 10^{-9})^3 \cdot \mathcal{N}_A) \sim 70$ mmol/L. Dispersed as nanogels at a reasonable volume fraction of 0.1 % in a culture gel of 2 millimeter high, the absorbance is already $\sim 0.8$. This means that the irradiation with light will not be homogeneous through the gel.

To improve the kinetics of release without modifying the structure of the gel, the photocleavable dye must be replaced by one with the following properties. Its molar extinction coefficient must be low – in the order of 5,000 L/mol/cm – to allow the light to penetrate the gel. Its quantum yield must be as high as possible, to rely on the lowest irradiation power. And finally its photolysis kinetics must be faster than the one reported for the nitrobenzyl group. The first two points do not leave a lot of room for improvement, but "faster" systems can easily be found in the literature, at the expense of a lower quantum yield. In reference [139] is described a set of nitrophenyl-based molecules whose photocleavage rate depends only on the intensity of light ($k \propto I_0$, where $I_0$ in the intensity of incident light). Contrary to the previously reported system, the molecule is directly cleaved upon irradiation, without going to intermediate states – these intermediate states are often the limiting ones, and are probably responsible for the slow time reported before.

[1] For reviews on photocleavable groups, refer to references [132–136].

### Azobenzene-based dissassemblies

As reported in the part about liposomes, azobenzene can be used to build light-sensitive assemblies. The β-cyclodextrine/azobenzene host/guest association has been used as crosslinks of a PEG-based hydrogel [140]. The polymer self-assembled into 250 nm sized microgels, which are also covalently crosslinked. The host/guest crosslinks are destroyed upon UV light irradiation (365 nm), which allows the gel to swell, without destruction due to the covalent crosslinking. A blue light irradiation (450 nm) allows the gel to shrink again. No encapsulation/release tests are reported with this system yet.

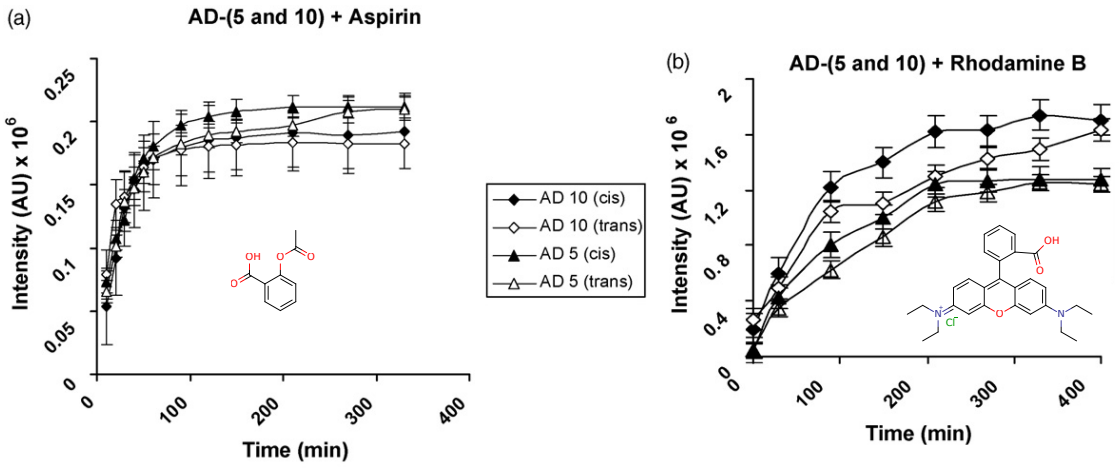


**Figure 3.7.** *Adapted from reference [141]. Azobenzene-crosslinked dextran nanogels, loaded either with (a) aspirin or (b) rhodamine B. "trans" means that the sample has been kept into the dark, while "cis" means that it has been irradiated with UV light continuously (365 nm).*

Dextran hydrogels have also been crosslinked with azobenzene, relying on the self aggregation of this molecule in its trans conformation. 200 nm sized particles, loaded with aspirin or rhodamine B, release their content with UV light irradiation (365 nm). The release rate is in the timescale of 2 hours [141].

### Photo-polymerization/-depolymerization

Coumarin is another member of the light-sensitive molecules, which goes from their initial state to another with a wavelength and comes back to the initial one with another (see figure 3.8. Linked to polymers, they act as photodegradable cross-linking agents. They have been introduced in hydrogels, as reported in reference [142]; this system is shown on figure 3.9. Briefly, a copolymer made of a PEG block and a coumarin functionalized polyNIPAM block is self-assembled into micelle above polyNIPAM LCST. The micelles are crosslinked with UV light (310 nm), thanks to the coumarins, and are turned into nanogels by lowering the temperature below the LCST. A further UV irradiation (260 nm) breaks the coumarin dimers and allows the gel to swell, releasing the entrapped molecules. Here,

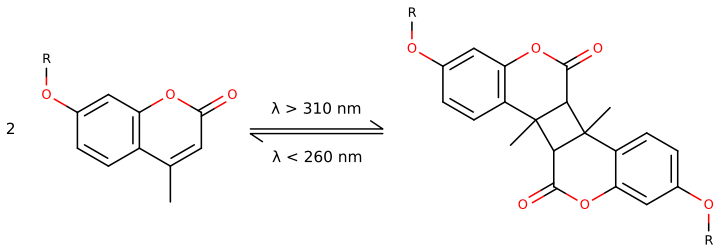


**Figure 3.8.** *Light-induced (UV) coumarin dimerization. The process is reversible upon irradiation with UV of shorter wavelength. From reference [142].*

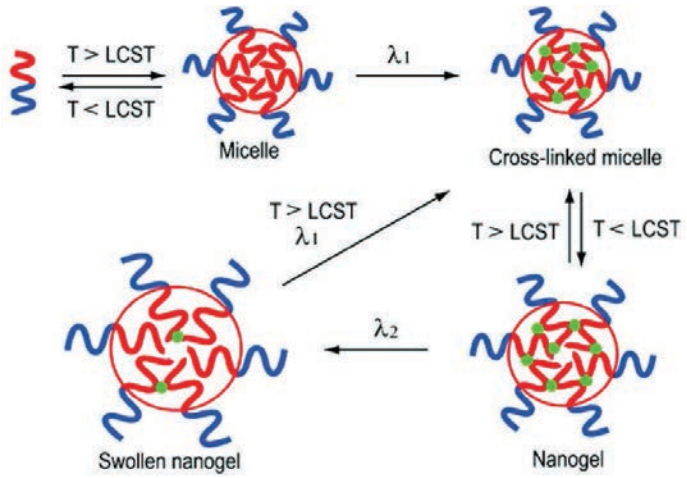


**Figure 3.9.** *Block-copolymer assembled into light-sensitive hydrogels. The blue part is made of PEG and the red one of polyNIPAM functionalized with coumarins. Reprinted from [142].*

dipyridamole (504 g/mol) is released, but light stimulation only leads to a 1.5 increase in release kinetics compared to non-stimulated gels.

### 3.1.1. Nucleid-acid based hydrogels

Recently a hydrogel encapsulation system made of plasmids crosslinked with ethylene glycol diglycidyl ether (EDGE, a di-epoxide) was reported. The gel self-disassembles upon blue light irradiation (400 nm, unknown power), which releases both entrapped material and the plasmid itself. The mesh size of the system has been characterized experimentally and is in the range of 30–40 Å. The release of the plasmid occurs within 500 hours, with the entrapped material, such as BSA, lysozyme or FITC-dextran (77 kg/mol). The timescales associated with the release depends on the entrapped molecules 200 hours are reported for BSA and dextran, while 48 hours are for lysozyme [143, 144]. The hydrodynamic radius of the lysozyme is ≈ 16 Å, smaller than the mesh size, while the radius of BSA is ≈ 35 Å and the one of the dextran 55 Å; this explains why the release of lysozyme is faster than the

other molecules. However, the comparison with the other systems is not obvious, as the gel particles are macroscopic (millimetric). The mechanism of degradation suggested by the authors is the self degradation of ethers in water under light irradiation. Linked to nucleic acid, the wavelength of maximum degradation efficiency is 400 nm.

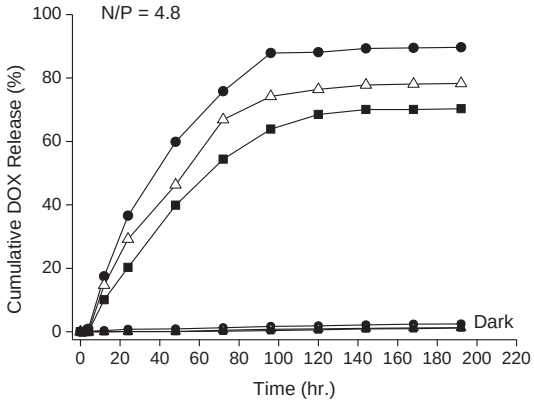


**Figure 3.10.** *Reprinted from reference [145]. Release of doxorubicin from plasmid nanogels crosslinked with EDGE and polyethylene imine. ●: 0.08 %, △: 0.1 %, ■: 0.15 % EDGE cross-linking.*

A slight variation of this system is shown in reference [145]. The size of the particle is reduced to the range of 500 nm to 5 µm. The plasmids are crosslinked both with EDGE and a diamine. While EDGE-based crosslinks can be destroyed with light, the diamine-based ones are permanent. The synthesized particles do not dissolve upon light irradiation, but rather swells. Several anti-cancerous drugs have been loaded in these gels, doxorubicin, epirubicin, paclitaxel, and released also with blue light (400 nm). The characteristic time associated with the release is approximatively 50 hours for these drugs (see figure 3.10).

## 3.2. Light-triggered gel collapse

### PolyNIPAM based hydrogels

PolyNIPAM is a shortening for poly(*N*-isopropyl acrylamide). This polymer in water undergoes a solubility transition when heated above a threshold temperature called the lower critical solubility temperature (LCST). Above the LCST polyNIPAM is collapsed, while below it, it swells. This phenomenon has been exploited to create temperature-sensitive hydrogels, which have been then converted to light-sensitive hydrogels.

Gold nanoparticles and infrared light have been used to this aim [146–148]. Here, a specific type of particles with a near-infrared absorbance peak is used. They are made of a gold sulfide core surrounded by a gold shell. These particles have been used to sensitize 40 nm size polyNIPAM nanoparticles loaded with methylene blue, ovalbumin or BSA. Irradiating the samples with infrared light (1,064 nm) only doubles the release rate of methylene blue or triples the one of ovalbumin or BSA (see figure 3.11); the resulting temperature in the sample

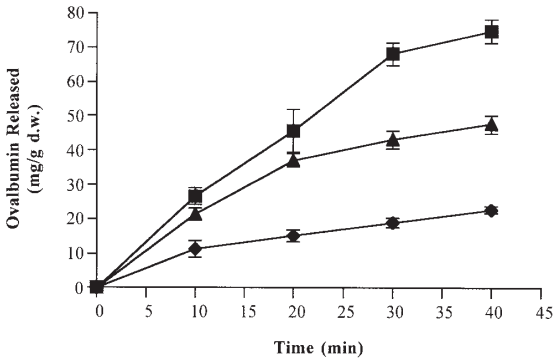


**Figure 3.11.** *Reprinted from reference [146]. polyNIPAM based gel loaded with ovalbumin. Amount of release ovalbumin as a function of time, under continuous infrared (1,064 nm, 10 Hz pulses) light irradiation. ◆: non-irradiated gels, ▲: irradiated gel without gold nanoparticles, ■: irradiated gels with nanoparticles.*

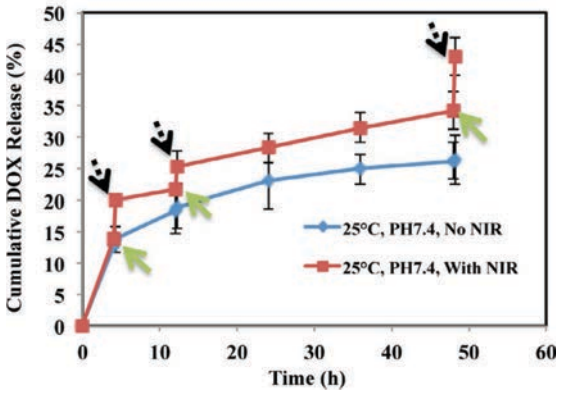


**Figure 3.12.** *Release of doxorubicin from polyNIPAM nanogel sensitized with carbon nanotubes. Blue curve: sample kept in the dark. Red curve: sample irradiated periodically (between the green and black arrow) with infrared light (808 nm).*

is unknown, but must be above 40 ℃, the LCST of the polyacrylamide used. The associated timescales are in the range of 5 minutes for the methylene blue and 30 minutes for the proteins [146]. The release relies here on a local heating of the nanogel with nanoparticles; the density of nanoparticles must be sufficient to cross the LCST of the polymer. The generation of heat is balanced by the dissipation: the smaller the particle, the higher the dissipation. This suggests the existence of a threshold of nanogel size and of density of gold nanoparticles below which the release will never occur. There is no mention of such thresholds in the presented systems, though.

Another method to convert light to heat relies on the use of carbon nanotubes. 200 nm sized nanogels were loaded with carbon nanotubes and doxorubicin. Heating the nanogels above the LCST less than doubles the released amount of doxorubicin. The associated timescale is the hour. Irradiating the sample with infrared light increased slightly the amount of released doxorubicin, compared to the sample kept in the dark (see figure 3.12). Only 40 % of the initial load of doxorubicin was released within 72 h, under IR irradiation (808 nm, 1 W/cm²) [149]. These nanogels were synthesized by radical polymerization, either in reverse emulsions [150], or in aqueous media [146].

The LCST of "raw" polyNIPAM is 32 ℃ in water, which means that under physiological conditions (37 ℃), the gel is already collapsed, and is of no use for hydrogel-based release. One solution is to tune the LCST of the polyNIPAM using additives, often introduced as co-monomers: hydrophilic ones increase the LCST, while hydrophobic ones decrease it [148]. In reference [149], hydrophilic cross-linkers have been used to increase the LCST above 37 ℃, which made the nanogels compatible with their experiments with cells.

### Other systems

The system developed in reference [151] relies on temperature-induced deprotonation of a protonated amine. The hydrogel is made of PEG and polyacrylate chains bearing protonated amine functions, decorated with gold nanoparticles. This polycationic network has the ability to retain anionic molecules, by electrostatic interactions. When the hydrogel is heated, the amines are deprotonated and the entrapped molecules can escape the gel. This phenomenon has been attributed to a dependence of the pKa to the temperature [152]. A high power green laser (514 nm, 39 W/cm²) is used to heat the sample containing 200 nm size hydrogels loaded with pyrene tetrasulfonic acid. About 25 % of the loaded amount of acid is released during 8 minutes of continuous irradiation (see figure 3.13). The high power of the laser combined with the absorbance of the particles lead to an elevation of 8 ℃ of the suspension, going from 25 ℃ to 33 ℃. Heated in a quartz cell without light irradiation, the nanogels were also able to release their content, and seems so occur since 25 ℃.

This review was essentially focused on nanometer-sized hydrogels, but a lot of light-sensitive bulk hydrogels have also been developed [153, 154]. They include azobenzene crosslinked hydrogels, azobenzene-modified LCST polymers (polyNIPAM notably), spiropyrane modified LCST polymers, orthonitro benzene or di-coumarin crosslinked networks. One notable example – the azobenzene-modified polyNIPAM – did not lead to the development of nanogels. In fact, the isomerization of azobenzene shifts the LCST by several degrees. The typical shift obtained is at most 6 ℃, which is rather restrictive for biological applications: to prevent an accidental release from such hydrogels, the temperature must be regulated precisely. This may explain the absence of azobenzene-based polyNIPAM nanogels.

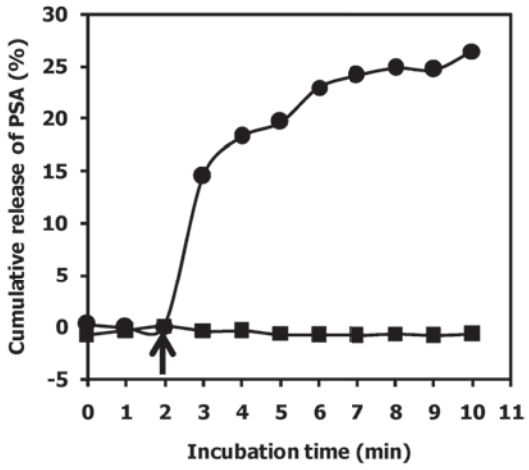


**Figure 3.13.** *Reprinted from reference [151]. Release of pyrene tetrasulfonic acid from a polycationic hydrogel, ■: in the dark and ●: under continuous irradiation (514.5 nm, 39 W/cm², starting at the black arrow).*

## 3.3. Encapsulation yield and loading constraints

### Impact of the synthesis procedure on the protein encapsulation

Several methods have been reported for the synthesis of the nanogels [155]:

**Micromolding** The monomers or the polymer chains are molded in a PDMS matrix. Particles as small as 100 nm have been reported. While it is possible to obtain arbitrary shapes with this method, the "2D" synthesis limits the throughput of the gel production.

**Reverse emulsion** The gels can be prepared from the emulsion of an aqueous phase containing the monomers and the molecule to encapsulate, dispersed in an oil phase. The size of the emulsion fixes the size of the nanogels. Several methods have been proposed to prepare the emulsion: surfactants+ultrasounds, microfluidic devices and injection of the aqueous phase in the oil through a porous membrane.

**Homogeneous polymerization** The monomers and a polymerization initiator can be dissolved in an aqueous medium. The gels will grow from a nucleation point, until the polymerization is stopped (either by lack of monomers or by losing the reactivity). The size of the gels depends on when the polymerization is stopped.

At the exception of the technique relying on ultrasounds, all of them are a priori compatible with the process of proteins.

The molecules of interest are loaded in the gel either during its synthesis or after. For the emulsion-based procedures, the protein can be added to the emulsified aqueous phase. Unless the protein is excluded from the matrix during the polymerization, high encapsulation yields are expected; the same is expected for the molding process. For the homogeneous polymerization, the protein can also be added to the reaction mixture. If no specific affinity is developed between the encapsulated molecule and the matrix, the encapsulation yield is limited by the volume fraction of the aqueous phase actually included in the matrix. If the mesh size of the gel permits it, the protein can also be entrapped in the gel after its synthesis; the role of the size mesh will be discussed further in this section.

Concerning the synthesis conditions, all the systems reported in the previous section are made by radical polymerization. Adding the protein in this step is questionable, as the protein activity can be damaged by radicals [156]. The damages are particularly important in presence of oxygen, and include protein cross-linking (via the histidine residues), protein fragmentation, protein oxidization and protein unfolding.

### Impact of the mesh size

In systems encapsulating proteins by the entrapment in a polymer matrix, the mesh size must be slammer than the encapsulated molecule to avoid the escape by passive diffusion. Yet, the real mesh size is seldom characterized. The few examples we got can be compared

to the characteristic size of a protein. First, the protein radius can roughly be derived from its molecular weight by the formula $R_{\text{min}} = 0.066 \sqrt[3]{M}$, where $R_{\text{min}}$ is its radius in nanometers and $M$ its molecular weight in g/mol [157]. The typical radius of a 50 kg/mol protein is in the range of 2.5 nm, which means that the protein is retained by both the nanoPARCEL system (3.6 nm) and the DNA based system (4 nm). To compare with usually used hydrophilic drug, the size of doxorubicin is ≈ 0.5 nm, which means that the gel is not able to retain them. For a complete off/on delivery, nanogels are therefore specific to high molecular weight molecules like proteins.

The tight entrapment of the protein has a negative impact on the kinetics of release. A complete release requires the hydrolysis of a significant amount of the light-sensitive cross-linkers, which leads to a slow release. The fastest reported system release caspase within 20 s, but the characteristic response time of the other systems is rather in the 10 minutes scale The kinetics of release can be increased both by increasing the kinetics of hydrolysis of the light-sensitive moiety, or by increasing the light intensity.

One possible solution to overcome the slow hydrolysis of the gel is proposed in reference [158]. The light-sensitive gel is used only to build the shell of the particle. The protein is no longer entrapped in the gel, but rather in the aqueous core of the particle. And the thinnest the membrane, the faster the release, while the amount of entrapped protein stays the same. As soon as a hole is poked in this membrane, all of its content can be released. The mechanism is the same as liposomes sensitized with the pore-making polymer. This kind of objects belongs to the polymer capsule family, and will be developed in the next part.

# 4. Aqueous core—polymer shell capsules

Systems made of an aqueous core surrounded by a light-sensitized polymer shell combine a priori the advantages of both liposomes – a mild aqueous medium – and the ones of gels – mainly their mechanical resistance. Though most examples in the literature do not consider protein encapsulation, they illustrate the degree of control that can be expected.

Polymer capsules can classified into three main classes, depending on their synthesis procedure. It can be done by covering a pre-formed liquid or solid core with alternating layers of polyelectrolytes with opposite charges, leading to a *layer-by-layer* capsule. Polymers – in particular amphiphilic diblock polymers – can self-assemble into vesicles, leading to objects somehow similar to liposomes, and called *polymersomes*. Finally, the polymer can also be synthesized or deposited at the water/oil interface in an emulsified system, leading to also to capsules. All these systems are schematically represented on figure 4.1.

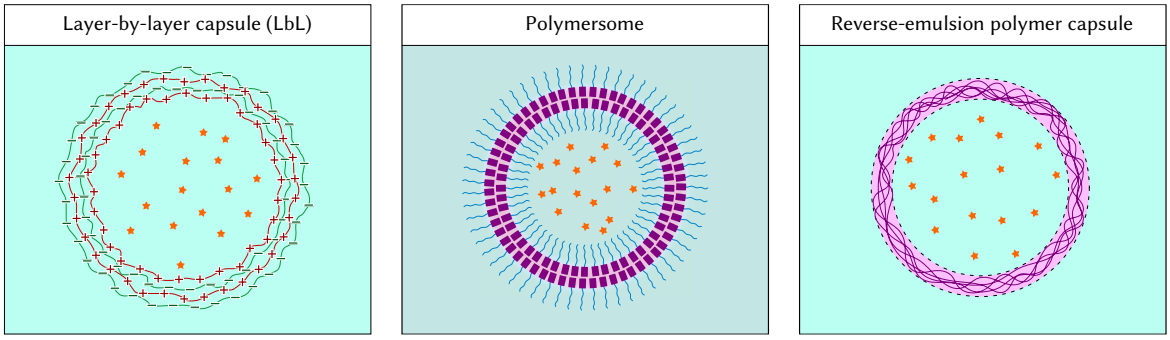


**Figure 4.1.** *Schematic view of the three classes of polymer capsules: the layer-by-layer assemblies, the polymersomes and the polymer capsules made by reverse emulsion. The hydrophilic part of the membrane is represented in blue, while the hydrophobic one is represented in purple.*

## 4.1. Layer-by-layer assemblies

### 4.1.1. System description

Layer-by-layer capsules are made from assemblies of polyelectrolytes of opposite charges created around a pre-synthesized template. This template can be a solid organic or inorganic sphere, or even a droplet in an emulsion [159]. The layers are deposited one after the other,

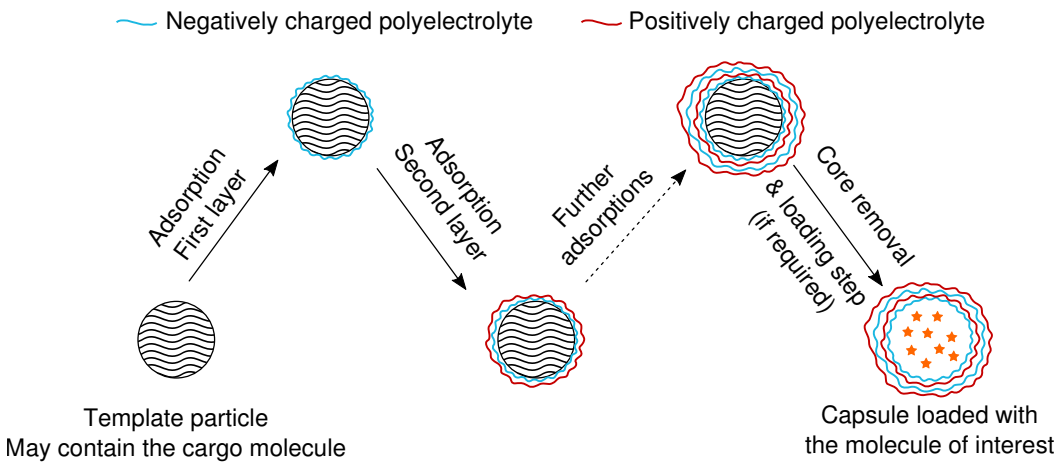


**Figure 4.2.** *Layer-by-layer capsule synthesis procedure. Adapted from reference [159].*

as shown on figure 4.2. The core template is removed by various ways, depending of the nature of the core itself. Compared to liposomes, they are claimed to be less permeable and mechanically more resistant.

### 4.1.2. Light-induced release

Two mechanisms lead to the release of entrapped molecules from LbL capsules: namely, the capsule can remain intact but its permeability increases, or the capsule can burst under a mechanical stress.

#### Photochrome-doped LbL capsules

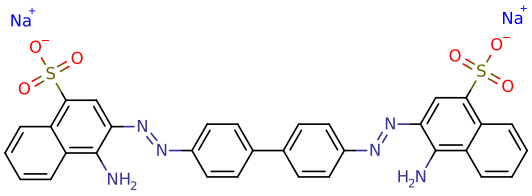

**Figure 4.3.** *Congo red, an azobenzene-containing ionized dye.*

Azobenzene has once more proven reliable to confer light sensitiveness to a drug-encapsulating object. In the system shown in reference [160], an azobenzene-based dye is added to a layer-by-layer assembly made from polystyrene sulfonate/polyamine, yielding 5 µm sized capsules. Irradiated with UV light, the dye isomerizes and perturbs locally the organization of the LbL assembly, which is made permeable. While carboxyfluorescein was not retained in the capsules, UV light irradiation ($\lambda > 400$ nm, unknown power) was

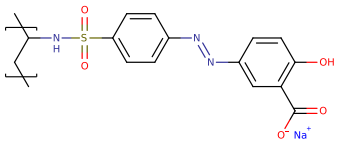

**Figure 4.4.** *Azobenzene-containing cationic polyelectrolyte. From reference [161].*

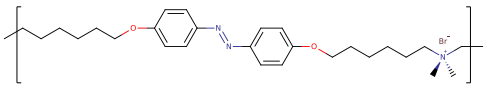

**Figure 4.5.** *Azobenzene-containing cationic polyelectrolyte. From reference [162].*

required to release dextrans. Dextrans smaller than 66 kg/mol were released within 1 hours, while a 464 kg/mol one required two hours. Bigger dextrans remained indefinitely in the capsule.

Azobenzene can also be covalently attached to one of the polyelectrolytes [161] (see figure 4.4). Both a neutral dextran (10 kg/mol) and a polyanionic one (3 kg/mol) have been loaded in polymersomes preformed with this polymer and poly(vinyl sulfonate), by passive diffusion. All were released upon UV light irradiation, which caused the capsule to shrink. Its diameter goes from ≈ 4.7 µm to ≈ 2.6 µm within 10 hours of continuous irradiation. No more precisions were available from the article. Another polymer is reported in reference [162] (see figure 4.5). 4 µm sized capsules were made with this polymer and a polyanionic carrageenan, but no release experiments were performed.

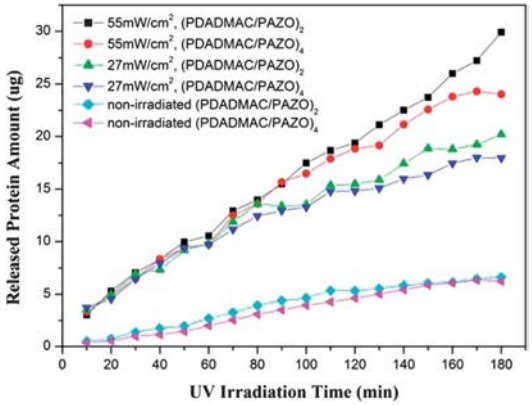


**Figure 4.6.** *Reprinted from reference [163]. UV induced release of BSA from azobenzene-based LbL capsules.*

Azobenzene has been used to induce the disruption of a LbL capsule made with the polymer shown on figure 4.4 and a poly(allyl dimethylammonium chloride) [163]. BSA was introduced in these particles by precipitating it with calcium carbonate, in the template synthesis step. After assembling the membrane, the dissolution of the core with EDTA yields free BSA stuck in 5 µm scaled capsules. A continuous UV irradiation (366 nm, 55 mW/cm²) only multiplied the release rate by a value ranging from 2.5 to 4 (see figure 4.6). 2 hours of irradiation were sufficient to break the particles, though. The limited amount of released BSA (16 % after 2 hours) is attributed by the authors to an irreversible interaction of the protein with the capsule.

### Light-induced elevation of temperature

Inorganic light-absorbing particles have also been used to break layer-by-layer assemblies. Silver nanoparticles were embedded in 2 µm capsules made of polystyrene/polyamine by synthesizing them in situ from a silver salt [164, 165]. Less than 1 second of a green laser irradiation (532 nm, 25 mW) was sufficient to break the capsule shells. The burst mechanism is based on the temperature elevation induced by the silver nanoparticles [164]. These capsules have been used to release 10 kg/mol fluorescent dextran inside living cancerous cells [166].

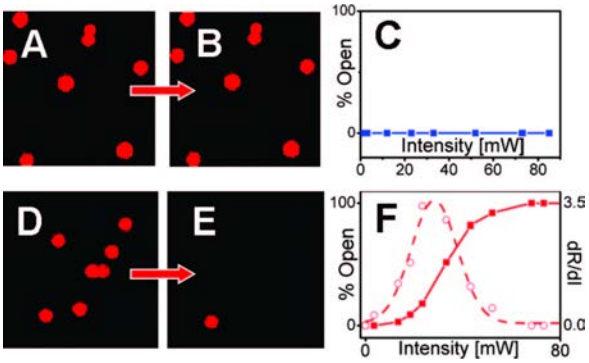


**Figure 4.7.** *Reprinted from reference [167]. LbL capsules loaded with Alexa Fluor 555 dextran. From the left to the right: confocal pictures taken before and after irradiation at 830 nm, 65 mW for 10 s; the graph represents the percentage of opened capsules after irradiation (continuous line) and its derivative (dashed line). A,B,C: LbL capsules without nanoparticles D,E,F: LbL capsules loaded with gold nanoparticles*

Gold has also been embedded in such capsules, with similar results. In reference [168], 5 µm sized capsules are used to deliver 10 kg/mol dextran into cells, upon laser irradiation (830 nm, 2.3 mW/25 µm², less than 1 second). However, it was shown that this high laser intensity, while in the infrared region, impaired the cells. This even led to cell death at higher powers (31 mW). A similar system is reported in reference [169]. Aggregates of gold nanoparticles have also been used, as this configuration improve the absorption of light, which lead to irradiations with lower intensities [167]. As the mechanism of release rely on an elevation of temperature, the capsules are loaded in their permeable state, by elevating the temperature of the buffer. Temperatures of 50–60 ℃ are reported, which is sufficient to cross the LbL glass transition temperature; this makes the membrane porous and allow the loading and the release. Fluorescent labeled dextran (10 kg/mol) has successfully been released from these capsules upon infra-red light irradiation (830 nm, 65 mW, 10 s), as shown on figure 4.7. In reference [170], lysozyme is entrapped as crystals in poly(allyl amine)/poly(styrene sulfonate) capsules, sensitized with gold nanoparticles. Lysozyme is claimed to be released upon infra-red light irradiation (1,064 nm, 50 mJ/cm²).

Layer-by-layer assemblies were also be doped with dyes. In reference [164], the membrane of 2 µm LbL capsules made from poly(allyl amine)/poly(styrene sulfonate) is loaded with an

IR absorbing dye (IR-806), and broken with a laser irradiation (830 nm, less than 1 second, 60 mW/25 $\mu m^2$).

### 4.1.3. Encapsulation yield and loading conditions

#### Synthesis of LbL capsules

Several templates are reported, both organic and inorganic ones, but most of them are incompatible with the pre-encapsulation of proteins, due to the harsh conditions used for their removal. Melamine beads are removed with hydrochloric acid at 0.1 mol/L. Polystyrene beads are also reported; their removal relies on dissolution with a water-miscible organic solvent, e.g. tetrahydrofuran. Inorganic particles have also been used for this application. Silica beads are removed with hydrofluoric acid, while calcium carbonate ones are dissolved with EDTA. The template may also not be dissolved at all, if it is porous. In this case, the molecule of interest can be loaded into the template before the synthesis of the membrane.

#### Loading conditions

The encapsulated protein or molecule can be entrapped in the template or loaded after its dissolution. As reported at the beginning of this section, the dissolution procedures are harsh and not compatible with the manipulation of proteins. Acids and organic solvents are known to denaturate proteins, and EDTA is known to inactivate enzymes with a metallic center, like the metalloproteases. Only a loading after the synthesis of the LbL assembly and the dissolution of the core is conceivable.

Up to now, only two examples of protein release using light-sensitive layer-by-layer assemblies has been found. We will however extend this discussion on large molecular weight molecules, like dextran. A first method relies on loading crystals of proteins in the capsules, in conditions preventing the crystal dissolution. This has been applied successfully to lysozyme [170], but it is limited to a small range of proteins, which are crystallizable in conditions where the layer-by-layer assembly stays either intact or permeable. The principle is interesting but not general, because only a few proteins can be crystallized properly at the low salt conditions required to assemble the LbL membrane and after replacing the encapsulation buffer by a physiological one.

The second method relies on the coprecipitation of proteins in calcium carbonate, to build the template core. They are obtained by mixing calcium chloride (330 mmol/L) and sodium carbonate (330 mmol/L). The pH of the sodium carbonate solution if above 11, which can affect the stability of the entrapped proteins, depending on how long they will stay in this solution. BSA is known to unfold irreversibly to coat hydrophobic surfaces: it may be encapsulated in a denaturated and aggregated form, which could explain the low release yield obtained (16 %) [163]. The encapsulation yield also is unknown, and is probably dependent on the affinity of the protein to the inorganic cluster. The role of EDTA, used to dissolve the core, has already been discussed.

The third method relies on temperature-sensitive capsules that can be loaded at high temperature; this temperature increase makes the membrane permeable. This has been applied to the loading of dextrans. Temperatures as high as 60 ℃ are reported, which is denaturing form several proteins. The encapsulation yield is limited by the volume fraction inside the capsules and will not be substantial, except if the inner compartment binds the protein – which is likely to slow down the release of the protein.

#### Size of the capsules

The size of the capsules reported as light-sensitive was never smaller than 1 µm. However, the size of the layer-by-layer assemblies depend on the size of the core, and can be decreased by using smaller ones: capsule ranging from 10 nanometers to several micrometers are reported [159]. The thickness of the membrane can also be tuned, by varying the number of layers deposited around the core.

#### Release rate

The faster releases are obtained by breaking the membrane. Characteristic times of 1 second are evoked, but rely on pulsed or high-power laser irradiation.

### Conclusion

Altogether, it is concluded that encapsulation is the major drawback to be solved in the case of LbL capsules, to be immediately relevant for an application to proteins, where a high encapsulation yield and a preservation of the protein activity is required. Concerning the object itself, it can be noted that light-sensitive LbL capsules are not common objects. Most of the stimuli-responsive LbL capsules reported respond either to pH, ionic strength or temperature [159, 171, 172].

As a last remark against these capsules, we may also add that the dissolution of the core can leave toxic species inside the capsules, as it has been reported with melamine [173]. If not impairing the activity of the proteins, it may affect the cell activity and should be avoided.

## 4.2. Polymersomes

### 4.2.1. System description

Polymersomes are self-assembled polymer capsules made of an aqueous core and an polymer shell containing di- or triblock amphiphilic copolymers. The polymers self-assemble into vesicles, due to the property of the hydrophobic blocs to aggregate and the balancing steric repulsion between the hydrophilic blocs that alleviate micellization. Polymersomes and liposomes share several features. However, using synthetic objects in place of lipids

allows more chemical flexibility and the possibility to build thicker membranes with several advantages regarding their stability, their permeability or their mechanical resistance [174].

## 4.2.2. Light-triggered release mechanisms

### Azobenzene-based systems

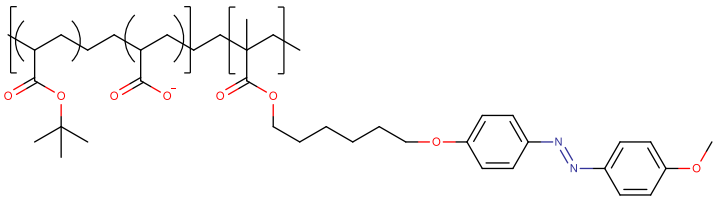

**Figure 4.8.** *Azobenzene-containing diblock polymer. The hydrophilic block is made of a acrylate/acrylic acid copolymer. The hydrophobic one is made of azobenzene pendant groups. From reference [175].*

The light-induced isomerization of azobenzenes has been exploited to build light-sensitive polymersomes. An example of a block copolymer sensitized with azobenzene moieties is shown on figure 4.8. This acrylate/acrylic acid based polymer has been used to prepare vesicles in dioxane/water (16 % vol.) mixtures, which disassemble under UV light irradiation (360 nm, 34 mW/cm²) and reassemble under blue light (440 nm, 24 mW/cm²) [175]. Adding water above 21 % vol. the polymer aggregated. No encapsulation and release experiments have been conducted with this system.

A similar polymer (see figure 4.9) was reported to make light-sensitive vesicles without organic solvents, when associated with a non-sensitive polymer [176]. It has been shown that UV irradiation (365 nm, 1 W/cm²) induced the rupture of 10 µm-sized vesicles by the

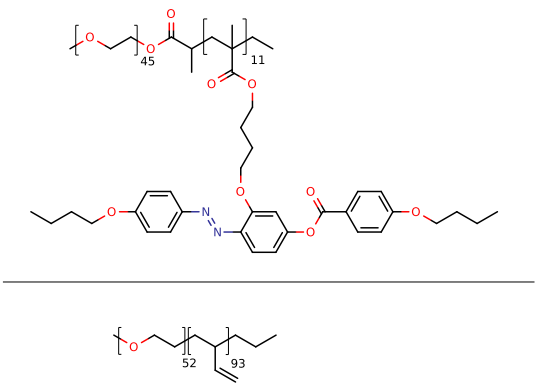

**Figure 4.9.** *Polymers used to build UV-sensitive polymersomes in reference [176].*

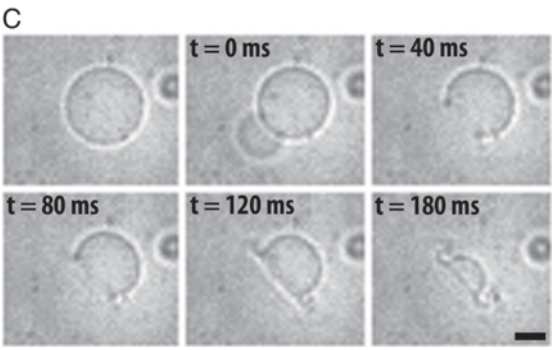


**Figure 4.10.** *Reprinted from reference [176]. Polymersome pore opening, upon UV light-irradiation.*

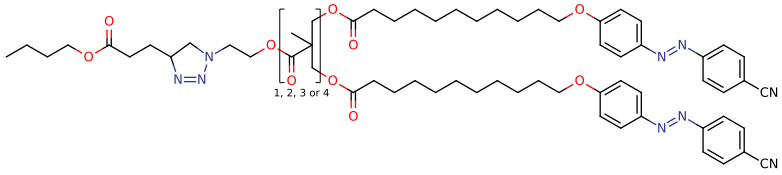


**Figure 4.11.** *Dendrimer used to build polymersomes, from reference [177].*

creation of pores (see figure 4.10). The timescale associated with the pore opening is 100 ms, but this phenomenon occurs randomly during the 5 minutes of UV irradiation.

A similar system is reported in references [177, 178], in which the linear acrylic polymer is replaced by a PEG chain connected to several azo-bearing chains to build dendrimers (see figure 4.11). The vesicles made with this polymer have been shown to break within 35 minutes of UV irradiation (365 nm, 150 mW/cm²), with no other details on the kinetics.

In all the systems reported above, the azobenzene is present in the hydrophobic part of the block copolymers. In its trans form, it is hydrophobic because its polarity is near zero. Irradiating the polymer with UV light converts the azobenzene to the cis isomer, whose polarity is significantly higher than the trans one. This destabilizes the hydrophobic assembly of the polymersome and leads to its disassembly [175].

A host/guest based system built around a synthetic supramolecular cycle and an azobenzene is reported in reference [179]. Mitoxantrone, a small hydrophilic drug, has been encapsulated in these vesicles and released with UV light irradiation (365 nm, power unknown). Irradiating the polymer with UV light yields cis azobenzene, which escapes the supramolecular cycle and disassemble the vesicle. At a physiological pH, the kinetics of release is slow: 3 hours are required to release 60 % of the entrapped drug.

### Light-induced ionization

Block copolymer have been made with spiropyrane moieties [180]. The only reported assemblies are micelles, which disassembles upon UV light irradiation. No polymersomes were reported yet, though the adjustment of the block length should favor such assemblies.

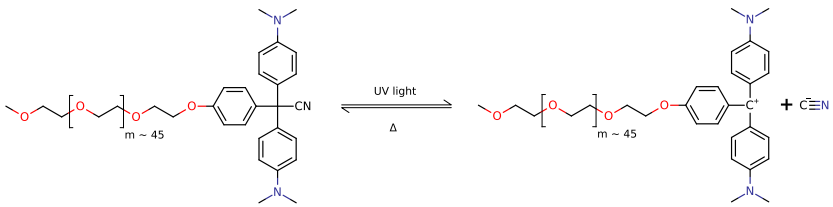


**Figure 4.12.** *Light-sensitive diblock polymer used in reference [181]. The hydrophilic part is made of poly(ethylene glycol), while the light-sensitive hydrophobic part is made of malachite green. Upon UV irradiation, the cyanide anion detaches from the triphenyl group.*

Malachite green is another example of molecule able to ionize under light irradiation. The reverse process occurs spontaneously by thermal relaxation. PEG polymers ended with malachite green, shown on figure 4.12, have been used to build 100 nm vesicles [181]. They disassemble within 500 s of UV light irradiation (Hg lamp, 900 mW/cm²), and reform themselves spontaneously when kept in the dark. No precise kinetics of disassembly or release have been performed.

### Photocleavable chains

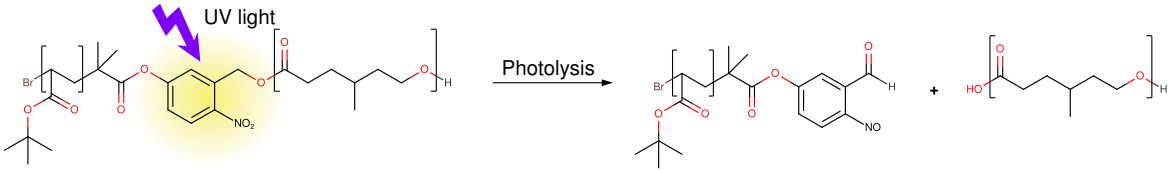


**Figure 4.13.** *Light-induced photolysis of a diblock polymer. UV light is absorbed by the orthonitrobenzene group, highlighted in yellow. From reference [182].*

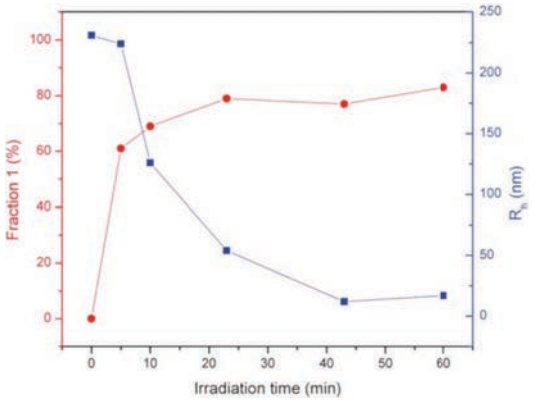


**Figure 4.14.** *Reprinted from reference [183]. Release of eGFP from light-cleavable polymersomes (●) and evolution of the diameter of the objects in the sample (■) upon UV light irradiation (365 nm, 200 mW/cm², 10 min).*

Orthonitobenzyl esters have been used to link the blocs of diblock polymers, as shown on figure 4.13. These polymers have been assembled in 70 nm sized vesicles loaded with various molecules including a protein (fluorescein, ATTO665 and eGPF). The encapsulation efficiency of eGFP have been evaluated to 22 %. Irradiating these vesicles with UV light (365 nm, 700 mW/cm²) triggers the lysis of the orthonitrobenzyl ester moieties, leading to the breaking of the chains, as shown on figure 4.13. The characteristic release time of vesicle lysis has been evaluated to 30 minutes by DLS measurements. 10 minutes irradiation at 200 mW/cm² are sufficient to release the entrapped eGFP (see figure 4.14), while 1 hour was required to release only 60 % of the fluorescein, suggesting that this small dye interacts

with the polymers [182, 183]. Encapsulation and release of biocytin in similar systems is also reported [184]. The release occurred within 6 hours of UV light exposure (365 nm, 55 mW/cm²). One strategy brought up in reference [185] to increase the kinetics of release relies on adding multiple orthonitrobenzyl ester groups per polymer chain. It has been only proved with micelles, though.

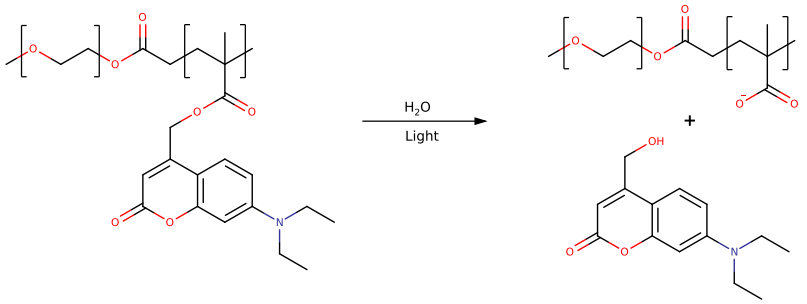


**Figure 4.15.** *Diblock polymer, made of PEG and coumarin-bearing methacrylate. Upon light-irradiation (UV or IR 2 hv), the coumarin ester bond hydrolyses to let place to methacrylic acid, turning the hydrophobic block in an hydrophilic block. Developed in reference [186].*

Coumarins groups can also be hydrolyzed by light irradiation. In the system reported in reference [186], they are introduced along the hydrophobic chain, as shown on figure 4.15 and assembled into micelles. UV light (365 nm) or IR (2 photons, 794 nm) turned the hydrophobic core in an hydrophilic one, by the creation of a poly(methacrylic acid). The micelles were broken in the timescale of 2 hours. No vesicles were reported with this polymer.

### Light-induced local heating

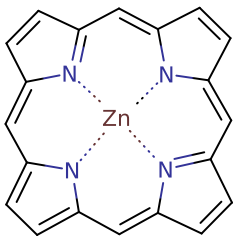


**Figure 4.16.** *A porphyrin complexing a zinc ion.*

Porphyrines are macrocycles made of four pyrrole units, as shown on figure 4.16. Loaded with ferritin in polymersomes made of PEG-b-polybutadiene block copolymer, the polymersomes become sensitive to UV light (365 nm). Only a small amount (25 to 50 %) of the entrapped biocityn is released after 4 hours of continuous irradiation [187]. The release

relies on the presence of ferritin, but it can be replaced by dextran for the same effect [188]. The mechanism involved here is a local heating due to the absorption of light by the porphyrin. The protein is suspected to adsorb on the inner membrane and cause a differential stiffening of the leaflets, leading to budding and subsequently leading to the release of the entrapped content [187].

Capsules sensitized with gold nanoparticles were reported in reference [189]. They were inserted in the hydrophobic layer of vesicles made from poly(L-lactic co glycolic acid)/polyNIPAM. These particles, irradiated with visible light (488, 532 and 633 nm), made the polyNIPAM chains collapse and destroyed the vesicles in the timescale of the minute. No specific release experiment was performed.

### 4.2.3. Preparation conditions and encapsulation yield

Several techniques are reported, enabling to control the size of the polymersomes and the encapsulation yield[1]. Some techniques are based on organic solvents. One of the most reported method relies on dissolving the polymer in an organic solvent. The aqueous solution to encapsulate is added dropwisely to the organic solvent, yielding vesicles whose size is in the 100 nm – 3 µm range. Details on the other techniques are available in references [190–192]. Not compatible with the handling of proteins, they will not be discussed here.

The lipids can be dissolved in a volatile solvent and made to dry on a flat surface to make a polymer film [190]. Upon hydration, vesicles in the 50 – 800 nm range are formed; monodisperse objects of a defined diameter can be obtained by extrusion through a filter. The size of the filter pores defines the size of the obtained polymersomes. Electroformation applied to the polymer film will lead to micrometer-sized polymersomes. However, low encapsulation yields are expected. Similar to the techniques used for the preparation of liposomes, yields in the 10 % range are expected.

Several case of self-assembly of the polymer directly in the aqueous medium are reported. In the specific case of the formation of the vesicle via host/guest associations, encapsulation yields as high as 76 % for the MTZ drug have been reported [179].

The reverse emulsion method – similar to the scheme shown on figure 2.35 page 36 – can be used to process the block copolymers. 10 µm vesicles have been obtained with this method [176]. Transposed to microfluidic devices, larger vesicles can be made; 200 µm objects are reported [189]. The encapsulation yield is expected to be high, as most of the aqueous phase containing the molecule of interest will be entrapped in a vesicle.

All the solvent-less process reported above are compatible with the processing of proteins. Concerning the encapsulation yield, the results obtained with the liposomes suggests that is should be the most efficient method. This technique is compatible with the process of proteins, and meets the requirements of encapsulation yield.

[1] The thickness of the membrane depends on the molecular weight of the chains [174].

### Conclusion

Light-sensitive polymersomes are a potential candidate for the release of fragile molecules in a cell culture medium. However, the characteristic release time of the reported systems is in the timescale of 10 minutes, which is slow. One system shows fast openings of pore (100 ms), but this event was not predictable and occurred randomly within the 5 minutes of irradiation. This makes the polymersomes to respond slowly on average,

Finally, it should not be surprising to observe a slow release rate from polymersomes, because their membrane is more stable than the one of liposomes. They are probably not the good choice for our application, due to the kinetics of release.

## 4.3. Capsules made of solid polymers

### 4.3.1. Polystyrene capsules

Commercial polystyrene-acrylic based capsules have been loaded with carbachol (a small hydrophilic molecule) or fluorescein, by swelling the dry particles with a mixture of propanol/chloroform/ammonia containing the molecule of interest. These capsules were manipulated using optical tweezers, allowing to position them precisely in a culture medium. They are broken with a high-power laser pulse (337 nm, 1 ns, 0.25 µJ) centered on the 1 µm sized capsule. The release of the entrapped molecules occurs almost instantly: fluorescein escapes the capsule in the timescale in the timescale of 100 ms. Cell experiments have also been conducted with this system: carbachol released near a CHO cell was responsible for the increase of calcium concentration inside the cell [45]. The mechanism underlying the capsule rupture is not known yet, but may include light pressure, plasma generation of photolysis [193].

Concerning the usefulness of these systems to protein release, it seems somehow compromised. Loading these objects in the propanol/chloroform/ammonia mixture will surely lead to the protein denaturation.

### 4.3.2. Capsules made by the reverse emulsion technique

#### Synthesis conditions and encapsulation efficiency

To obtain capsules with an aqueous core, the synthesis relies on creating a highly insoluble polymer shell around drops in an inverse emulsion (see figure 4.17). The aqueous phase dispersed in the oil phase contains the molecule of interest and one reactant, which alleviate the loading step. The oil contains a second one of the reactant, leading to the formation of the polymer shell upon contact between the two phases – e.g. by polyaddition. The choice of the oil is crucial: the synthesized polymer must not be soluble in it, but the monomeric reactant has to be well dispersed in it. Depending of the conditions, in particular the concentration of both reactants, capsules or particles can be obtained with this procedure [194].

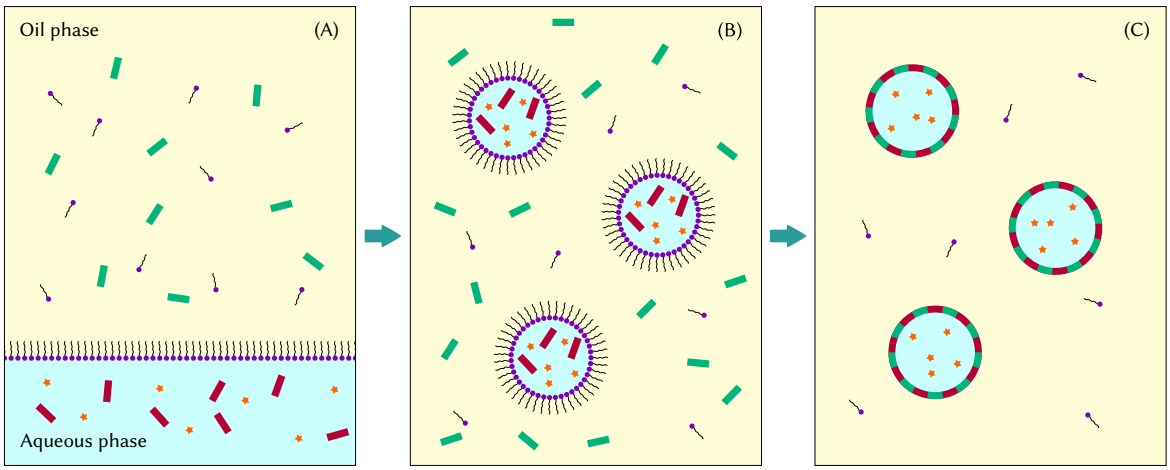


**Figure 4.17.** *Preparation of polymer capsules with an aqueous core by the reverse emulsion method. (A): the aqueous phase, containing the molecule to encapsulate (the orange stars) and a reactant (the red rectangles) is made to contact of the oil phase, containing a stabilizer (the purple circle with a tail) and another reactant (the green rectangles). (B): the system in (A) is emulsified to give (B), where the water phase is dispersed in the oil phase. (C): the reactant in the oil phase reacts with the one in the aqueous phase at the water/oil interface, to give a polymer shell.*

A mild method used to disperse water phase in oil phase is based on a nano-emulsion technique. Ultrasounds [194] or phase inversion temperature processes [195] are also reported. In all cases, emulsion breaking is prevented by adding non-ionic surfactants in the oil phase. The use of block copolymers leads to capsules in the range of 100 nm [196–198].

A typical system reported in the literature is based on the interfacial polyaddition between an oil-soluble diisocyanate and a water soluble diol or diamine, leading respectively to polycarbamates or polyureas. The reactivity of amines is high enough to perform the reaction at room temperature – low reactivity of alcools requires heating to 60 ℃ [194, 199].

Once they have been synthesized in the continuous oil phase, the capsules must be transfered into water. Several methods of transfer from the oil to water are reported in the literature, and rely on the volatility of the oil (cyclohexane, hexane). The suspension of capsules in the oil is basically re-emulsified in an excess of water. The oil is removed by heating the suspension [196], or at room-temperature under stirring [200] or in an ultrasonic bath [197]. One example of oil removal by freeze-drying has been reported. This attempt was unsuccessful though, as the dried capsules stuck irreversibly, leading to aggregates in dispersed in the aqueous medium [194].

The encapsulation yield has been characterized using a fluorescent dye (sulforhodamine 101). A value of 90 % is reported [199].

This synthesis procedure is somehow versatile, as it can be “reversed” to produce oil-containing capsules suspended in water [201], or even capsules filled with a mixture of non-aqueous polar liquids suspended in an oil [202]. Various “monomers” have been reported to build the capsules. They range from simple $C_6$ diols [194] to polyols like glycerol [197] or even biosourced polymers like starch [196, 203], dextran [194, 197] or

lignin [204]. Simple $C_6$ diamines, arginine [194], diethylenetriamine [197] can be added to this list. Finally, proteins like albumin [205], are also reported to be crosslinkable at the oil/water interface to form robust membranes of polymeric capsules.

### Light-sensitive systems

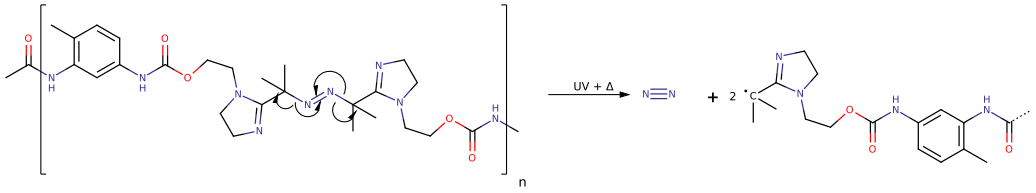


**Figure 4.18.** *Light and temperature sensitive polymer, from which nanocapsules have been built. From reference [200].*

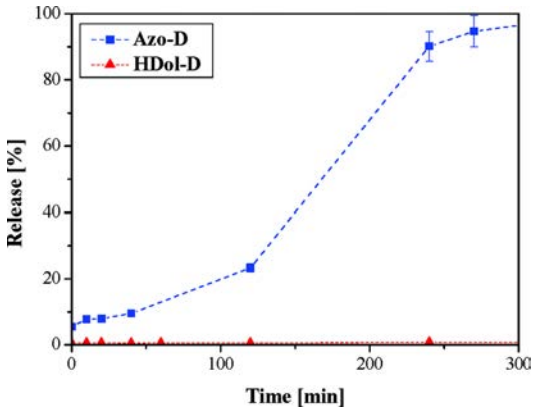


**Figure 4.19.** *Reprinted from reference [200]. Release of sulforhodamine 101 from azo-capsules (Azo-D) and hexane diol based ones (HDol-D), under continuous UV light irradiation. No release is expected from hexane-diol based capsules, because they are not light-sensitive.*

Photo-cleavable diazo moieties (see figure 4.18) has been used to build 200–400 nm sized capsules [200]. The release is claimed to be triggered either by pH, temperature or light stimulation; all these stimuli lysed the azo bonds, ultimately leading to the destruction of the capsule. Entrapped sulforhodamine 101 is released in the timescale of the hours and requires UV irradiation (Hg lamp, unfiltered, unknown power), see figure 4.19. pH and temperature did not perform better. The slow kinetics of release is attributed to the slow decomposition of the azo molecule.

In reference [198], the lysis of a polyester membrane is triggered by UV irradiation and light, as shown on figure 4.20. No specific light-sensitizer is required. However, the conditions required to break the capsule are harsh: one hour at 80 ℃ and under UV

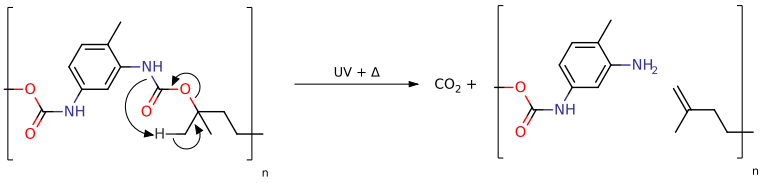


**Figure 4.20.** *Temperature and light induced degradation of a polyester-based polymer. From reference [198].*

irradiation was required to release the entrapped sulforhodamine 101. No precisions on the kinetics of release were given.

### Discussion

Little is known yet about the compatibility of such an encapsulation method with fragile proteins. As the capsules are synthesized around the aqueous phase containing the molecule of interest, high encapsulation yields are expected as it was the case for liposomes prepared by the *reverse emulsion method*. Only one evaluation of the encapsulation yield has been performed though [199]. Values ranging from 80 to 96 % are reported for the encapsulation of sulforhodamine 101 in polyurethane capsules. At this point, similar values should be expected for proteins.

Various preparation conditions are reported, which should allow to optimize a procedure that avoid harsh processing conditions for proteins. All are based on a reverse emulsion synthesis, which should prevent any contact between the protein and the oil phase, thus avoiding solvent-based denaturation. A surfactant is used to stabilize the reverse emulsions; non-ionic low-HLB ones are generally used, recognized as compatible with the preservation of the protein activity. The emulsification is mostly done using high-intensity ultrasounds, which may affect the proteins. However, PIT emulsification, which relies only on a temperature-based phase inversion, are also reported. Well-chosen surfactants can prevent from crossing the limit of 37 ℃, thus alleviate or minimize protein denaturation. A broad range of capsule size is accessible, and depends on the size of the emulsion. The typical capsule size is 200 nm.

Concerning the synthesis itself, it can be conducted at room temperature. In a majority of the cases reported, a primary amine reacts with the oil soluble monomer (a diisocyanate). One should therefore pay attention to reactivity of the encapsulated protein itself, as it also bears primary amine functions. This has even been exploited to build capsules from BSA. Protein competes however with organic amines added to the aqueous phase; 24 hours at 25 ℃ are required to synthesize the capsules from BSA [205], while 3 hours at 25 ℃ are sufficient for diamine based ones [206].

Concerning the light-sensitivity of these systems, only a few examples are reported, badly characterized and requiring long-lasting deep UV irradiation, one even combined to 80 ℃ heating. This is redhibitory for any protein application. Yet, no specific efforts

have been made to introduce light-sensitive moieties in the membrane of these capsules. The versatility of the synthesis procedure gives a lot of space for developing efficient light-sensitive capsules.

## 4.4. Hybrid membranes

We describe here some "exotic" light-sensitive systems which somehow mixed the principle of building a polymer capsule around an aqueous core with another basic architecture, such as a hydrogel or temperature-sensitive assemblies. They are all reported in this short section, as only a couple of examples are reported in the literature for each of them.

### 4.4.1. Hydrogel capsules

An hybrid system, composed of a hydrogel capsule around a liquid core, is reported in reference [158]. The synthesis procedure also differs from the other systems: the capsules are obtained from poly(*N*-vinylformamide) particles by a sequence of hydrolysis and crosslinking, using sodium hydroxide and glutaraldehyde in methanol. This lead to ≈ 2 µm sized capsules with a 300 nm thick shell. The capsules were found to be permeable to fluorescein and dextran, up to 250 kg/mol. Loaded by diffusion, the capsules are made impermeable to dextrans down to 2 kg/mol with hyaluronic acid. Sensitized with gold nanoparticles, the capsules are completely destroyed by pulsed laser irradiations (532 nm, 50 mJ/cm²). However, no characterization of the release kinetics has been performed.

### 4.4.2. Nanoparticles bridged by organic polymers

The system reported in reference [207] is made of gold squares assembled in boxes, as shown on figure 4.21. Box faces are kept together with polyNIPAM chains. When the chains are swollen, the box is tight, but increasing the temperature make the chains collapse and the particle release its content. The LCST of polyNIPAM has been tuned to 39 °C, to match the biological conditions. Several molecules have been encapsulated in these boxes (doxycycline, lysozyme and alizarin-labelled PEG), simply by stirring a suspension of the boxes in their leaky state and the molecule to encapsulate. The release was triggered by infra-red irradiation (10–40 mW/cm²) for 2 minutes, and occurred in the timescale of 2–4 minutes.

In reference [208] are reported 1 µm capsules made from the assembly of 20 nm spherical particles. These particles were functionalized with a cinnamic acid derivate: a light irradiation allowed to cross-link the particles by dimerization of the cinnamate (see figure 4.22). These capsules are synthesized in a water/oil/water emulsion: the nanoparticles are suspended in the oil sheet (toluene) and the inner aqueous drop contained the encapsulated materiel (here cyclodextrines). UV irradiation leads to the crosslinking of the nanoparticles, giving a mechanically resistant capsule. This step was followed by the removal of the

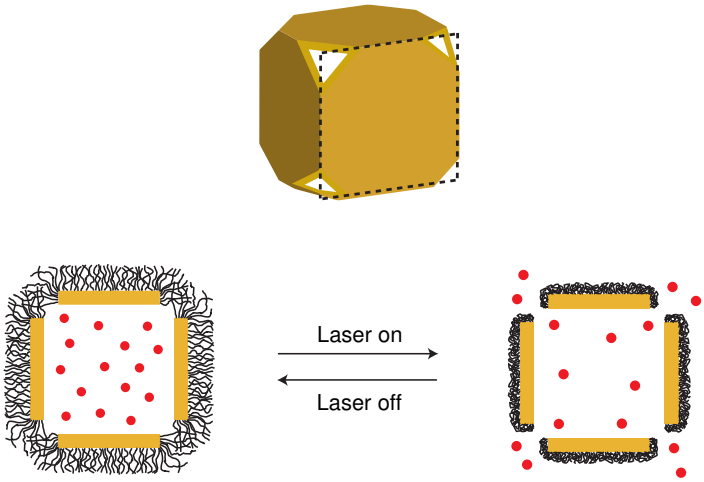


**Figure 4.21.** *Cubic boxes made of self-assembled gold* faces*, kept together with polyNIPAM chains (black lines). The box is tight while the chains are swollen, and made leaky when they are collapsed. Reprinted from [207].*

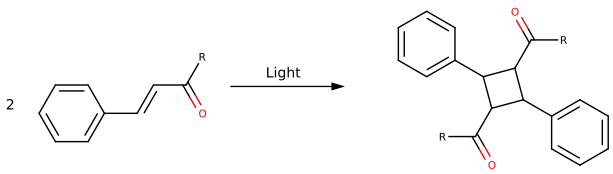


**Figure 4.22.** *Light-induced cinnamic acid derivative 2+2 cycloaddition.*

toluene to yield a suspension of functional capsules. The release of the entrapped cyclodextrines occurred upon UV light irradiation (254 nm, unknown power). The kinetics of release are unknown.

A similar system reported in reference [209], in which the capsules are made of gold nanoparticles cross-linked by semi-fluorinated PEG chains. At room temperature the 80 nm sized obtained capsules are tight, but elevating the temperature to 62.5 ℃ or irradiating the suspension with a green laser (532 nm, 250 mW) make them leaky, which allowed to load them with rhodamine B. With the green laser, the release of the encapsulated dye occurs in the timescale of one minute.

## 4.5. Role of the stimulation wavelength

One major point has not yet been discussed, as it is common to all systems, and concerns the stimulus itself. Three main parameters are relevant here: the wavelength of light irradiation, its surface power and the duration of the stimulation.

Various wavelengths are used to trigger the release from the light-sensitive systems shown in this review, ranging from infra-red to deep ultraviolet. From a practical point of view, infra-reds are preferred, as they are less scattered and can penetrate the tissues deeper than lower wavelengths [210]. Anyway, this practical limitation is only relevant for in vivo applications or for the study of thick samples. From another point of view, high-energy photos can be harmful for the cell, the surrounding tissues and even the encapsulated molecule of interest. 250 nm UV can be absorbed by virtually any organic material, leading to its destruction. It is in fact one of the mechanism of rupture alleviated for the polystyrene capsules. As it is not specific to the capsule, it can lead to the destruction of the collagen gel and the encapsulated material. UV, in particular the UV-B (315–280 nm) and the UV-C (280–160 nm), are known to cause oxidative damages to collagen network [211]. Cells behavior is also affected by UV light, and the results ranges from a modification of its metabolism to its death, depending of the light intensity [212]. Concerning the encapsulated material, UV in the 298–250 nm range is known to break disulfide bonds, which results in protein denaturation [213], and has even been used as a method to break disulfide-crosslinked hydrogels, as shown before. Therefore, visible or infra-red light must be the preferred stimulus for our system. Three trails can be followed: tune the light sensitive moieties to make them visible or infra-red absorbing, use two-photon stimulation or use up-converting particles to generated UV from visible light in situ. The relevance of using up-converting particles in contact with biological systems is discussed, as they are made of toxic materials [52].

The harmfulness of the light-stimulation comes also from its intensity. The threshold above which damages occur are wavelength dependent [214]. We need also to keep in mind that the femtosecond lasers used for non-specific triggered release purposes have also been used to disrupt organelles directly inside the cells [215]. In that case, a precise space control is required to prevent any cell damage. Thresholds of 0.47 J/cm² for blue light (457 nm) and 1,900 J/cm² for IR (810 nm) are reported for epithelial cells [216].

# Summary

Several systems in the literature appear as promising to address the question of a fast and localized protein delivery. All the systems used to release proteins or macromolecules are summarized in tables on page 70. If we focus on fast-releasing systems not triggered by UV light, several candidates arise. The polymer-sensitized liposomes are of interest, even if the release time is 30 minutes. In fact, the slow kinetics is linked to the size of the vesicle. The estimated characteristic release time of a 50 kg/mol protein from 10 µm sized vesicles is 133 s, while it decreases to 8 ms for a 200 nm sized one (see appendix C.4.2, p. 201). The dye-sensitized liposomes are also of interest, thanks to the instant release and visible light stimulation; the high energy required may be a problem, as the dye itself, due to its potential cell toxicity. As for nanogels, no candidates arise. The fastest system reported has a 20 s characteristic time; faster systems can probably obtained by building looser gels, at the expense of a spontaneous protein release. The most promising systems are probably the capsules, as they combine the advantages of both the liposomes and the nanogels. By the reverse emulsion process, the protein can be encapsulated in an aqueous core, under physiological conditions, with a high encapsulation yield. Only two light-sensitive systems made by this technique are reported. They do not seem to have been developed for fast and/or efficient light-triggered release: hard and long-lasting UV irradiations are required. The performances of the two other kinds of capsules, the polymersomes and the layer-by-layer assemblies, suggest that there is a possibility to develop efficient light-sensitive capsules by this technique.

To conclude, two systems seem worth to be investigated: the liposome-based delivery systems and the photo-breakable polymer capsules. Both have been studied during this thesis and are developed in the next chapters.

| Sensitizer | Light effect | Mechanism | λ | Power | τ (s) | Ref. |
|---|---|---|---|---|---|---|
| Azobenzene on polymer | Isomerisation, polarity shift | Pore opening | Visible | unknown | 30 min | [97] |
| None (bare lipids) | Heating/Photolysis | Membrane rupture | 355 nm | ≈ μJ | instant | [43, 44] |
| Orthonitrobenzyl ester | Lipid lysis | Membrane disruption | 355 nm | unknown | 20 s | [98] |
| DiD (lipidic dye) | Local heating | Membrane disruption | 645 nm | 560 nJ | instant | [102–104] |

**Table 4.1.** *Light-triggered release of proteins from liposomes, summary*

| Sensitizer | Light effect | Mechanism | λ | Power | τ (s) | Ref. |
|---|---|---|---|---|---|---|
| Orthonitrobenzyl ester | Crosslink lysis | Gel disruption | 365 nm | 10 mW/cm² | 20 s | [124] |
| Nucleid acid | Crosslink lysis | Gel disruption | 400 nm | unknown | 48–200 h | [143] |

**Table 4.2.** *Light-triggered release of proteins with nanogels, summary*

| Object type | Model drug | Sensitizer | Light effect | Mechanism | λ | Power | τ (s) | Ref. |
|---|---|---|---|---|---|---|---|---|
| Layer-by-layer | Dextran | Azobenzene dye | Isomerization | Permeabilization | > 400 nm | unkown | ≈ hour | [161] |
| Layer-by-layer | BSA | Azobenzene | Isomerization | Membrane rupture | 366 nm | 55 mW/cm² | 2 hours | [163] |
| Layer-by-layer | Dextran | Silver NP | Heating | Membrane rupture | 532 nm | unknown | < 1 s | [166] |
| Layer-by-layer | Lysozyme cystals | Gold NP | Heating | Membrane rupture | 1064 nm | 50 mJ/cm² | instant? | [170] |
| Polymersome | EGFP | Orthonitrobenzyl ester | Polymer lysis | Membrane rupture | 365 nm | 700 mW/cm² | 10 min | [182, 183] |

**Table 4.3.** *Light-triggered release of water-soluble macromolecules from polymer capsules, summary*

# Part II.

# Light-sensitive liposomes

# Introduction

This chapter addresses the question of liposome photobreakage, with a focus put on the achievement of fast (< 1 s) response-times to irradiation; this is required to enable a local delivery of the entrapped molecules. Systems that absorb light strongly are certainly fast (cf. chapter 2). However, as they rely on a local heating to break the liposomes, they are not compatible with applications in thick hydrogels used for cell-culture: the energy will be dissipated throughout the whole cell culture medium and may cause structural damages to it. From the bibliography, we identified photochrome-containing liposomes as promising capsules. In fact, the release does not rely on a local increase of temperature and were seemingly sensitive to exposure to light at low irradiance and low total power (< 10 min at $\sim$ mW/cm$^2$), diminishing the risk of increasing the temperature of the sample. Yet the possibility to design fast-responsive photoliposomes and the optimization of their rate of response to stimulation were generally not investigated.

Here we report experimental assessments of the rate of liposome breakage or permeabilization in the presence of two models of photoisomerizable chromophores: an azobenzene-containing surfactant (azoTAB) and amphiphilic macromolecules grafted with azobenzene (150-15C8-10Azo). Both model photochromes bind to lipid bilayers and can break or permeabilize the membrane depending on their degree of photo-isomerization. The surfactant is representative of systems that were reported for releasing small molecules in less than 100 s upon shining UV or blue light [72, 75, 79, 80]. The polymer comes from systems launched in our team by F. Vial and S. Sebai [97, 217] and is a simple tool that adsorbs tightly photochrome groups on lipid membranes, which in practice may alleviate toxicity issues due to exchanges of surfactants or small azo-containing lipids with cell membranes [97]. Important results published on photochrome-containing liposomes suggested however that the perturbation of the bilayer was rather weak, and essentially ascribed to shifts of lipid phase transition, or local scrambling of the lipid order. No evidence for membrane breakage or poration were shown. When this thesis was launched, it was accordingly decided to experimentally assess the possibility to optimize liposome composition for on-demand protein release, which needs either to form photo-breakable or photo-porable systems. These systems should in addition be compatible with fast leakage. The first section reports the study by light scattering of "liposome to micelle" transitions in mixed lipid:azoTAB solutions. The second part reports on polymer-coated small liposomes permeabilization studied by light-scattering, and calcein leakage experiments.

# 5. Surfactant sensitized vesicles

## Introduction

In the presence of an excess of surfactant, liposomes may dissolve into mixed micelles of nanometer size. The process has been extensively investigated, e.g. with Triton X-100. It can be fast, but the details on the intermediate pathways involved in the lipid-bilayer dissolution-mechanisms are still discussed [218]. A generally accepted scheme is summarized in figure 5.1.

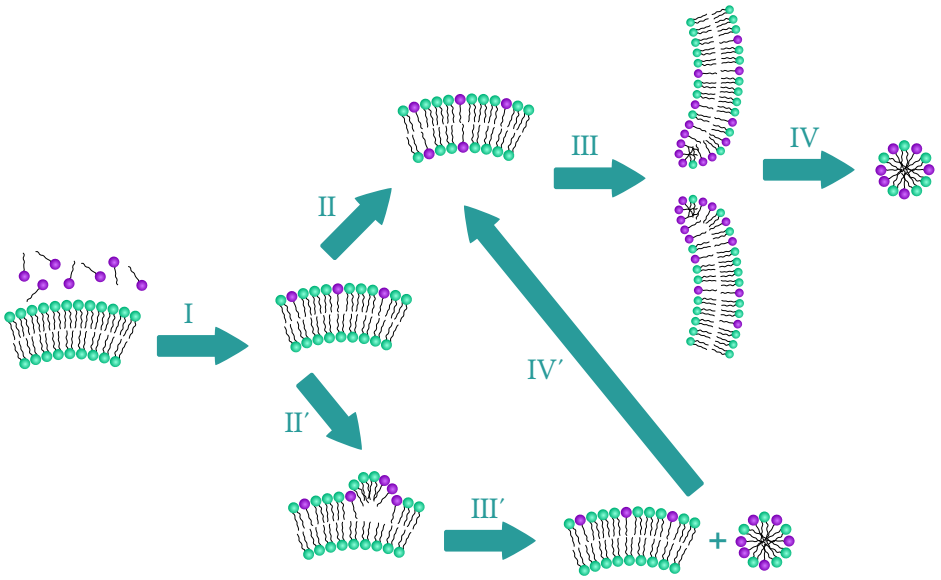


**Figure 5.1.** *Adapted from reference [218]. I: detergent monomers inserted in the vesicle outer monolayer. II: detergent equilibrates between the inner and the outer monolayer through rapid flip-flop. III: pores are formed in the bilayer. IV: Lipid-detergent mixed micelles are formed. When rapid flip-flop is not possible, then an alternative pathway occurs. II′: insertion of multiple curvophilic detergent molecules cause a large increase in the curvature of the outer bilayer. III′: lipid-detergent mixed micelles are shed from the bilayer, and this process leads to IV′: detergent trans-bilayer movements. The system can then undergo processes III and IV.*

Irrespective of the main pathway(s), the formation of pores is involved at the stage of liposome "opening" (III) and formation of prolate or oblate mixed micelles. Liposome dissolution is thus expected to indicate compositions and environment conditions (pH, temperature, ionic strength, etc.) close to conditions of poration. As a rule of thumb, it is

generally admitted that a critical lipid:surfactant ratio must be reached to make the bilayer fragile and to enable the formation of pores. Experimentally, the ratio of lipid to total surfactant is controlled, and the partition of surfactants between the aqueous phase and the lipid one modulates the position of the systems above or below this critical ratio. Based on this premises, it is expected that upon switching the polarity of azoTAB by shining light, one should control the stability of lipid:azoTAB mixed assemblies.

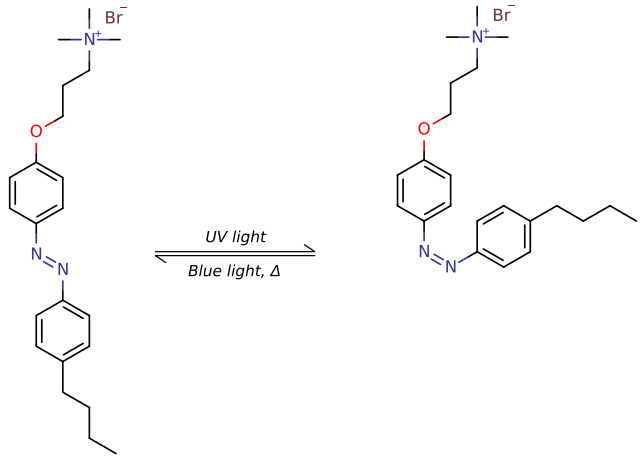


**Figure 5.2.** *The azobenzene-based surfactant, referred to as* azoTAB. *Like many azobenzene-containing molecules, azoTAB is isomerized with a specific wavelength.*

Under UV light, the azobenzene is in a predominantly cis – polar – configuration, which means that the surfactant is more soluble in water. This should diminish or minimize the perturbation of the membrane. Under visible light, the azobenzene shifts to its trans isomer form, lowering at the same time its solubility in water, which makes it more prone to bind to the membrane. The structure of the surfactant we used is shown in figure 5.2. AzoTAB was straightforward to synthesize at the laboratory and its physico-chemical properties were well characterized [219, 220]. Its molecular weight is 434 g/mol (with bromide counter-ion), its CMC in water is below 0.8 g/L for the trans isomer and equal to 1.6 g/L for the cis isomer. The micelle radius was measured by DLS: < 3.5 nm, and by SAXS: 2.7 nm outer radius, aggregation number of 60 [220]. One advantage of azoTAB is its long characteristic thermal relaxation time from the cis to the trans isomer, which takes about two days at 20 ℃ (see figure 5.3). When measurements – conducted in the dark – are short compared to the relaxation time of the cis isomer, one can in practice neglect the variations of the cis-isomer fraction. This enables to perform experiments without irradiating the samples continuously, thus minimizing the amount of light shone on samples. Finally, the extinction coefficient of azoTAB (ca. 58 L/g/cm at 350 nm) enables to reach the photostationary state of predominantly cis isomer in solutions up to 1 g/L using UV LED lamps at an irradiance below 3 mW/cm². It was determined that 84 % cis isomers and 16 % residual trans ones equilibrate upon shining 365 nm UV light (by $^1$H NMR, ref. [219]).

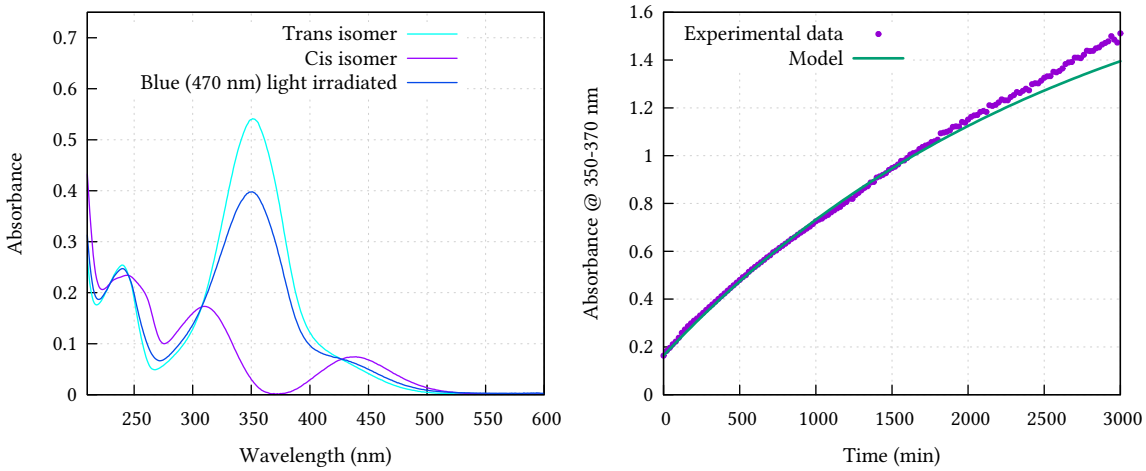


**Figure 5.3.** Left: *trans and cis isomer of the azoTAB surfactant in water, at 9.2 mg/L. The attenuation coefficient of trans azoTAB at 353 nm is 58.6 L/g/cm.*
Right: *thermal relaxation of azoTAB (34 mg/L) in water, followed by the absorbance of the solution at 350–370 nm. The characteristic time of relaxation (2,700 min) has been inferred from the initial absorbance (0.16), the measured all-trans absorbance (2.0) and the initial slope of the curve (see appendix* C.3.2 Measurement of azoTAB relaxation time by UV-Visible spectroscopy*, p. 197).*

# 5.1. Liposome solubilization by the azoTAB surfactant

## 5.1.1. Determination of azoTAB:lipid critical ratio

To determine the surfactant concentration required to dissolve the liposomes into mixed micelles, we mixed DOPC lipid and azoTAB and measured by dynamic light scattering the hydrodynamic diameter and scattered intensities of these samples. As lipid vesicles are non-equilibrium assemblies, whose diameter strongly depends on production procedures, the influence of the preparation of stock solutions was assessed. To this aim, lipid and azoTAB were mixed in aqueous solutions using two different protocols: at low (< 0.1 g/L) or higher (> 1 g/L) lipid concentrations, with or without sonication, with azoTAB added before or after the formation of lipid vesicles.

In the first protocol, a suspension of 200 nm DOPC liposomes was prepared by the film hydration method in deionized water and extrusion. Aggregates of lipids were removed by centrifugation (10 minutes at 14,000 g) to yield small vesicles at approximatively 1 g/L lipids (2.06 mmol/L). Aliquots of DOPC vesicles were mixed with azoTAB solutions and incubated at room temperature (detailed protocol reported in appendix *E.2.2 "Low lipid concentration" protocol*, p. 210).

The second protocol consisted in the hydration for 30 min of a dry film of DOPC prepared as above, with a 20 g/L solution of azoTAB in deionized water, then sonicated the mixture and let the solution rest for 24 h at room temperature. A more detailed description of the experimental conditions is given in appendix *E.2.2 "High lipid concentration" protocol*, p. 210.

When the mixtures were prepared with trans azoTAB, and after 24 h incubation, both the intensity of scattered light and the hydrodynamic diameter suggested the presence of liposomes until the azoTAB:lipid ratio increased above a threshold value. Liposomes prepared by the first protocol dissolved into small, presumably micellar, objects above azoTAB:lipid ratios between 6 and 8. In the more concentrated solutions prepared by the second protocol, the signal from liposomes essentially vanished above a ratio of 5.5 (see table 5.1). This ratio is similar to the usual dissolution ratios measured with conventional surfactant:lipid mixtures [221–223]. In addition, it was not affected by dilution of the stock solutions into PBS buffer (not shown). The smaller diameter of liposomes prepared at higher concentrations are not surprising due to the sonication step that usually form small vesicles (< 50 nm diameter).

The initial radii and intensities measured within a few minutes after preparation of dilute mixtures (by extrusion and post-addition of azoTAB) indicated however that at short times vesicles were present in the whole experimental window of compositions. The dissolution of liposomes by azoTAB added in the outer aqueous phase was clearly evolving during incubation. This contrasts with the effect of Triton X-100, able to dissociate the liposomes within the time needed for mixing and DLS measurements.

| $C_{azoTAB}$ (g/L) | | 0.00 | 0.17 | 0.34 | 0.50 | 0.67 | 0.84 | 1.68 | 3.36 |
|---|---|---|---|---|---|---|---|---|---|
| $I_{diff}$ (kcps) | 0 h | 21 | 15 | 17 | 22 | 19 | 18 | 18 | 15 |
| | 24 h | 22 | 14 | 21 | 16 | 3.0 | 1.4 | 2.7 | 3.0 |
| | Δ (%) | +6 | −3 | +21 | −25 | −84 | −92 | −85 | −79 |
| $D_h$ (nm) | 0 h | 525 | 443 | 418 | 419 | 375 | 408 | 388 | 401 |
| | 24 h | 468 | 462 | 413 | 312 | 79 | *no fit* | *no fit* | *no fit* |
| | Δ (%) | -11 | +4 | −1 | −26 | −79 | | | |

**Table 5.1.** *Hydrodynamic diameter ($D_h$) and intensity of scattered light ($I_{diff}$, in kilo counts per seconds) of mixtures of trans-azoTAB and vesicles (DOPC, 0.1 g/L), after preparation and 24 hours later. no fit indicates that correlograms were too noisy to enable the determination of $D_h$, indicating the absence of detectable liposomes.*

| azoTAB:DOPC w. ratio | | 2.4 | 3.6 | 4.8 | 6.0 | 10.0 |
|---|---|---|---|---|---|---|
| 20 g/L azoTAB | $I_{diff}$ (kcps) | 288 | 156 | 113 | 60 | 44 |
| | $D_h$ (nm) | 150 | 30 | *no fit* | 2 | 2 |
| PBS diluted | $I_{diff}$ (kcps) | 95 | 12 | 9.5 | 7 | 8.2 |
| | $D_h$ (nm) | 75 | 11 | 9 | 5 | *no fit* |

**Table 5.2.** *Scattered light intensity ($I_{diff}$) and hydrodynamic diameter ($D_h$) of azoTAB/DOPC mixtures after 24 hours of incubation. The results are shown for the "raw" mixtures (20 g/L azoTAB), and after dilution in PBS (0.8 g/L azoTAB).*

When mixtures were prepared with predominantly cis azoTAB, the results were similarly that at short time liposomes were always detected, whereas at time 24 h samples with high a azoTAB:lipid ratio contained micelles. Liposomes were dissolved into small micelles ($D_h$ < 3 nm) above a critical cis-azoTAB:lipid w. ratio of about 16.

| $C_{azoTAB}$ (g/L) | | 0.00 | 0.17 | 0.34 | 0.50 | 0.67 | 0.84 | 1.68 | 3.36 |
|---|---|---|---|---|---|---|---|---|---|
| $I_{diff}$ (kcps) | 0 h | 21 | 24 | 25 | 26 | 26 | 27 | 35 | 24 |
| | 24 h | 22 | 20 | 25 | 29 | 30 | 18 | 6.1 | 3.2 |
| | Δ (%) | +6 | −16 | 0 | +11 | +16 | −34 | −83 | −87 |
| $D_h$ (nm) | 0 h | 525 | 477 | 476 | 446 | 430 | 387 | 363 | 348 |
| | 24 h | 468 | 438 | 408 | 369 | 349 | 295 | *no fit* | *no fit* |
| | Δ (%) | −11 | −8 | −14 | −17 | −19 | −24 | | |

**Table 5.3.** *Hydrodynamic diameter ($D_h$) and intensity of scattered light ($I_{diff}$, in kilo counts per seconds) of mixtures of cis-azoTAB and vesicles (DOPC, 0.1 g/L), after preparation and 24 hours later. no fit indicates that correlograms were too noisy to enable the determination of $D_h$, indicating the absence of detectable liposomes.*

It is observed for the trans isomers that the liposome dissolution upon post-addition of the surfactant (first protocol) occurs at a total azoTAB concentration close to the CMC. Dissolution similarly occurs near the CMC of the cis azoTAB in the dilute lipid solution (0.1 g/L, see table 5.3). CMC has been reported to be of the order of magnitude of the association constant of surfactant near the saturation of lipid membranes. It is thus predictive of liposome breakage essentially when the lipid concentration is well below CMC – i.e. when binding of surfactants in the liposomes negligibly affects the concentration of surfactant in the aqueous phase.

### 5.1.2. Kinetics of dissolution

To estimate the characteristic time of light-triggered dissolution of liposomes, we choose from table 5.3 the samples still containing liposomes in the presence of cis azoTAB at time 24 h. We describe first the case of post-addition of azoTAB in preformed liposomes. Just after addition of azoTAB (under its predominantly cis form), samples were irradiated with blue light (470 nm, 1 mW/cm²). These experiments were conducted at various concentrations of azoTAB: 0.340 g/L, 0.503 g/L and 1.26 g/L. Immediately after shinning blue light, the intensity of scattered light was recorded every 5 minutes for 14 hours. Details of the experimental procedure are described in appendix *E.2.2 Determination of azoTAB-mediated liposome dissolution kinetics*, p. 211.

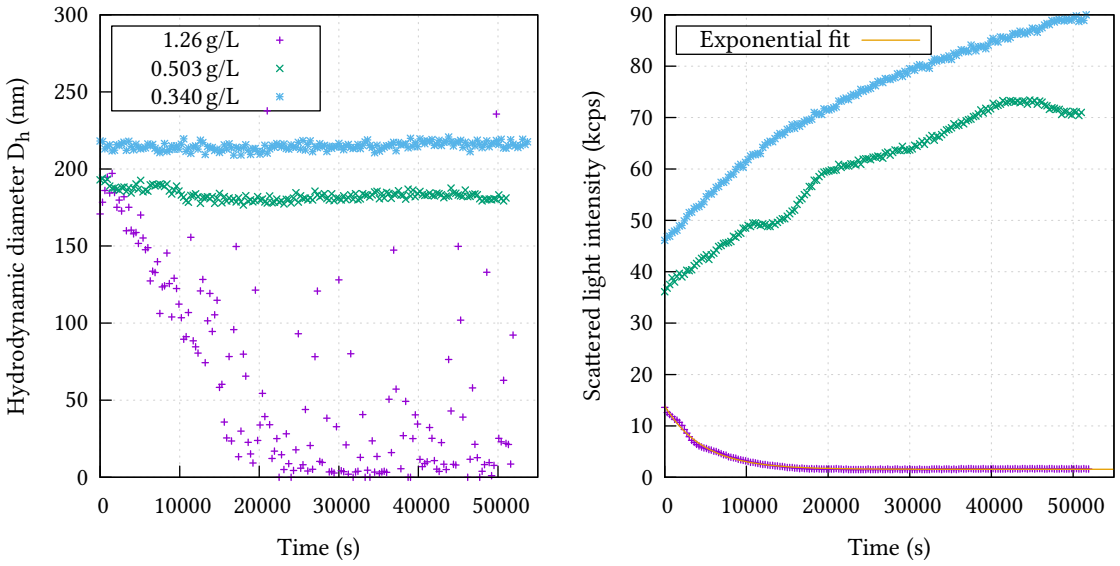


**Figure 5.4.** *Dissolution of liposomes with azoTAB in water (no NaCl, no buffer) under blue light irradiation (470 nm, 92 mW/cm²), followed by dynamic light scattering. The initial suspension contained 0.06 g/L DOPC and either 0.340, 0.503 or 1.26 g/L cis-azoTAB.*

The hydrodynamic diameter and the intensity of scattered light are shown in figure 5.4. For the highest concentration of surfactant, both the diameter and scattered intensity decreased regularly starting immediately. Diameters lower than 5 nm were reached beyond 20,000 s (5.5 h). Tentative fit of the intensity decay by an exponential decay yielded the relaxation time of 4,700 s (1.5 h); this time gives us an order of magnitude of the characteristic time of liposome dissolution. Obviously, membrane dissolution is hours-long, irrespective of the details of the mechanism and/or model that may be used to analyze this data.

As regard to lower azoTAB concentrations, exposure to blue light triggered hours-long slow increases of the scattered light intensity. The amplitude of increase was however below 30 %, suggesting that the variation of the shape or size of assemblies were small. A possible interpretation is that this increasing intensity, with essentially unchanged diameter, can be attributed to the adsorption of the surfactant in bilayers, as reported in reference [218].

### 5.1.3. Effect of salt on the dissolution kinetics

The slow kinetics may be due to electrostatic repulsion between the surfactant molecules. In order to evaluate the role of coulomb repulsion in the rate of reorganization of mixed lipid:azoTAB solutions, the same experiments were conducted in buffers with added NaCl.

In pure water, the ionic strength is dictated by the surfactant. At 1.26 g/L (2.9 mmol/L), the associated Debye length is 5.6 nm. The typical area per molecule in azoTAB-related CTAB micelles is 0.536 nm² [224], which corresponds roughly to 0.7 nm between two surfactant molecules in the micelles. As it is much lower than the Debye length, this can explain a significant contribution of coulomb repulsion to kinetics of adsorption of

azoTAB in liposomes. Adding 150 mmol/L NaCl – which in addition brings the experimental conditions closer to biocompatible osmolarities – reduces the Debye length to 0.77 nm. If the electrostatic repulsion in the aqueous medium is responsible for the slow kinetics, the presence of salt should significantly accelerate these kinetics.

The following modifications were made to the previous protocol. The initial liposome suspension was prepared by hydrating the film with an aqueous solution of sodium chloride at 150 mmol/L, and extrusion. AzoTAB in 150 mM sodium chloride was mixed to an aliquot of liposome solution to reach 0.06 g/L lipids, and either 0.340, 0.503 or 1.26 g/L of cis azoTAB in 150 mmol/L sodium chloride.

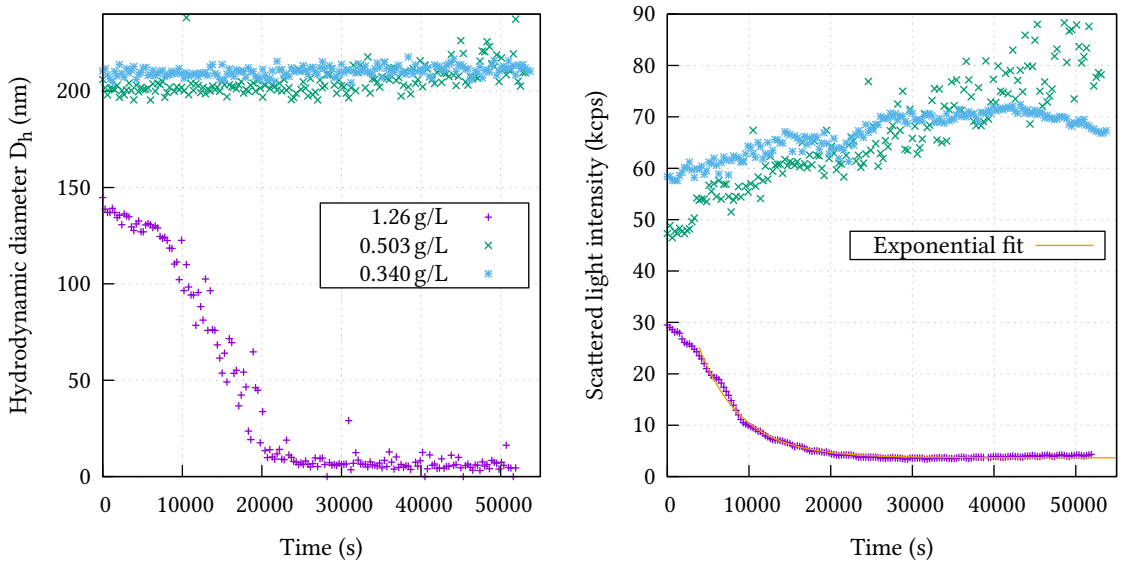


**Figure 5.5.** *Dissolution of liposomes with azoTAB under blue light irradiation (470 nm, 92 mW/cm²) in presence of salt, followed by dynamic light scattering. The initial suspension contained 0.06 g/L DOPC, 150 mmol/L sodium chloride and either 0.340, 0.503 or 1.26 g/L cis azoTAB.*

The kinetics of dissolution in 150 mM NaCl solutions (figure 5.5) were similar to the ones obtained without salt. At 1.36 g/L azoTAB, the scattered intensity decayed gradually during about 20,000 s, with an associated characteristic time of 5,300 s (1.5 h) from the fit to a monoexponential decay. A visibly slower initial decay of the decrease of the hydrodynamic diameter, during about 8,000 s, is the major difference with the kinetics recorded with no NaCl. At low azoTAB concentrations, the hydrodynamic diameter did not significantly vary, while one observed an increase of the intensity. Adding salt did not accelerate the dissolution. This clearly rules out the hypothesis of a limiting rate due to coulombic repulsions in the surfactant-containing liposomes.

Only a few references on the kinetics of liposome dissolution by surfactants are available in the literature. From these references, it can be concluded that non-ionic surfactants [221, 222] dissolve liposomes faster than their ionic counterparts [223, 225]. Authors suggest that one rate-limiting stage is the translocation of the surfactant through the bilayer, which is

essential because the surfactant is generally added on preformed liposomes and is initially adsorbed in the outer leaflet. The origin of the slow kinetics may be worth to study using the "trick" of the photoswitchable dissolution as we showed here. These investigations goes however beyond the scope of designing biocompatible capsules, which is in practice strictly constrained by the fixed pH, ionic strength and temperature of the biocompatible fluids.

### 5.1.4. Investigating the light-sensitivity of azoTAB:DOPC mixtures

We restricted here the study to preliminary trials, seeking to confirm the importance of the presence of azoTAB in the internal and/or external compartments of liposomes, and to estimate whether fast responses may be achieved in these conditions. To this aim, we measured by DLS the effect of exposure to light on liposomes prepared by the second protocol, based on sonicated mixtures of azoTAB and lipids. These stock solutions were diluted 25 fold, to reach 0.8 g/L azoTAB in PBS 1×.

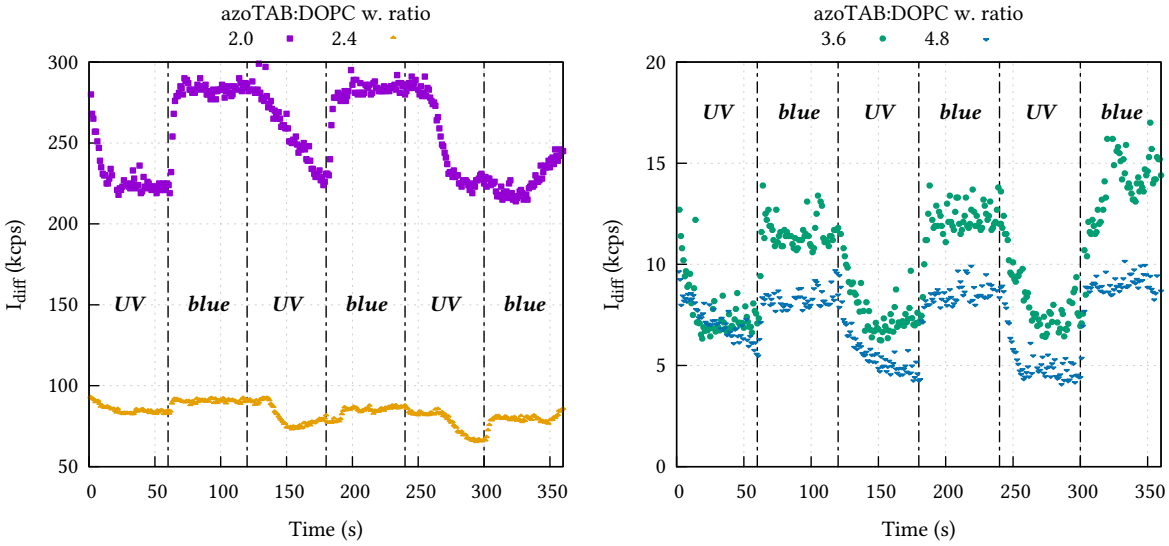


**Figure 5.6.** *AzoTAB:DOPC mixtures, at 20 g/L azoTAB, submitted alternatively to UV light (365 nm, 35 mW/cm²) and blue light (470 nm, 92 mW/cm²). The intensity of scattered light was recorded as a function of time.*

When mixed liposomes were present in the stock solution (azoTAB:lipid w. ratio below 5), the absence of variations in the diameter and the decrease of scattered light intensity upon UV-light irradiation indicates that cis azoTAB presumably desorbs from the membranes (see figure 5.6). This variation occurred in a few seconds, which is the typical time needed for trans to cis photoisomerization exposed to irradiances above 1 mW/cm². Unfortunately, the quantification of the photoconversion rate was hampered by geometrical constraints in the DLS measurement apparatus. Due to the high OD of the solution and variability of the distance between the light source and the sampled volume in the DLS vials, only an order of magnitude of 10 s can be estimated. The amplitudes of the scattered intensity

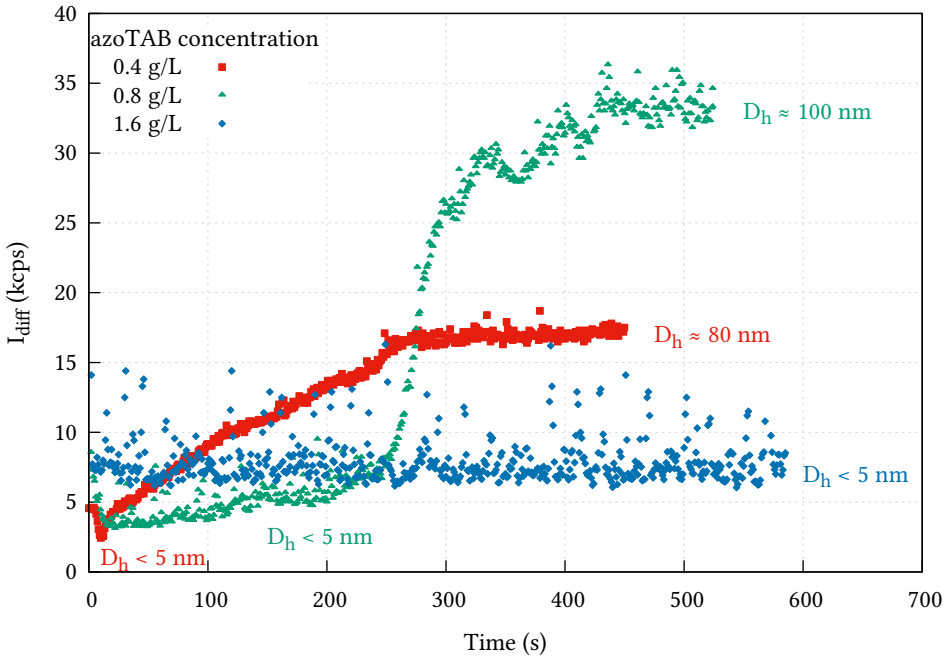


**Figure 5.7.** *Light scattering from solutions of azoTAB:DOPC (10:1 g/g) in PBS exposed to UV light at time zero.*

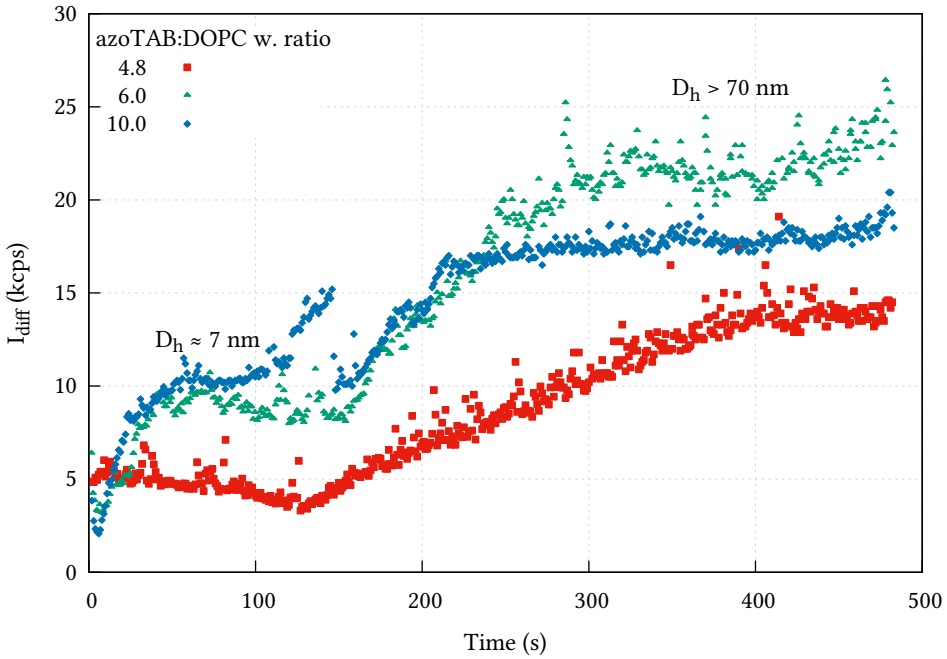


**Figure 5.8.** *Light scattering from solutions of 0.4 g/L azoTAB:DOPC in PBS exposed to UV light at time zero.*

variations (≈ 20–30 %) are of the same order of magnitude as the slow hours-long increases observed upon exposure to blue light of liposomes supplemented with surfactants in their outer leaflet. The reversibility of variations suggests that neither significant breakage, nor liposome reorganization, has occurred, and that equilibrium with the azoTAB was quickly reached in these conditions.

When the preparation procedure yielded mixed micelles of azoTAB:lipid – i.e. at azoTAB: lipid ratios higher than 5 g/g – the solutions exposed to UV light showed much lower scattered intensity. Yet the sensitivity to UV-vis irradiation, the responses in the timescale of the second and the reversibility were preserved at irradiation times below 1 min. Results are shown in figure 5.6. An UV irradiation for typically longer times than 3 minutes was needed to trigger a marked increase of scattering accompanied by the formation of objects with diameters above 30 nm. At azoTAB concentrations lower than 0.8 g/L, and irrespective of the azoTAB:lipid ratio, a long exposure under UV light (10 mW/cm² on the top layer of the sample) triggered an irreversible transition to slow formation of > 30 nm scattering species accompanied by increasing scattered intensity after a lag time of about 3 minutes. At higher concentrations, no effect of light could be detected (see figures 5.7 and 5.8). Cis isomerization presumably destabilized micelles, inducing formation of lipid aggregates. Control experiments included:

- the stability of scattering, and absence of large objects, in solutions diluted 12 fold (i.e. at azoTAB 1.6 g/L) and
- the stability of scattering and preservation of small (< 3 nm) micelles in the absence of lipid in solutions of azoTAB.

Further investigations of these responses are going on, but were not completed during the time of this thesis.

It is concluded that mixed DOPC:azoTAB assemblies can reorganize rapidly over second to minute timescales, upon trans to cis isomerisation of the surfactant in dilute conditions. When the surfactant is initially evenly distributed among the lipids (e.g. present in both leaflets of vesicles, or in mixed micelles) the formation of cis isomers apparently decreases the molecular weight of assemblies, confirming the poorer affinity for lipids of the cis compared to the trans isomer.

### 5.1.5. Dissolution of liposomes from encapsulated azoTAB

Cutting the presence of azoTAB in the outer compartment/leaflet has a major practical advantage. Upon dilution of liposomes, any azoTAB molecule present outside the liposomes can desorb and be lost (e.g. by dialysis) and may be toxic to cell cultures. It was thus of interest to assess the possible photosensitivity of liposome-encapsulated surfactants. To this aim, lipid films were hydrated with a cis azoTAB solution in PBS, to yield suspensions containing 1 g/L lipid and either 1.0, 1.5, 2.0 or 5.0 g/L of cis azoTAB. When liposomes

| $C_{azoTAB}$ (g/L) | 1.0 | 1.5 | 2.0 | 5.0 |
|---|---|---|---|---|
| **$D_h$ (nm)** | 251 | 183 | 98 | 21 |
| **Disp.** | 0.36 | 0.24 | 0.32 | 0.25 |
| **Intensity (kcps)** | 92.5 | 63.4 | 9.2 | 3 |

**Table 5.4.** *Hydrodynamic diameter ($D_h$), polydispersity (Disp.) and intensity of scattered light of lipids:cis-azoTAB samples. DOPC concentration: 1 g/L.*

were obtained, the outer azoTAB was removed by gel filtration. Samples in the dark were characterized by DLS, as shown in table 5.4.

As expected from section 5.1.1, above an azoTAB:lipid w. ratio of 5:1 (ca. 9:1 mol/mol), the intensity and the diameters indicated the formation of mixed micelles. Below this threshold ratio, stable liposomes could be manipulated. Both 1 g/L and 1.5 g/L samples contained mixed liposomes. They were purified (to remove unbound azoTAB) by gel permeation chromatography (fractionation ability of the gel: $4{\cdot}10^4$–$2{\cdot}10^7$ g/mol, dextran). The fraction with the highest concentration of liposomes was selected based on its scattered light intensity. The evolution of the intensity of scattered light and the hydrodynamic diameter were recorded by DLS, upon exposure to blue light (one measurement every 5 minutes for 14 hours). The detailed protocol is available in appendix *E.2.2 Light-sensitivity assessment of azoTAB-loaded liposomes*, p. 211.

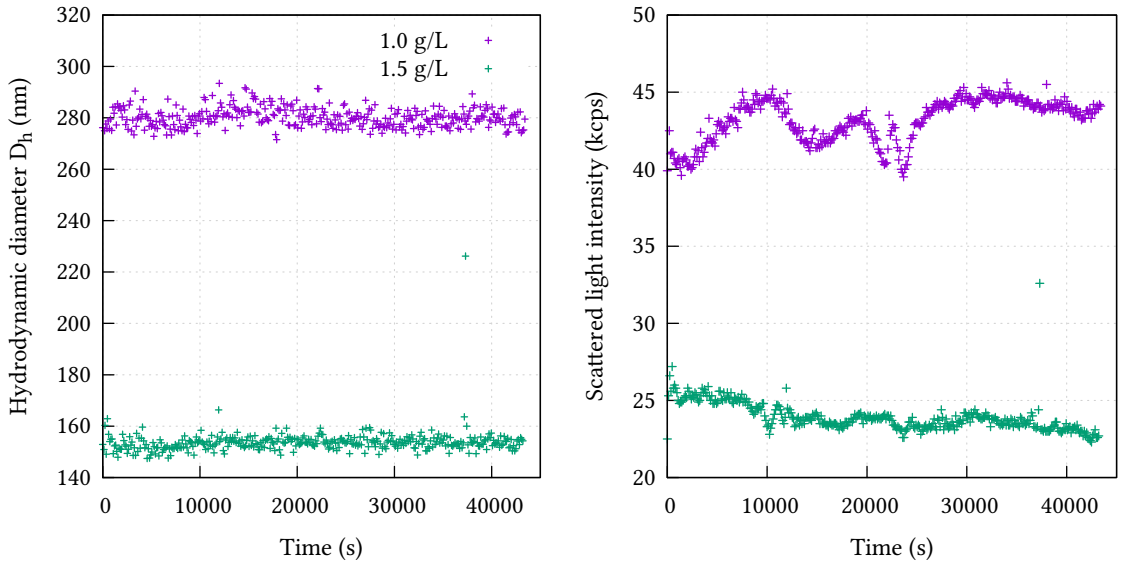


**Figure 5.9.** *Liposomes loaded with surfactant, irradiated with blue light (470 nm, 92 mW/cm²). They are made here from a lipid film hydrated with a solution of azoTAB at either 1.0 g/L or 1.5 g/L in water.*

Under these conditions, the mass of azoTAB trapped in one liposome of diameter 200 nm should be roughly the same as the mass of lipid. Any leakage of the surfactant should accordingly markedly decrease the scattered intensity. The results shown in figure 5.9

indicate that the diameter did not vary and that no significant evolution of the intensity occurred. At 1 g/L or 1.5 g/L azoTAB in the sole internal compartment, dissolution of liposomes was not phototriggerable.

## Conclusion

Liposomes containing azobenzene-surfactants can be made light-responsive by adjusting the azobenze:lipid ratio. Experimentally, light-sensitive liposomes were observed below a weight ratio of 4–5 azoTAB per lipid, or in dilute solutions, below the CMC of the cis azoTAB. The window of compositions was sufficiently broad to enable robust responses, in particular the adsorption/desorption of trans/cis azoTAB in bilayers. The breakage of liposomes requires however stricter conditions.

When present outside the vesicle under its cis (polar) form at concentrations higher than the CMC, the surfactant was able to dissolve highly diluted liposomes (< 0.1 g/L). However, the hours-long kinetics observed is not compatible with the application to the fast and local delivery. The limiting kinetic barrier has not been identified yet, and at least cannot be managed by small variation of salt concentrations (in a range compatible with applications in biology). The use of neutral surfactants may be an alternative to fasten the responses

We may also consider that a full dissolution is not required to achieve a controlled release. As shown in reference [218] and on figure 5.1, holes can be opened in membranes with no breakage of the liposomes. Assuming that the limiting steps of the breakage mechanism are steps II′ and III′, the slow dissolution primarily depends however on translocation of the surfactant, which should be fast in the presence of pores. A slow dissolution indicates therefore a slow translocation process. Failure to find compositions showing fast micellization clearly points to the lack of stable pores in the membranes.

Finally, a constraint with molecular surfactants is that they can rapidly diffuse in, and partition between, all membranes present in the solution, including cell membranes. Toxicity can thus be an issue. The trials to make light-sensitive liposomes after removal of azoTAB from the outer medium was not convincing, indicating that optimization of membrane breakage without an excess of surfactant in both leaflets is not an easy task. This lessens the hope to build a functional system with azobenzene-based surfactants unless they are not freely diffusing and exchanging in solution.

# 6. Azobenzene-based polymer sensitizer

## Introduction

### Choice of the system

This section summarizes studies of azobenzene-containing amphiphilic polymers. The perturbation of lipid bilayers by such macromolecules is likely to be similar to the one achieved by small molecular surfactants. However due to the presence of multiple hydrophobic side-chain groups on these macromolecules, they are unlikely to be removed from the membranes by dilution – thanks to the multiple bindings of the polymer to the membrane provided by these hydrophobic groups. Hence they can be prepared with negligible amount of free (unbound) azobenzene-containing polymer in the solutions. This is an important advantage for the design of robust, light-responsive lipid capsules.

In addition, polymer-coated liposomes become sensitive to light. As mentioned in chapter 2, the photo-triggered release of FITC-labeled Dextran or proteins have been established in the case of polymer-coated giant unilamellar vesicles. The compatibility of the polymer with cell cultures has already been assessed, and no toxicity was found at the concentrations required to permeabilize the giant liposomes [226].

Possible adjustments of these polymer-coated liposomes, for the sake of a local and fast release, were thus worth to study. The major concerns were at the beginning of this thesis:

1. the slow (30–40 minutes long) release time from giant vesicles (5 to 30 µm diameter),
2. the absence of data on properties of small (< 300 nm) vesicles coated with azopolymers.

It was thought that the permeabilization time could be significantly decreased in small vesicles (≈ 200 nm) due to a smaller inner volume (see appendix C.4.2, p. 201).

As a model system, we studied an azobenzene-containing polymer, shown in figure 6.1. This polymer has already been used for the permeabilization of giant vesicles in references [97, 226]. Permeability was mainly studied by the leakage of a fluorescent dye, calcein. The section below describes these results.

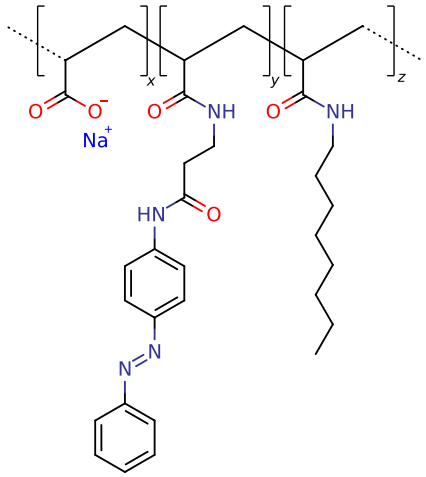


**Figure 6.1.** *Azobenzene-containing polymer used to sensitize the liposomes. x, y and z are respectively the fraction of acrylic acid, azobenbzene and $C_8$ alkyl chain in the polymer. The polymer used corresponded to x = 0.75 mol %, y = 0.10 % and z = 0.15 %, and a molecular weight of 9 kg/mol.*

### Permeabilization principle

Due to the presence of hydrophilic and hydrophobic moieties along the chain, the polymers shown in figure 6.1 binds on lipid bilayers. With increasing the degree of grafting by hydrophobic side groups, the chains can 1) stick to the membrane without significant perturbation, 2) scramble the lipid order, and finally 3) dissolve liposomes into mixed micelles (cf. references [68, 227] and ref. therein). As for surfactants, the hydrophobicity of azobenzene side-groups in the polymers can be switched by shining light: an UV irradiated polymer will be more hydrophilic – thus less permeabilizing – than a blue irradiated one. Due to the poly(carboxylic acid) nature of the polymer, permeabilization is also sensitive to pH and ionic strength. With the adequate balance between the presence of octyl groups in the polymer and the amount of azobenzene, it is thus possible to achieve a permanently tight association with liposomes under both UV and blue irradiation, while preserving the integrity of the membrane in the UV-adapted (predominantly cis) conditions. A switch to the trans azobenzene isomer makes the liposomes permeable [97].

In the case of giant liposomes (GUV, made with DOPC) containing from 0.01 to 0.1 polymer:lipid w. ratio, the impermeable membranes prepared in the presence of UV-adapted polymers turned leaky upon exposure to blue light. The average leakage time was of the order of 30–40 min, but a marked heterogeneity of the time pattern of release was observed between isolated vesicles (see figure 6.2). The variety of observed release behaviors includes for instance gradual leakage for several tens of minutes, as well as abrupt (faster than 1 s) transitions to an empty vesicle. It has not been possible from the investigation of diverse GUV preparations to establish the origin of such an heterogeneity. The impact of the average composition on the release rate was negligible at the level of the population-

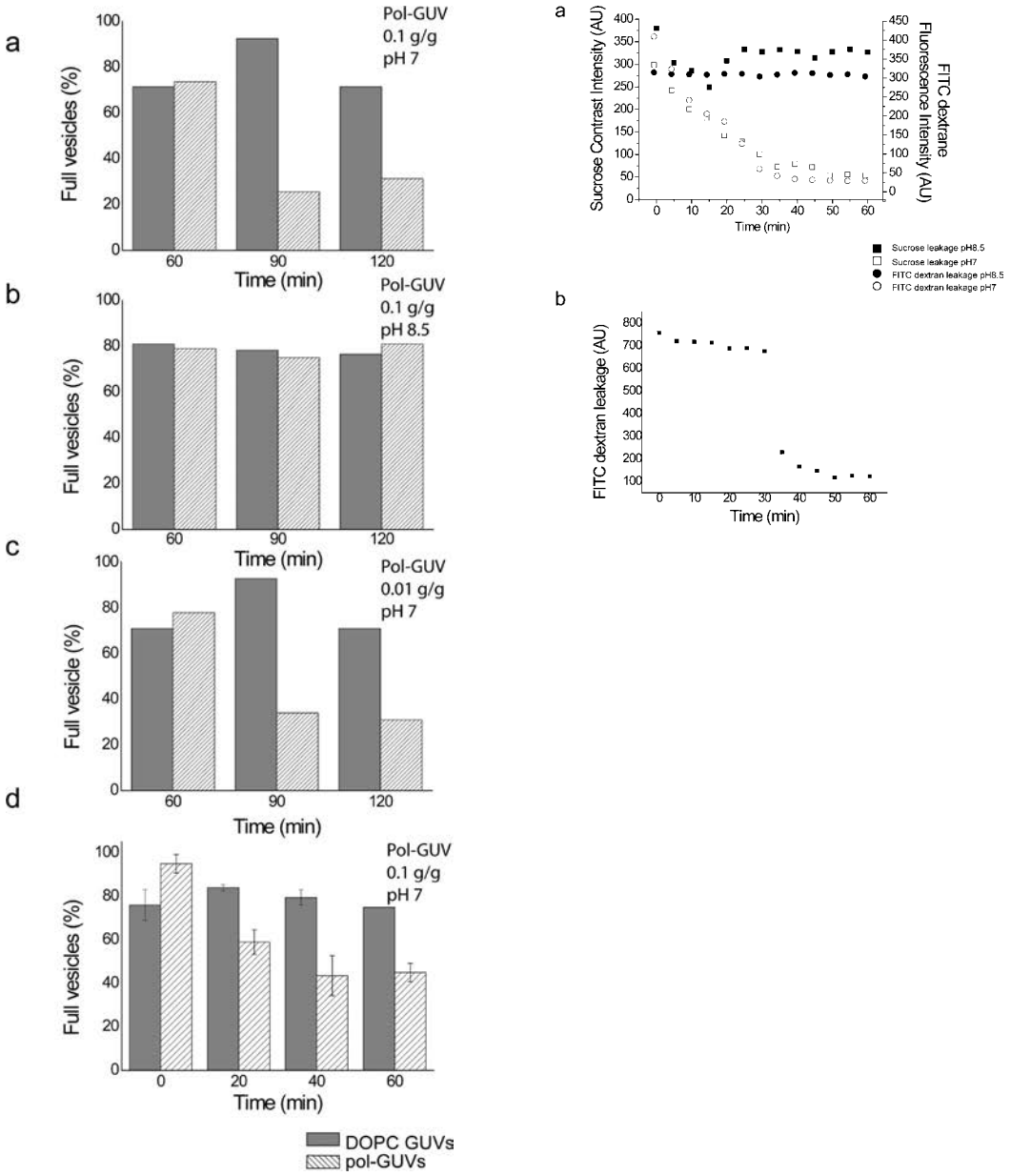


**Figure 6.2.** *Reprinted from reference [97].* Left: *Histograms representing the percentage of full pol-GUVs (dashed columns) and DOPC control GUVs (gray column) with varying AMP:DOPC ratio, pH, and irradiation conditions as a function of time. (a) 0.1 g/g pol-GUVs and DOPC GUVs were initially irradiated at 365 nm for 3 min at pH 7. The vesicles were maintained in the dark for 60 min. At t = 60 min cis pol-GUVs were briefly (1 min) irradiated at 436 nm. The percentage of empty vesicles was followed over 1 h at pH 7. (b) Same conditions as (a) at pH 8.5. (c) Same conditions as (a) at a ratio of AMP:DOPC of 0.01 g/g. (d) Same condition as (a) with 0.1 g/g pol-GUVs and DOPC GUVs irradiated at 365 nm for 3 min at pH 7 and immediately irradiated at 436 nm. The error bars represent higher and lower values from three sets of experiments.* Right: *Leakage profiles of three isolated pol-GUVs. (a) Sucrose leakage kinetics at pH 8.5 and 7 (full and empty squares, respectively) and FITC dextran leakage kinetics at pH 8.5 and 7 (full and empty circles, respectively). (b) FITC-dextran leakage profile of another isolated pol-GUV at pH 7 as a function of time.*

averaged leakage time – i.e. neither the degree of azobenzene side group in the chains, neither the polymer:lipid ratio changed the 30–40 min leakage time needed in practice to reach 40 % of empty GUVs.

The purpose of this section is to assess whether leakage by induced by this polymer out of LUV can be more robust and tunable.

## 6.1. Experimental conditions

### 6.1.1. Principle of the experiment

The kinetics of release from 200 nm vesicles was assessed by measurements of calcein fluorescence. Calcein is a commonly used fluorescent dye for leakage studies [72, 76, 88, 91, 92, 217], due to its self-quenching properties. At concentrations higher than 15 µmol/L, calcein self-quenches, which leads to a drop of fluorescence down to a negligible value compared to the fluorescence of dilute solutions. The threshold concentration is typically 0.2 mmol/L. At concentration below 200 µmol/L fluorescence varies roughly in proportion to concentration (see emission pattern in figure 6.3). Using an optimal (high) concentration of calcein entrapped in liposomes, it is possible to assimilate the variation of fluorescence in suspensions to the emission of calcein being diluted upon release. This enables to follow the release in situ.

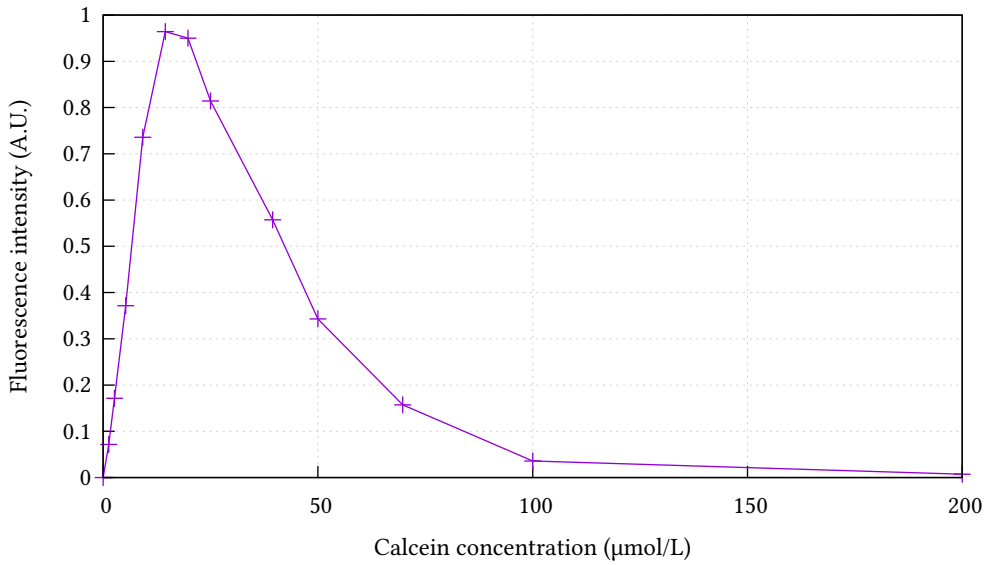


**Figure 6.3.** *Fluorescence intensity of a calcein solution in water. Excitation wavelength: 495 nm, emission wavelength: 515 nm. Reprinted from reference [228].*

### 6.1.2. Sample preparation

DOPC liposomes were prepared by the film hydration method as described in appendix E.1.1, p. 209. In the following experiments, the dry lipid films (evaporated from a chloroform: methanol solution) were always made of lipids mixed with the azo-polymer at 9:1 weight ratio. Cholesterol was possibly present, and in these cases the total DOPC + cholesterol was considered as the weight of lipids. Unless specified, the dry film was hydrated with a solution of 25 mmol/L calcein in PBS 1× added at the ratio of 1 µL aqueous solution per 1 µg of dry film. Vesicles were obtained by mild shearing by pipetting, then sonication, three cycles of freeze/thaw and 3 extrusions through a syringe filter with a pore size of 200 nm. This process is used to avoid multilamellar objects, which may complicate the kinetics of release.

This yields a suspension of liposomes at ca. 1 g/L, with 25 mM calcein both outside and inside the vesicles. At this step, the azobenzene-containing polymer was photoisomerized to form cis isomers. At 25 mmol/L, calcein solutions absorb significantly the light at 365 nm. Therefore, the vesicle suspension was deposited in a wide flat-bottom glass container to expose a thin layer (< 1 mm) to irradiation.

Finally, the excess calcein present outside the liposomes was removed by gel permeation chromatography. The fraction containing the highest amount of liposomes was collected (identified as the one showing the highest scattering by DLS). N.B.: Prior to measurements, the presence of calcein-loaded liposomes was evaluated. Fraction freshly collected from gel filtration were diluted in PBS buffer (addition of 20 µL of the purified sample to 2 mL of buffer), and the fluorescence was recorded prior and after mixing with an excess of Triton X-100 (20 µL of 100 g/L TX100). Samples showing a relative variation of fluorescence intensity lower than 10 % upon TX100 treatment were discarded.

## 6.2. Interpretation of typical photo-triggered release patterns

*All the following steps were performed rapidly (within the 2 hours following the gel filtration step), in the dark or under weak ambient light, to prevent the trans isomerization of azobenzene. In a typical experiment, the stock solution of liposomes was diluted (about 100 fold) in the running buffer (1× PBS) and the fluorescence of calcein was recorded (excitation at 495 nm, emission at 515 nm) before and after exposure of the sample to blue light, and finally after supplementation with TX100, a surfactant that fully dissolve the liposomes. A typical fluorescence pattern is shown in figure 6.4.*

The initial fluorescence intensity corresponds to solutions containing polymers in their "predominantly cis" isomer form. It was checked that this intensity was stable for about 100–500 s in the fluorimeter. The stability (absence of leakage) was also revealed by the repeatability of the initial fluorescence of liposomes solutions prepared from their stock

solution at times 20 min, and 40 min after the first measurement (i.e. subjected to additional incubation in the dark).

The sample was then irradiated with blue light (370 ± 10 nm) for 1 or 5 min (14 mW/cm²). (N.B.: during irradiation, the recorded signal had no meaning as the excitation mirror was moved to prevent damages to the detector). After stopping the light source, fluorescence measurement was immediately resumed and its variation was recorded typically for 30 minutes. Finally, 20 µL of a 100 g/L Triton X-100 was added in the 2 mL sample, which achieves a ratio of 120 molecules of Triton X-100 per molecule of lipid (see appendix *E.2.3 Forced release test*, p. 212). The immediate dissolution of vesicles in the presence of TX100 is reflected by an abrupt jump of fluorescence intensity that indicates the release of the entrapped calcein. The final intensity corresponds to a complete release from the liposomes (see figure 6.4). The experimental procedures involved here are detailed in appendix E.2.3, p. 212.

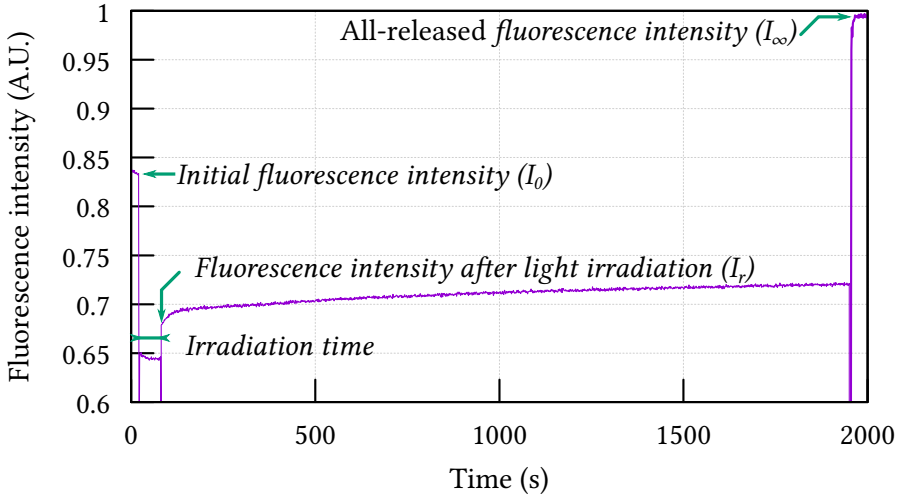


**Figure 6.4.** *Representative fluorescence variations by a solution polymer-containing liposomes loaded with 25 mmol/L calcein. In this example, the weight ratio of components were 7:1:2 DOPC:polymer:cholesterol, dispersed at a total concentration of 1g/L lipid, purified by gel filtration, and finally diluted 100 fold in PBS.*

Using a conventional interpretation, it is expected that leakage is primarily responsible of the variation of fluorescence, and one generally assumes that the difference between intensities measured at time $t$ and at time 0 – here before irradiation – varies in proportion to the amount of released calcein. However, we observed in practice that the intensities measured immediately after exposure to blue light was always lower than before irradiation, making the use of conventional interpretation difficult. Possible bias or artifacts that may affect measurements are:

**Effect of internal filter or turbidity** In the case of high effective absorbance of solutions near wavelength of excitation or emission, variation of UV-vis spectra can change the apparent fluorescence.

**Quenching** Azobenzene molecules are efficient quenchers. The cis-trans isomerization may change the quenching efficiency and affect the fluorescence. The quenching properties of the azobenzene are well-known, and they even lead to the development of efficient commercially-available quenchers, like the Black Hole Quenchers ® by Biosearch Technologies and DABCYL by Invitrogen.

**Bleaching** Calcein absorbs blue light (470 nm) significantly and may slowly bleach upon irradiation in water.

In order to analyze the fluorescence data, we estimated the possible contributions of each bias cited above.

### 6.2.1. Negligible quenching and negligible internal filter effects

First, the expectation of proportionality of the emission with the concentration of free calcein shall be valid. The encapsulated volume fraction in the sample was lower than $8{\cdot}10^{-5}$ (this value is obtained by assuming that all the lipids were collected from the stock solution of liposomes, see appendix C.4.1, p. 200), the corresponding total concentration of calcein was therefore below 180 nmol/L. This is the maximal possible value, and is ten times lower than the threshold concentration of calcein self-quenching (see figure 6.3, p. 90).

Second, the absence of quenching and the absence of bias due to absorbance by the polymer was experimentally controlled in calcein solution without liposomes. To this aim, the fluorescence of a 200 nmol/L calcein solution in PBS was measured before and after addition of 10 g/L of cis azo-polymer to reach a final polymer concentration of 0.99 mg/L (addition of 20 µL in 2 mL). The drop of fluorescence shown in figure 6.5 is essentially due to the 1 % dilution, and any contribution of (cis)polymer absorbance represent less than 1 % change in fluorescence.

Every 5 minutes the sample was irradiated for 1 minute alternatively with UV or blue light, to form predominantly trans or cis isomers. The details of the experiment are described in appendix C.3.3, p. 199. The fluorescence intensity for the *1 minute irradiation* was not sensitive to UV/blue irradiation cycles, showing that the effects of absorbance of the solution, and quenching by the polymer were negligible.

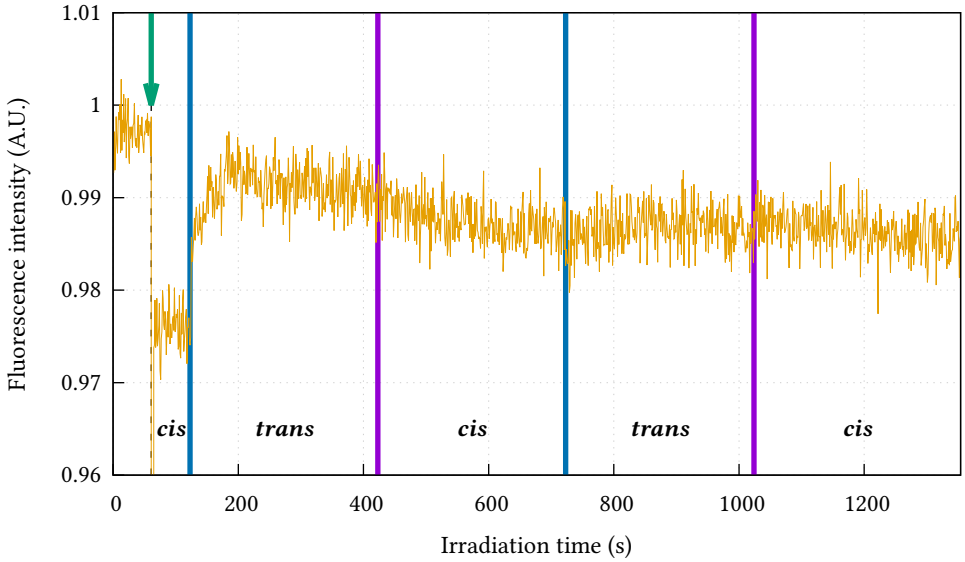


**Figure 6.5.** *Fluorescence intensity of a 200 nmol/L calcein solution in PBS. Green arrow: (cis) azo-polymer is added to yield a solution of 198 nmol/L calcein and 0.99 mg/L azo-polymer (1 % dilution). At each plain vertical bar, the recording was stopped for 1 minutes and the solution was irradiated with UV (purple bar) or blue light (blue bar). Blue light specifications: 470 nm, 14 mW/cm². UV light specifications: 365 nm, 5 W/cm².*

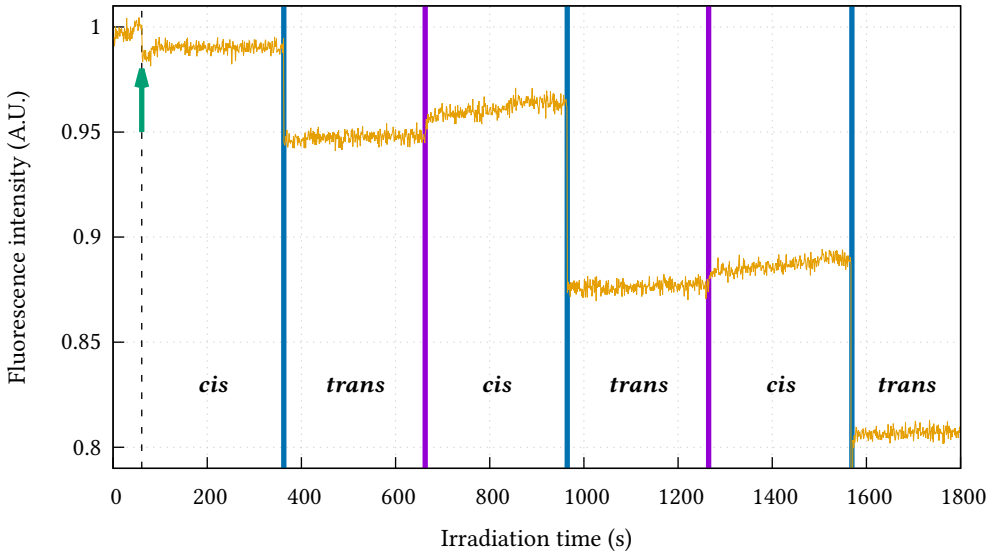


**Figure 6.6.** *Fluorescence intensity of a 200 nmol/L calcein solution in PBS. (cis) azo-polymer was added in the solution (final concentration 0.99 mg/L, green arrow). At each plain vertical bar, the recording was stopped for 5 minutes and the solution irradiated with UV (purple bar) or blue light (blue bar) for 5 minutes.*

### 6.2.2. Contribution of bleaching at long irradiation times

To assess whether bleaching may occur, we considered longer exposure to blue light. Similarly as reported above, a freshly prepared solution of calcein+polymer (no lipid) was exposed to cycles of UV/blue irradiation, but for 5 minutes instead of 1. The resulting fluorescence variation is shown in figure 6.6. The initial addition of the polymer approximately diluted the solution by 1 %. The irradiation with UV light did not significantly affect fluorescence, compared to irradiations with blue light that decreased the fluorescence intensity by resp. 4 %, 9.5 % and 10 % at each successive exposure. The impact of 5 minutes irradiation with blue light can not be neglected.

For that reason we controlled the preservation of total calcein fluorescence by a comparison of the liposomes-containing samples prior and after exposure to blue light (comparison of the total fluorescence recovered after addition of TX100, by solutions prepared from the same stock liposome, and subjected or not to 1 min exposure under blue light prior to addition of excess TX100). These controls revealed that exposure to 1 or 5 min blue light did not decrease the fluorescence by more than the experimental uncertainty – the variation of intensity ratios in TX100 containing solution are similar to the error resulting of pipetting that is reflected by the variation of the ratios of initial intensities $I_0$, see table 6.1.

| **Sample ref.** | **S1** | | **S1 NaCl** | | **S2** | | **SChol50%** | **S1 TX** |
|---|---|---|---|---|---|---|---|---|
| **Irradiation time** | 1 min | 5 min | 1 min | 5 min | 1 min | 5 min | 5 min | 5 min |
| $\frac{I_\infty \text{ (blue)}}{I_\infty \text{ (blank)}}$ | 1.03 | 0.99 | 1.08 | 1.07 | 0.98 | 0.79 | 0.83 | 1.00 |
| $\frac{I_0 \text{ (blue)}}{I_0 \text{ (blank)}}$ | 1.04 | 1.09 | 1.0 | 0.98 | 0.97 | 0.81 | 0.93 | 1.07 |

**Table 6.1.** *Ratios of fluorescence of liposomes solutions with (*blue*) or without (*blank*) exposure to blue light (irradiation time shown in sample code). N.B.:* blue *and* blank *refer to different samples.* $I_\infty$ *is the fluorescence measured after addition of TX100,* $I_0$ *the initial fluorescence before irradiation. Sample codes refer to the following compositions: "S1" DOPC:polymer 0.9:0.1 g/g; "S1NaCl" = S1 supplemented with a NaCl solution at time zero; "S2" DOPC liposomes supplemented at time zero with a solution of polymer; "Schol 50%" DOPC:cholesterol/polymer 5:5:1 g/g; "S1 TX" DOPC:polymer 9:1 g/g supplemented at time zero with TX100 at CMC/10 (details on sample preparation are given in the next section).*

It is concluded that the effect of bleaching can be generally neglected, and if not, measurements of intensities in presence of TX100 (such as reported in table 6.1).

## 6.3. Data analysis

Because the main origin of the "after-blue" drop of intensity was not identified, a quantitative evaluation of the degree of leakage from curves such as the one shown in figure 6.4 were not straightforward. The fluorescence values of interest are the initial fluorescence intensity ($I_0$), the intensity measured immediately after exposure to blue light ($I_r$), the intensity at

long time, somewhat arbitrarily fixed at time 20 minutes ($I_{+20\,\mathrm{m}}$) and the total final intensity with excess TX100 ($I_\infty$).

From these data an apparent degree of release – corresponding to the fraction of intensity variation effectively observed between $I_r$ and $I_{+20\,\mathrm{m}}$ – is calculated by $L_{\mathrm{app}} = (I_{+20\,\mathrm{m}} - I_r)/(I_\infty - I_r)$. A priori, this ratio underestimates the degree of leakage, because it does not account for the release occurring during blue irradiation. In particular, the $L_{\mathrm{app}}$ is systematically lower from measurements on samples that were irradiated for 5 min compared to similar samples irradiated for 1 min. As shown in figure 6.7, longer irradiation times lead to missing a fast initial leakage taking place in the 0–5 min interval.

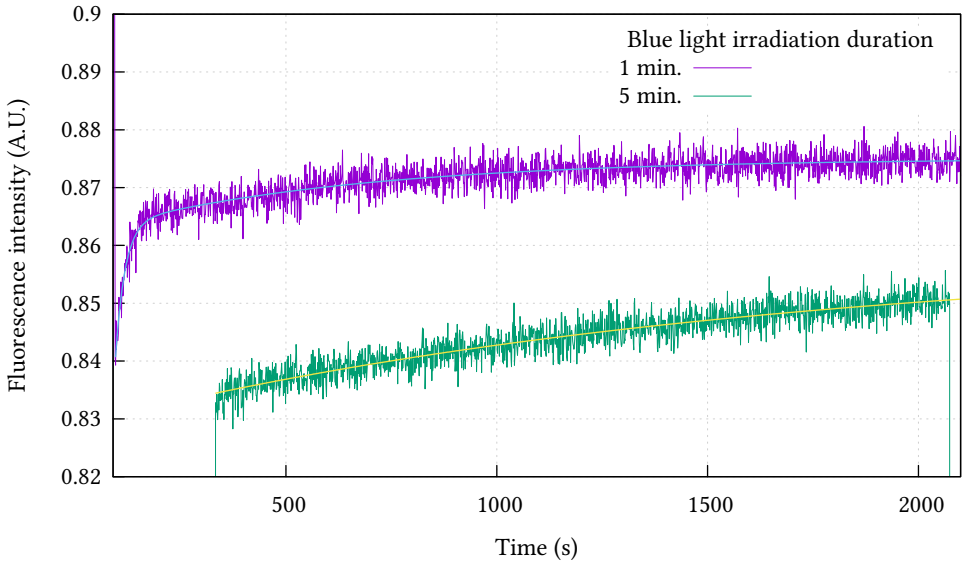


**Figure 6.7.** *Fluorescence intensity of a suspension of $DOPC_{0.9}$/azo-$polymer_{0.1}$ liposomes, recorded after blue light irradiation. The fluorescence increase after irradiation was fitted by a monoexponential curve for 5 minutes irradiation ($\tau$ = 1590 ± 120 s) and a biexponential for the 1 minute experiment ($\tau_1$ = 22.7 ± 1.3 s, $\tau_2$ = 608 ± 33 s).*

An alternative analysis of data is based on an assumption about the origin of intensity loss just after exposure to blue light. We showed in the previous section that quenching by polymer in the bulk solution, bleaching and absorbance do not provide adequate corrections. We propose that the variation of the initial intensity is due to changes occurring in liposomes, where polymer and calcein are both highly concentrated. Quenching of a residual fluorescence from the polymer-containing liposomes is possible for instance, and is expected to increase upon cis to trans isomerization – due to the marked increase of the azobenzene absorption peak at about 350 nm. The extrapolation of the value of the initial intensity after photoisomerization toward the trans form should accordingly enable to estimate the degree of leakage. To this purpose, we assumed that fluorescence intensities can be written before blue irradiation as follows:

$$I_0 = \alpha^{\mathrm{cis}}_{\mathrm{bulk}} \cdot [\mathrm{calcein}]_{\mathrm{bulk}} + \alpha^{\mathrm{cis}}_{\mathrm{ves}} \cdot [\mathrm{calcein}]_{\mathrm{ves}} \tag{6.1}$$

and after blue irradiation:

$$I_r = \alpha_{\text{bulk}}^{\text{trans}} \cdot [\text{calcein}]_{\text{bulk}} + \alpha_{\text{ves}}^{\text{trans}} \cdot [\text{calcein}]_{\text{ves}} \tag{6.2}$$

$$I_\infty = \alpha_{\text{bulk}}^{\text{trans}} \left( [\text{calcein}]_{\text{bulk}} + [\text{calcein}]_{\text{ves}} \right) \tag{6.3}$$

where [calcein] is the concentration of calcein, and $\alpha$ factors taking into account the quenching by the azobenzenes ; *ves* stands for *vesicles*.

Our measurements showed that $\alpha_{\text{bulk}}^{\text{trans}}$ and $\alpha_{\text{bulk}}^{\text{cis}}$ are equal. It comes at $t = 0$ (extrapolation of $I_r$ to an hypothetic zero time where all the trans isomers would already be formed):

$$I_r - I_0 = k \left( I_\infty - I_0 \right), \text{with } k = \frac{\alpha_{\text{ves}}^{\text{trans}} - \alpha_{\text{ves}}^{\text{cis}}}{\alpha_{\text{bulk}} - \alpha_{\text{ves}}^{\text{cis}}} \tag{6.4}$$

The value of the correction factor, $k$, was constrained by physical relevancy of calculated intensities. First, a minimum value was determined from calculation of $(I_r - I_0)/(I_\infty - I_0)$ for all the samples studied: if low or no leakage occurred in one sample, this ratio is expected to be equal to $k$ and its absolute value diminishes when $I_r$ corresponds to a sample with partial leakage. This constrained $k$ to be below −0.8. On the other hand, the correction applied to $I_0$ cannot produce zero or negative fluorescence intensities, which limited the value of $k$ to be above −1.4. Using this range of values, we could extrapolate the maximum degree of leakage from experimental measurements. Interpolated leak results are summarized in table 6.4, p. 99.

### 6.3.1. Liposomes without cholesterol

A representative variation of fluorescence in samples containing DOPC:polymer (9:1 w.) liposomes is shown in figure 6.7. Somewhat arbitrarily the increase with time of fluorescence was fitted by exponential variations, allowing to extract one (monoexponential) or two (biexponential) characteristic time. If the permeability is low, or if poration/breakage of liposomes is a random process, the concentration of calcein outside the vesicles should follows an exponential-like law, as reported in appendix C.4.2, p. 201. Clearly, we could essentially estimate the order of magnitude of the fast characteristic time, mainly captured after 1 min exposure to blue light. The time associated to longer processes was also a rough estimate as it was of the same order as the experimental time. However we were interested primarily by accelerating the release, and a lack of calcein release at time above 10 min was indicative of poor practical efficiency of the photo-stimulation.

The characteristic release time associated with different external conditions of buffer are shown in table 6.2.

In one set of experiments, quoted *S2*, DOPC:polymer (9:1 w.) liposomes were diluted in PBS supplemented with additional "free" polymer (at a concentration of 0.001 g/L and under its cis isomer form, this concentration almost double the total concentration of polymer in the solution). This was performed to establish whether the polymer free in solution may fragilize the membranes. In another set, the ionic strength was slightly increased.

| Sample ref. | S1 | S1 NaCl | S2 | S1 TX |
|---|---|---|---|---|
| **1 min blue irradiation** | 23 ± 1 | 14 ± 1 | 30 ± 1 | – |
| | 610 ± 30 | 640 ± 20 | – | – |
| **5 min blue irradiation** | 1600 ± 100 | 2800 ± 100 | – | 1100 ± 100 |

**Table 6.2.** *Release times obtained from the fit of the fluorescence curves by one or two exponential decay processes, after 1 or 5 minutes of blue light irradiation. Sample codes refer to the following compositions: "S1" DOPC:polymer 9:1 w. ; "S1NaCl" = S1 supplemented with a NaCl solution at time zero; "S2" DOPC liposomes supplemented at time zero with a solution of polymer ; "S1 TX" DOPC:polymer 9:1 w. supplemented at time zero with TX100 at CMC/10 (details on sample preparation are given in the next section). The absence of results, due to non-fittable data, are replaced by a dash.*

The azo-polymer is a polyacid that behaves as a polyelectrolyte at neutral pH. Adding sodium chloride to the buffer has been shown to increase the kinetics of release [217] (case of an amphiphilic polyacrylate similar to the present one, but without azobenzene). Phosphate saline buffer pH 7.4 (PBS) contains 150 mmol/L sodium chloride and 10 mmol/L phosphate, reaching the ionic strength of 172 mmol/L. To change the ionic strength of liposomes, sodium chloride was added to the PBS buffer equilibrating the gel filtration column, and used to elute the liposomes just before leakage experiments. In the example shown, a concentration of 62.5 mmol/L of sodium chloride was used; the sample is quoted *S1NaCl*.

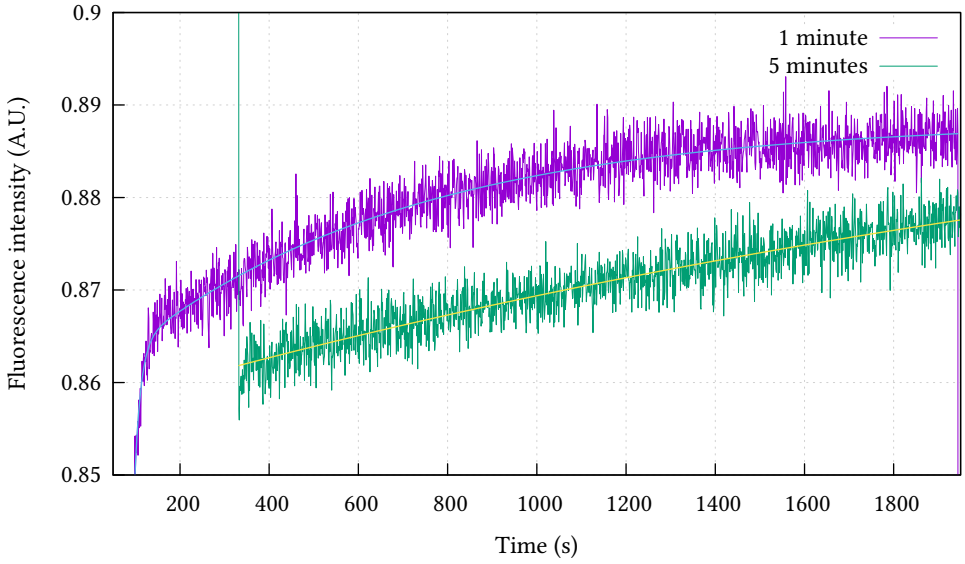


**Figure 6.8.** *Fluorescence intensity of a liposome suspension (90 % DOPC, 10 % azo polymer) in PBS + 62.5 mmol/L sodium chloride.* 1 minute *and* 5 minutes *refer to the blue light irradiation duration.*

In all these conditions, the order of magnitude of the "fast" release time – determined after 1 min exposure to blue light – was 15–30 s, and a longer time of about 10 min was

sometimes needed to match with experimental data. Obviously the apparent slow release time estimated after 5 min exposure under UV light may represents a tail of the initial leakage (usually a residual 10% of apparent release), and converge to the experimental time of observation suggesting that a longer measurement time is required to accurately determine this slow process.

| $C_{\text{Triton X100}}$ (mg/L) | 14.4 | 28.8 | 71.9 | 144 |
|---|---|---|---|---|
| **CMC fraction** | 1/10 | 1/5 | 1/2 | 1 |

**Table 6.3.** *Triton X100 concentrations added to the sample prior fluorescence measurement.*

Finally, we considered the addition of a low concentration of TX100 to fragilize the liposomes, prior to their exposure to blue light (sample quoted *S1 TX*). Triton X100 was added to liposome suspensions to obtain the concentrations shown in table 6.3. Even at CMC/10, the concentration of surfactant (23 µmol/L) was higher than the concentration of lipids (< 13 µmol/L).

At CMC/5 and above all the entrapped calcein was released prior to irradiation, indicating that liposomes were leaky and emptied within the time needed to fill the cell with the sample. The sample at CMC/10, did not show significant fast variation of intensity after 1 minute exposure to blue light. This may be due to either a much faster release, or to the absence of release.

In order to evaluate whether initial release could be faster than a few tens of seconds, and would have been missed in the fluorescence variation, we used the correction of initial intensity $I_0$ described in the previous section. Results are summarized in table 6.4 and show an order of magnitude of 30 % to 50 % release in most cases. Differences between the renormalized degree of release, and experimentally observed (apparent) release ratios is particularly important in the TX100 fragilized liposomes. This suggests that a fast release, occurring in less than 10 s, was reached. However, the lack of release from at least 50 % of the liposomes at time 20 min, even after a 5 min long irradiation, is not understood yet.

| **Sample ref.** | **S1** | **S1NaCl** | **S1 TX** | **S2** | **S2NaCl** |
|---|---|---|---|---|---|
| $L_{\text{app}}$ | 0.28 | 0.27 | 0.03 | 0.29 | 0.20 |
| $L_{k=-0.8}$ | 0.11 | 0.30 | 0.35 | 0.29 | 0.33 |
| $L_{k=-1.2}$ | 0.29 | 0.44 | 0.48 | 0.44 | 0.47 |

**Table 6.4.** *Apparent and extrapolated release ratios of liposome preparations irradiated with blue light for 1 minute. S1: DOPC:azo polymer 9:1 w. S2, same as S1, with azo polymer added to the buffer. S1 TX: same as S1, with Triton X-100 added to the buffer, at a concentration of CMC/10. NaCl means that 62.5 mmol/L sodium chloride was added to the buffer.*

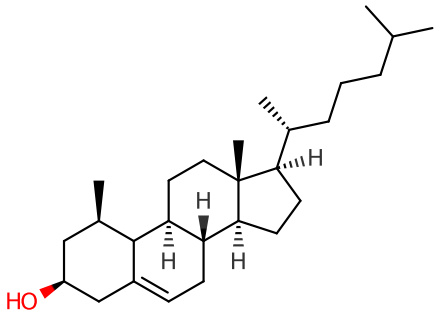


**Figure 6.9.** *Skeletal representation of cholesterol.*

### 6.3.2. Cholesterol-containing liposomes

Cholesterol is a small hydrophobic molecule present in the membranes of mammalian cells. In vitro, it has been shown to modulate the membrane fluidity and the packing of phospholipids in bilayers, and to prevent their transition to gel phase at low temperature. The effect of cholesterol on photoinduced leakage has been reported in the case of azobenzene-containing lipids [73, 75, 77].

Samples were prepared as described in the experiments with DOPC:polymer liposomes, by simply adding cholesterol at the stage of film drying. The azo-polymer was kept at 10 % by weight, and the 90 % lipids included DOPC plus cholesterol. The relative weight amounts of cholesterol and DOPC are summarized in table 6.5.

| **Sample name** | **SChol5** | **SChol10** | **SChol15** | **SChol20** | **SChol50** |
|---|---|---|---|---|---|
| **DOPC (%)** | 94.4 | 88.9 | 83.3 | 77.8 | 44.4 |
| **Cholesterol (%)** | 5.6 | 11.1 | 16.7 | 22.2 | 55.6 |

**Table 6.5.** *Relative lipid composition of films. The sample name derives from the global amount of cholesterol in the lipid film, made of azo-polymer (10 % w.), cholesterol and DOPC.*

As before, the fluorescence intensity of the suspension was recorded before and after irradiation, and finally after adding an excess of Triton X-100. An example of fluorescence variation is shown in figure 6.10, here for the *20 %* sample and does not significantly differ from data recorded without cholesterol. The characteristic release times, the apparent degree of calcein release at time 20 minutes, and the renormalized degree of leakage are shown in table 6.6 and table 6.7.

Concerning the 5 minute irradiation samples, the amount of apparent release varied from 5 % to 17 %, which is comparable to values measured without cholesterol. The fraction of cholesterol in the membrane does not make sense to rank apparent degrees of leakage, and data seem rather subjected to fluctuation from sample to sample. The strong variability in the results does not permit to draw any conclusion regarding the evolution of the apparent release. Renormalizing data to account for the initial drop of intensity after blue light

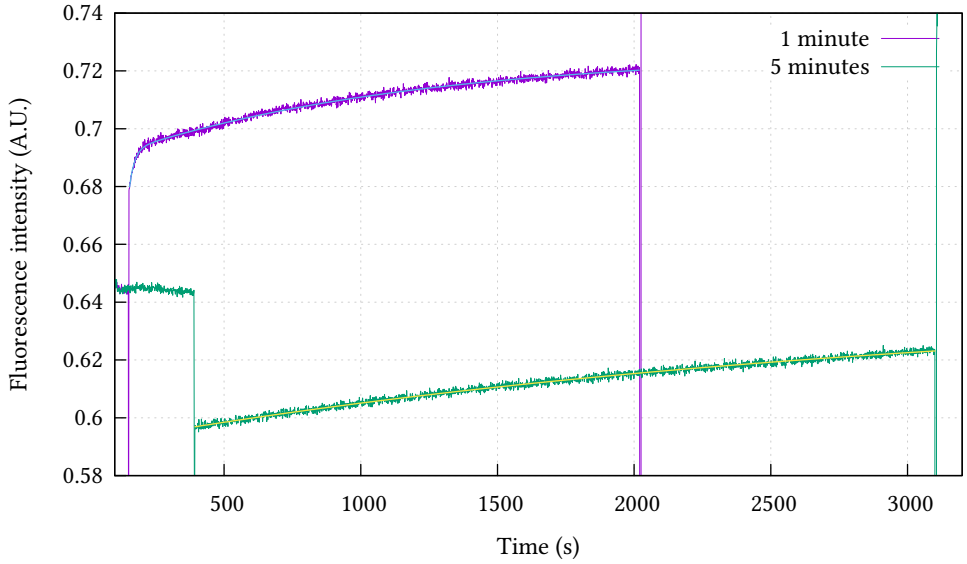


**Figure 6.10.** *Fluorescence intensity of a liposome suspension prepared from the DOPC(83.3 %)/cholesterol(16.7 %) film, after 1 and 5 minutes of blue light irradiation.*

| **Sample name** | **SChol5** | **SChol10** | **SChol15** | **SChol20** | **SChol50** |
|---|---|---|---|---|---|
| **Release times (s)** | 1254 ± 24 | ∞ | 22.1 ± 4.1<br>985 ± 35 | 18.62 ± 0.79<br>1083 ± 15 | 15.02 ± 0.83<br>1043 ± 80 |
| $L_{\text{app}}$ | 0.10 | 0.02 | 0.07 | 0.07 | 0.02 |
| $L_{k=-0.8}$ | 0.13 | 0.50 | 0.22 | 0.25 | 0.22 |
| $L_{k=-1.2}$ | 0.31 | 0.60 | 0.38 | 0.40 | 0.38 |

**Table 6.6.** *Characteristic release times, apparent release ratios and extrapolated release ratios for liposomes made of DOPC:cholesterol:azo polymer loaded with calcein, after 1 minute of blue light irradiation. ∞ means here that the fluorescence intensity curve was almost flat and the exponential fit did not converge.*

| **Sample name** | **SChol5** | **SChol10** | **SChol15** | **SChol20** | **SChol50** |
|---|---|---|---|---|---|
| **Release times (s)** | 2000 ± 100 | 920 ± 50 | 2300 ± 300 | 2900 ± 100 | 1600 ± 100 |

**Table 6.7.** *Characteristic release times for liposomes made of DOPC:cholesterol:azo polymer loaded with calcein, after 5 minutes of blue light irradiation.*

exposure, suggest that degree of fast leakage of the order of 20 % to 30 % could be the effective leakage. This fraction of leakage is similar to the case of liposomes with no cholesterol, and the fast release time is not accessible to our experimental setup.

# Conclusion

Light sensitive liposomes were prepared by inclusion of azobenzene-containing cis-polymers in the lipid, DOPC or DOPC:cholesterol, membranes. Exposure to blue light generally triggers the release of loaded calcein in the medium. In practice, we never measured 100 % release. And reasonable order of magnitude leveled up to 30% (both apparent and renormalized degrees of release). It was surprising that a significant fraction of calcein and/or liposomes did not leak out, in particular in the presence of low concentration of Triton X-100 (CMC/10) that fragilizes the membranes. A fast, partial release may be hidden behind the blue light irradiation, but the lack of full release suggests that the efficiency of polymers has to be questioned further.

The choice of calcein self-quencher, and more generally of fluorescence, to study the release from azobenzene-sensitized liposomes introduces difficulties of quantification due to possible quenching that are essentially unknown as it shall depends on molecular configurations and local concentrations in and around the liposome membranes. It has been chosen for its simplicity of implementation, and the possibility to follow the release in real time. However, the origin of the fluorescence intensity decrease after irradiation remains unknown, and can be attributed neither to photobleaching nor quenching.

For accurate results based on fluorescence, one should replace the calcein by a fluorophore with a red shifted absorption band, which may solve both the photobleaching with the blue light irradiation and the undesired release caused by the fluorescence excitation beam.

# Part III.

# Temperature-sensitive capsules made by the reverse emulsion method

# Introduction

This chapter presents polymer capsules based on thermo-responsive polymers. As mentioned in chapter 4, capsules containing stimuli-responsive polymer membranes are interesting alternatives to liposomes, but they were often prepared in harsh conditions that are not compatible with protein manipulation. Our goal was to adapt the mild procedures of polymer capsule preparation to form capsules with an aqueous core that can be released on demand. The shell of the capsule is composed of water insoluble polymers, which ensures a tight encapsulation. Two main mechanisms can lead to the destruction of the capsule wall:

1. The polymer constitutive of the membrane can be hydrolyzed, or more generally degraded into smaller chains (e.g. photo-cleavable monomers introduced in the chain). Depending on solubility of the products, the membrane is broken into insoluble aggregates or is dissolved.

2. The solubility of polymer constitutive of the membrane can depend on stimulation, but is not involved in chemical reaction.

We implemented the second strategy, based on polymers which dissolve upon stimulation. We believe that absence of hydrolysable monomers should be an advantage for the preservation of stability in complex environments (e.g. enzyme-containing cell culture media). As temperature-responsive systems can be readily turned into light-responsive ones (see chapter 4, e.g. nanoparticle-doped capsules), we studied the introduction of temperature-sensitive chains into capsules.

## Polymer selection

Solubility of polymers depends on the temperature (T). In water, one distinguish polymers that become insoluble at high temperature, and represent the majority of water-soluble chains, from polymers soluble at high T and precipitated at low T.

The upper critical solution temperature (UCST) is the temperature above which a chain becomes soluble. Conversely, below the lower critical solution temperature (LCST) polymers are soluble, while they become insoluble at higher temperature, as shown in figure 6.1. The transition between insoluble and soluble behavior is generally sharp.

To control the permeability of capsules, the critical temperature must be adjusted to the practical conditions of use. A few examples of polymers with a UCST near 37 ℃ in biological mediums are reported [229]. Several polymers with a LCST in water that can be varied

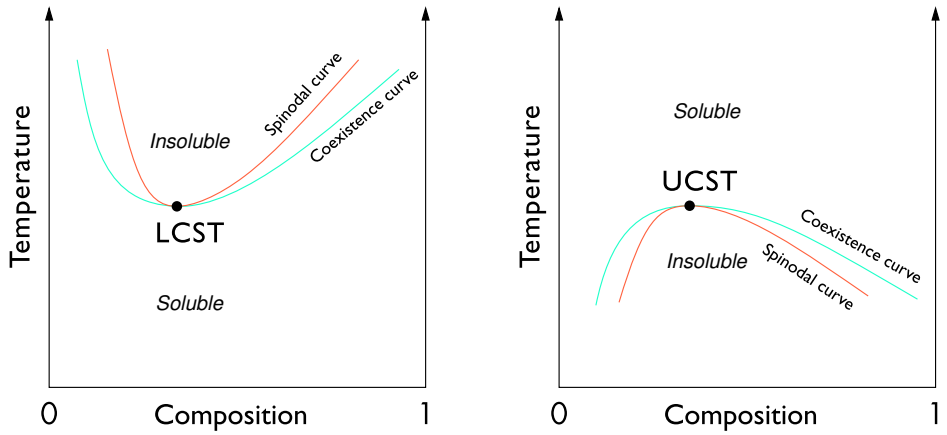


**Figure 6.1.** *Phase diagrams of LCST and UCST polymers in solution, as a function of temperature and the composition of the solution. LCST polymers – left diagram – are soluble at low temperature and insoluble when heated above theirs LCST. UCST polymers – right diagram – are soluble at high temperature and become insoluble when cooled below their UCST.*

to reach values of interest are reported. Popular examples include polyacrylamide and poly(ethylene glycol) derivatives. One of the most developed LCST polymer for biological applications is probably the poly(*N*-isopropyl acrylamide), abbreviated polyNIPAM, whose LCST in biological buffers is near the physiological temperature, ≈ 32 ℃. It is commercially available under various chain lengths and chains ends. Furthermore, polyNIPAM derivatives – imparted with light sensitive properties by the introduction of azobenzene moieties – are under investigations at the laboratory.

We studied one model system based on a LCST polymer, and another one based on UCST polymers. On one hand, the LCST polymer – polyNIPAM – is commercially available. This enables to obtain rapidly a proof on concept of temperature-sensitive capsules, and to characterize the permeability and the degree of release as a function of the temperature.

On the other hand, UCST polymers present several advantages for application, in particular in biological experiments. When the release can be triggered by an increase of temperature, first the tight encapsulation at low temperature facilitate manipulations, and second various localized heating procedures may be implemented – e.g. using an infrared laser, or loading nanoparticles in the capsules[1]. However, neutral UCST polymers are neither common in water nor commercially available. Y. Zhao's team (Sherbrooke University, Canada) is currently developing such polymers [230], and they reported temperature-sensitive polymer micelles, from UCST polymer:polystyrene diblock copolymers. He kindly provided us three polymers, whose general formula is shown in figure 9.1. They differ by their UCST in PBS: 35 ℃, 43 ℃ and 47 ℃, and will be referred later by the value of their UCST.

[1]Gold nanoparticles ability to convert visible or infrared light into heat has been described in part I. We reported liposomes (p. 31), nanogels (p. 46) and LbL capsules (p. 54) made light-sensitive with such particles.

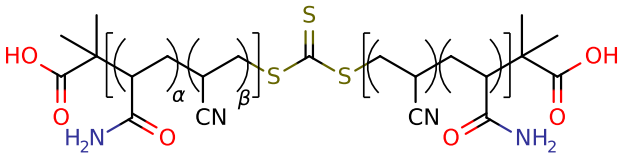


**Figure 6.2.** *Common skeletal formula of the UCST polymers. Molecular weight: ∼ 15 kg/mol. The UCST of the polymer depends on the acrylamide/acrylonitrile ratio. Polymer* 35 ℃*: α = 67.9 %, β = 32.1 %. Polymer* 43 ℃*: α = 66.1 %, β = 33.9 %. Polymer* 47 ℃*: α = 65.8 %, β = 34.2 %.*

## Capsule preparation

Three different strategies have been used to prepare polymer capsules (see chapter 4 page 51): the layer-by-layer assemblies, the polymersomes and the capsules made by interfacial polymerization. Layer-by-layer assemblies and polymersomes have however a limited encapsulation yield and exhibit poor kinetics of release performances. We choose therefore to form capsule shells based on polymerization on droplet surfaces. The group of K. Landfester developed this kind of chemistry based on interfacial polyaddition in inverse emulsion, one reactant being in the water droplets (hexamethylene diamine, HMDA), the other in the oily continuous phase (toluene diisocyanate, TDI)[2]. This strategy allows to reach almost quantitative encapsulation yields. Furthermore, the TDI reactant can be associated with different water-soluble reactants provided that they display amine or alcohol functions.

We adapted this strategy to the synthesis of thermoresponsive capsules using amino-functionalized water-soluble polymers as one of the reactants, or introducing non-reactive polymers in the nascent membranes by spontaneous adsorption. To facilitate the observation of permeabilization, we have in addition considered millimeter-sized capsules – large enough to be viewed by optical microscopy – allowing to check the integrity of the membrane or the fluorescence of an encapsulated dye in real time. In the first section, we describe millimeter-sized capsules made from polyNIPAM, and their response to variation of temperature. The next section presents the basic process that can be used to form nanometer-sized capsules with polyNIPAM. Finally, the last section focuses on the characterization of millimeter-sized UCST capsules.

[2]For details, see section *4.3.2 Synthesis conditions and encapsulation efficiency*, p. 62.

# 7. PolyNIPAM-based millimeter sized capsules

We aimed first at building millimeter-sized capsules, whose shell was composed of a thermoresponsive polymer, namely α,ω diamino terminated polyNIPAM (polyNIPAM-$(NH_2)_2$, or "reactive" polyNIPAM). The shell was obtained by interfacial polyaddition in inverse emulsions. This section is split into three parts. The first one details the modifications of the protocol of K. Landfester that were required in order to obtain millimeter-scaled capsules. The second one presents the synthesis and properties of purely polyNIPAM based millimeter sized capsules. Finally, the third one describes the influence of mixed membrane composition on temperature-triggered release.

## 7.1. Adaptation of published protocols

### 7.1.1. Analysis of K. Landfester's protocol

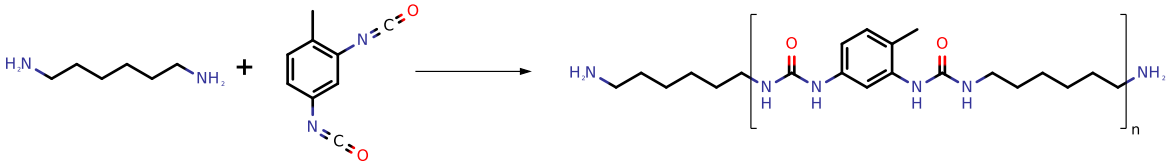

**Figure 7.1.** *Polyaddition occurring between hexamethylene diamine (HMDA) and toluene diisocyanate (TDI). This is the main reaction leading to the formation of capsules.*

The nanometer-scaled capsules reported in reference [231] are made from hexamethylene diamine (HMDA) and toluene diisocyanate (TDI). HMDA is highly soluble in the aqueous phase, at concentrations as high as 100 g/L, but is not soluble into the oil phase – typically cyclohexane. The diisocyanate is soluble in the oil phase, but not soluble in the aqueous one. Polyaddition thus primarily takes place at the water/oil interface, yielding a polyurea based shell, as shown in figure 7.1. This polymer is neither soluble in the oil phase nor in the aqueous one, which leads to the formation of an impermeable and insoluble membrane.

To produce capsules with a diameter below 300 nm, the aqueous phase (containing hexamethylene diamine) is dispersed in the oil phase by sonication in the presence of surfactants. TDI (in the oil) is added at various ratios compared to HMDA, which was

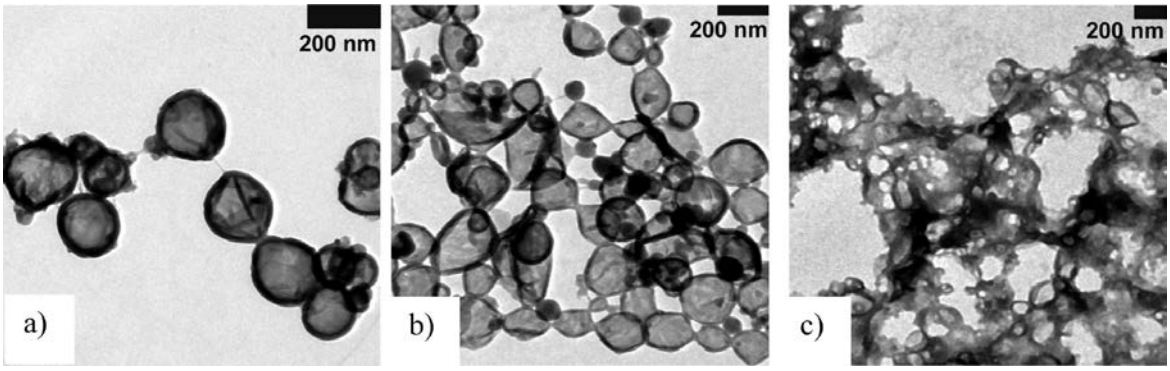


**Figure 7.2.** *Nanocapsules made of HMDA and TDI, viewed by transmission electron microscopy (TEM), directly from cyclohexane. The three samples differs from the HMDA:TDI mol. ratios. (a) 1:2, (b) 1:1.5, (c) 2:1.*

shown to modulate the thickness of the membrane, in the range of 10 nm: the higher the TDI concentration, the thicker the membrane (see figure 7.2). Amounts lower than 1:1 mol. TDI:HMDA did not yield to stable capsules.

### 7.1.2. Synthesis of millimetric capsules

The preparation of millimeter sized capsules does not require high energy emulsification steps. A drop of aqueous phase is simply hanged from a needle in the oil phase composed of cyclohexane and TDI. ≈ 12 drops could be made in each vial without collapse, nor inter-drop attachment. The preparation procedure is detailed in appendix *F.1.2 HMDA millimeter-sized capsules*, p. 218, and is summarized on figure 7.3. The aqueous phase was made of HMDA dissolved in PBS, at the following concentrations: 10 mg/L, 100 mg/L, 1 g/L, 10 g/L and 100 g/L.

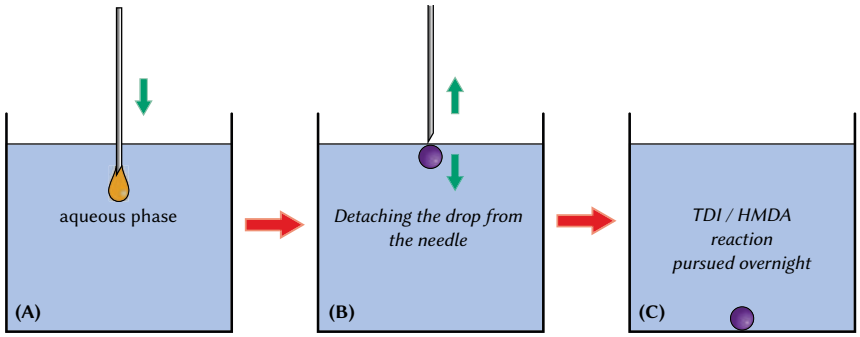


**Figure 7.3.** *Synthesis procedure of model HMDA millimeter-sized capsules. (A) A drop (1 µL) of the aqueous phase is created in the TDI/cyclohexane mixture with a microsyringe/ Depending on the concentration in HMDA, a crumpled membrane appears instantly. (B) The drop is unhooked from the needle at the approach of the oil/air interface. (C) The TDI/HMDA reaction is pursued overnight.*

| **Sample (HMDA conc.)** | 10 mg/L | 100 mg/L | 1 g/L | 10 g/L | 100 g/L |
|---|---|---|---|---|---|
| **Membrane (t = 0)** | No | No | No | Yes* | Yes* |
| **Membrane (t = 12 h)** | No | No | Yes* | Yes | Yes |

**Table 7.1.** *Presence of a membrane around the aqueous phase drop, immediately after adding the drops inside the cyclohexane (t = 0) and 12 hours later (t = 12 h). "*" means that the membrane was not mechanically resistant.*

The drops were observed with naked eye in the cyclohexane, first immediately after introduction in the oil and after overnight incubation (12 hours). Results are summarized in table 7.1.

With the 10 g/L and 100 g/L samples, an opalescence appearing immediately after immersing the drop in the oil phase suggests that the membrane is rapidly formed. Reactions times in the timescale of the minute were however not sufficient to create mechanically resistant membranes, and contact with the side of a needle was sufficient to break the film at that stage of the reaction. Nothing happened in the same timescale with the other samples. 12 hours later, no visible membrane was present around the 10 mg/L and 100 mg/L drops. When two drops were put in contact, they immediately coalesced. The 1 g/L drop was wrapped with a thin film that did not resist to the lateral side of the needle. The film around the last two samples was resistant, and the capsules could be displaced with the needle or a pipette without rupturing it.

The required concentration of HMDA to build resistant capsules – 10 g/L – is substantially higher than the one reported in reference [194]. This may probably be explained by the ability of the diisocyanate to react with water. At low concentration in HMDA, the side-reaction between the isocyanate and the water can't be neglected, and a polyurea matrix is probably created, with inferior mechanical properties. For the next experiments, the concentration of 10 g/L HMDA in the aqueous phase will be used.

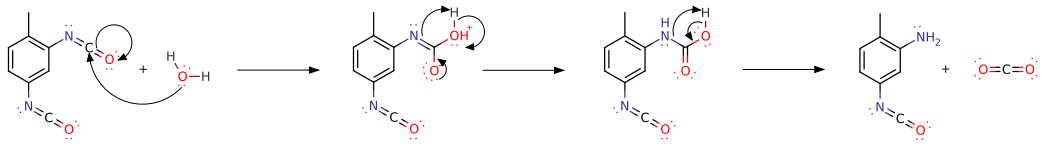

**Figure 7.4.** *Hydrolysis of one isocyanate function of TDI. This reaction leads to the formation of a primary aromatic amine, which can in turn react with an isocyanate function. This will eventually lead to the formation of a polyurea chain.*

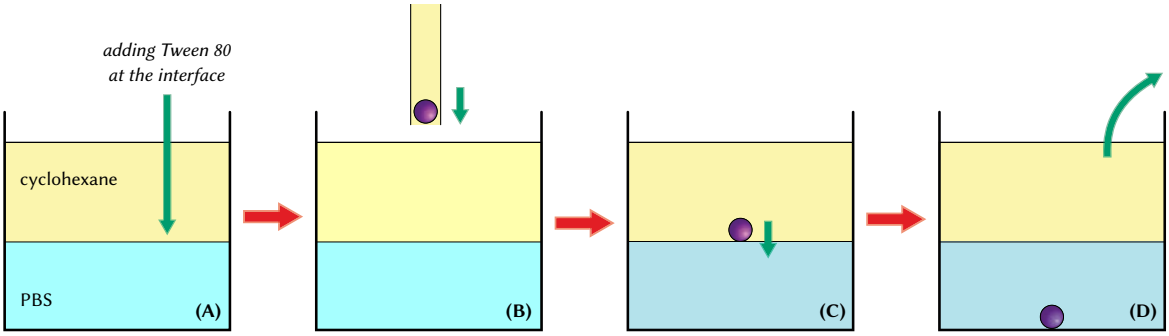


**Figure 7.5.** *Transfer of a millimeter-sized HMDA-based capsule. (A): PBS and cyclohexane are poured in a vial, a small amount of Tween 80 is added at the water/oil interface. (B): The capsule is added in the oil phase and (C) falls on the interface. Due to the presence of the surfactant at the interface and the density of the capsule, the interface is crossed. (D): the capsule is ready for use in an aqueous phase.*

### 7.1.3. Transfer into the aqueous phase

Transferring the capsules into water is a crucial step for further applications of these systems in biological conditions. When the capsule was deposited with cyclohexane on the surface of an aqueous medium, it remained at the oil/water interface. The addition of surfactant in the aqueous phase – e.g. Tween 80, SDS or Triton X-100 – or in the oil phase – Span 80 – did not ease the interface crossing. Pushing the capsule with a pipette or short centrifugation cycles 2,000 rpm for 30 seconds) only led to the rupture of the membrane.

To successfully transfer the capsule in the water phase, 1) we increased the density of the encapsulated aqueous phase, by adding either sodium chloride or sucrose (12 % w. in the case of NaCl, 20 % w in the case of sucrose), and 2) we added a small amount of Tween 80 at the PBS/oil interface, before introducing the capsule. The main disadvantage of this method is the lack of control on the amount of surfactant deposited at the interface. In fact, when "high" amounts were deposited, a gel appeared at the interface preventing the capsules to cross it. Better control was finally achieved by adding a saturated solution of Tween 80 in cyclohexane instead of pure Tween 80. The final transfer procedure is shown in figure 7.5.

## 7.2. PolyNIPAM-based capsules

*Unless explicitly stated,* polyNIPAM *will refer to* α,ω diamino-terminated polyNIPAM *in this section (7.2).*

### 7.2.1. Synthesis of polyNIPAM-based capsules

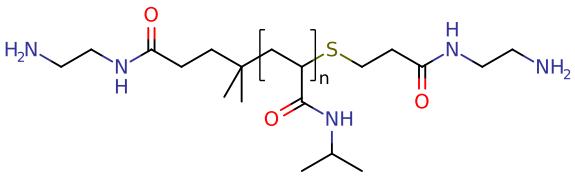


**Figure 7.6.** *Skeletal representation of α,ω diamino-terminated polyNIPAM. Polymer molecular weight: 4,600 g/mol.*

To introduce polyNIPAM in the membrane we replaced the diamine by α,ω diamino-terminated polyNIPAM[1] (see figure 7.6 for the skeletal formula). As polyNIPAM is temperature sensitive, the temperature of preparation needs to be controlled.

1. A gradient of TDI in cyclohexane is created by depositing TDI at the bottom of the vial. Being denser than the oil, the TDI remains here and the concentration at the top of the vial is too low to yield stable membrane.

2. The drop of aqueous phase is created in the oil at a temperature below the LCST of polyNIPAM. This prevents the polymer to make macroscopic aggregates.

3. The temperature of the reaction vessel is then increased above the LCST, to precipitate polyNIPAM that goes partially to the interface; this gives birth to a primitive membrane with poor mechanical properties.

4. The drop is released from the needle and plunge to the bottom of the vial, where the primitive membrane is reinforced by formation of urea bonds between the polyNIPAM chains via reaction with the TDI.

This preparation procedure is summarized on figure 7.7, and detailed in appendix *F.1.1 Capsule preparation*, p. 215.

Concerning the transfer of the capsules in the water phase, the protocol used for HMDA capsules can be reused. The only requirement is to keep the capsules at a temperature above the LCST to prevent their destruction.

[1] This polymer was not commercially available. Commercial α,ω dicarboxy terminated polyNIPAM (Polymer Source, CA) was converted to diamino terminated ones with a carbodiimide-mediated reaction with ethylene diamine. For details on the reaction, refer to appendix *C.2.2 α,ω diamino-terminated poly(NIPAM) synthesis*, p. 195.

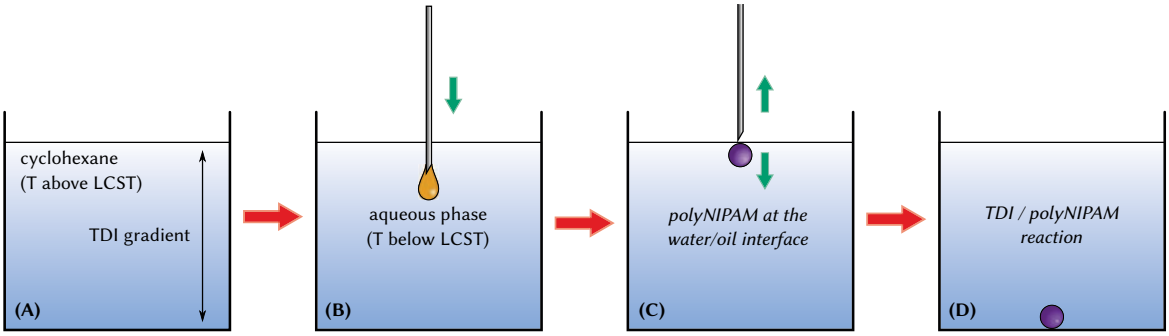


**Figure 7.7.** *Synthesis of the capsule in the oil phase. (A) a gradient of TDI concentration is created in cyclohexane, at a temperature above the LCST. Under these conditions, the concentration in TDI at the top of the cyclohexane is considered null. (B) a drop of the aqueous phase is introduced in the oil with a microsyringe. The syringe and its content are at a temperature below the LCST, allowing the solution to flow through the needle. (C) as the oil is at a temperature above the LCST, the polyNIPAM inside the drop precipitates and goes to the water/oil interface. As the drop was kept in the higher levels of cyclohexane, where no TDI can be found, no reaction occurred yet. (D) the drop is made to fall at the bottom of the cyclohexane, were the membrane is synthesized.*

### Effect of the additives on the LCST of polyNIPAM

In the last section, sodium chloride or sucrose were used to increase the density of the capsule, in order to ease the transfer from the cyclohexane to the aqueous phase. Both have been reported to decrease the LCST of polyNIPAM, as shown in figures 7.8 and 7.9. The concentration of sodium chloride and sucrose were respectively 2.22 mol/L (12 % w.) and 0.63 mol/L (20 % w.). This means that the LCST of polyNIPAM is expected to decrease to ≈ 29 ℃ with sucrose and ≈ 8 ℃ with sodium chloride.

Experimentally, a PBS solution containing 10 g/L in polyNIPAM and 20 % w. sucrose is opaque at room temperature (20–25 ℃), but becomes transparent when cooled below 15 ℃. In presence of sucrose, it is thus possible to make the capsule at room temperature, with a cooled syringe to process the polyNIPAM in its soluble form. A solution of polyNIPAM containing sodium chloride at 2.22 mol/L also appeared opaque at room temperature. The polyNIPAM redissolved only when cooled below 5℃. An interesting consequence of these conditions is that the polyNIPAM membrane will be in contact with two different media: the internal medium and the external one (PBS, in which the LCST of polyNIPAM is 32 ℃). The release experiments will determined whether the polyNIPAM is affected by the internal medium, the external medium of both of them.

### Results

The protocol of synthesis of millimeter sized capsules is detailed in appendix *F.1.2 Evaluation of the effect of sucrose and NaCl on polyNIPAM capsules*, p. 218, and compositions of the aqueous core is reported in table 7.2.

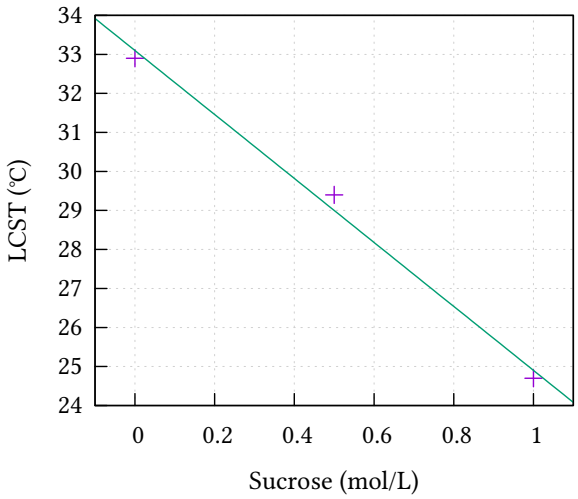


**Figure 7.8.** *Evolution of non-reactive polyNIPAM LCST in water, as a function of sucrose concentration. Polymer concentration: 1 g/L, polymer molecular weight: 16 kg/mol. Reprinted from reference [232] (ESI).*

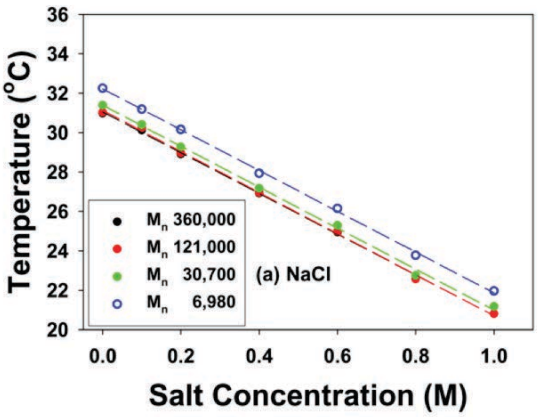


**Figure 7.9.** *Evolution of non-reactive polyNIPAM LCST as a function of the concentration of sodium chloride and the molecular weight of the polymer. Polymer concentration: 10 g/L. Reprinted from reference [233].*

| Sample name | Buffer | [polyNIPAM] (g/L) | additive | $C_{additive}$ |
|---|---|---|---|---|
| **NaCl** | PBS | 10 | sodium chloride | 2.22 mol/L |
| **Sucrose** | PBS | 10 | sucrose | 0.63 mol/L |

**Table 7.2.** *Aqueous phase compositions.*

In both cases, we obtained capsule-like objects in oil. However, the capsules containing sodium chloride did not tolerate the transfer in the aqueous phase: all the processed capsules (≈ 12) burst either at the oil/water interface or within a few seconds in the water phase. The ones made with sucrose were not as fragile and could be transferred into the aqueous phase.

This difference of behavior can be tentatively attributed to the difference of the LCST in both samples. With sugar, the LCST is just below the room temperature; at RT, the aqueous phase looks like a suspension of fine aggregates. With salt, the temperature is much lower. Heating the aqueous phase at room temperature gives a coarse suspension, which may explain why the capsules are fragile. Therefore, we only used sucrose-based samples in the next experiments.

In addition, when capsules were based on longer chains – 22,000 g/mol polyNIPAM, compared to experiments based on 4,200 g/mol one – neither sodium chloride nor sucrose-containing capsules could resist mechanical stress during the transfer in PBS. When the polymer length is increased, the number of amine functions per capsule is decreased, as there is only two amine functions per chain. Increasing ratio between TDI and NIPAM certainly contributes to better resistance due to the insolubility of the aromatic moieties

in water. Finally as a control, we build the capsules from solutions of the commercial dicarboxy-terminated polyNIPAM (4,200 g/mol). In this case, no membrane appeared, even 12 hours after pouring the drops in the cyclohexane + TDI mixture, and drops coalesced when they were brought into contact. This observation confirms that the amine functions at the end of the polymer chains are required to build the capsules.

### 7.2.2. PolyNIPAM capsules: characterization

Pure polyNIPAM (4,200 g/mol) capsules once transferred into PBS at 45 ℃ (> LCST) appeared mechanically resistant. To assess their permeabilization upon temperature shifts, two series of experiments were performed. The first set was to check visually the integrity of the membrane as a function of the temperature. This was performed on a microscope with a temperature-regulated plate, to determine the temperature of membrane breakage at micrometer resolution.

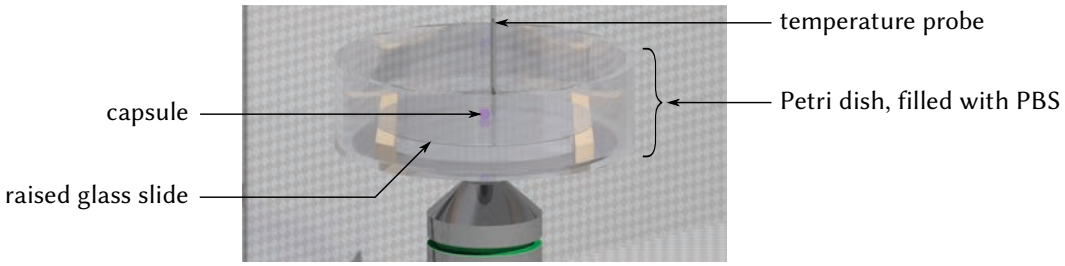


**Figure 7.10.** *Schematic representation of the microscope-based setup used to characterize the capsules. The capsules is placed in the PBS filled Petri dish, whose temperature is controlled with a Peltier microscope plate (not represented). If required, the capsule can be elevated with a glass slide, as shown in the picture. The temperature was measured in the water phase, near (< 1 mm distance) the capsule with a temperature probe.*

The second set of data assessed the permeability of the capsules to various molecules. Capsules were loaded with fluorescent-labeled molecules to estimate, by epifluorescence measurements, the amount of entrapped molecules. The procedure is described in details in appendix *F.1.1 Capsule characterization by microscopy*, p. 217. The setup, at the exception of the Peltier plate, is shown in figure 7.10. To ensure that the whole capsule was at the same temperature as the PBS, it was deposited on an elevated glass slide. Especially this prevented the capsule to be in contact with the bottom of the dish, whose temperature may not be the same as the one of the PBS.

#### Integrity of the capsules as a function of the temperature

We prepared polyNIPAM (4,600 g/mol) capsules with sucrose 20 % w. as reported before. When cooled to ≈ 0 ℃ (ice bath), the capsules may remain apparently intact; however, gentle stirring of the medium completely destroyed them, leading to a dispersion of fine sheets. The same process applied to capsules kept at 45 ℃ did not destroy them.

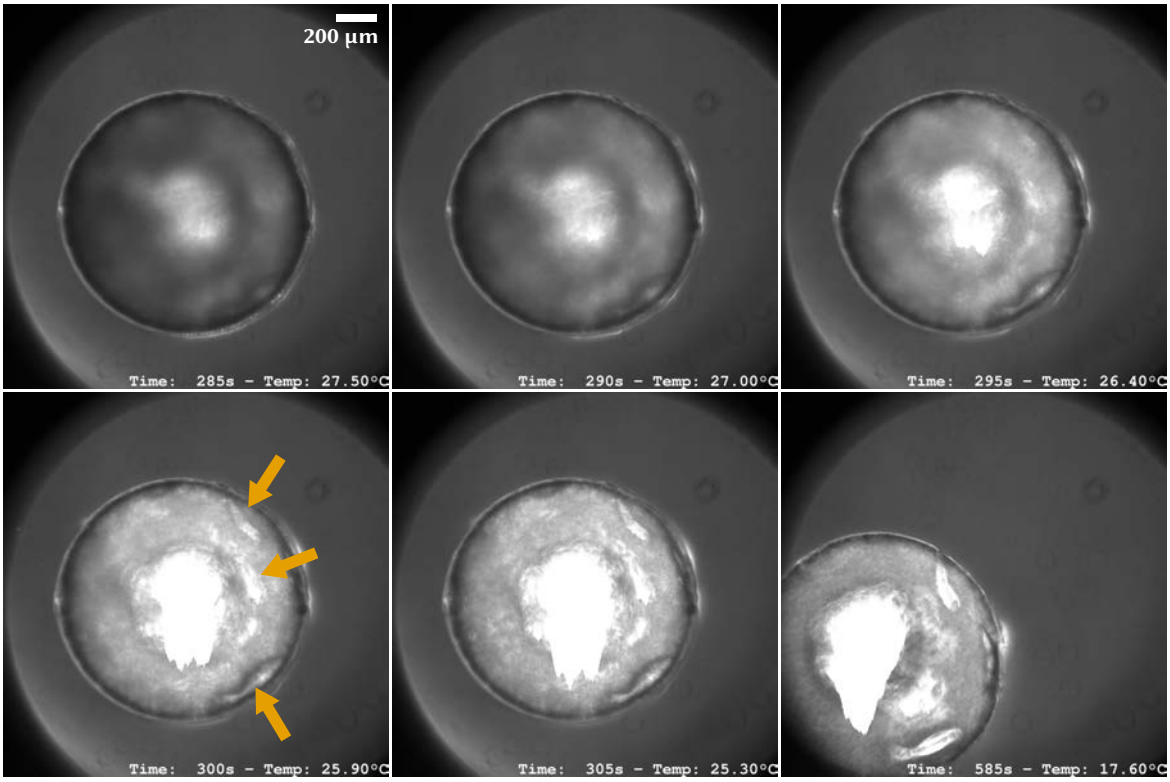


**Figure 7.11.** *Phase contrast images of a polyNIPAM (10 g/L) + sucrose (20 % w.) capsule, upon a decreasing ramp of temperature. Initially, the capsule appear homogeneous. Decreasing the temperature below 27 ℃ made the capsule to appear brighter while lacerations appeared in the membrane (orange arrows).*

Pictures of the capsules were taken by phase contrast microscopy, every 5 seconds, along a ramp of temperature, decreasing from 45 ℃ to 15 ℃ at 10 ℃/min; the temperature was kept at 15 ℃ at the end of the ramp. Examples extracted from a complete pile of photographs is shown figure 7.11. At the beginning of the ramp, the capsule looks homogeneous. When the temperature decreased below 27 ℃, the membrane became spotted by brighter domains and lacerations appeared. At this stage, any movement of the capsule, produced by moving the microscope plate, achieved to disrupt the membrane.

### Characterization of the membrane permeability as a function of the temperature

To characterize the release from these objects, various fluorescent dyes were encapsulated inside the capsules, ranging from small hydrophilic molecules (sulforhodamine 101) to large antibodies. To this aim, the fluorophores were dissolved in the aqueous phase used to produce capsules. The dyes and their concentrations, in the micromolar range, are reported in table 7.3. The detailed preparation and characterization procedures are reported in appendix *F.1.2 polyNIPAM capsules release tests*, p. 219.

| Molecule | Dye | $C_{molecule}$ | $C_{dye}$ |
|---|---|---|---|
| Sulforhodamine 101 | – | 50 µmol/L | 50 µmol/L |
| Dextran (3 kg/mol) | Texas Red | 50 mg/L | ≈ 10 µmol/L |
| Dextran (10 kg/mol) | fluorescein isothiocyanate | 250 mg/L | ≈ 15 µmol/L |
| BSA (66 kg/mol) | Texas Red | 1 g/L | ≈ 40 µmol/L |
| Netrin (68 kg/mol) | fluorescein isothiocyanate | 60 mg/L | 1.9 µmol/L |
| Antibody (150 kg/mol) | fluorescein isothiocyanate | 67 mg/L | 1 µmol/L |

**Table 7.3.** *Fluorescent probes entrapped in polyNIPAM capsules.*

**Sulforhodamine 101** Sulforhodamine 101 is a small (606.8 g/mol) hydrophilic molecule, whose skeletal formula is shown in figure 7.12, best known for its sulfonyl chloride derivative called *Texas Red*. This molecule has been selected because it is reported to bleach less easily than other commonly used fluorophores (e.g. fluorescein isothiocyanate) and because its fluorescence does not depend on the temperature [234].

The temperature and fluorescence intensity inside the capsules are reported on figure 7.13. The fluorescence intensity is quasi-constant at the beginning of the experiment, but decreases when the temperature crosses 36 ℃. This is characteristic of a release of the entrapped dye. The release rate seems to be significant below 34 ± 2 ℃. Approximatively 25 % of the initial fluorescence intensity is lost 10 minutes after crossing the critical temperature (t = 300 s). However waiting longer did not increase this value. 3 hours after, only 30 % leak is attained. Two phenomena can explain this result:

1. A slow diffusion through the membrane (if the membrane becomes permeable, but is not broken). In this case, the fast burst-like release shall presumably be due to

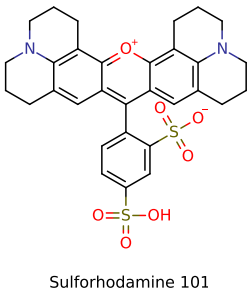


**Figure 7.12.**

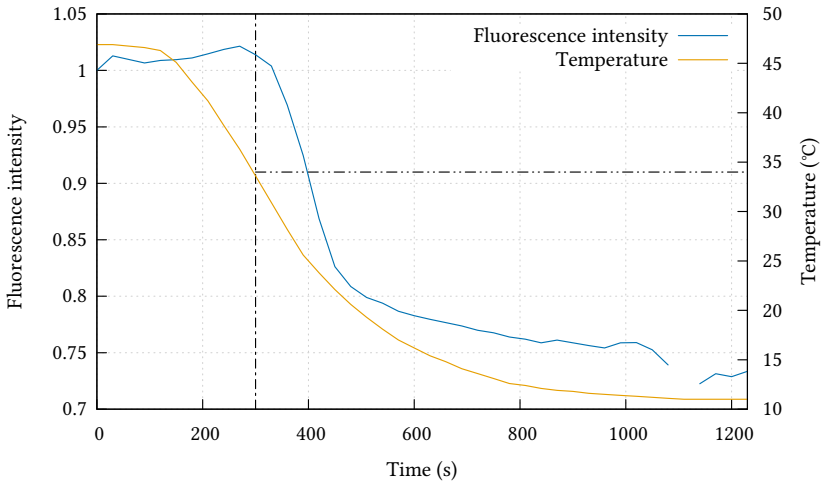


**Figure 7.13.** *Fluorescence intensity of a polyNIPAM capsule loaded with sulforhodamine 101 (50 µmol/L).*

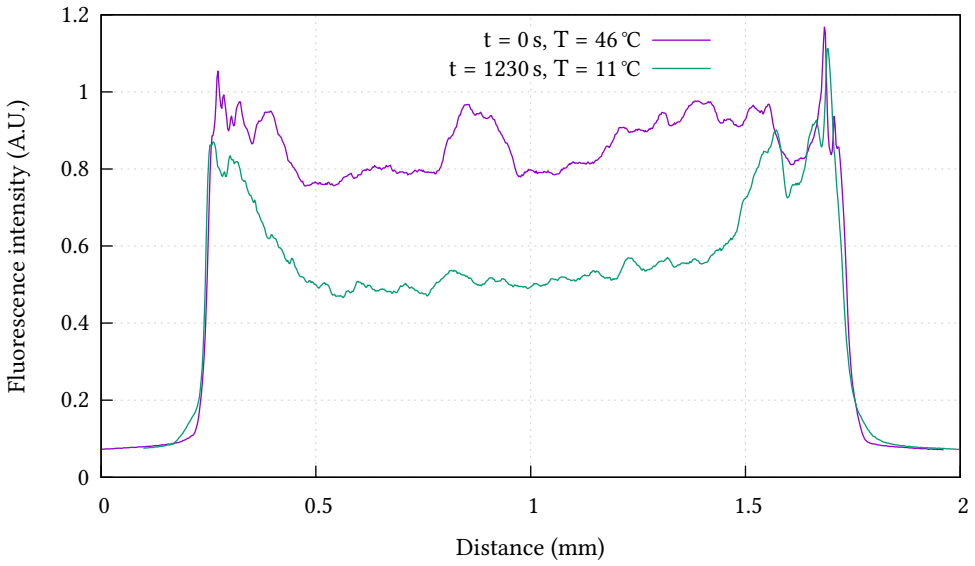


**Figure 7.14.** *Fluorescence intensity profile of a polyNIPAM capsule loaded with sulforhodamine 101, at high temperature (t = 0 s) and low temperature (t = 1,230 s).*

transient opening of large transmembrane pathways under the effect of osmotic pressure difference inside and outside the capsule.

2. The sulforhodamine is trapped inside the capsule and/or the membrane.

We saw that at low T the capsule is torn apart, thus an almost free diffusion of the sulforhodamine outside the capsule is expected. The associated timescale ($t$) can be evaluated with $\tau \sim l^2/D$, where $l$ is the radius of the capsule (1 mm) and $D$ is the diffusivity of sulforhodamine ($\sim 500\,\mu m^2/s$). Evaluating this expression gives about ten minutes, which likely explains the slow release of the entrapped dye.

The fluorescence profile of the capsule at the beginning and at the end of the temperature ramp is shown in figure 7.14. The fluorescence of a sphere projected on a plane, as viewed by a microscope, has a spherical profile. For a 0-centered sphere with a radius $r$, the fluorescence intensity profile is given by the equation:

$$I_{\text{sphere}} = \begin{cases} |x| \leq R, & \sqrt{R^2 - x^2} \\ |x| > R, & 0 \end{cases} \tag{7.1}$$

where $x$ is the profile abscissa (called *distance* in the profile plots). If only the membrane of the capsule is fluorescent, the fluorescence profile becomes:

$$I_{\text{membrane}} = \begin{cases} |x| \leq R, & \sqrt{(R+e)^2 - x^2} - \sqrt{R^2 - x^2} \\ R < |x| \leq R + e, & \sqrt{(R+e)^2 - x^2} \\ R + e < |x|, & 0 \end{cases} \tag{7.2}$$

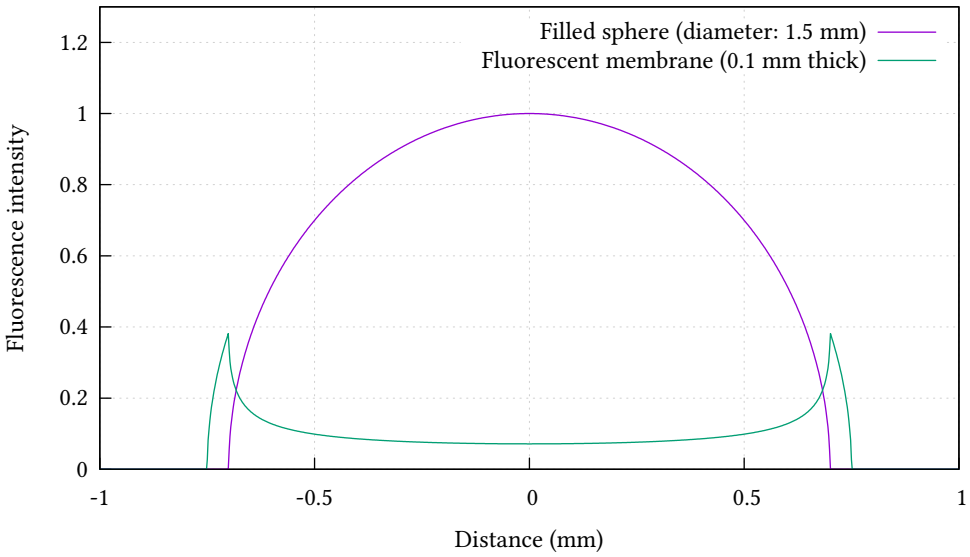


**Figure 7.15.** *Theoretical fluorescence profile of an homogeneous sphere with a radius of 0.75 mm and the one of a membrane surrounding this sphere, with a thickness of 0.1 mm. The concentration of dye is the same in both compartments.*

where $R$ is the radius of the inner capsule core and $e$ the thickness of the membrane. An example is shown in figure 7.15. Lateral peaks, with in between a flat fluorescence profile are thus characteristic of a dye-stained membrane. The fluorescence profile at low T showed typically such a shape. This means that sulforhodamine stained irreversibly the membrane of the capsule, possibly due to hydrophobic binding. This result contradicts what is claimed in references [199, 205], where sulforhodamine 101 is presented as a dye that do not alter membrane composition, and was used to quantify the loading efficiency and the release properties of capsules. Even if the systems are not strictly identical – in reference [199], capsules are made from 1,6-hexane diol and in reference [205] from albumin – this raises some doubts concerning the inactivity of sulforhodamine 101 towards the reaction and its relevance for the characterization of the capsules.

**Dextrans and proteins** Dextran is a branched polysaccharide made from glucose monomers, connected together with α-1,6 glycosidic linkages – branches emerge from α-1,3 linkages. These uncommon linkages are not hydrolyzed by endogenous enzymes, which confers the polysaccharides an improved stability. Thanks to these properties, they are commonly used as hydrophilic macromolecular models. We used here 3 kg/mol and 10 kg/mol dextrans, whose respective hydrodynamic radius are 1.2 nm and 2.3 nm. Finally, we used also fluorescently-labeled proteins. We report here bovine serum albumin labeled with Texas Red (BSA-TR), an antibody labeled with FITC and netrin-1 labeled with FITC[2].

[2]Netrin-1 labeled with FITC is not commercially available. The labelling protocol with fluorescein isothiocyanate is reported in appendix C.2.1, page 194.

In the case of dextran, a typical curve of release is shown in figure 7.17, here for dextran-Texas Red. Fluorescence profiles of the capsules exhibit a spherical shape, as illustrated on figure 7.16. This confirms that fluorescent dextran does not stain the membrane.

The fluorescence intensity slightly decreased at high temperatures; this leak is constantly seen with dextran-loaded capsules. This indicates that capsules are slightly permeable, even at high temperature. Decreasing the temperature made the fluorescence intensity to decrease strongly when a critical temperature was reached. In contrast to the example of sulforhodamine, long term experiments show an almost complete disappearance of the fluorescence inside the capsule. The amount of released dye has been estimated for both dextrans, 10 minutes and 3 hours after crossing the critical temperature. The results are summarized in table 7.4. Finally, dextran loaded capsules – even at a concentration as low as 10 mg/L – are more fragile than the previous ones, and are slightly permeable even at 45 °C. It may be caused by an interference of the dextran with TDI reaction during formation of the membrane (e.g. reaction of hydrophilic dextran with TDI, competing with the polyaddition of NIPAM chains).

Fluorescence intensity curves for BSA-TR and the antibody are shown respectively on figure 7.18 and figure 7.19. The results are summarized in table 7.4.

| **Probe** | **Critical temperature (°C)** | **Released amount** | |
|---|---|---|---|
| | | **10 min** | **3 h** |
| Sulforhodamine 101 | 34 ± 2 | 25 % | 30 % |
| Dextran Texas Red | 27 ± 1 | 19 % | 84 % |
| Dextran FITC | 29 ± 2 | 24 % | 88 % |
| BSA-FITC | 29 ± 1 | 30 % | 40 % |
| Netrin-FITC | – | 0 % | 0 % |
| Netrin-FITC + BSA | 29 ± 2 | 31 % | 76 % |
| Antibody-FITC | 31 ± 1 | 13 % | 25 % |

**Table 7.4.** *Release of fluorescent proteins from polyNIPAM capsules. Temperature of release, amount of dextran released 10 minutes and 3 hours after crossing the critical temperature.*

The amount of protein released 3 hours after crossing the critical temperature is rather low: 25 % for the antibody and 40 % for the BSA, and 0 % for netrin-1. These proteins can react with the diisocyanate and be integrated to the membrane. In fact, we show in the bibliographical review that BSA can be used to create capsules, when reacted with the toluene diisocyanate. To increase the released amount of these proteins from the capsules, one could add a high concentration of BSA in the aqueous core of the capsule. This will decrease the amount of the protein of interest entrapped in the membrane.

This has been tested successfully with netrin-1. BSA was added in large excess (32 times the w. amount of netrin-1). The aqueous phase was therefore made of 60 mg/L netrin-1 and 1.92 g/L unlabeled BSA. From 0 % of release, we obtained the results shown in table 7.4. The

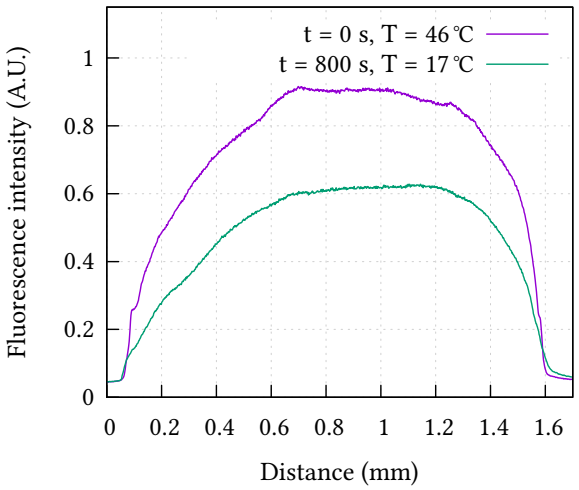


**Figure 7.16.** *Fluorescence profile of a dextran-FITC loaded capsule, at the beginning of the experiment (t = 0 s) and at the end of the temperature ramp (t = 800 s).*

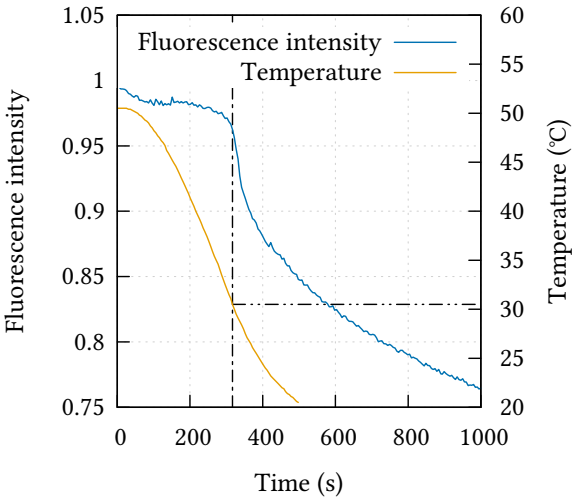


**Figure 7.17.** *Fluorescence intensity of a polyNIPAM capsule loaded with dextran-Texas Red (3,000 g/mol, 50 mg/L), upon a decreasing ramp of temperature.*

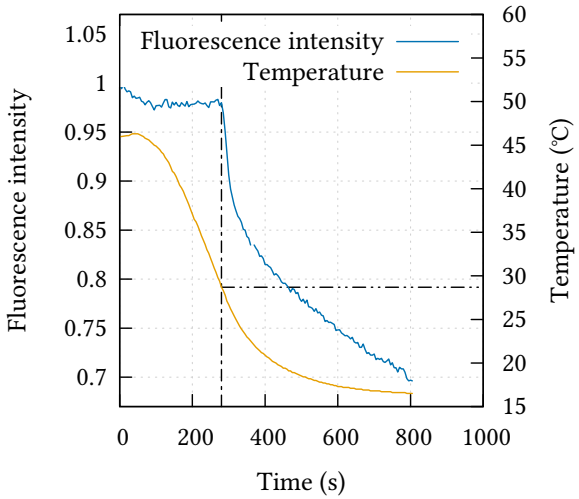


**Figure 7.18.** *Fluorescence intensity of a polyNIPAM capsule loaded with BSA-Texas Red upon a decreasing ramp of temperature.*

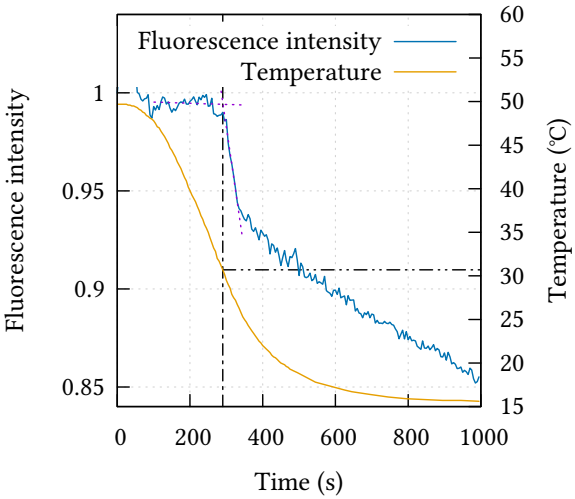


**Figure 7.19.** *Fluorescence intensity of a polyNIPAM capsule loaded with an antibody labeled with FITC upon a decreasing ramp of temperature.*

hypothesized effect of BSA is verified, as 75 % of the entrapped netrin-1 are released within 3 hours.

### Conclusion

The critical temperature and the release are summarized in 7.4. The temperature of release is between 27 ℃ and 31 ℃, typically around 29 ℃, which is close to the LCST of regular polyNIPAM in PBS. Of practical importance, the LCST refers here to critical temperature measured in the outer buffer, not in the solution composition present inside capsules before leakage. The critical temperature of the polyNIPAM+sucrose mixture (≈ 15 ℃) appears clearly below permeabilization conditions.

Embedding the polymer into the membranes does not affect much the dissolution temperature compared to LCST in PBS. The hydrophobic ureas, formed upon attachment of diisocyanate, can explain a slight decrease of critical temperature of release (29 ℃) compared to polyNIPAM LCST (32 ℃).

Finally, we confirmed that a high efficiency of release can be reached if the encapsulated molecule does not interact with the membrane. Concerning the proteins, when encapsulated alone the release was poor, presumably because of the reactivity of amine-containing amino-acids. Indeed, proteins such as BSA can be used to form the shell of the capsule with TDI. Adding an excess of unlabeled BSA increased the performances of the capsules as it competes with the target protein (here netrin) for reaction and formation of the inner surface of the shell.

## 7.3. Effect of mixed membrane composition

In the last section we described temperature-sensitive capsules made of pure α,ω di-amino-terminated polyNIPAM. In order to finely tune the encapsulation and release properties of the capsules, we modulate the composition of the shell by using both HMDA and polyNIPAM. To figure out whether homogeneous distribution of both HMDA and NIPAM polymers can be obtained, the Hildebrand solubility parameters (δ, expressed in $cal^{1/2}{\cdot}cm^{-3/2}$) were estimated. When the difference between the solubility parameters is higher than (e.g. more than one unit), polymers are considered to be not miscible. For polyNIPAM, this value equals 10.0 $cal^{1/2}{\cdot}cm^{-3/2}$; the value for the polyurea obtained from HMDA+TDI is not available in the literature, but has been calculated to 18.8 $cal^{1/2}{\cdot}cm^{-3/2}$ using the values given in reference [235]. The two polymers are thus not compatible: depending on the concentration ratio of both compounds, we may observe *domains* of one polymer entrapped in a matrix made of the other, as illustrated on figure 7.20. If polyNIPAM domains are entrapped in an insoluble polyurea matrix, the LCST of these plug-like domains should be essentially unaffected by the surrounding matrix. On the other hand, more homogeneous mixing and copolymerization is expected to produce membrane

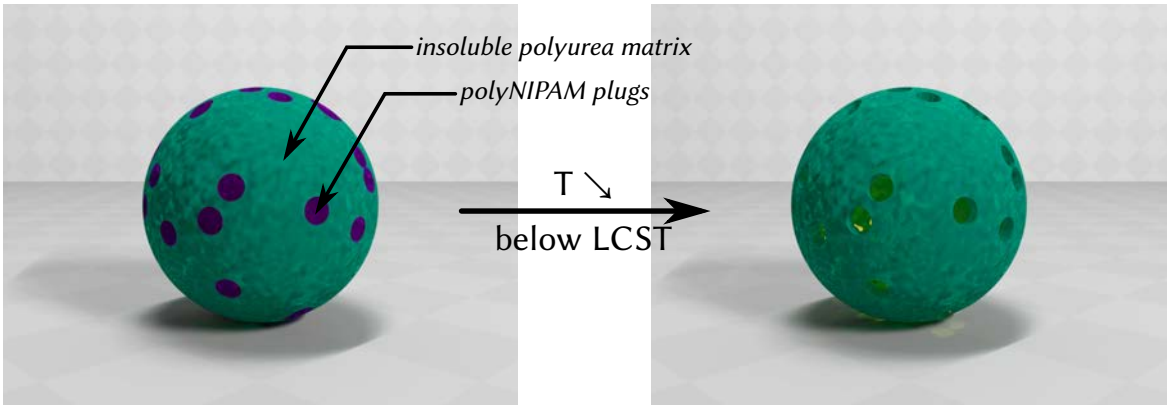


**Figure 7.20.** *Illustration showing, on the left, a capsule made with an insoluble polyurea matrix (in green, made from HMDA + TDI) entrapping plugs of polyNIPAM (in purple). Above the LCST of polyNIPAM, the plugs are impermeable and stays in place. When the temperature is decreased below the LCST – picture on the right – the plugs dissolve and the content of the capsules is released by the newly created holes.*

whose permeabilization occurs at decreasing temperature with increasing HMDA or that are not responsive at all to temperature shifts.

In this section we describe capsules made from mixtures of HMDA and polyNIPAM. We assessed the effect of varying ratio between α,ω diamino-terminated polyNIPAM (4,600 g/mol) and HMDA.

### 7.3.1. Reactive polyNIPAM and HMDA mixtures

The capsules were prepared as reported in the previous section, from α,ω diamino-terminated polyNIPAM and HMDA mixtures. The total weight concentration of "monomers" – i.e. polyNIPAM and HMDA – in the aqueous phase was kept constant and equals to 10 g/L. Various composition of capsules were tried; their composition is reported in table 7.5 (the detailed preparation and characterization procedures are reported in appendix *F.1.2 Reactive polyNIPAM+HMDA capsule release tests*, p. 219).

| **Sample name** | 5 % | 10 % | 25 % | 50 % |
|---|---|---|---|---|
| **$C_{polyNIPAM}$ (g/L)** | 0.5 | 1.0 | 2.5 | 5.0 |
| **$C_{HMDA}$ (g/L)** | 9.5 | 9.0 | 7.5 | 5.0 |
| **Release** | No | No | Yes | Yes |
| **Glucose** | Yes | Yes | Yes | No |
| **Temperature (°C)** | – | – | 20 ± 1 | 30 ± 1 |

**Table 7.5.** *Composition of the aqueous phase used to build capsules, release conditions (presence of glucose) and temperature of release.*

The first batch of capsules was loaded with dextran-Texas Red (3,000 g/mol, 50 mg/L). However, we were not able to transfer the capsules with a low amount of polyNIPAM (5 %, 10 % and 25 %) in the aqueous phase. They all burst at the oil/water interface during the dispersion process, regardless the presence of Tween 80 at the interface. Replacing the dextran with sulforhodamine 101 (50 µmol/L) allowed to build capsules transferable to water, but all burst within minutes in the aqueous phase after the transfer. This was attributed to osmotic pressure. Therefore, we replaced both the transfer buffer and the one used for the fluorescence measurements with PBS supplemented with 11 % w. glucose. This enabled to equals the concentration of sucrose in the capsules, while ensuring that the density of the transfer buffer (1.04) remained lower than the one of the capsules (1.08). Due to the presence of glucose, a decrease of the polyNIPAM LCST is expected. With 11 % w. glucose (≈ 0.63 mol/L), the LCST is expected to decrease to 27 ℃ (see figure 7.21).

The samples 5 %, 10 % and 25 % were processed with 11 % w. glucose. The 50 % capsules were solid enough and have been processed without glucose. The fluorescence intensity of the first three samples are reported on figure 7.22.

Samples 5 % and 10 % did not release their content upon a temperature decrease. Conversely, the sample 25 % gives a fluorescence curve comparable to the ones obtained for capsules made of 100 % polyNIPAM. The critical temperature of release is 20 ± 1 ℃, which is below the expected LCST of polyNIPAM in presence of glucose (11 % w.). Increasing the polyNIPAM/HMDA ratio led to more resistant capsules. At 50% polyNIPAM, a behavior comparable to the one of the 100 % capsules was obtained (see figure 7.22). All the results are summarized in table 7.5.

These results confirm the possibility to build temperature-sensitive capsules from polyNIPAM/HMDA mixtures, though they appeared to be of lower mechanical stability than pure polyNIPAM-based capsules. A minimum concentration ratio exists below which the capsules are no longer temperature-sensitive, and it is located between 10 % and 25 % polyNIPAM: when the concentration of HMDA is higher than 75 %, the membrane made mostly of insoluble polyurea matrix dominates.

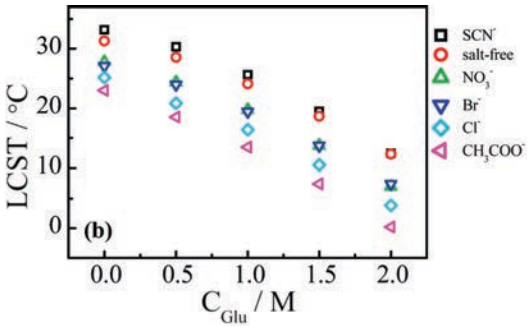


**Figure 7.21.** *Evolution of polyNIPAM LCST in water, as a function of glucose concentration, and in presence of various ions. Here, only the salt-free case is of interest (the red circles). Polymer concentration: 1 g/L, polymer molecular weight: 16 kg/mol. Reprinted from reference [232].*

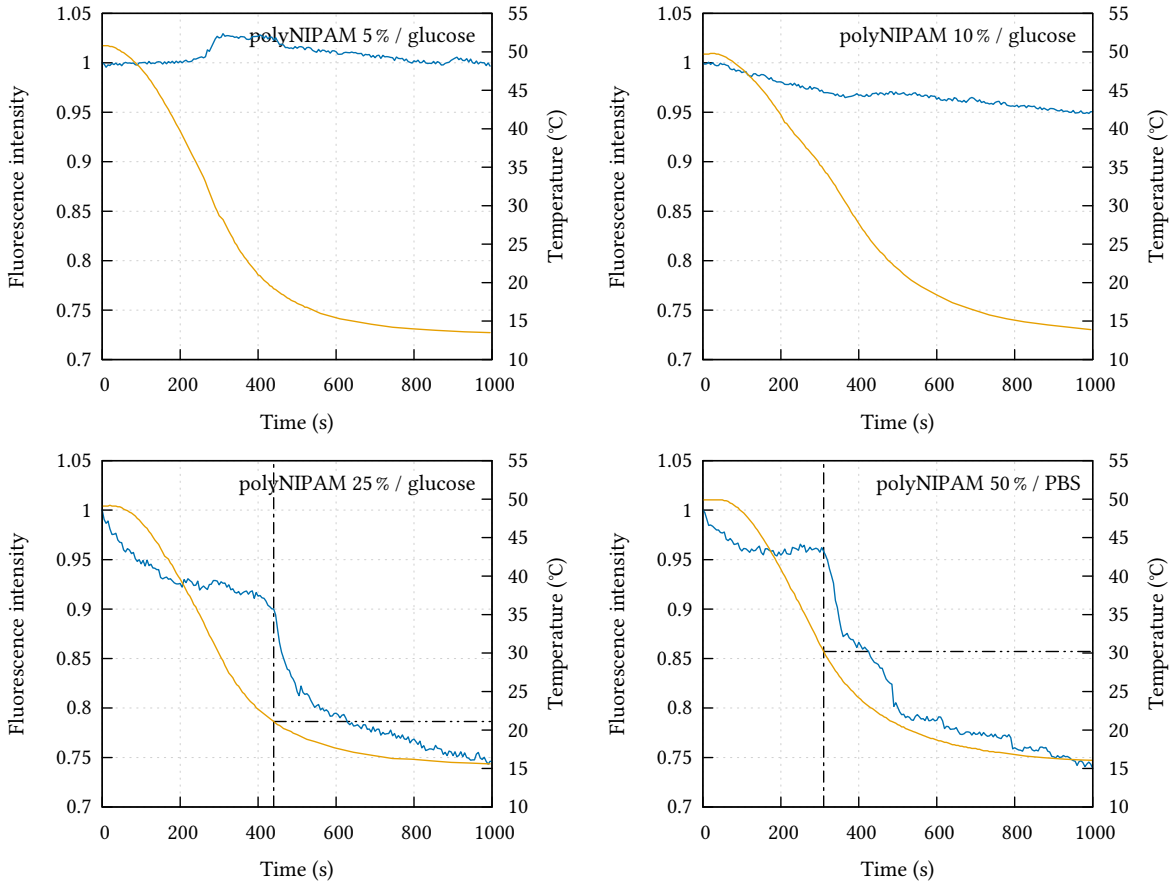


**Figure 7.22.** *Fluorescence intensity of capsules made from HMDA/α,ω diamino terminated polyNIPAM mixtures, filled with 50 µmol/L sulforhodamine 101, submitted to a decreasing ramp of temperature. —— temperature, —— fluorescence intensity.*

### 7.3.2. Unreactive polyNIPAM and HMDA mixtures

Finally, we prepared capsules from HMDA and non-reactive polyNIPAM mixtures. To keep the length of polyNIPAM chain constant, the commercial precursor of the reactive polyNIPAM was used, a α,ω dicarboxylic acid terminated polyNIPAM.

Samples were prepared as before, by adding the non-reactive polyNIPAM and HMDA to the aqueous phase. The processed samples are reported in table 7.6 (the detailed preparation and characterization procedures are reported in appendix *F.1.2 Unreactive polyNIPAM+HMDA capsule release tests*, p. 220). The capsules were loaded with dextran-Texas Red (50 mg/L). The capsules obtained with this probe were resistant enough to be transferred into the aqueous phase, even in the absence of glucose.

| **Sample name** | 5 % | 10 % | 25 % | 80 % | 90 % | 95 % | 100 % |
|---|---|---|---|---|---|---|---|
| **[polyNIPAM] (g/L)** | 0.5 | 1.0 | 2.5 | 8.0 | 9.0 | 9.5 | 10.0 |
| **[HMDA] (g/L)** | 9.5 | 9.0 | 7.5 | 2.0 | 1.0 | 0.5 | 0.0 |
| **Solid capsule** | Yes | Yes | Yes | Yes | Yes | No | No |
| **Temperature-sensitive** | No | No | No | No | Yes | – | – |
| **Temperature of release** | – | – | – | – | 40 ± 1 ℃ | – | – |

**Table 7.6.** *Capsules made from amino-terminated polyNIPAM and HMDA, composition of the aqueous phase and properties of the capsules.*

In contrast to the results obtained with the reactive (amine-terminated) polyNIPAM, 25 % and 50 % polyNIPAM did not yield temperature-sensitive capsules with the non-reactive polymer. This suggests that amino-terminated polyNIPAM was incorporated into the membrane via its reaction with TDI. At higher polyNIPAM/HMDA ratio temperature-sensitive objects were however formed, as reported in table 7.6. Three regions can be extracted from this table. Below 80 % polyNIPAM, capsules are not temperature-sensitive: no release was detected when they were submitted to the decreasing temperature ramp. Between 80 % and 95 %, fragile temperature-sensitive capsules are obtained. Above 95 %, the reaction did not lead to capsules, even after 12 hours reaction, and drops coalesced rapidly in the oil or burst when transferred in the aqueous phase.

The responsive capsules differ from the ones containing amino-reactive polyNIPAM by the release temperature. Here, a clear rupture was observed at 40 ℃. The origin of this deviation to the LCST of polyNIPAM has not been found yet. The LCST of the α,ω dicarboxylic acid terminated polyNIPAM in PBS (3 g/L) is 32 ℃; the presence of two carboxylates in the chain does not shift significantly the LCST. Any effect of the matrix should also be unlikely, as capsules made from 50 % reactive polyNIPAM and 50 % HMDA release their content at 30 ℃ in PBS. Complementary experiments have to be performed to improve the statistics of present data.

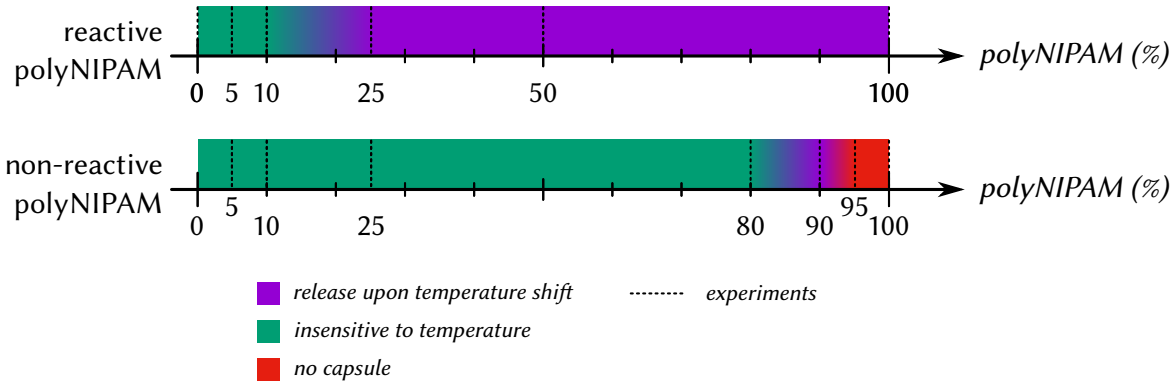


**Figure 7.23.** *Temperature-sensitivity of the capsules made from polyNIPAM, as a function of the relative amount of polyNIPAM in the aqueous phase.*

### 7.3.3. Conclusions

The range of composition compatible with formation of temperature-sensitive capsules are illustrated on figure 7.23. When the polyNIPAM reacts with diisocyanate, and is covalently attached at the interface and *de facto* integrated to the membrane, relatively low [polyNIPAM]/[HMDA] ratios yield temperature-sensitive objects. On the contrary, control experiments with non-reactive polyNIPAM show the lack of responses in most cases. It is likely that the HMDA matrix pushes the polyNIPAM outside the membrane; this is supported by the low miscibility of the two polymers. High concentrations of polyNIPAM in water can nevertheless affect the interface, because of adsorption of polymer aggregates during membrane formation – the temperature is elevated above the LCST at the beginning of the synthesis procedure. Adding just enough HMDA to get a resistant membrane allowed to prepare temperature-sensitive objects without amine-ends in the polyNIPAM. This observation supports the scheme drawn at the beginning of this section, where the polyNIPAM would be entrapped in an insoluble polyurea matrix, and act as soluble plugs.

Another interesting point observed with these capsules is their fragility. For the ones made with reactive polyNIPAM and a high amount of HMDA, we added glucose to equilibrate the osmotic pressures and prevent their burst. This fragility of the membrane is rather surprising, because both polyNIPAM and HMDA are known individually to make mechanically-resistant and impermeable capsules. However, they differ by their flexibility. HMDA lead to flexible membranes, easily deformed; polyNIPAM lead to stiffer membranes (above LCST), not deformed with a similar strain. If the membrane is effectively composed of a continuous insoluble polyurea matrix with inclusions of polyNIPAM domains, this means that stiff domains are surrounded by flexible ones. The capsule is submitted to high shear stresses during the aqueous phase transfer protocol, which probably facilitate breakage of heterogeneous membranes at the frontier between soft and rigid doamins. The transfer protocol could probably be improved to reduce the shear stress.

# 8. PolyNIPAM-based nanocapsules

Besides the synthesis of thermoresponsive capsules, one of our long term objectives is to be able to generate gradients of proteins inside culture gels. When encapsulated in a collagen gel, macrocapsules won't be able to freely diffuse inside the gel. Once their content has been released in the medium, a second release is impossible as no filled capsules can reach the zone. With that system, only pulses of concentration can be generated. To obtain a gradient, a continuous source of protein is required. Therefore, a diffusion of the capsules is necessary in order to refill the zone that was stimulated with loaded objects. For capsules freely diffusing inside the gel, the capsule size has to be smaller than the mesh size of the gel. Objects of around 200 nm seem appealing for that application. This chapter thus focuses on the synthesis and characterization of polyNIPAM-based nanometer-sized capsules.

This work is divided into two parts. The first one deals with the synthesis of the nanocapsules and their re-dispersion in the aqueous phase. The last one focuses on the characterization of the capsules, including the determination of their diameter, their morphology and their release properties.

## 8.1. Description of the synthesis of nanometer sized capsules

### 8.1.1. Analysis of the synthesis procedure described in the literature

The synthesis of nanocapsules by interfacial polyaddition has been described by the group of K. Landfester (see section 4.3.2, page 62). This procedure of preparation of nanometer sized capsules, shown on figure 8.1, involves two steps: the preparation of an fine emulsion followed by an interfacial polyaddition.

The size of the capsules derives from the size of the aqueous droplets involved in the reaction with the diisocyanate. While a syringe was sufficient to create these drops to build millimeter-sized capsules, a more complex method here is required. As we aim to build 200 nm capsules, the droplets must be in the same range. Emulsions with a droplet size in the 20–200 nm range are called nano-emulsions[1]. To reach such a small size of droplets,

[1] As reported in reference [236], several names are given to 20–200 nm sized emulsion: nano-emulsion, miniemulsions, ultrafine emulsions or submicron emulsion. Only the term nano-emulsion will be used thereafter.

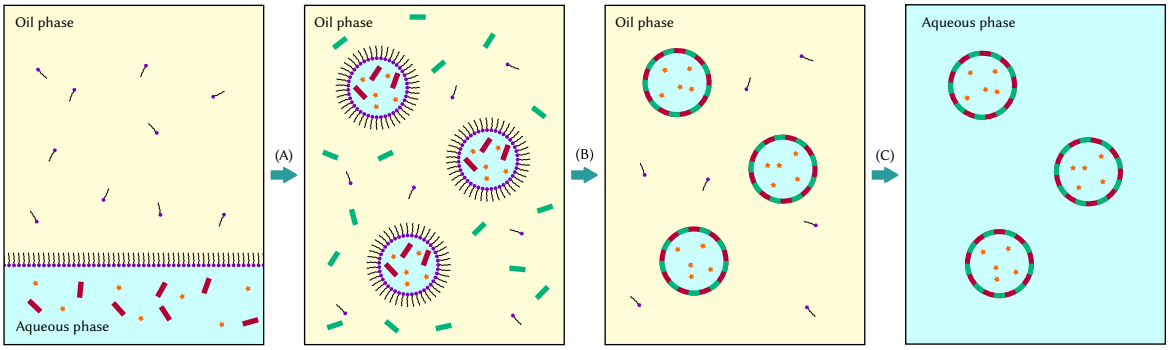


**Figure 8.1.** *Schematic representation of the steps involved in the nanocapsules preparations. (A) the oil phase and the aqueous phase are emulsified to yield a nanometeric scaled emulsion. The aqueous phase initially contains one of the reactant, there a diamine-terminated polyNIPAM (red rectangles) and the molecule to encapsulate, shown as orange stars. After emulsification, the oil-soluble toluene diisocyanate is added (green rectangles). (B) the diisocyanate reacts with the amine chain ends of polyNIPAM at the water/oil interface, leading to the formation of capsules. (C) at the end of the synthesis, the capsules are transferred to the oil phase.*

high energy ultrasounds are often applied to the system [236]. However, we have to keep in mind that these high energy ultrasounds can have a negative impact on the activity of the protein. Fortunately, low-energy methods yielding water-in-oil nano-emulsions have emerged recently [237]. For more details on the nano-emulsions, one may refer to reviews [236–239].

### Choice of the surfactant

In this study, only the ultrasound technique was used to prepare the water-in-oil emulsion. However, we are conscious that this step may have deleterious effects on encapsulated proteins. Therefore, we decided to give priority to surfactants that have also been used in low energy methods. The surfactant can be chosen from one of the following classes:

- anionic molecule, like SDS, potassium oleate,
- cationic molecule, like oleylammonium chloride, oleylamine,
- non-ionic one, like the PEG based $C_xE_y$, Tween or Span.

As the surfactant will enter the aqueous phase, ionic ones must be avoided to prevent the denaturation of the encapsulated protein.

Conversely, the Tween and Span family is often proposed to prepare nano emulsions, as the diversity of available surfactants enable to match the HLB required to emulsify a specific aqueous phase in a specific oil.

Associated in pairs, i.e. one Tween and one Span, a broad range of HLB can be covered, depending on the relative amount of each surfactant. They are thus been used to prepared water-in-oil and oil-in-water emulsions [240–242], and as well as oil-in-water

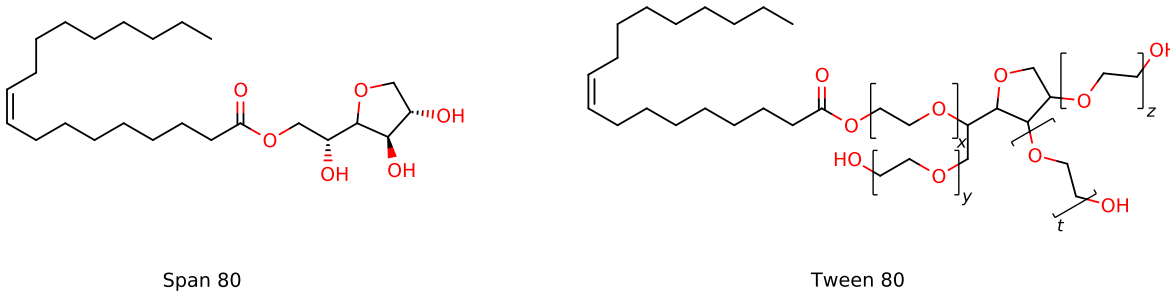


**Figure 8.2.** *Skeletal representation of Span 80 and Tween 80, two biocompatible non-ionic surfactants. Tween 80: $x + y + z + t = 20$, HLB = 15. Span 80: HLB 4.3.*

nano-emulsion [243] and water-in-oil nano-emulsion [244–247]. Moreover, these surfactant are biocompatible – Tween 80 and Span 80, two members of this family shown on figure 8.2, have already been approved as drug and food additives.

### Transferring the capsules from the oil phase to an aqueous phase

The interfacial polyaddition-based synthesis has been conducted in cyclohexane as this solvent was reported to be well suited for the synthesis of nanocapsules [194, 196–200, 231, 248].

As it was the case with the millimeter-sized capsules, the newly synthesized objects must be transferred from the oil to the aqueous buffer. Several methods have already been discussed in the bibliographical review, section 4.3.2 page 62. Briefly, the oil phase containing the suspended capsules is emulsified in an aqueous buffer, with the aid of a surfactant, and then the oil is evaporated, either by heating the emulsion or by stirring for some time at room temperature. Concentrated SDS solutions (≈ 1 g/L) and high power ultrasounds are reported [194]. We decided to exploit this technique to explore the feasibility of synthesizing capsules in oil and transferring them in an aqueous phase, despite the fact that it may be deleterious for encapsulated proteins.

## 8.1.2. Synthesis of HMDA based nanocapsules

The first set of experiment aimed at verifying the possibility to replace the surfactants used in the literature by the Span/Tween mixture. Two things needed to be verified: the stability of the obtained emulsions and the possibility to prepare capsules from HMDA and toluene diisocyanate.

### Emulsions studies

The key point of this study is to find the correct mixture between Span 80 and Tween 80 which lead to stable nano-emulsions of the required size. The aqueous phase contains HMDA at 100 g/L and fluorescein at 1 mmol/L in PBS. The aim of fluorescein was not to

follow the system by fluorescence, but rather to localize the aqueous phase, as this dye is not soluble in cyclohexane. This helped to see with naked eyes whether the system demixed or not. As mentioned before, the HLB of Tween 80 and Span 80 strongly differ, being respectively 15 and 4.3. HLB, the hydrophilic-lipophilic balance, is an empiric value used to quantify the hydrophilic or hydrophobic degree of a surfactant. This value is used to predict whether a surfactant will lead to direct (oil-in-water) emulsions or inverse (water-in-oil) emulsions. HLBs in the 9–15 range tend to make oil-in-water emulsions, while water-in-oil ones are obtained with lower values, in the 3–6 range. For the mixtures of surfactants, one may estimate the HLB of the mixture by the formula $\mathrm{HLB}_{\mathrm{mixture}} = \mathrm{HLB}_{\mathrm{A}} \cdot w_{\mathrm{A}} + \mathrm{HLB}_{\mathrm{B}} \cdot w_{\mathrm{B}}$, where A and B are the two considered surfactants, and $w_{\mathrm{A}}$, $w_{\mathrm{B}}$ their respective weight fractions.

| Span:Tween vol. ratio | HLB | Initial aspect of the emulsion | Aspect 12 h later |
|---|---|---|---|
| 100:0 | 4.3 | Yellow, trouble, homogeneous | Idem |
| 90:10 | 5.4 | Yellow, trouble, homogeneous | Idem |
| 80:20 | 6.6 | Yellow, trouble, homogeneous | Idem |
| 70:30 | 7.7 | Yellow, almost transparent, homogeneous | Idem |
| 60:40 | 8.8 | Yellow, translucent, homogeneous | Idem |
| 50:50 | 9.8 | Yellow, translucent, homogeneous | Demixing |
| 40:60 | 10.9 | Aqueous phase gelation | — |
| 30:70 | 11.9 | Aqueous phase gelation | — |

**Table 8.1.** *Emulsion aspect of the obtained emulsion, unaided eye observation.* Idem *means that no evolution could be detected. HLB estimated with the formula* $HLB_{mixture} = HLB_A \cdot w_A + HLB_B \cdot w_B$.

We prepared emulsions from the different Span to Tween ratio, as reported in table 8.1. The details of the experimental procedure are given in appendix C.3.1 *Characterization of nano-emulsions prepared from Tween 80/Span 80 mixtures* page 197. Depending on the surfactant mixture, yellowish transparent, translucent or opaque emulsions are obtained. Stable emulsions are obtained for the highest ratios of Span 80. For 50 % vol. Span (HLB = 9.8) the emulsion demixed after 12 hours. This is not surprising, as the HLB of the surfactant mixture is outside the water-in-oil HLB range. For the lowest ratios of Span, the preparation of the emulsions was even hindered by the gelation of the aqueous phase. This can be attributed to the high amount of Tween used. Being only partly soluble in the oil, it concentrates in the aqueous phase thereby inducing the transition to a gel state. The aspect of the other emulsions can be explained by the size of the droplets.

Each sample was characterized by dynamic light scattering at t = 0 and t = 12 h, without dilution. The results – the diameter and the associated polydispersity – are summarized in table 8.2. As expected, emulsions prepared with the highest ratio of Span exhibited small droplets sizes and high stability. With lower values, typically the Span:Tween 70:30 vol. ratio, the diameter decreased with time after preparation while no demixing was observed.

| Span:Tween | t = 0 | | t = 12 h | |
|---|---|---|---|---|
| vol. ratio | $D_h$ (nm) | Disp. | $D_h$ (nm) | Disp. |
| 100:0 | 198 | 0.22 | 200 | 0.10 |
| 90:10 | 201 | 0.18 | 221 | 0.12 |
| 80:20 | 197 | 0.18 | 215 | 0.29 |
| 70:30 | 185 | 0.21 | 115 | 0.25 |
| 60:40 | 199 | 0.20 | 276 | 0.25 |
| 50:50 | 222 | 0.20 | – | – |

**Table 8.2.** *Diameter of the emulsified droplets, as measured by dynamic light scattering. The measurements were conducted on emulsions without dilution, immediately after preparation and 12 hours later.*

This suggests that we were close to the micro-emulsion domain, where the emulsions are thermodynamically stable. Decreasing the Span:Tween ratio further lead to unstable emulsions, as seen with the increasing diameter of the 60:40 sample and the demixing of the last one.

### Capsule synthesis

All the previously detailed emulsions with a Span ratio comprised 100 % and 50 % were mixed with toluene diisocyanate. A polyurea shell should be formed from the reaction between TDI and HMDA. All the samples in the range 100–50 % vol. Span reported in table 8.2 were processed. After this reaction step, the samples were transferred into aqueous phase, by emulsifying the oil suspension in a solution of sodium dodecyl sulfate and evaporating the cyclohexane at 70 ℃ for 30 minutes under magnetic stirring. The aqueous samples were filtered on 1.2 µm cellulose acetate prior DLS measurements. The protocol is detailed in appendix F.2.1, p. 222. The diameter of the synthesized objects both in cyclohexane and in water, after filtration, are summarized in table 8.3.

| Span:Tween | In cyclohexane | | In SDS, filtered | | |
|---|---|---|---|---|---|
| vol. ratio | $D_h$ (nm) | Disp. | $D_h$ (nm) | Disp. | kcps |
| 100:0 | 5,190 | 0.32 | 208 | 0.16 | 17 |
| 90:10 | 10,700 | 0.42 | 206 | 0.23 | 5 |
| 80:20 | 1,980 | 0.40 | 218 | 0.11 | 19 |
| 70:30 | 633 | 0.29 | 204 | 0.19 | 10 |
| 60:40 | 344 | 0.22 | 218 | 0.17 | 27 |
| 50:50 | 322 | 0.22 | 217 | 0.17 | 52 |

**Table 8.3.** *Diameter of the capsules in cyclohexane (after synthesis) and in SDS solution obtained by dynamic light scattering.*

In cyclohexane, high amounts of Span lead to aggregated samples, as shown by the high diameter and polydispersities. Conversely, with 60:40 and 50:50 Span:Tween vol. ratios, the diameters of the capsules are close to the diameter of the droplets in the initial emulsion. After dispersion in the aqueous phase, all sample exhibited a diameter close to 200 nm, which suggests some aggregation in the oil phase. However, the intensity of scattered light differs strongly from one sample to the other. Low intensities are obtained with Span 80 concentration in the 100–70 % range, which means there is only a few objects remaining in the aqueous phase. The aggregates visible in the oil phase were probably stuck in the filter. Conversely, high intensities were measured for the two samples obtained with 60 and 50 % vol. Span. These values are highly encouraging. Therefore, the samples prepared in the next parts will be synthesized in the presence of 60:40 and 50:50 Span 80:Tween 80 mixtures.

### 8.1.3. Application to the synthesis of polyNIPAM nano-capsules

In this part, HMDA has been replaced by the diamine-terminated polyNIPAM used in the previous chapter, whose structure is reminded figure 8.3. In the case of polyNIPAM, the preparation procedure has to be adapted to the temperature sensitivity of the polymer.

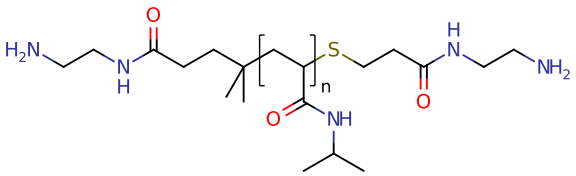


**Figure 8.3.** *Skeletal structure of the α,ω diamino terminated poly(N-isopropyl acrylamide).*

In the last chapter, we demonstrated that replacing a fraction of polyNIPAM with HMDA did not affect the responsiveness of the membrane. Therefore, two series of capsules were synthesized, one with 100 % diamino-terminated polyNIPAM and another one with a 50 %/50 % polyNIPAM/HMDA mixture. As explained in the previous chapter, polyNIPAM solutions needs to be processed at low temperature. Here, the high concentration of polyNIPAM causes the LCST to decrease, even if no salt nor sucrose were added. Unless specified, all the next steps performed at 10 °C. The detailed preparation procedure is available appendix F.2.2, p. 223.

The size of the obtained droplets has been assessed at 25 °C after emulsification and prior adding the TDI. The capsules obtained after the reaction with TDI were characterized at 40 °C both in oil and in the final aqueous phase. The DLS measurements are reported in table 8.4.

The diameter of the emulsions obtained in the presence of polyNIPAM is slightly higher. Indeed, polyNIPAM may increase the viscosity of the dispersed phase, thus reducing the efficiency of ultrasounds. As before, the capsules in oil tend to aggregate, which makes the measurements unreliable, and gives diameter in the micrometer range. When transferred to

| Composition | Emulsion | | Capsules in oil | | Capsules in SDS (40 °C) | | |
|---|---|---|---|---|---|---|---|
| | $D_h$ (nm) | Disp. | $D_h$ (nm) | Disp. | $D_h$ (nm) | Disp. | kcps |
| pNIPAM 100 % | 359 | 0.20 | 760 | 0.25 | 176 | 0.09 | 120 |
| pNIPAM 50 %/HMDA 50 % | 315 | 0.22 | 3,260 | 0.25 | 171 | 0.22 | 89 |

**Table 8.4.** *Diameter of the emulsion and the capsule suspension, measured by dynamic light scattering. SDS samples were filtered on cellulose acetate (1.2 µm) prior to measurement.*

the aqueous phase, objects with a diameter in the expected range are obtained. The factor of two between the diameters of the emulsion and the capsules in the aqueous phase may be the sign that capsules are, at least, partly broken in the process.

These preliminary experiments confirmed the possibility to build objects with a diameter close to 200 nm using a mixture of Span/Tween. This opens the way to low-energy emulsification procedures, compatible with the encapsulation of fragile molecules.

## 8.2. PolyNIPAM nanocapsules characterization

### 8.2.1. Temperature effect on the hydrodynamic radius

PolyNIPAM capsules were prepared from 100 % diamino-terminated polyNIPAM, according to the previously exposed protocol. After being transferred in the aqueous phase, the resulting suspension was characterized by DLS. We measured the hydrodynamic diameter and the intensity of scattered light, above the LCST (50 °C), and below the LCST (20 °C) immediately after decreasing the temperature, as well as 24 hours and 8 days later. These results are summarized in table 8.5.

| Time | Temperature (°C) | $D_h$ (nm) | kcps |
|---|---|---|---|
| 0 | 50 | 218 | 57 |
| ≈ 15 min | 20 | 413 | 65 |
| 24 h | 20 | 562 | 64 |
| 8 d | 20 | 440 | 69 |

**Table 8.5.** *Hydrodynamic diameter and intensity of scattered light of a suspension of polyNIPAM capsules.*

When the temperature is decreased below the LCST of polyNIPAM, the diameter of the objects increases from 218 nm to 413 nm; this might correspond to the swelling of the polymer. Long term measurements show no significant evolution of the hydrodynamic diameter or of the intensity of scattered light. We do not observe the dissolution of the whole capsule. This is compatible with the observations made on millimeter size capsules, where the capsule did not dissolve either, but was rather torn into pieces.

### 8.2.2. Temperature-induced release

For the millimeter-sized capsules, it was possible to follow the fluorescence intensity directly inside the capsule as their size permits it. The dye concentration inside the capsule could be directly linked to the intensity of fluorescence inside it. However, it is not possible to follow nanometer-sized objects by this technique. The main obstacles here are the Brownian motion, causing a continuous movement of the capsule, and the diffraction of light, which make the observation of a single capsule rather difficult.

With the vesicles, this issue was addressed by using a specific fluorophore or combination of molecules, whose fluorescence is quenched inside the capsules and reappeared when released. Amongst the different possibilities, we choose to focus on calcein and cobalt(II) complexes. As reported in references [249–252], calcein and cobalt(II) ions form non-fluorescent complexes. Adding EDTA to the outer buffer make the fluorescence reappear when the complex leak out of the capsule, as EDTA is a stronger ligand for cobalt than the calcein. While one calcein is able to complex one cobalt ion, they are encapsulated at a 1:2 mol. calcein:cobalt ratio.

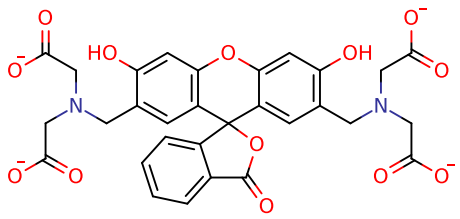


**Figure 8.4.** *Skeletal representation of calcein, in its ionized form. The four carboxylates complex cobalt(II) ions.*

The concentrations we choose to encapsulate were 250 µmol/L calcein – two order of magnitude lower than the concentration used for self-quenching – and 600 µmol/L cobalt(II), introduced as $CoCl_2$.

In order to check the validity of the technique, we recorded the emission spectra of calcein (3.2 µmol/L)+ cobalt(II) chloride (7.7 µmol/L), with and without 10 mmol/L EDTA, in PBS. The excitation wavelength was 495 nm; the obtained spectra are shown on figure 8.5. Adding EDTA caused a strong increase of the fluorescence intensity. At the maximum emission wavelength (525 nm), the intensity ratio with and without EDTA is 280.

Based on the these observations, we encapsulated the calcein/cobalt(II) complex in polyNIPAM/HMDA capsules. Several polyNIPAM:HMDA w. ratios have been tested: 100/0, 90/10 and 80/20. The detailed protocol is reported in appendix F.2.3, p. 224.

We were not able to reproducibly synthesize capsules made of 100 % polyNIPAM capsules, as irreversible macroscopic aggregates formed either in the oil phase or after their transfer in the aqueous phase. Therefore, we did not characterize the release from these objects, but rather focused capsules containing mixtures of HMDA and polyNIPAM. Conversely, the fluorescence intensity dependence on the temperature of the 90/10 and 80/20 samples

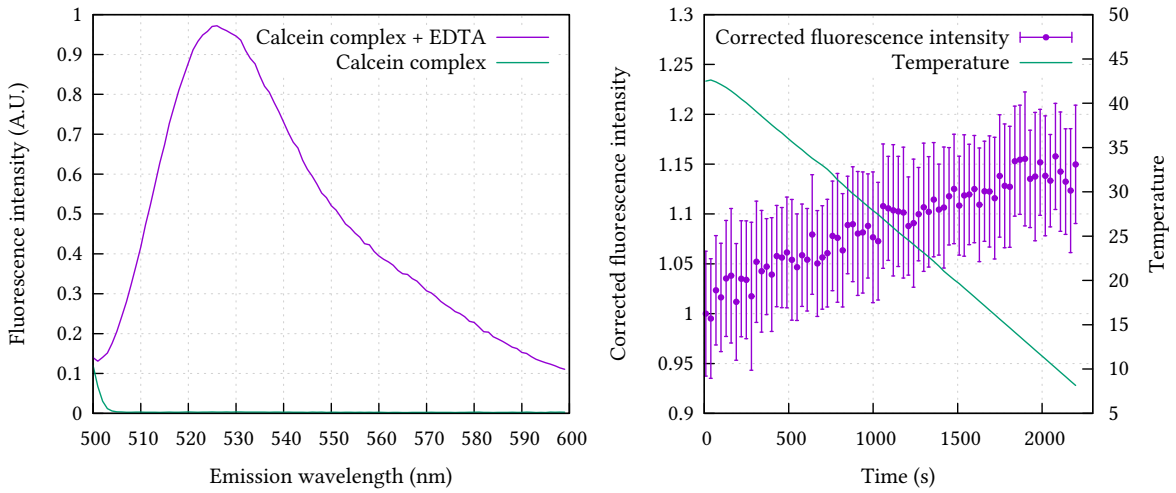


**Figure 8.5.** Left: *fluorescence intensity of a solution containing 3.2 µmol/L calcein sodium salt and 7.7 µmol/L $CoCl_2$ in PBS, without and with 10 mmol/L EDTA.*
Right: *fluorescence intensity of polyNIPAM/HMDA 80/20 capsules, encapsulating calcein/cobalt complex, suspended in 10 mmol/L EDTA in PBS. The suspension is submitted to a decreasing temperature ramp. The temperature dependence of the fluorescence intensity has been corrected. Excitation wavelength: 488 nm. Emission wavelength: 526 nm.*

was recorded. An example of the curves obtained from these experiments is shown on figure 8.5, and is representative of the ones obtained for both samples.

The fluorescence intensity was found to slightly increase when the temperature is decreased; no slope discontinuity is observed. In particular, crossing the LCST of the polyNIPAM (32 ℃) does not alter the shape of the fluorescence intensity curve. This means that either the capsules are not made leaky with the decrease of temperature, or that they were already empty before this experiment. The initial raw value of fluorescence, 53,580 for the 80/20 sample and 17,000 for the 90/10 one, is in the range of what is expected for a complete release, which confirms that all the encapsulated content was already released at the beginning of the experiment.

### 8.2.3. Morphology of the capsules imaged by electron microscopy

We showed in the previous paragraph that calcein is completely released even before decreasing the temperature. This suggests that either the membrane synthesis leads to leaky shells, or that capsules are destroyed in any of the following steps. We tried therefore to analyze the shape of the obtained capsules by cryoTEM. To this aim, we prepared capsules with the compositions reported in table 8.6. The capsules were prepared as reported before, without any dye. After their transfer in the aqueous phase, the SDS in the buffer was removed by gel permeation chromatography conducted at 50 ℃. This additional step was required, as SDS micelles appears on cryoTEM pictures, adding unwanted noise. The

| Sample number | 1 | 2 | 3 |
|---|---|---|---|
| **HMDA (g/L)** | 100 | 50 | 20 |
| **diamino-terminated polyNIPAM (g/L)** | 0 | 50 | 80 |

**Table 8.6.** *Composition in diamine terminated monomers of the aqueous phases used to prepared the capsules for the transmission electron microscopy.*

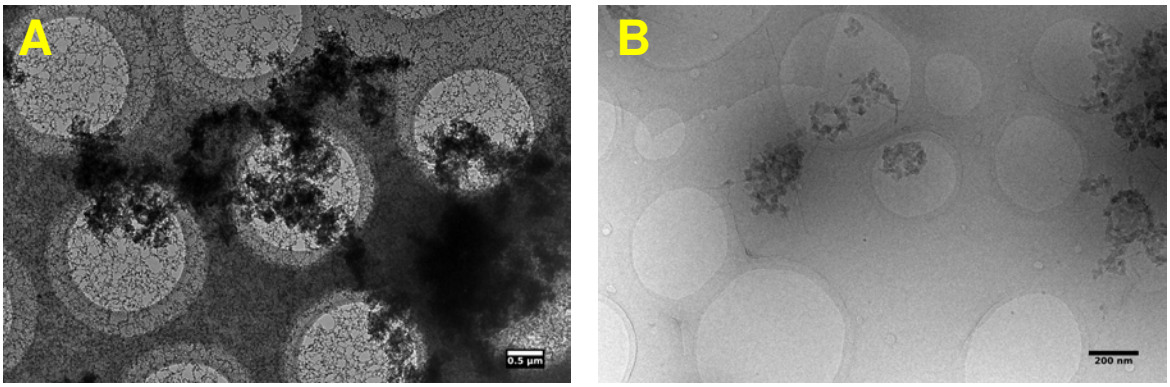


**Figure 8.6.** *Suspensions of capsules viewed by cryoTEM. A: capsules made of 50 g/L HMDA/50 g/L polyNIPAM, 3200×. Scale bar size: 500 nm. B: capsules made of 100 g/L HMDA, 11000×. Scale bar size: 200 nm.*

protocol is detailed in appendix F.2.3, p. 224. Pictures obtained for samples 1 and 2 are shown on figure 8.6.

On picture A is shown the suspension of capsules made from 50 % polyNIPAM/50 % HMDA – pictures obtained for the 80 % polyNIPAM were similar. The sample seems to consist mainly of aggregates of spherical objects; no tight capsules could be seen on this picture. We note also the presence of a black network on the whole sample. Picture B shows objects made from 100 % HMDA. They are spherical, and their diameter is in the expected range of 200 nm. They seem also to be made of aggregates of small spheres or patches. In this case, no network is observed, but we can see filaments emerging from the 200 nm objects.

Conversely, 100 % HMDA capsules prepared in reference [231] are shown on figure 8.7. The capsules looks partly collapsed, as the samples are not frozen prior imaging in this case. However, they seem to be made from a homogeneous and continuous membrane. The only difference between this reference and our experiment is the surfactant used to stabilize the emulsion. In our case, we used Span 80/Tween 80 mixtures, while they used a polyisobutene-succinimide pentamine (Lubrizol U).

Span 80 and Tween 80 contains both 3 alcohols functions susceptible to react with the diisocyanate. The high functionality of these molecules will lead to the formation of a cross-linked network, which explains the black mesh on the electron microscopy pictures. This issue is not observed with Lubrizol, as it only carries one amine function. In our system, we have both primary amine functions, at the end of our "monomers" – polyNIPAM

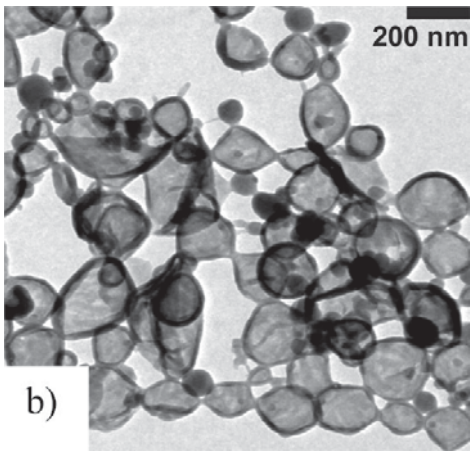


**Figure 8.7.** *TEM picture of capsules made from HMDA+TDI, from reference [231].*

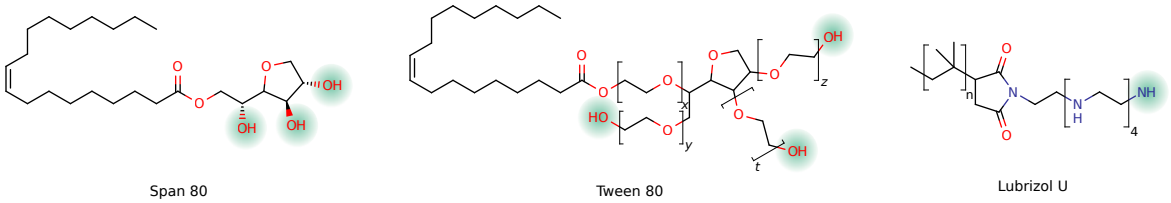


**Figure 8.8.** *Tween 80 and Span 80 contains both three functions thay may react with an isocyanate, while Lubrizol U contains only one. These functions are highlighted in green, and are alcohols for Tween/Span, and a primary amine for Lubrizol.*

or HMDA – and alcohols on the surfactants. We expected that the diisocyanate would mostly react with the amines, as both were introduced in almost quantitative proportions. Furthermore, amines are more reactive than alcohols. However, this seems not be the case. Span 80 is not soluble in water, and is probably mostly present in the oil phase, even after the emulsification. Span 80 and the disocyanate are thus in the same phase making their reaction easier, thus creating the network.

## Conclusion & perspectives

Transposition of the synthesis procedure of nanocapsules described in the literature to polyNIPAM based systems was a priori a simple question of adjusting emulsification conditions. We choose the couple Span 80/Tween 80 to emulsify the system because they enable to form water-in-oil emulsions by a low energy emulsification strategy.

In the published articles, no mention is made of the importance of the nature of surfactant in the synthesis of the capsules, but our attempts to use Tween/Span mixtures proved that it matters. Calcein/cobalt assay and morphology of capsules shown in transmission electron microscopy images suggest ill-defined surfaces. In practice, only leaky objects were obtained. Interfacial reactivity was certainly be affected by surfactants. The presence of

alcohols in the surfactant molecules may lead to side reactions; this work should be pursued by a systematic evaluation of the surfactants that could be used to stabilize the emulsion, for instance the Brij family. As Tween/Span, they can be used to prepare nanoemulsions by low energy processes, at constant temperature [247], and are also biocompatible (see figure 8.9).

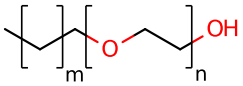


**Figure 8.9.** *General formula of a Brij surfactant. This molecule is made of an alkyl chain and a PEG tail; the alkyl chain may be unsaturated.*

Finally, the procedure to redisperse the capsules in an aqueous phase has to be optimized. Indeed, the ultrasounds step might be too violent both for the capsules and their load. Centrifugation may be an alternative, and it has already been used to make water droplets crossing the oil/water interface, as shown section 2.4.3, page 36, for the preparation of liposomes by the reverse emulsion method. We may also consider to replace progressively the oil with solvents of increasing polarity, e.g. by cycles of gentle centrifugation and redispersion of the capsules in polar solvents, like alcohols of decreasing chain length, while avoiding the dissolution of the polyNIPAM shell.

# 9. UCST polymer-based millimeter-sized capsules

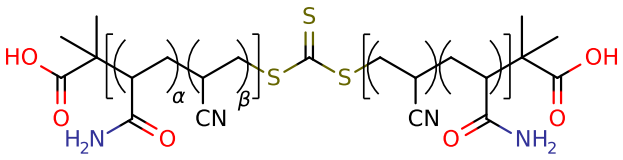


**Figure 9.1.** *Common skeletal formula of the UCST polymers. Molecular weight: ∼ 15 kg/mol. The UCST of the polymer depends on the acrylamide/acrylonitrile ratio. Polymer* 35 ℃*: α = 67.9 %, β = 32.1 %. Polymer* 43 ℃*: α = 66.1 %, β = 33.9 %. Polymer* 47 ℃*: α = 65.8 %, β = 34.2 %.*

This chapter presents the use of UCST polymers to build temperature sensitive capsules. As mentioned in the review chapter, UCST polymers are appealing for biological applications as an increase of temperature will induce their dissolution and thus the destabilization of the capsule shell and the release of the encapsulated content. The work reported here mainly focuses on three of the polymers provided by Y. Zhao, whose general structure is shown back in figure 9.1. The UCST of these polymers was 35 ℃, 43 ℃ and 47 ℃ in PBS, and they will be referred later by these values.

Like the commercial polyNIPAM derivative we used in the last chapter, the UCST polymer chains are end-functionalized by carboxylic acid functions. We planned to incorporate these polymers in the same way we incorporated the polyNIPAM. Due to lack of time, the conversion of the polymers to "reactive" amine-terminated chains was however not accomplished. A first preliminary study was carried out to assess the preparation of capsules from non-reactive precursors.

## 9.1. Characterization of the UCST polymer

The UCST of polymers is sensitive to the composition of the aqueous phase, but these effects were not characterized when this work was launched. As we use sucrose or NaCl to increase the density of the inner aqueous phase during capsule preparation, it was important to measure the impact of these osmolytes, and of other alternative additives used to increase capsule density – including glucose and heavy water – have been characterized.

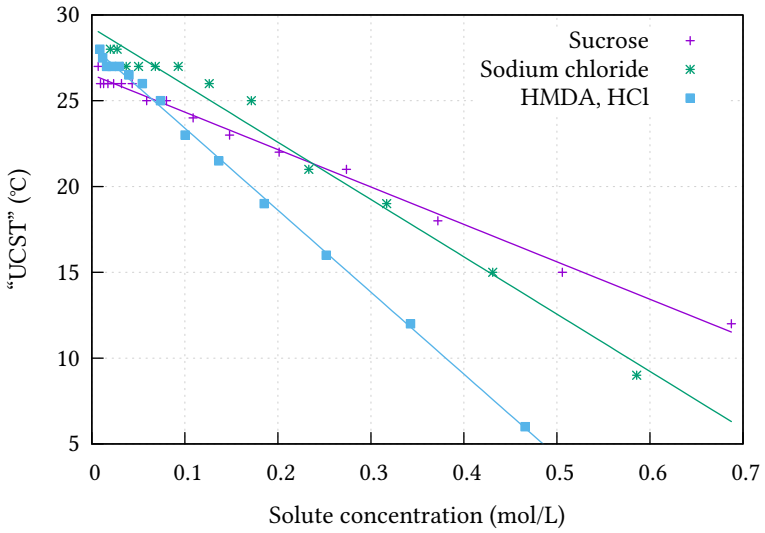


| Solute | Slope (℃/mol) | $y$-cept. (℃) |
|---|---|---|
| Sucrose | − 22 ± 1 | 27 ± 1 |
| NaCl | − 33 ± 1 | 29 ± 1 |
| HMDA | − 48 ± 1 | 28 ± 1 |

**Figure 9.2.** Left: *evolution of the UCST of polymer "35 ℃" as a function of the concentration of various solutes: HMDA (hydrochloride), sucrose and sodium chloride.*
Right: *fit results (y-cept. stands for y-intercept).*

### 9.1.1. Solute effects on the UCST

#### Effect of sucrose, NaCl and HMDA on the UCST of the polymers

We studied the effect on various solutes – HMDA, sodium chloride and sucrose – on the UCST of the 35 ℃ polymer, as a function of the solute concentration. We first determined the cloud point of solution of polymers by stepwise decrease of temperature (steps of 1 ℃), and observation of emerging turbidity; the detailed protocol is reported in appendix *C.3.5 Evaluation of UCST as a function of solute concentration*, p. 200. The results are shown in figure 9.2.

With all the solutes, the UCST decreased almost linearly with increasing concentration of solute. This enabled us to extrapolate the UCST for the concentrations required in the capsules. For sucrose at 0.63 mol/L, the expected UCST is 13 ℃ (< RT); for sodium chloride at 2.22 mol/L, – 44 ℃…[1] Thus the impact of the two osmolytes, sucrose or sodium chloride, is high and would decrease the UCST below the temperature of experiments.

Whereas all UCST polymers quickly dissolved in water with sucrose or NaCl above a threshold temperature, their mixtures with HMDA turned into translucent gels within minutes or hours, even at high temperature. Cooling the mixtures below the UCST (ice bath) did not induce to precipitate, which was surprising. When they are dissolved in water or PBS, the diamine and the polymer are of opposite charges, which may explain that gel were formed by coulombic associations. To alleviate this effect, we added two equivalents

[1] Those concentrations are the ones used for the synthesis of HMDA or polyNIPAM-based millimeter-sized capsules.

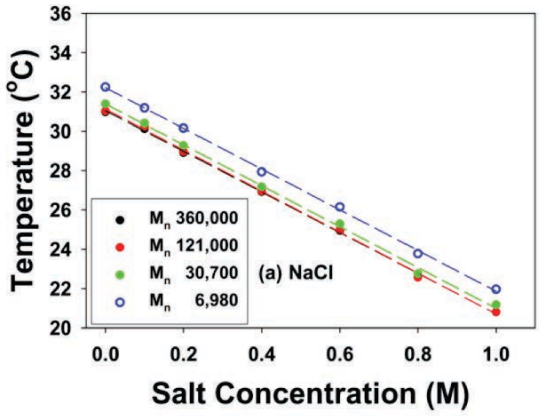


**Figure 9.3.** *Evolution of polyNIPAM LCST as a function of the concentration of sodium chloride and the molecular weight of the polymer. Polymer concentration: 10 g/L. Reprinted from reference [233].*

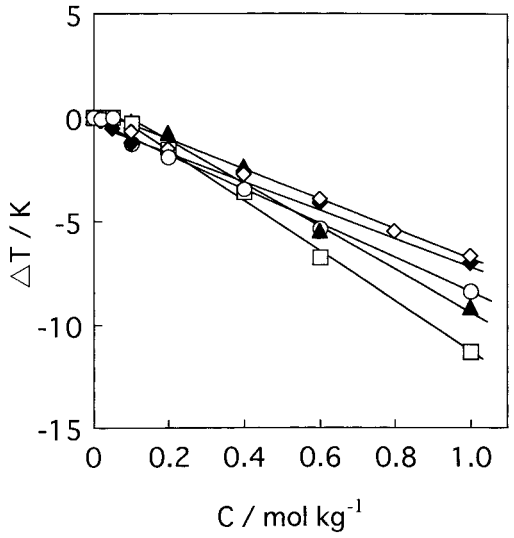


**Figure 9.4.** *Reprinted from reference [253]. Relationship between ΔT (LCST with sugar – LCST in water) and concentration of sugars: fructose (◆), xylose (◇), glucose (○), sucrose (▲) and maltose (□), for a polyNIPAM crosslinked hydrogel.*

of HCl per HMDA, turning the solution to slightly acidic before adding the polymer under its acid form.

We can compare the effect of the solutes on the polyNIPAM and on the UCST polymer. The evolution of polyNIPAM LCST in presence of sodium chloride is shown in figure 9.3. The slope of the curve is approximatively – 10 ℃/mol, one third of the value obtained with the UCST polymer, which means that the effect of NaCl is much higher in the case of UCST polymers. Sucrose also decreases the LCST of polyNIPAM, as shown in figure 9.4. The slope is also in the range of – 10 ℃/mol.

To achieve the reverse response to additives, we finally used heavy water.

### Effect of heavy water on the UCST

The UCST of the polymers in $D_2O$ was assessed by following the absorbance of polymer solutions by UV-visible spectroscopy upon decreasing temperature. Details on the experimental setup and conditions are available in appendix C.3.2, page 198.

Reference spectra for polymers at 5 g/L in PBS were provided by Y. Zhao, and are reprinted on figure 9.5. The spectra obtained in heavy water are shown in figure 9.6. The UCSTs are defined here as the temperature when the transmittance is decreased by 50 %. The values are summarized in table 9.1. For all three polymers, the UCST in heavy water was ≈ 10 ℃ above the one obtained in PBS. The UCST temperature of polymer 1 is 45 ℃ in heavy water, which means that capsule loaded with high density solutions can be prepared while

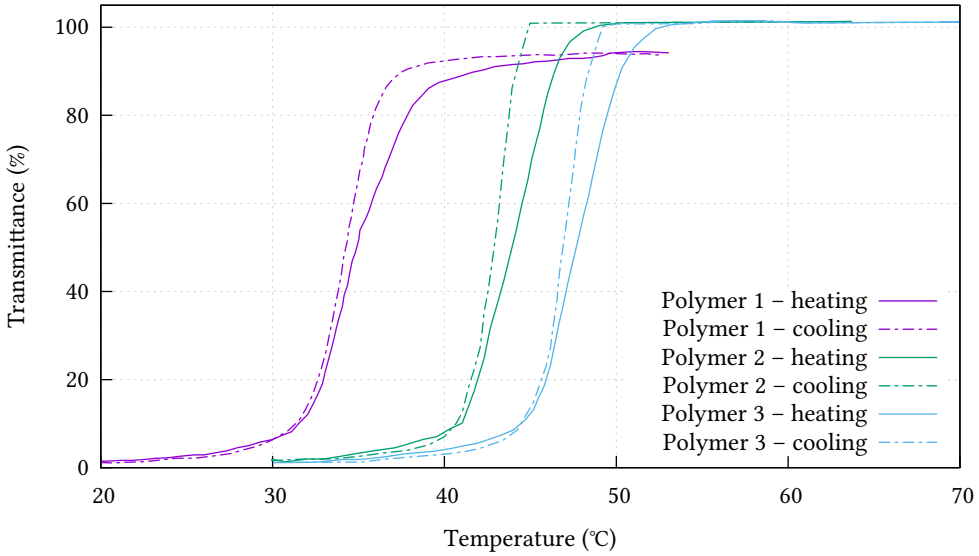


**Figure 9.5.** *The three UCST polymers used in this work. They are named by the value of their UCST, defined as the middle of the transmittance ramp, upon cooling. Polymer 1: ≈ 34 ℃, polymer 2: ≈ 43 ℃ and polymer 3: ≈ 47 ℃. Data provided by Y. Zhao.*

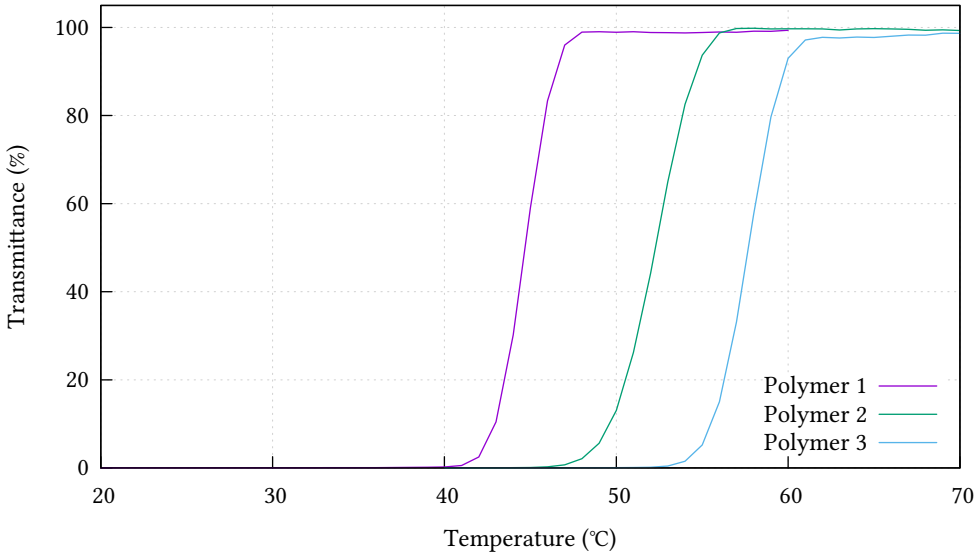


**Figure 9.6.** *Transmittance of UCST polymers at 3 g/L in $D_2O$, upon cooling. Polymer 1: ≈ 45 ℃, polymer 2: ≈ 52 ℃, polymer 3: ≈ 58 ℃.*

| Polymer | 1 (35 °C) | 2 (43 °C) | 3 (47 °C) |
|---|---|---|---|
| **UCST in PBS (°C)** | 34 | 43 | 47 |
| **UCST in $D_2O$ (°C)** | 45 | 52 | 58 |
| **ΔT (°C)** | 11 | 9 | 11 |

**Table 9.1.** *UCST of the three polymers, in PBS and in heavy water.*

preserving the response to a temperature jump above RT (or above 37°C if application in biological environments are sought). If the processing temperature of 50 °C is too high (e.g. induce the degradation of the protein encapsulated), addition of sucrose or sodium chloride could be used to decrease the UCST.

## 9.2. Adaptation of the capsule preparation procedure to the UCST polymers

To build capsules with UCST polymers, we had to replace HMDA by another reactant that do not form gels with the polymer. In reference [194], various "monomers" are reported to lead to the formation of capsules in conjunction with TDI: starch, dextran and 1,6-hexane diol. We tried to build capsules from 1,6-hexane diol, using an aqueous phase made of 10 g/L 1,6-hexane diol and 20 % w. sucrose in PBS. However, this did not lead to capsules; even after 12 hours of reaction, the aqueous drops were not covered with a mechanically resistant membrane. The other monomers reported by K. Landfester's team are proteins, bovine serum albumin and ovalbumin (OVA) [205]. 170–190 nm capsules were prepared from an aqueous phase made of protein (BSA or ovalbumin), of deionized water and sodium chloride. The weight concentration of "monomer" is the same here as the one reported for the capsules made from HMDA. We decided to adapt this strategy to build capsules in the presence of UCST polymers. As for polyNIPAM, we mixed the UCST polymer and ovalbumin while keeping their total weight constant – 100 g/L.

The final synthesis procedure – aqueous phase transfer excepted – is represented on figure 9.7. The aqueous phase – containing the ovalbumin, heavy water and the UCST polymer – must be processed at a temperature where the polymer is soluble, that is above the UCST in presence of heavy water. Conversely, the cyclohexane:TDI mixture must be added below the UCST to react on interfaces that contain polymers. For all polymers, we worked at room temperature (20 °C), as their UCST is above 34 °C.

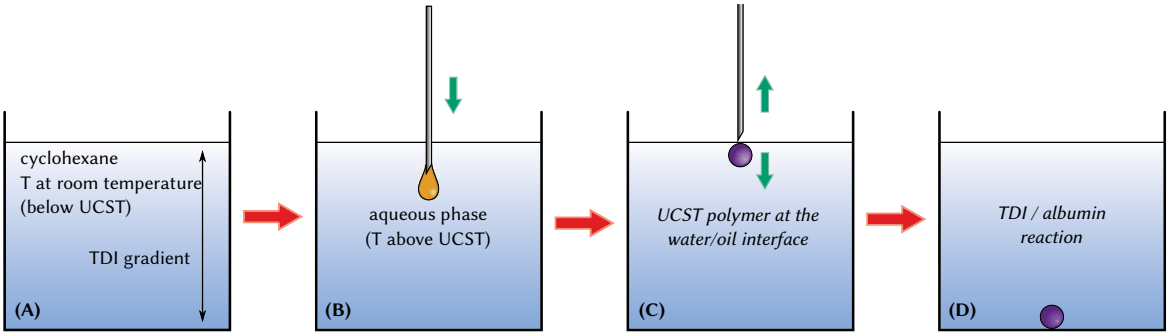


**Figure 9.7.** *Synthesis of the capsule in the oil phase. (A) a gradient of TDI concentration is created in cyclohexane, at room temperature (below UCST). Under these conditions, the concentration in TDI at the top of the cyclohexane is considered null. (B) a drop of the aqueous phase is introduced in the oil with a microsyringe. The syringe and its content were heated above UCST, allowing the solution to flow through the needle. (C) the UCST polymer inside the drop precipitates and goes to the water/oil interface. As the drop was kept in the higher levels of cyclohexane, where no TDI can be found, no reaction occurred yet. (D) the drop is made to fall at the bottom of the cyclohexane, were the membrane is synthesized.*

## Results

*The experiments performed in this section have been done in parallel of the characterization of the UCST polymers. Thus, the density of the aqueous phase was increased with sucrose for the capsules made with 10 g/L of proteins, and with heavy water for the 100 g/L ones. The detailed procedure is available in appendix* F.1.2 Determination of the working UCST+albumin composition, *p. 220.*

Four sets of aqueous phases were prepared, with BSA or ovalbumin with a concentration of 10 g/L or 100 g/L. Dextran TexasRed was used as the fluorescent probe. The composition of these phases are reported in table 9.2. Due to some experimental constraints – mainly the concentration of fluorescent probes in stock solutions – the concentration of heavy water used was 71.7 % vol.

All the aqueous phases lead to mechanically resistant capsules transferable to PBS. Fluorescent profiles for all samples are shown in figure 9.8.

| Albumin | $C_{albumin}$ | Additive | $C_{additive}$ | Fluorescent probe | $C_{probe}$ |
|---|---|---|---|---|---|
| Ovalbumin | 10 g/L | Sucrose | 20 % w. | Dextran Texas Red | 100 mg/L |
| Ovalbumin | 100 g/L | $D_2O$ | 71.7 % vol. | Dextran Texas Red | 10 mg/L |
| BSA | 10 g/L | Sucrose | 20 % w. | Dextran Texas Red | 100 mg/L |
| BSA | 100 g/L | $D_2O$ | 71.7 % vol. | Dextran Texas Red | 10 mg/L |

**Table 9.2.** *Composition of the aqueous phases used to build model capsules from albumin. The solvent of all the phases is PBS. The fluorescent probe here is Texas Red labeled dextran (3,000 g/mol).*

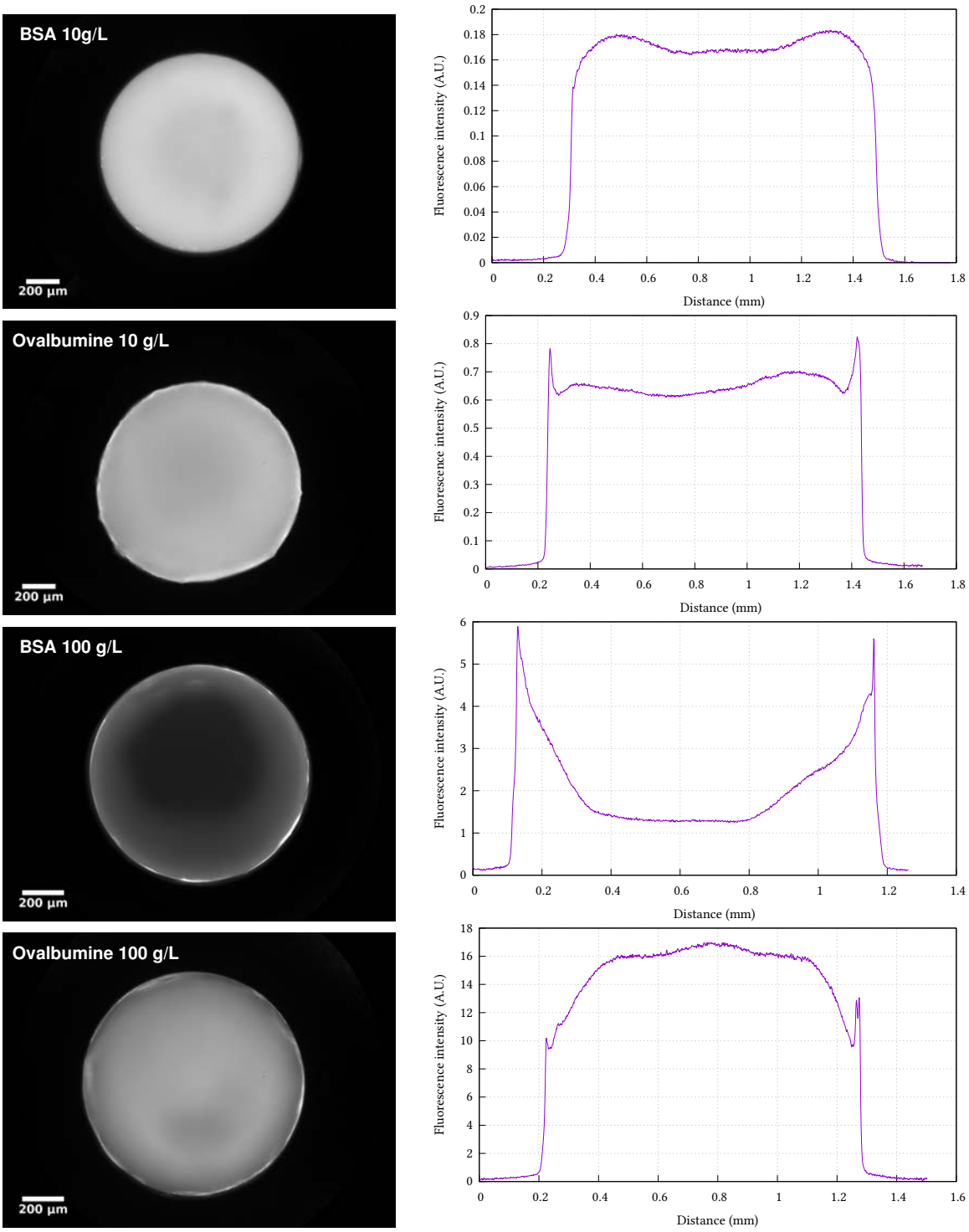


**Figure 9.8.** *Capsules made from albumin and filled with dextran-TexasRed. Left: epifluorescence picture. Right: fluorescence profile.*

Capsules made from low protein concentration (10 g/L) show almost flat fluorescence profiles, which suggest that the TexasRed labeled dextran is partially entrapped in the membrane. This is probably due to a reaction between the diisocyanate and the dextran. The reactivity of the dextran compared towards the diisocyanate has even been exploited to build nanocapsules from it, as reported in references [194, 197].

For BSA (≈ 65 kg/mol), 10 g/L corresponds to 0.154 µmol/L. BSA probably reacts with the isocyanates by its primary amine functions, brought by the lysine residues. The number of lysine residues in BSA is evaluated to 12 [254]. This increases the concentration of reactive functions to 1.85 µmol/L. For dextran (162.14 g/mol per monomer), 0.1 g/L corresponds to a concentration of 0.617 µmol/L. As each dextran monomer bears three alcohol functions, this leads to a concentration of 1.85 µmol/L reactive species. The same calculation has been performed for ovalbumin; all the results are summarized in table 9.3.

| **Reactant** | **BSA** | **Ovalbumin** | **Dextran** |
|---|---|---|---|
| **$M_w$ (monomer)** | 65 kg/mol | 43 kg/mol | 162.14 g/mol |
| **Reactive functions/monomer** | 12 (lysine) | 20 (lysine) | 3 (alcohol) |
| **Concentration** | 10 g/L | 10 g/L | 0.1 g/L |
| **Reactive functions concentration** | 1.85 µmol/L | 9.30 µmol/L | 1.85 µmol/L |
| **Concentration** | 100 g/L | 100 g/L | 10 mg/L |
| **Reactive functions concentration** | 18.5 µmol/L | 93.0 µmol/L | 0.185 µmol/L |

**Table 9.3.** *Reactant concentrations in 10 g/L capsules (loaded with 100 mg/L dextran Texas Red) and 100 g/L capsules (loaded with 10 mg/L dextran Rexas Red). Data for ovalbumin were extracted from Protein Data Bank, reference 1OVA.*

The concentration of reactive functions for dextran and the proteins is close, which may explain the integration of dextran in the membrane, as explained in section *7.2.2 Sulforhodamine 101*, p. 121. Even if amines are reported to be more reactive than alcohols, their number is probably overestimated. All the lysines have been taken into account, regardless of their position in the protein – some of them must be less accessible to the isocyanate, thus less reactive.

To overcome this competition between dextran and the albumin, we choose both to decrease the concentration of fluorescent-labeled dextran to 10 mg/L and to increase the concentration in albumin (100 g/L). The new concentrations in reactive functions are shown in table 9.3. The ratio albumin-functions:dextran-functions is now 100 for BSA (1 before) and ≈ 500 for ovalbumin (5 before). The corresponding fluorescence profiles are shown in figure 9.8. For BSA, the profile plot has the shape of a reverse sphere (convex curve), which is characteristic of a fluorescent membrane (cf. section 7.2.2 page 121). The dextran is still incorporated in the membrane, even with optimized conditions. A different profile is obtained with ovalbumin, though. Its concave shape confirms that dextran is less integrated in the membrane in this case.

These results show that the synthesis of UCST polymer based macrocapsules is possible. In reference [205], where nanometer-sized capsules from albumin are described, it is shown that ovalbumin lead to capsules with higher performances than their BSA-based counterparts. They report a higher loading efficiency of sulforhodamine 101. The morphology of the capsules also differs (see figure 9.9). Ovalbumin capsules seemed more defined than the BSA ones.

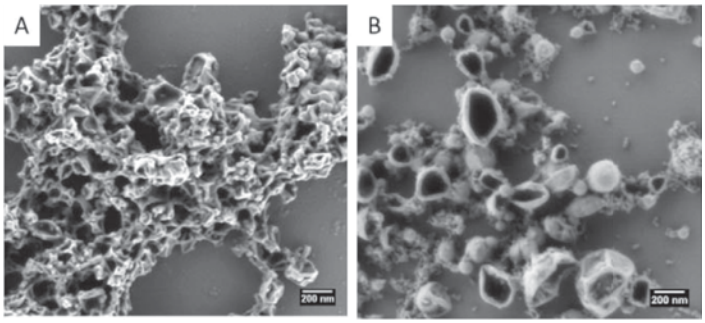


**Figure 9.9.** *Reprinted from reference [205]. Capsules made from albumin by the reverse emulsion emulsion method, viewed by scanning electron microscopy. A: capsules made from bovine serum albumin (BSA). B: capsules made from ovalbumin.*

These observations, together with our results, allowed us to conclude that capsules made from ovalbumin should be preferred, because encapsulated molecules are less susceptible to react with the diisocyanate, and because the performance of nanometer-sized capsules built from ovalbumin are higher.

## 9.3. Characterization of capsules made from UCST polymers and ovalbumin

This section focuses on the characterization of the thermal properties of capsules made from UCST polymer and ovalbumin. The experiments were conducted mainly on the 43 ℃ polymer. Due to a lack of time, only a limited set of measurements has been done with the 35 ℃ polymer. We decided not to use the 47 ℃ one as its UCST in heavy water is 58 ℃, and experimentally, its mixture with protein was accompanied by gelation likely due to protein denaturation at high temperature – at this temperature, the denaturation rate of ovalbumin is in the range of 100 minutes [255]. For the other two UCST polymers, we explored the influence of the composition of the shell on release properties.

### 9.3.1. Choice of the encapsulated fluorophore

In order to determine the best fluorophore to study the thermal properties of the UCST polymer-based capsules, we prepared capsules from aqueous solutions containing OVA,

UCST polymers and 3 different fluorophores. The composition of the aqueous phases is reported in table 9.4. The experimental procedure is detailed in appendix *F.1.2 UCST polymer-based capsules: choice of the fluorophore*, p. 221.

| Dye | $C_{dye}$ | $C_{ovalbumin}$ (g/L) | $C_{UCST\ polymer\ (43\,°C)}$ (g/L) |
|---|---|---|---|
| BSA-FITC | 167 mg/L | 80 | 20 |
| Calcein | 10 µmol/L | 80 | 20 |
| Dextran-TexasRed | 10 mg/L | 100 | 10 |

**Table 9.4.** *Composition of the aqueous phase used to made fluorophore-filled capsules. All contained also 71.7 % vol. $D_2O$ and were buffered with PBS.*

BSA-FITC loaded capsules looked initially (i.e. at RT) homogeneous. Bright spots (likely aggregates) appeared upon temperature increase. The size and brightness of these aggregates increased with increasing the temperature (see figure 9.10), while the background became darker which suggests that some BSA-FITC is associated with the aggregates. Aggregation may be either due to the increase of temperature or a co–precipitation of the BSA with the polymer.

The mean fluorescence intensity over the all volume of the capsule was plotted as a function of the temperature (see figure 9.10). It has been shown to increase with the temperature, with a 300 seconds lag time. The origin of this unexpected increase is possibly rooted in BSA aggregation and/or denaturation.

Similar experiment conducted with calcein as the fluorophore preserved the homogeneous appearance of membrane fluorescence, even when heated to 51 °C (see figure 9.10). In the example shown, the total fluorescence inside the capsule increased with the temperature, fluorescence intensity and temperature curves being remarkably superimposed, which suggests the absence of leakage and the effect of T on the fluorescence of this fluorophore. Calcein and FITC belong to the same class of fluorophores. FITC being known to have a T-dependant quantum yield, this speaks for a strong influence of the temperature on calcein too.

Finally, dextran-TexasRed loaded capsules looked homogeneous in fluorescence, independently of the temperature. The fluorescence of Texas Red is almost constant with temperature [234]. Increasing the temperature made the fluorescence intensity decrease (see figure 9.10). The magnitude of the decrease – 25 % over 55 °C – was however low.

As a control experiment, we evaluated the behavior of non encapsulated TexasRed in an aqueous solution of similar composition as the inner phase of the capsule – 100 g/L OVA and 100 mg/L Dextran TexasRed. The fluorescence intensity recorded as a function of temperature, as shown on figure 9.11, display a clear increase when the temperature decreased, and variations were essentially reversed by reversing temperature shifts. The amplitude of the variation was of the same order of magnitude as the variation measured in the capsules, which suggest that capsules were impermeable.

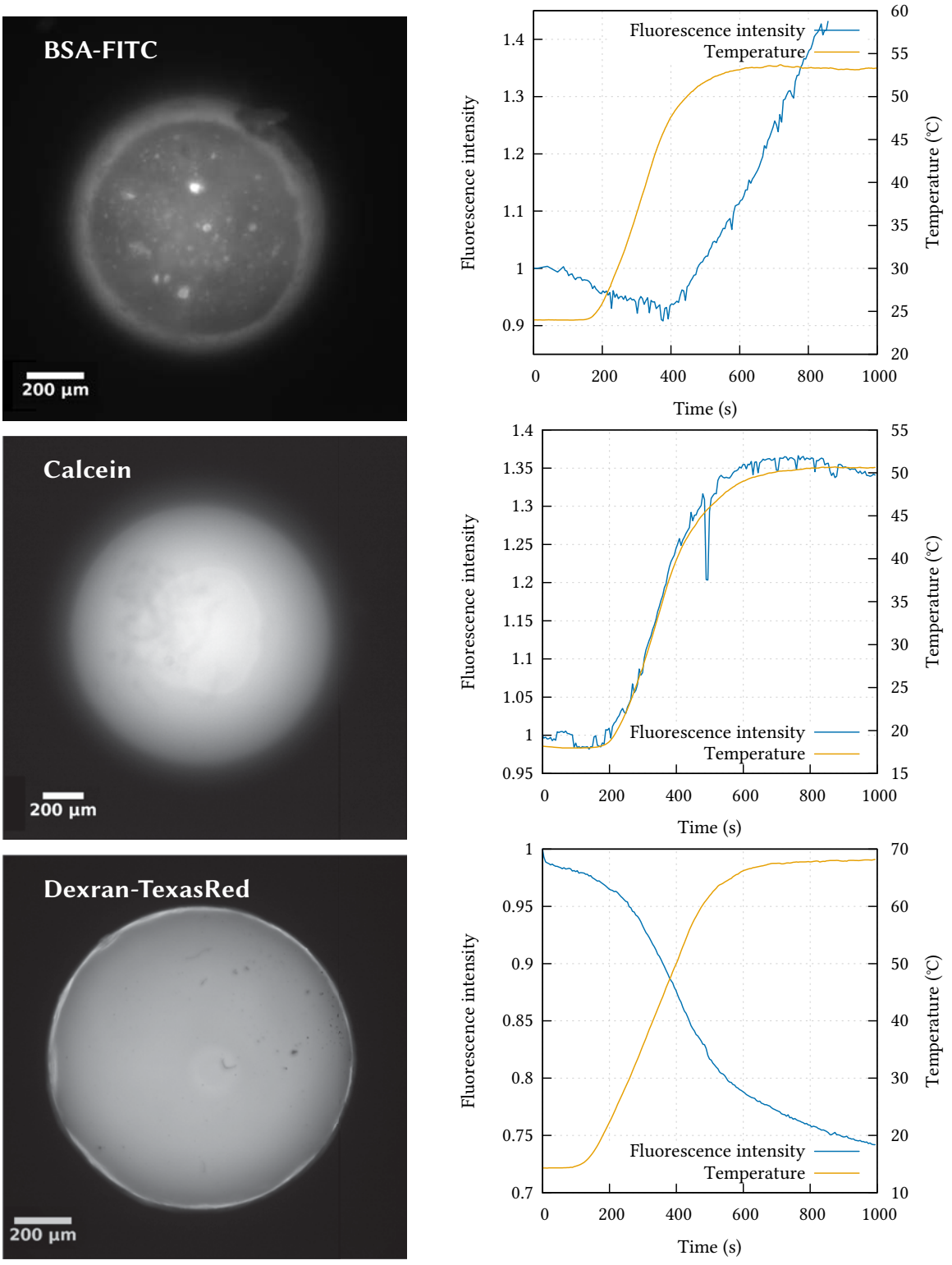


**Figure 9.10.** *Capsules made from ovalbumin and UCST polymer, filled with fluorescent probes and submitted to an increasing ramp of temperature. Left: epifluorescence pictures. Right: fluorescence intensity of the capsule and temperature as a function of time.*

In practice, we nevertheless observed release (of internal aggregates or microscopic heterogeneities) because it was accompanied by their burst out of the capsule, visible on the pictures recorded with the epifluorescence microscope. An example of this burst is shown on figure 9.12, where a capsule made from 80 g/L UCST polymer (43 ℃) and 20 g/L ovalbumin is heated from 15 ℃ to 55 ℃. We defined the temperature of release as the temperature of capsule burst.

### 9.3.2. Influence of the membrane composition on the temperature-sensitivity of the capsules

To assess the influence of membrane composition (varied by variation of the inner aqueous phase during membrane formation) on temperature sensitivity, capsules were prepared from a solution of ovalbumin, UCST polymer (43 ℃) and heavy water in PBS. Capsules were tested within 24 h after their preparation. The composition of the processed aqueous phases is reported in table 9.5 (the detailed protocol is reported in appendix *F.1.2 Temperature-sensitivity of UCST:ovalbumin capsules*, p. 221).

| **Sample name** | 0 % | 10 % | 20 % | 30 % | 50 % | 70 % | 80 % | 90 % | 100 % |
|---|---|---|---|---|---|---|---|---|---|
| $\mathbf{C_{UCST\ polymer\ 43\,°C}}$ **(g/L)** | 0 | 10 | 20 | 30 | 50 | 70 | 80 | 90 | 100 |
| $\mathbf{C_{Ovalbumin}}$ **(g/L)** | 100 | 90 | 80 | 70 | 50 | 30 | 20 | 10 | 0 |
| **Solid membrane** | Yes | Yes | Yes | Yes | Yes | Yes | Yes | Yes | No |
| **Ruptured capsules (/2)** | 0 | 1 | 0 | 0 | 0 | 0 | 2 | 2 | – |

**Table 9.5.** *The aqueous phases were prepared from heavy water 71.7 % vol. and 10 µmol/L calcein in PBS, alongside the compounds shown in the table above.*

Capsules were submitted to a temperature ramp, while controlling the integrity of the capsule by fluorescence microscopy. The results are reported in table 9.5. Except the 100 % sample containing only UCST polymer, all the aqueous phases used lead to mechanically resistant capsules, transferable to PBS. Capsules made from less than 80 % UCST polymer were not temperature-sensitive. The capsules made from 80 % and 90 % UCST polymer were found to burst when the temperature was increased.

These results are comparable to the ones obtained for capsules made from polyNIPAM and HMDA. A low polyNIPAM:HMDA ratio lead to non-permeable capsules, insensitive to the temperature, while high ratios did not lead to capsules at all. The temperature-sensitive capsules were found in a narrow window of concentrations, comparable to the one obtained with polyNIPAM. The existence domains of these capsules are reported on figure 9.13.

To determine the temperature of burst , and possible statistical fluctuations from capsule to capsule, series of similar preparations have been studied: two with the 43 ℃ UCST polymer and one with the 35 ℃ UCST polymer, subjected to an increasing sweep of temperature (from 15 ℃ to 50 ℃, ≈ 7 ℃/min; the detailed protocol is reported in appendix *F.1.2 Determination of*

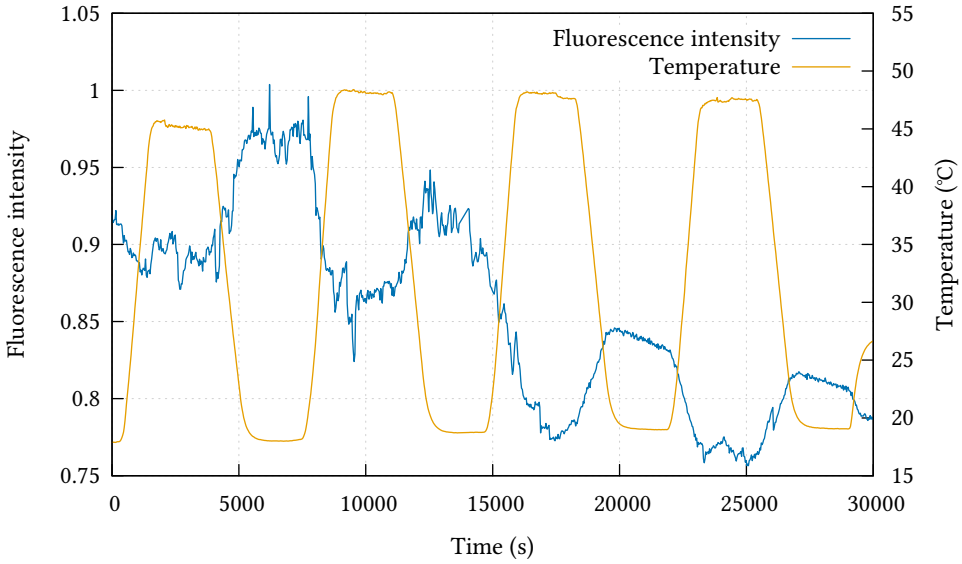


**Figure 9.11.** *Fluorescence intensity of a solution composed of 100 g/L ovalbumine, 100 mg/L Dextran TexasRed in PBS. Viewed on a microscope; the solution was sealed between two glass slides. Sample thickness: 120 µm.*

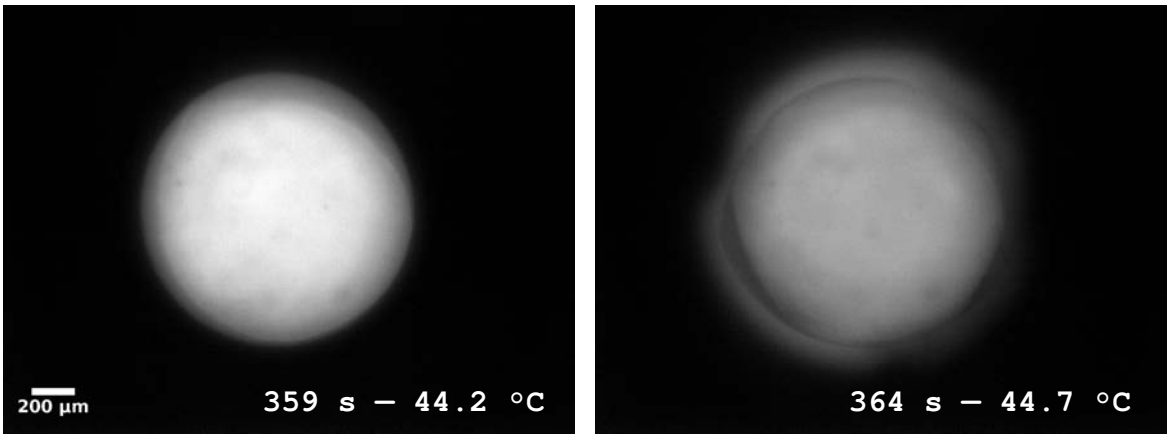


**Figure 9.12.** *Example of capsule explosion, viewed on an epifluorescence microscope. The capsule here is made of 80 g/L UCST polymer (43 °C), 20 g/L ovalbumin and 71.1 % vol. $D_2O$.*

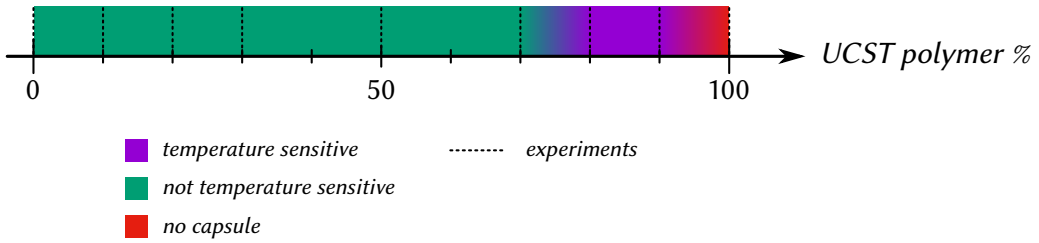


**Figure 9.13.** *Temperature-sensitivity of the capsules made from UCST polymer (43 ℃), as a function of the relative amount of polymer in the aqueous phase.*

*the burst temperature of UCST:ovalbumin capsules*, p. 221). An example of a "burst" seen by epifluorescence microscopy has been shown in figure 9.12, p. 155.

### 90 % 43 ℃ UCST polymer – 10 % ovalbumine capsules

We prepared 17 capsules from an aqueous phase composed of 43 ℃ UCST polymer and ovalbumine, at a 90:10 w. ratio. The buffer composed of PBS containing 71.7 % vol. heavy water. 14 of them exploded during the increasing ramp of temperature (82 %). 13 "bursting" temperatures have been determined (cf. table 9.6); the leakage from the 14th one was not sharp enough to allow the extraction of one temperature.

| **Sample** | 1 | 2 | 3 | 4 | 5 | 6 | 7 | 8 |
|---|---|---|---|---|---|---|---|---|
| **Burst temperature (°C)** | 35.9 | 48.0 | 40.3 | 31.3 | 44.6 | 48.0 | 42.7 | 34.6 |

| **Sample** | 9 | 10 | 11 | 12 | 13 | **avg** | **stddev** |
|---|---|---|---|---|---|---|---|
| **Burst temperature (°C)** | 40.6 | 45.5 | 41.5 | 36.7 | 33.0 | *40.2* | *5.6* |

**Table 9.6.** *Burst temperature of capsules made from 90 % 43 ℃ UCST polymer.* ***avg*** *and* ***stddev*** *stand respectively for* average temperature *and* standard deviation.

The mean temperature at which the release occurs is 40 ± 6 ℃. This is close to the UCST of the polymer in PBS, 43 ℃. This is similar to what we observed with polyNIPAM: thermal behavior of the mixed capsules can be achieved near the critical solution temperature of the polymer "physically" adsorbed in the membranes.

### 80 % 43 ℃ UCST polymer – 20 % ovalbumine capsules

Preliminary data of capsules prepared from a mixture of 43 ℃ UCST polymer and ovalbumin at a 80:20 w. ratio (same buffer as above: PBS at 71.7 % vol. heavy water) are reported in the table 9.7.

The average burst temperature seems lower than the previous one, but the standard deviation suggest that variability between capsules has a marked impact. The statistic is not sufficient to draw clear conclusion in this case.

| **Sample** | 1 | 2 | 3 | **avg** | **stddev** |
|---|---|---|---|---|---|
| **Burst temperature (°C)** | 25.7 | 36.5 | 40.5 | *37.5* | *9.0* |

**Table 9.7.** *Burst temperature of capsules made from 80 % 43 °C UCST polymer.*

### 90 % 35 °C UCST polymer – 10 % ovalbumine capsules

Finally, a series of capsules was prepared from an aqueous phase, composed of 35 °C UCST polymer and ovalbumine, at a 90:10 w. ratio. The buffer was composed of PBS (71.7 % vol. heavy water). BSA-Texas Red was used as the fluorescent reporter. The results are shown in table 9.8.

| **Sample** | 1 | 2 | 3 | **avg** | **stddev** |
|---|---|---|---|---|---|
| **Burst temperature (°C)** | 22.4 | 25.0 | 20.8 | *22.7* | *2.1* |

**Table 9.8.** *Burst temperature of capsules made from 90 % 35 °C UCST polymer.*

The mean temperature is significantly lower in this case, compared to capsules containing the 43°C UCST polymer. Considering the poor statistic, no quantitative relationship can be established between UCST and temperature capsules breakage. Nevertheless, the T of response is here again lower than UCST. Changing the polymer affects burst temperature.

## Conclusion

Kindly provided by Y. Zhao's team (Sherbrooke University, Canada), the UCST polymer used were end-functionalized by carboxylic acid functions and thus could not be chemically attached into the capsule membranes. Using proteins, serum albumin or ovalbumin as monomers reacting on TDI, capsules were shown to incorporate UCST polymers and form thermosensitive membranes in a narrow range of composition. Ovalbumin gave the best results, which is consistent with the results reported by the group of K. Landfester [205].

Results are promising, as capsules were found to burst at a temperature close to the UCST of the polymer. In addition, the limited range of efficient compositions is comparable to the results obtained with non-reactive polyNIPAM. This suggests that significant improvement should be reached by making the UCST polymer end-reactive for covalent attachment to the capsules.

The use of NaCl, sucrose and $D_2O$ modulate the UCST of the polymers that can accordingly be chosen well below or above the room temperature. As mentioned in the review part, UCST polymer based capsules are very appealing for biological applications as an increase of temperature can be induced locally to trigger the release. This study has established the proof a concept that such capsules can be prepared.

# Conclusions & perspectives

# Conclusions & perspectives

The present work aimed to identify promising routes for the design of molecular tools that are capable to improve controlled chemical activation of cells. A need for non-invasive and local activation was identified in the context of academic biological studies, in particular studies of the early stages of cell growth, migration or polarization. To maximize the chance for successful encapsulation and fast on-demand delivery of fragile proteins or peptides, several functional assemblies were evaluated from literature. The specific constraints of biological environments and the need for a robust spatio-temporal control on responses primarily limits the candidates to 1) light-responsiveness – the milder and most versatile stimulus – with the alternative of temperature-responsiveness coupled to exposure to light, 2) systems compatible with mild encapsulation in aqueous core(s).

None of the systems currently used can reach all the requirements exposed below.

- Release and control on timescales faster than the biological responses to study.
  Typically, fast subcellular reorganization of the cytoskeleton is observable in the timescale of seconds, but minutes and hours are also of interest.

- Localized activation.
  If the release must occur in a limited region of space, or generate gradients to activate subcellular levels ($\sim \mu m$), it should be faster than diffusion of the released agents. Capsules have ideally to become permeable at subsecond timescales.

- Manipulation of fragile molecules, such as proteins, in conditions ensuring the preservation of their activity.

- Finally, toxicity of capsules or of the stimulus may be issues that deserve to be assessed.

In the present thesis, experimental investigations were focused on promising candidates that may fulfill the above requirements once optimized: liposomes and polymer capsules with an aqueous core, primarily because breakage of a thin membrane upon exposure to stimuli is likely to provide the fastest release. Although light can provide harmless stimulation and excellent spatial control, we also considered temperature-responsive systems as models. They represent the first step in the development of visible or infrared-sensitive systems – both can be implemented from the temperature-sensitive ones via the encapsulation of dyes or nanoparticles.

## Liposomes

Liposomes have been found to be "easily" turned into light-sensitive vehicles. Despite permeabilization to small molecules was extensively reported and sounded as promising basis, different principles are involved for the controlled release of proteins. To release quickly a high molecular-weight molecule, the membrane must indeed be disrupted or pores larger than several nanometers must be opened. Our model, light-sensitive liposomes, was based on the incorporation of azobenzene in the lipid bilayers, under the form of surfactants or polymers. The azobenzene-containing surfactant (azoTAB) proved efficient to solubilize liposomes, and solubilization was light-triggerable. A switch from UV-adapted cis-azoTAB to blue-adapted trans isomer triggers dissolution. However, the kinetics of dissolution was highly sensitive to the amount and distribution of azobenzene surfactant in the leaflets. Low amounts, or more surprisingly absence of surfactant in one of the two leaflets at the time of exposure under blue light markedly slowed down the kinetics. The timescale of hours emerged, thus indicating that such systems are not robust to dilution or to any competitive partition of the surfactants between other membranes (e.g. cell membranes). The reversible and fast responses (seconds) observed in mixed solutions of lipid and azobenzene surfactants near CMC showed however that reorganization and membrane dissolution can be rapid in conditions that distribute evenly the molecular partners.

To maintain azobenzene moieties in permanent proximity with the membranes, we used amphiphilic polymer "anchors". Previous studies performed in our laboratory showed that this polymer triggers the formation of pores in the membrane of giant vesicles, when irradiated with blue light. Our application to smaller liposomes indicates similar efficiency, and a fast release time of the order of tens of seconds. Detailed studies based on fluorescence were however hampered by the irradiation time during which no measurement was possible, and by complicated quenching effects in the liposomes.

Finally, two points deserve future studies that were out of the scope of the present work.

1. The absence of conditions that can afford full (100 %) release of encapsulated fluorophores is not understood. Assessment of the leakage of azobenzene surfactants and/or polymer-containing liposomes complicated by the high quenching efficiency of azobenzene may be carried out by an alternative method, based on FRAP and differences in the diffusion coefficients of encapsulated and released molecules. This method has been optimized during this thesis and will be considered in future experiments.

2. The literature reports on the kinetics of liposome dissolution by surfactants are scarce – which contrast with the extensive reports on phase diagrams at equilibrium – and mostly rely on DLS analysis. A more precise analysis of transition from micelles to vesicles in liposome/surfactant interaction is certainly required. It is planned to resume the study initiated in the present work by the analysis of the transitions by time-resolved small angle X-ray scattering.

## Polymer capsules

As an alternative to liposomes we considered polymer capsules. They were reported in the literature to be versatile objects, able to encapsulate molecules with a high yield and to release their content by the disruption of the membrane. In 2012, the date at which this work started, no particularly successful results on light-sensitive polymer membranes were available in the literature, and most responsive systems did not enable simple encapsulation of fragile molecules. We choose to build capsules based on interfacial polyaddition approaches (aromatic diisocyanate + polyamines) known at the time to yield non-responsive systems, but to facilitate encapsulation in mild conditions. Adjustment of membrane composition was anticipated to enable responsiveness by integration of polymers that dissolves upon a temperature shift. Because of its vast potential for chemical adjustments and extensive reports existing in literature, the model of polyNIPAM was considered as representative of polymer chains with LCST. On the other hand, studies of a more original system, based on UCST of neutral chains in water, were initiated in collaboration with the group of Y. Zhao (Sherbrooke Univ.).

Preparation of macrocapsules with a diameter of the order of the millimeter was an important preliminary step, because this configuration enabled direct observations and identification of artifactual phenomena, due to adsorption or covalent attachment of fluorophore probes in the capsule membranes. Based on these model macrocapsules, it is possible to conclude that membranes can be made by covalent attachment between aggregates of polyNIPAM. In addition, mechanically resistant mixed membranes can be made by the addition of short amines with hydrophobic isocyanates in the presence of polyNIPAM or of the UCST polymer. They were found to be easily processed and impermeable to small hydrophilic molecules when kept respectively above the LCST or below the UCST.

Amine-terminated polyNIPAM formed temperature-responsive membranes in a broad range of composition – copolymerization with non-responsive hydrophobic amines, in the window of 25 % to 100 % w. Variation of composition provided a tuning parameter to modulate the membrane rigidity and hydrophobicity. The window of compositions yielding temperature-responsive capsules was in comparison relatively narrow when the temperature-responsive chains are not covalently bound. This result came from a control experiment showing that in the main part of the composition range, covalent attachment was required. But it may in practice speak in favor of preparation of capsules from any commercially available polymer showing a transition of solubility. In the absence of a tight attachment of the responsive chains, variability may however emerge in the temperature of responses, as revealed by the standard deviation of several degrees of the temperature of breakage (capsules containing UCST polymers). One shall prefer to introduce reactive (amine) end groups in the chain and to form the membrane by copolymerization with short amines, which in our hands (with polyNIPAM) yielded well controlled temperature of permeabilization, close to LCST of the responsive polymer in the outer medium of capsules.

Finally, to achieve obvious responses to temperature, and high degree of release of encapsulated probes (including proteins), it is critical to control the conditions of addition.

In practice, it has been difficult to alleviate cross-interaction with additives, including surfactants, osmolytes (sucrose, NaCl), and side reaction of isocyanates with hydroxyl and/or amine groups that were present on proteins. This may be a practical issue Preparation of capsules based on the reaction of a protein (ovalbumin, BSA) added in excess improved clearly the system, by preserving the protein of interest (in this work fluorescent probes) from being irreversibly bound to the membranes. It was also forming apparently more homogeneous membranes than with the polyamine:TDI precipitates.

In general, we highlight that the adaptation of the protocol and in particular the nature of molecules present in internal compartment of droplet at the stage of capsule polymerization has a critical impact on capsule functionality. Our work identified important parameters, and contribute to progress toward the rational design of robust and biocompatible responsive systems, which is a demanding task becoming now within our reach.

# Part IV.

# Appendices

# Table of Contents


**A. Role of molecular gradients on biological systems** **171**
A.1. Gradients role during embryogenesis . . . 172
A.1.1. From the symmetric embryo to gastrulation . . . 172
A.1.2. Tissue and cell scale . . . 175
A.2. Immune system . . . 176
A.3. Cancer development . . . 177

**B. Currently used gradient generators** **179**
B.1. Diffusion-based gradient generators . . . 179
B.1.1. Coculture based assays . . . 179
B.1.2. Pipette based assays . . . 180
B.1.3. Diffusion in culture chambers . . . 182
B.1.4. Diffusion in hydrogels . . . 184
B.2. Flow-based systems: microfluidic devices . . . 186
B.2.1. Cells in the flow of the microfluidic device . . . 187
B.2.2. Cells in low shear-stress channels . . . 189

**C. Materials & Methods** **193**
C.1. Materials . . . 193
C.1.1. Chemical and biological materials . . . 193
C.1.2. Specific laboratory furnitures . . . 194
C.2. Sample preparation procedures . . . 194
C.2.1. Fluorescein isothiocyanate netrin-1 labeling . . . 194
C.2.2. α,ω diamino-terminated poly(NIPAM) synthesis . . . 195
C.3. Sample characterization . . . 196
C.3.1. Dynamic and static light scattering . . . 196
C.3.2. UV-visible spectroscopy . . . 197
C.3.3. Fluorescence intensity measurements . . . 198
C.3.4. Maximum bubble pressure tensiometer . . . 199

C.3.5. Other characterizations . . . 200
C.4. Various calculations . . . 200
C.4.1. Evaluation of the encapsulated volume fraction in a liposome suspension . . . 200
C.4.2. Evaluation of the characteristic time of release from a porous liposome 201

**D. Experimental techniques 203**
D.1. Maximum bubble pressure tensiometer . . . 203
D.1.1. Principle . . . 203
D.1.2. Determination of surfactant concentration . . . 205

**E. Preparation and characterization of liposomes 209**
E.1. Sample preparation procedures . . . 209
E.1.1. Liposome suspensions preparation . . . 209
E.1.2. Liposome purification by GPC . . . 209
E.2. Sample characterizations . . . 210
E.2.1. Systematic size and concentration characterization . . . 210
E.2.2. AzoTAB-mediated dissolution of liposomes . . . 210
E.2.3. Characterization of the release from azo polymer-sensitized liposomes 212

**F. Preparation and characterization of polymer capsules 215**
F.1. Millimeter-sized capsules . . . 215
F.1.1. General procedures . . . 215
F.1.2. Assays description . . . 218
F.2. Nanometer-sized capsules . . . 222
F.2.1. HMDA-based capsules . . . 222
F.2.2. Synthesis and characterization of polyNIPAM capsules . . . 223
F.2.3. Determination of the temperature of release with the calcein+cobalt assay . . . 224
F.2.4. Morphological study by cryo electronic microscopy . . . 225
F.2.5. TexasRed fluorescence in presence of albumin . . . 226

**G. Quantitative and real-time FRAP measurements 227**
G.1. System description . . . 228
G.2. Theory . . . 229
G.2.1. The ideal system: an infinite picture . . . 229
G.2.2. Effect of the size of the recorded picture . . . 230
G.3. System implementation . . . 231
G.3.1. Setup description . . . 231
G.3.2. Data analysis . . . 231
G.3.3. Error function effect . . . 232

**Bibliography** **235**

**Abbreviations & acronyms** **263**

# A. Role of molecular gradients on biological systems

Whether it is a single isolated cell or a whole organism, biological system activity is regulated by several external signals of various nature. Both chemical and physical cues have been reported in literature.

Chemical signal family is very heterogeneous in term of cue and of target. It includes ions ($Ca^{2+}$, $Mg^{2+}$), dissolved gases ($O_2$, $N_2O$), small organic molecules (ionized or neutral, like acetylcholine), peptides and proteins of various sizes. The targets of these molecules can be either intracellular or extracellular. Magnesium ions have been reported to regulate gene expression in Humans, by interacting directly with enzymes and nucleic acid [256]. This is also the case for lactose; this sugar is normally not metabolized by enteric bacteria, like escherichia coli. However, its presence is sufficient to trigger on several bacteria strains the expression of several genes, which will lead to the production of proteins involved in the transport and the metabolism of lactose. As for external stimuli, numerous examples are reported. Neurotransmitters, hormones, growth factors are examples of molecules targeting receptors located on the cell membrane.

Cells are also sensitive to physical stimuli. Neurons or fibroblasts are known to discriminate their culture substrate by its stiffness [257, 258]. In the human body, some cells are even specialized to the transduction of physical signaling, like the photoreceptor cells for light, the lamellar corpuscle cells for pressure or the thermoreceptors for temperature. Electrical fields are used to propagate information along nerve fibers in most multicellular animals, but they are also reported to influence cell migration in wound repair or tumor genesis [25, 259].

Sensibility to signals can differ strongly from one cell type to another. Some react to the instantaneous concentration of the signaling molecule. This is the case for β-cell in the pancreas for example: they adapt their insulin secretion as a function of the glucose concentration. At the opposite, some cells are sensitive to the temporal and spatial distribution of a signaling molecule, and as often referred to as gradients. These gradients of chemical cues has been reported to play a role during the embryogenesis of vertebrates, to affect cells of the immune system or even play a role in the development of cancers. In many articles, the gradient is expressed by its relative slope on a characteristic length. The relative slope, noted $s$, is calculated as $s$ (in %) $= 100 \cdot \Delta C/C$, where $\Delta C$ is the difference of concentration between the two ends of the cell (or the ends of the studied part of the cell) and C is the mean value of the concentration along the cell. The characteristic length is the

length between these two ends, which is in the range of 10 µm, and often assumed to be exactly 10 µm (see figure A.1).

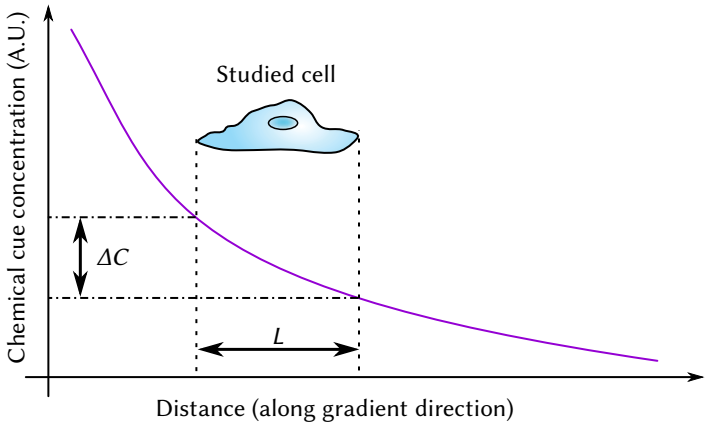


**Figure A.1.** *A cell in a gradient of a molecule of interest. The relative gradient steepness, $s$ in percentage, is defined as $s = 100 \cdot \Delta C/C$, where $C$ is the mean concentration on the cell level [22].*

## A.1. Gradients role during embryogenesis

Embryogenesis is a good example of chemical cue sensitivity, as the gradients affects the whole embryo, and are responsible for its evolution from a symmetric cell heap to a non-symmetric organism with differentiated cells. For reference, the anatomic axes of a differentiated mouse embryo are shown on figure A.2.

### A.1.1. From the symmetric embryo to gastrulation

The embryo begins as a symmetrical unicellular fertilized egg. In the early stages of development, the embryo morphology stays the same. The only evolution is owed to cell division, which increase the cell number. In the case of the mouse embryo, this process goes along with cell differentiation, from stage E3.5 onwards. As shown on figure A.3, the symmetric cell heap is replaced by the blastocyst, which consists in two differentiated cells. The trophectoderm cells are located on the periphery of the embryo, while the inner cell mass constitutes the inside of the blastocyst.

The symmetry of the embryo is broken shortly after its implantation, which occurs between stage E4.5 and E5.5. The embryo elongates along the proximal-distal axes to gain an egg shape. This elongation is accompanied by the localized expression of proteins from the TGFβ, Wnt and FGF families. The nodal protein from TGFβ family is expressed in the vicinity of the extraembryonic/embryonic visceral endoderm by the embryonic visceral endoderm cells (see figure A.3, the frontier between the pink and blue regions on the E5.5 stage). Nodal secretion is regulated by several mechanisms involving the

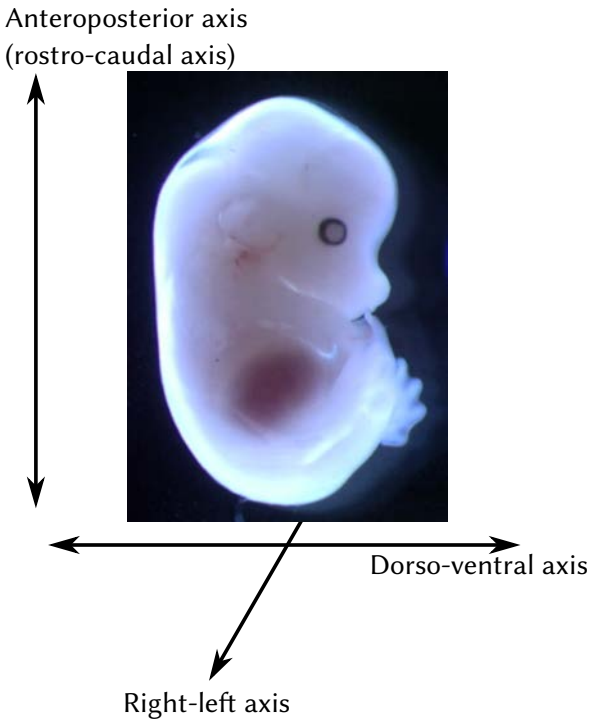


**Figure A.2.** *Mouse embryo, 14.5 days old. The three axes (anteroposterior, dorso-ventral and left-right) are represented by arrows.*

extraembryonic cells, leading to the formation of a proximal-distal nodal gradient. This gradient is responsible for the cell differentiation and organization along the proximal/distal axis [9].

The anteroposterior axis (see figure A.2) is defined by the gradient of Wnt [8–10], not only in the mouse but in most animals (see figure A.3, on the inferior part of the pink region). In mammals, Wnt is expressed in the posterior region, while a Wnt inhibitor is secreted in the anterior region, establishing a gradient of both proteins.

Nodal and Wnt are not the only two proteins involved during embryogenesis, and they are certainly not the only ones to be secreted as a gradient. Serotonin, inversin, polaris and various other proteins have been proteins have been reported [260].

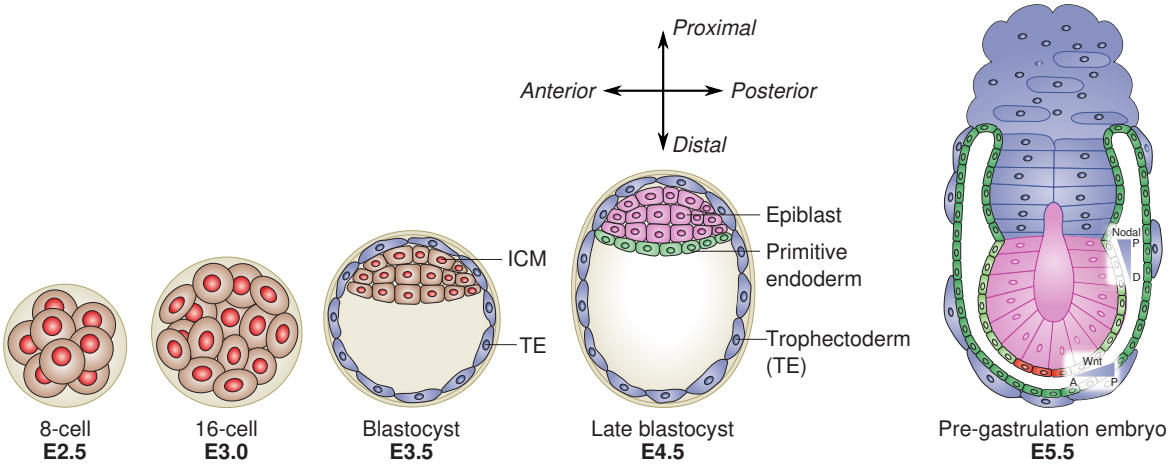


**Figure A.3.** *Early stages of mouse embryo development, from day 2.5 (E2.5) to day 4.5 (E4.5). The initial symmetry is broken at E3.5 when the blastocyst is formed by the segregation of the inner cell mass (ICM) and the trophectoderm cells (TE). Gradients of Nodal develops in the medial part of the embryo, below the extraembryonic (in blue) and embryonic (in pink) visceral endoderms. This give the direction of the proximal/distal axis. Wnt gradient develops at the distal extremity of the embryo which contributes to the development of the anterio-posterior axis. Adapted from [9].*

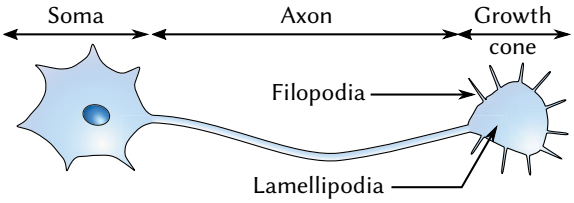


**Figure A.4.** *Schematics of a migrating neuron. The dynamic part, sensitive to netrin-1 is the growth cone.*

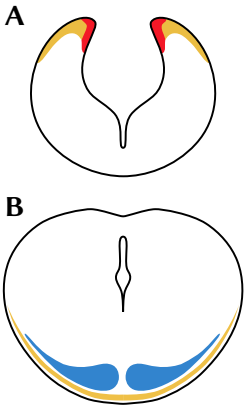


**Figure A.5.** *Precerebellar neurons migrate from the rhombic lip (A, in red) to the ventralregions of the ventral hindbrain regions (B, blue and yellow). Adapted from [261].*

## A.1.2. Tissue and cell scale

On a smaller scale, protein gradients are also responsible for the constitution of tissues during embryogenesis. The nervous system undergoes massive changes during this period, which involves neurogenesis, neuron migration and axon development. Precerebellar neurons (see figure A.5) are known to migrate from the rhombic lip to the ventral hindbrain [261]. This process is driven by a protein from a laminin related protein called netrin-1, also involved in neuron survival [13]. Neurons are *attracted* by increasing concentrations of this protein and are very sensitive to it. It has been reported that 5 molecules of netrin-1 are sufficient to trigger a morphologic response from the cell [44]. However, the relation between biological response and netrin-1 concentration is not obvious. While low doses are sufficient to trigger a response, its activity can be modulated by other proteins. Above a critical concentration, the Slit protein is able to annihilate netrin-1 activity. Without netrin-1, Slit is reported only as slightly repulsive. On Xenopus, it has also been found that a small fragment of laminin-1, a constituent of the extracellular matrix, is able to reverse the netrin-1 activity which becomes repulsive [262]. An interesting result, even more when remembering netrin-1 belongs to the laminin related-protein family.

Other protein gradients are also reported. FGF (fibroblast growth factor) family is involved in the development of neocortex, in particular in the development of its rostro-caudal axis and in its area patterning [263] (see figure A.6). TGFβ proteins are also found, along the bone morphogenetic protein (BMP), to be involved in spinal cord proliferation [264]. NGF (nerve growth factor) is a chemoattracting protein for neurons from rat superior cervical ganglion. It has been reported that the cell response is also dependent on the gradient steepness [2].

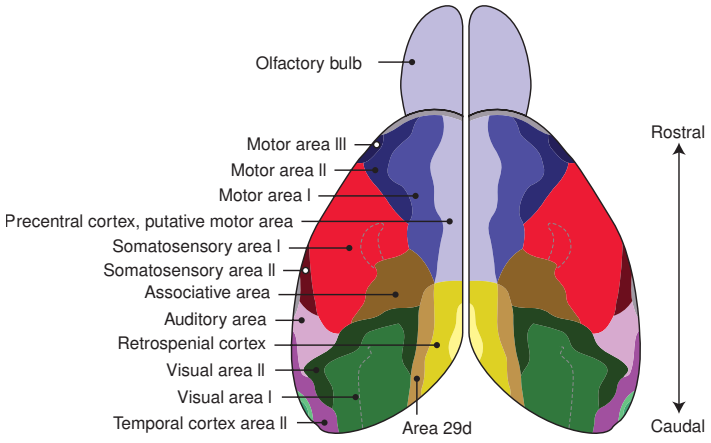


**Figure A.6.** *Areas of mouse neocortex, dorsal view. Reprinted from [263].*

## A.2. Immune system

Gradients of molecules cue plays also a role after the embryogenesis. Some families of cells are known to migrate in the direction of the increasing concentration of a particular molecule. This phenomenon is called chemotaxis. A part of the immune system response against a pathogen is based on chemotaxis. Macrophages are cells from the innate immune system specialized in phagocytosis. They are present in most tissues and represent the front-line of host defense against pathogens. Diverse receptors are expressed on its membrane to detect various antigens generally expressed on the surface of pathogens, like bacteria. When a pathogen is encountered and recognized by the macrophage, a phagocytic process is engaged, leading to the destruction of the foreign body. This process is accompanied by the secretion of several cytokines, including chemokines, like interleukine-1 (IL-1), IL-2, IL-8 or the tumor necrosis factor α (TNFα). These molecules will diffuse around the macrophage and eventually reach the blood flow. The surrounding tissue will also affect the surrounding tissues, leading to the inflammation.

Two kinds of cells will be recruited from the blood stream by the cytokines, the neutrophiles and the monocytes. Both are leukocytes which are normally present only in the blood flow. In particular, they are not found in healthy tissues. The final role is the same, to destroy the pathogen with a phagocytic process. While neutrophiles are directly able to fight, monocytes are not potent cells. They are only macrophage precursors and need to differentiate themselves, which only occurs after leaving the blood stream [265]. Figure A.7 summarizes this process.

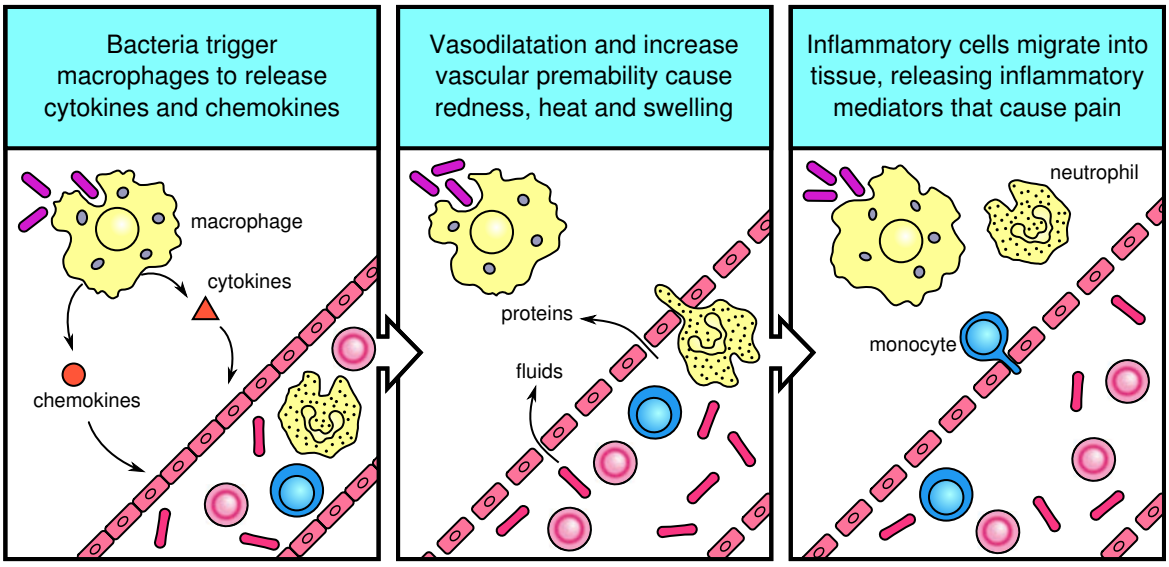


**Figure A.7.** *Some bacteria are detected by a macrophage. Neutrophiles and monocytes are recruited to the site of infection by the secretion of chemokines and other chytokines. Red cells represents erythrocytes. Adapted from [265].*

Neutrophils are highly sensitive cells: a gradient steepness lower than 1 % is sufficient to polarize the cells. This has been reported for *N*-formylmethionylmethionylmethione (fMMM), *N*-formylmethionylleucylphenylalanine (fMLP) [31] and IL-8 [32]. They also respond to a broad range of cytokines, as mentioned before. Due to these properties, neutrophils have become a widespread model to study chemotaxis [266]. Some pathways implicated in the chemotactic processes have described. The cytokine detection almost always involves the binding to a heterotrimeric G protein. If it seems simple outside the cell, the complexity increases drastically inside. Various intracellular signaling pathways have been identified: they involve phospholipases β2/3, phosphatidylinositide 3 γ, ion channels, adenylyl cyclases... This complex signaling pathways has numerous consequences, and amongst them is probably the non-linear response to cytokine concentration [267].

Several specific equipments have been developed to study the neutrophil chemotaxis. They range from simple chambers with a fixed uni-dimensional concentration gradient allowing 2D culture [31, 33] to more complex chambers allowing real time observation of cell polarisation in 3D collagen gel [268, 269]. Attempts to study the cells under a time-dependent gradient have also been reported [41].

## A.3. Cancer development

Chemotactic molecules are also reported to play a major role in cancer development and metastasis. Understanding the role of each molecule and the associated signaling pathways are considered to be a key to developments of new treatments. Targeting precise molecules or signaling pathways should lead to more efficient and specific treatments [270]. The task is far from being easy: the cancerous cells are sensitive to a large range of cytokines. It is even worse as the effect of one molecule varies from one cancerous cell type to the other.

Cancerous cells are called metastatic when they are able to leave their original tumor to spread to other organs. To achieve this, these cells must cross several barriers. The first is the tumor itself; the second one is the extra-cellular matrix of the surrounding tissues. The blood flow is reached by a process called the intravasation, which leads to a dissemination of the cells in the whole body. The cells will get out of the blood vessel by an extravasation process, which can be related to the leukocyte tissue invasion. It has been shown for several types of cancerous cells that the migration process is attributed to cytokine gradients. In the case of mesothelioma cells, a rare type of cancer which affects the mesothelium, several growth factors have been found to trigger a migration of cells. IGF-I and IGF-II are reported to both trigger the migration of the cells and direct their migration. To illustrate the complexity of the studied systems, the authors underline that these cells does not respond to aFGF, bFGF, GM-CSF and IL-6, while these molecules are known to stimulate the movement of carcinoma and sarcoma cells [271].

The stroma cell-derived factor-1 (CXCL12) involved in leukocyte migration has also been found to play a role in metastasis for several cancers: the breast cancer [39], the non-small cell lung cancer [38] or glioblastoma [272].

# B. Currently used gradient generators

## B.1. Diffusion-based gradient generators

These gradient generators are based only on passive diffusion of the molecule of interest, either in solution or in a 3D hydrogel.

### B.1.1. Coculture based assays

This technique is probably the first used to study the response from developing cells to gradients of chemotactic molecules. Its principle is simple: two populations of cells are cultured in a hydrogel. One is the studied population; the other one is secreting the chemotactic factors. Both populations are organized as clusters, facing themselves in the hydrogel [37]. The cluster of secreting cells acts as a localized source of molecules, as shown on figure B.1.

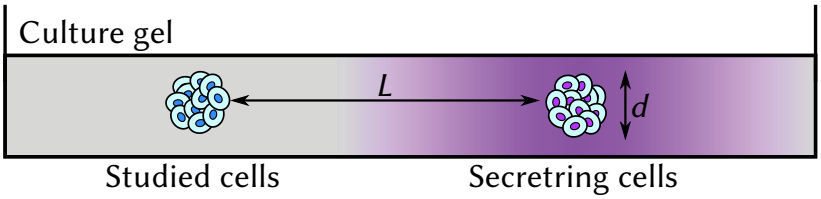


**Figure B.1.** *1D gradient generated in a culture gel with the coculture method. The gradient is represented in purple, and is established around the cluster of generated cells. The typical distance between the studied cells and the secreting cells $L$ is 1 mm; the size of both clusters $d$ is in the 100 µm – 1 mm range. Collagen is often used as the culture medium, at a concentration of 2–3 g/L [12, 13].*

The earliest reported assay was focused on the study of ganglion neurons from chicken embryos [37]. A gradient of NGF was supposedly generated by tissues taken from different organs (heart, kidney, colon). The cells from the ganglia responded by migrating towards the source of NGF. However, the secreting cells were not specialized in NGF secretion, which suggests that the NGF gradient was superimposed with gradients of other unknown molecules.

This issue was confirmed later by Lumsden et al. [273]. Neuron ganglions from mouse embryos were submitted to the gradient of NGF secreted by neuronal tissues. As in the previously mentioned experiment, the neurons were attracted by the NGF source, but a NGF inhibitor was not sufficient to repress this attraction. This observation suggests that

at least one more molecule secreted by the neuronal tissues has an attracting effect on neurons. The same conclusion has been done with laminin [274].

Using tissues known for secreting the molecule of interest enabled to show the chemotactic abilities of neurons. However, due to the various secreted molecules at the same time, it is impossible to determine the role of each molecule separately. Thanks to the progresses made in genetic engineering, it became possible to design cells specialized in the expression of the molecule of interest. This method has been applied to various chemotactic factors. Fibroblast growth factor (FGF-1) were efficiently secreted by transfection of NIH 3T3 cells to study neurons from rat spinal ganglia [275]. Several molecules from the semaphorin family (Sema III, E, IV) were also produced by this method and applied on neurons from superior ganglia of rats [276]. Other molecules, like netrin-1, have also been reported [13, 277].

This method, while having the advantage of being simple, suffers from several drawbacks. The gradient is not established immediately after the cells are put in the gel. The characteristic diffusion time can be estimated with the following formula: $\tau \sim L^2/D$, where $\tau$ is the characteristic diffusion time, $L$ is the characteristic diffusion length and $D$ the diffusivity of the studied molecules. For a protein which has no interaction with the culture gel, its diffusivity is in the range of 100 µm²/s. Under such conditions, we have $\tau \sim L^2/D = (10^{-3})^2/100 \cdot 10^{-15} = 10^4$ s. The gradient is established in approximatively 3 hours on the 1 mm separating the clusters. This kind of experiment is therefore limited to long-term studies, on large length scales. While it is sufficient to study neurons, it may not be sufficient for other cells. In fact, no other kinds of cells are reported. The other main limitation of this technique is the absence of control on the gradient. The molecule is secreted continuously, and there is no convenient way to quantify the concentration, either during the experiment or after. Gradients of proteins have been predicted using diffusion based models [278], but not confirmed by immunofluorescence due to an insufficient sensitivity of this technique. It is also reported that the steepness of the gradient and the mean value of the molecule concentration is mainly dependent of the distance between the two clusters [22]. The gradient is therefore not easily reproducible from on experiment to the other.

### B.1.2. Pipette based assays

The other commonly used technique used to create gradients from a punctual source use micropipettes, as shown on figure B.2. In the typical experiment, the point of the pipette is located at 100 µm from the studied part of the cell. The pipette body is commonly placed at 45° from an imaginary line drawn between the cell and the pipette tip [3]. The molecule is released most of the time on a pulsed regime using a pressure generator, although diffusion-based only processes are also reported [26]. Compared to a constant flux, the pulsed release prevents the flow to reach the cells, which may trigger an undesirable response. This system has been applied on various kinds of cells, ranging from neurons cultured in 3D

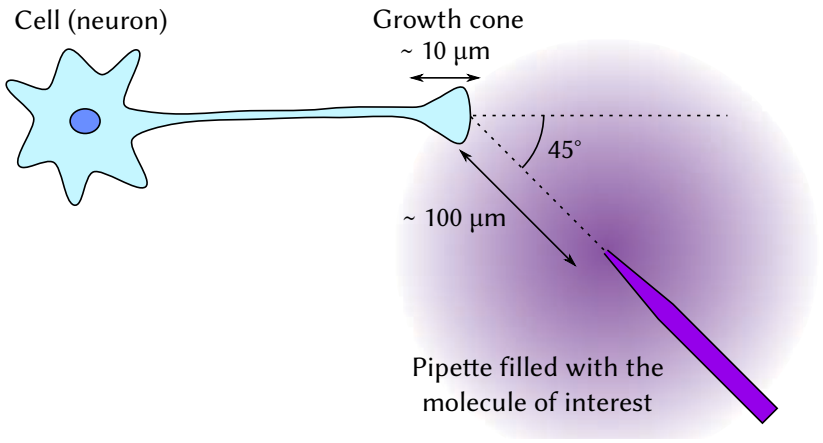


**Figure B.2.** *A pipette is used to create a local source of a molecule of interest in a culture medium. The gradient is represented in purple. The scale of the targeted cell (leukocyte) or part of cell (the growth cone of a neuron) is typically 10 µm. The pipette is located 100 µm away from the cell. The concentration of the molecule is assumed to be 1/1000 of the one in the pipette.*

collagen gel [2] to leukocytes [26] or cancerous cells [27] in 2D culture conditions. The same diversity is found for the released molecules, ranging from proteins [2, 28] to peptides [26].

The advantage of this technique compared to the previous one the possibility to control precisely the ejected amount of molecules in space and time. Reproducible gradients of high steepness can be reached by this method, in the range of 10–30 % [4, 11, 25]. The mean value of the molecule concentration around the cell can be controlled by the concentration of the molecule in the pipette. The time required for the gradient establishment is in the range of 10 minutes [4], but is considered table for longer periods, allowing to study cells on long timescales, in the range of one hour [23, 24]. However, the gradient range is in the 100 µm range, which can be reached by cells during the experiment. To maintain the cell in a gradient of defined concentration and range, it may be required to move the pipette during the experiment [279].

However, most of the cited publications in the last paragraph are based on a single article by Lohof et al. [3], where the characterization of the system is made. Authors often derive the concentration and the gradient slope from it without further characterization. This has been the subject of several discussions and criticisms [4–6]. A theoretical analysis of the pipette-based gradient generator and its experimental has been performed by Pujic et al [4]. The assumed linear relationship between the released molecule from the pipette and the pulse duration and frequency is not always true. The gradient is also often considered 2D, neglecting the vertical component. This is not verified experimentally by confocal imaging, which shows an heterogeneous of a labeled dextran along the vertical axis. These two observations turn the pipette-based in a qualitative-only assay, as the prediction of the local concentration of the released molecule is unreliable.

Unfortunately, this technique suffers from others drawbacks, independent from the characterization of the gradient. Only one cell can be studied at a time; to study N cells

in parallel, one should possess N micropipette devices, and probably N microscopes too if the observation is to be made live. To study the effect of more than one molecule, several pipettes should be used. It could be circumvented by mixing the molecules altogether, at the expense of having a fixed gradient of these molecules, which is somewhat limiting. Eventually, it should be noted that most of the experiments has been conducted with 2D cells cultures. The experiment has been conducted in 3D cultured cells (collagen gel) in only one of the cited references [2].

### B.1.3. Diffusion in culture chambers

Specifically designed culture chambers have been proposed to study the cells. Compared to the two previously cited systems, they produce a known an reproducible gradient, and due to their size, several cells can be studied at the same time, which make them an high-throughput system.

#### The Boyden chamber

The first reported chamber is the Boyden chamber [280], which is shown on figure B.3. The cells are studied in suspension, and are separated from a solution of the studied molecule by a classical filter membrane, in which the gradient is established. The chemotactic property of the molecule was assessed by counting the leukocytes trapped inside the membrane.

The system is simple, but suffers also from several drawbacks. It is not possible to track the cells in real time: the system must be emptied to isolate the filter. The gradient established near the filter is also not predicted, and is known to vary with time [6]. And finally, the cells are studied in suspension, which is not representative of the in vivo conditions.

This system is however used widely as a cell invasion model, as it occurs during cancer metastasis or during immune cell migration [281–283]. The filter is replaced by various membranes, ranging from simple collagen gels of various densities to more complex gels mimicking the extra-cellular matrix. To my knowledge, this system has not been applied to neuron migration.

A microfluidic version of this chamber has also been developed, enabling live-imaging of the migration and invasion process [284].

#### The Zigmond chamber

The Zigmond chamber can be viewed as an enhancement of the previous chamber. The chamber is made of two compartments linked by a small bridge (1 mm wide) where the gradient develops. The whole cell is made of glass, which allows to record the cell migration in live. The gradient was characterized using fluorescein isothiocyanate, and was found to be the steepest from 15 minutes to 90 minutes after filling the wells, and was considered to be steep and stable from 30 minutes to 90 minutes. No other characterization of the

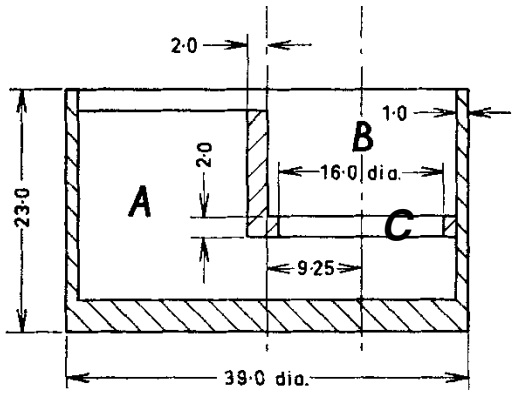


**Figure B.3.** *A side view of the Boyden chamber. A suspension of cells is placed in the compartment labeled B, and a solution of the studied molecule is placed in compartment A. The two compartments are isolated by a porous membrane, located in C. Adapted from [280].*

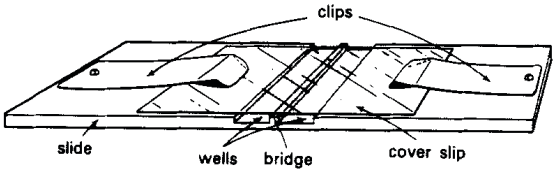


**Figure B.4.** *The original Zigmond chamber. The two wells act as sink and source, while the gradient is established in the bridge. Cells are cultured on the coverslip used to close the chamber. Reprinted from [31].*

gradient was done. The chemotaxis of human leukocytes to various peptides, like fMLP, is reported [31].

### The Dunn chamber

The Zigmond chamber is not sealed, which is problematic on long term experiments, as the culture medium is allowed to evaporate. The Dunn chamber is presented as an evolution of the previous chamber, overcoming the evaporation problem. Like the Zigmond chamber, the gradient is established in a small region linking two wells, acting as source and sink (see figure B.5) [33]. The gradient shape and time evolution has been described with a

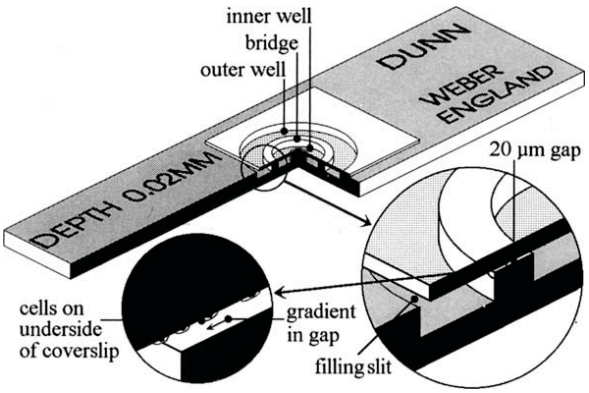


**Figure B.5.** *Schematic view of the Dunn chamber, reprinted from [29].*

numerical model and assessed experimentally with fluorescent molecules. A linear gradient of rhodamine labeled dextran is established in approximatively 20 minutes, and is sustained for several days. The slope of the gradient is in this case the highest one can expect from a linear gradient. This chamber has been used to study the chemotaxis properties of peptides on leukocytes [33] and proteins (macrophage colony stimulation factor) on macrophages [285], on long term experiments (90 minutes to 3 hours).

## B.1.4. Diffusion in hydrogels

### Gel printing

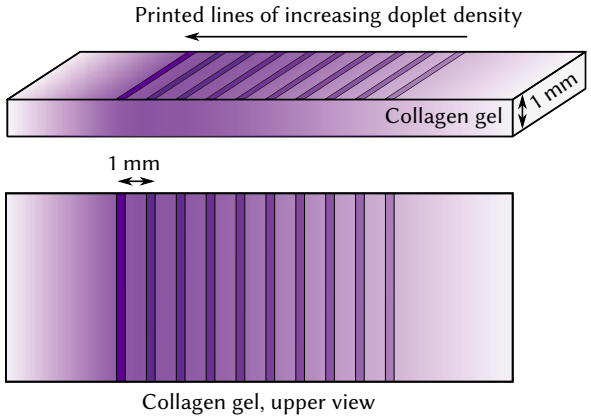


**Figure B.6.** *Generation of a molecule gradient inside a collagen by printing lines of increasing droplet density on its surface. The molecule of interest is represented in purple. The gradient is established by diffusion from the lines to the gel.*

Gradients inside a collagen gel have been generated by depositing the studied molecule on its top. The system described in ref [34] is shown on figure B.6; the theoretical analysis and experimental validation of this system is shown in ref [35]. Lines of increasing concentration in NGF have been printed on the top of a 1 mm-thick collagen gel containing the studied cells, which were neuron explants from rat embryos in this case. The same solution is deposited on each line; the increasing concentration pattern is achieved by increasing the droplet density from one line to the other. A linear gradient is established within 1 hours; before, its profile shows oscillations, due to the discrete pattern from which the gradient comes from. The gradient is established on a long range, 1 cm, and can persist more than 12 hours with a constant slope and mean concentration on almost 0.5 cm. However, these good performances are counterbalanced by several issues. The steepness of the generated gradient is rather low: gradients up to 0.4 % have been generated. It has been used to prove that neurons are sensitive to slope as low as 0.1 % with a mean concentration of 1 nmol/L, but all cells are not as sensitive. A dedicated equipment, specialized in dispensing drop of 1 nL on top of the collagen gel, is required, which proves expensive. These drawbacks may explain that only a few chemotaxis experiments are based on this technique [2].

This technique was not met with a great success: only a few chemotaxis experiments have been reported [2]. One way to make this technique more accessible may be to use desktop inkjet printers, as they have been successfully modified to allow cell printing, and are used in tissue engineering [286].

### Diffusion in a collagen bridge

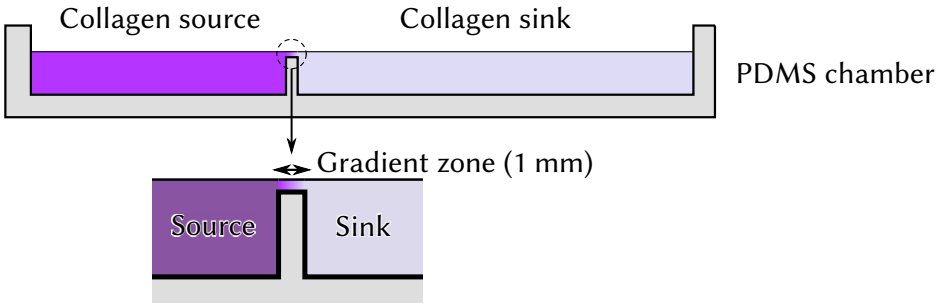


**Figure B.7.** *A gradient of molecules is established in the collagen junction between two chambers filled with collagen. One of the chambers contains the molecule and acts as a source, while the other one does not contain the molecule initially, and acts as a sink.*

Gradients have also been generated in systems as simple as the one shown on figure B.7 [36]. The system consists into two chambers isolated by a PDMS bridge 1 mm thick. Filled with collagen, the two chambers are connected by collagen bridge 1 mm thick and 200 µm high. One of the chamber is filled with collagen containing the studied molecule and acts as a source, while the other one acts a sink. A linear gradient is established within one hour in the collagen bridge, but evolves with time. The highest gradient steepness, 1.2 %, is reached in 6 hours, as reported by 40 kg/mol dextran labeled with tetramethyl rhodamine. Its value stays around 1 % for the next 18 hours. This system has been successfully used to study the chemotaxis properties of NGF and Slit2 against neurons from rat embryos. This device is probably by far the cheapest, and is sold by its creators as such. The most expensive part is the reusable mold used to make the PMDS chambers, with a price of $100. This chamber can prove to be very useful for long-term experiments requiring steady-states gradients. They can't however be used to study the cell response to a fast-established gradient, in the timescale of the second.

Some variations of this system are also reported. The collagen bridge can be replaced by a membrane [269].

### Towards the generation of gradients in 3D gels with microfluidic devices

A variation of this system using an inverse configuration, with refillable sink and sources, is shown on figure B.8 [30]. The 1D gradient is established in a millimeter-sized channel filled with an agarose gel, with either a linear shape or an exponential shape. The gradient is established initially within 7 hours, which is slow. The advantage in this resides in the

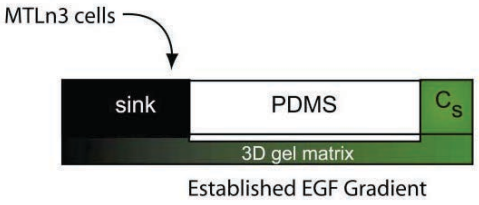


**Figure B.8.** *Gradient generated in channel filled with collagen gel. The channels two wells, which acts either as the source or the sink. Reprinted from [30].*

possibility to empty and fill again the sink and the source. If done regularly, at a frequency determined by a theoretical analysis of the system, it is possible to maintain the gradient for at least 10 days, in the case of the linear gradient. The theoretical results have been assessed with Alexa 488, a small hydrophilic fluorescent dye ($M_w \sim 400$ g/mol). They also used their chamber to study the chemotaxis of leukocytes in a collagen matrix against a gradient of fMLP.

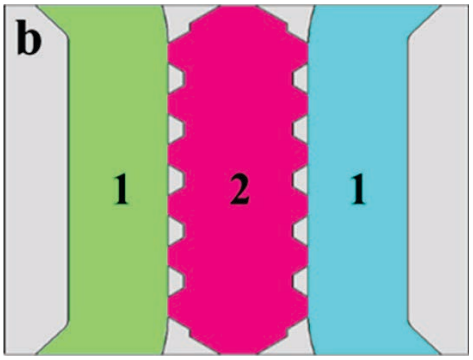


**Figure B.9.** *A diffusion-based gradient generator, implemented in microfluidic device. The inner chamber (in pink) is filled with a hydrogel containing the studied cells. The side channels (blue and green) acts as the source and the sink. Reprinted from [287].*

An automated version of this system has been implemented in microfluidic devices, as shown on figure B.9 [287]. As the dimensions of the diffusion chamber are also of millimeter scale, performances comparable with the previous system should be expected. No precise characterization of these systems was performed on a long time range, but a linear gradient is expected within 24 hours, as shown by their numerical predictions. Nevertheless, those systems were used to study the migration of human fibroblasts against a gradient platelet-derived growth factor or TGFβ.

## B.2. Flow-based systems: microfluidic devices

Microfluidic based devices has also reported to generate gradients of molecules in culture of cells. The simplest device is able to create a defined linear gradient in a liquid culture

medium, which has already been addressed by the various chamber-based systems shown above. The main difference between the two system is the possibility to create dynamic gradients in a microfluidic device, which was not possible in the steady-state chambers. Some systems specifically designed for biological applications are reviewed in various references [5, 6, 288–292].

In microfluidic devices, two phenomena are responsible for the creation of the gradient: the convection and the diffusion. Péclet number can be used to determine which phenomenon prevail above the other [292]. Its expression follows:

$$\text{Pé} = \frac{UL}{D} \tag{B.1}$$

where $U$ is the fluid velocity, $L$ the characteristic length of the microfluidic channel and $D$ the diffusivity of the considered molecule. At high Péclet regimes (Pé $\gg$ 1) convection is the dominant mass transport mode, while at low Péclet regimes (Pé $\ll$ 1), diffusion is the dominant mode.

## B.2.1. Cells in the flow of the microfluidic device

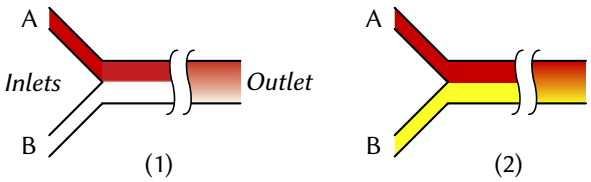


**Figure B.10.** *Y-shaped microfluidic device, as described in reference [293]. (1) a gradient of a molecule (in red) is obtained in the microfluidic channel. (2) same systems, with two molecules (the red one is introduced in A, the yellow one in B); two opposite gradients are obtained.*

The most simple device of this category is made of T- or Y-shaped microfluidic channels, as shown on figure B.10 [293, 294]. In such systems, the gradient is created by injecting a fluid containing the studied molecule and the buffer in two different outlets. A 1D gradient is created, but its slope depends on the position along the flow; steepest gradient are obtained near the source, while the lowest one are obtained downstream. The shape of the gradient can be predicted, and the accurateness of the results was confirmed with gradients of fluorescent dextran. The continuous flow allows maintaining the same gradient indefinitely, at the expense of using large volumes of the studies molecules. The typical flow rate for these experiments is 1 µL/min, which leads to almost 300 µL for a one-day experiment [6]. Such devices have been used to study the chemotaxis properties of leukocytes in a gradient of IL-8 [294] and T-lymphocytes in gradients of CXCL12 or CCL19 [293].

A different device using a set of premixing channels has been proposed by Dertinger et al. [295]. The chamber shown on figure B.11 allowed to generated 1D gradients of various shapes, ranging from linear one to parabolic (concave, convex). Evolutions of this

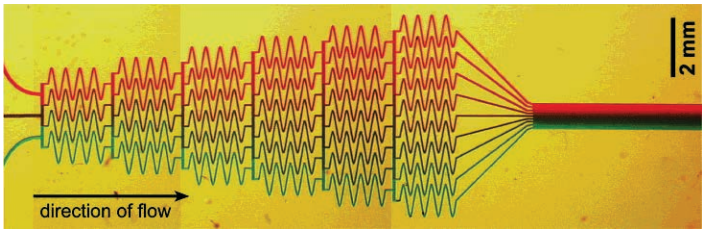


**Figure B.11.** *Microfluidic device designed by Dertinger and Whiteside for cell culture. A linear gradient in generated in the right part of the device (downstream), by a series of premixing channels. Reprinted from [295].*

microfluidic device relying on the multiplication of the input channels allowed creating more complex gradients, but always restrained to one dimension. Shapes like 3rd order polynomials or saw teeth with high slopes were obtained. Superimposition of two different gradients is also possible with this system. The characteristic length of the gradient ranges from 1 to 2 millimeters (channel width), and can persist for several millimeters along the flow.

The two previously developed devices work at high Péclet regime, meaning that convection is responsible for establishing the gradient. The gradient generation characteristic time is in the range of the second [292]. This, associated with the possibility to precisely predict the shape of the gradient, made this system interesting for cell studies on biological timescales, as far as 1D gradients in a liquid medium is sufficient. Thus, they have been used to study neutrophil chemotaxis, cancer cells chemotaxis, bacteria chemotaxis, stem cell differentiation, axon guidance, endothelial cell migration, and even prokaryotic cells, like yeast [289].

Dynamic gradients have been generated using these systems. The characteristic time associated with gradient modulation, in a pulsed regime, is in the timescale of the minute [296]; this can be determined by the relation $t_c = L_c/U$ at high Péclet, where $t_c$ is the characteristic time, $L_c$ the characteristic dimension of the channel and $U$ the flow velocity. The microsecond timescale can be reached using a in-situ mixer [297]. This mixer is made of a bubble trapped inside the microfluidic channel, and forced to vibrate with an external piezoelectric transducer operating at the bubble resonance frequency (70.1 kHz). The only restriction of this system is that the mixing device can only be used to turn a linear steep gradient to an homogeneous one. We may also wonder what are the effects of the acoustic vibrations on the studied cells.

Most of the developed systems generate linear gradients or even complex gradient along only one direction. More complex gradients, 2D in particular, can be developed at the expense of complex microfluidic devices [298].

## B.2.2. Cells in low shear-stress channels

The culture and study of cells directly in the microfluidic flow has several advantages. The systems remains simple, as the gradient generated in the flow is directly applied to the cells. Fast gradient modulation in time is possible, and is only limited by the flow when mixing does not rely on diffusion. However, the shear stress induced to the cells in those conditions has been reported to alter their behavior [14, 15]; the observed effects ranged from a modification of the cell skeleton to a collapse of the growth cone. The flow is even able to detach cells from the culture plate. To address this problem, several improvements relying on the isolation of the cell culture channel have been proposed.

### 1D-shaped gradients

One of the proposed methods relies on isolating the cell with a porous membrane. Two configurations have been proposed. The first one is made of a chamber filled with a hydrogel, with several microfluidic channels around it to establish the gradient. These devices have already been developed in part B.1.4, page 185. The second one is based on the same flow-based gradient generators shown before, the upper or the lower side of the microfluidic device is replaced by a membrane, upon or above which the cells are placed (see figure B.12). A steep gradient is obtained, and can be considered linear in a zone of 200 µm. Steady state was reached within 10 seconds for small molecules (GABA, 101 kg/mol) but it took 15 minutes for larger proteins (netrin-1, 75 kg/mol). This high time can be explained by the change of gradient-establishing process, which is diffusion based in this case, and depends on the diffusivity of the studied molecule.

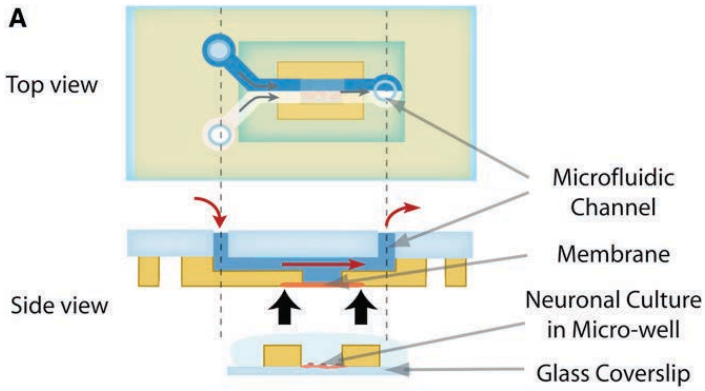


**Figure B.12.** *Cell culture above a microfluidic chamber, separated from it with a porous membrane, which allow th diffusion of the studied molecule. Reprinted from [17].*

The other proposed system is based on an isolation of the cells using walls with holes in it (see figure B.13). Depending of the size of the holes, their position and the thickness of the wall, the flow can be reduced to the point the cells do not sense it. In a device developed in reference [18], a quasi-linear gradient is obtained in a channel 200 µm wide, in 2 minutes

for 70 kg/mol dextran. The steepness of the gradient, and its position in the channel at the same time, depends on the pressure applied in the side channels. Similar devices are shown in other references, where they have been used to study neuron chemotaxis to netrin gradients [19] and the effect of Wnt3a on melanoma cells [20].

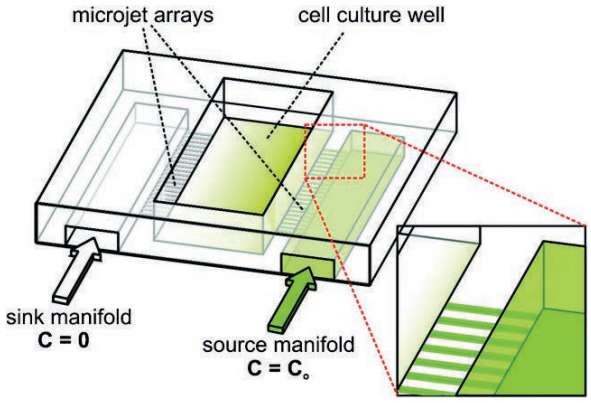


**Figure B.13.** *A microfluidic device to create 1D linear gradients for cell culture. This device is specifically designed for the study of neurons on glass slide, as the flow is almost zero near the neurons. Reprinted from [19].*

### 2D-shaped gradients

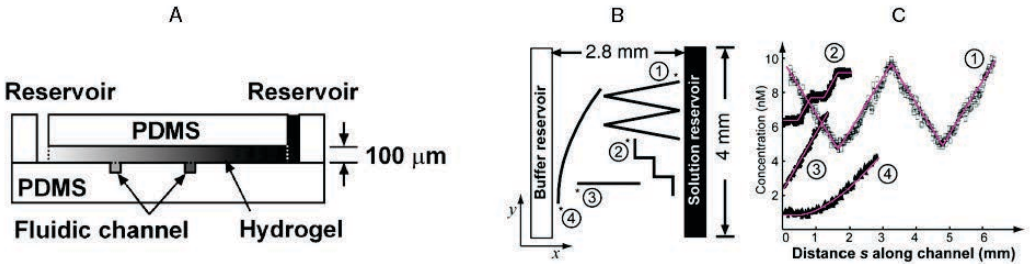


**Figure B.14.** *A microfluid/diffusion-based hybrid gradient generator. (A, B) a 1D gradient is created in a square hydrogel with two reservoirs, one filled with the molecule, the other one serving as a sink. The original shape of the gradient is modified with microfluidic channels under the gel. The shape of the channel impose the shape of the resulting gradient. (C) The shape of the concentration gradient along the channel. Reprinted from [299].*

2D gradients have been implemented in an hybrid of microfluidic and diffusion based device, as shown on figure B.14 [299]. A "steady-state" gradient is established in a square hydrogel 100 µm thick, with two reservoirs at opposite end of the gel. One plays the role of the source and the other one the sink. The almost-linear obtained gradient is modulated by microfluidic channels in contact with the lower side of the gel. This allows to create various shapes of gradients, which depend on the shape of the microfluidic channel. However, as

the 2D gradient depends on the shape of the channels tapped in the PDMS block, it is not possible to make this shape evolve with time. The time required to establish the linear gradient in the gel is long, due to its large size, and is estimated to be 10 hours for a small protein. The price of the arbitrary shaped gradient is high in term of system response speed.

Creating time-modulated gradient may be possible with this system, by changing the shape of the channel in real time. A laser-beam can be used to "draw" the channels in real time, as reported in references [300, 301].

### Dynamic gradients

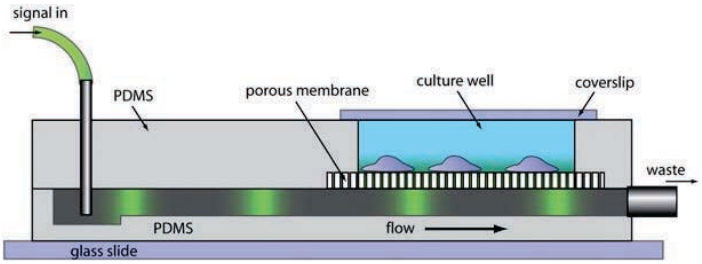


**Figure B.15.** *Dynamic gradient generation in a cell culture medium using a microfluidic device. Reprinted from [21].*

Dynamic gradients have also been implemented in these devices [21], as shown on figure B.15. However, even if the authors claims that the gradient is established quickly, it is in still in the timescale of the minute (45 seconds exactly). It is still out of the range of the biological timescale.

# C. Materials & Methods

*All the experimental procedures related to liposomes and millimeter-sized capsules are described in dedicated appendices. See respectively appendix E, Preparation and characterization of liposomes (p. 209) and appendix F, Preparation and characterization of polymer capsules (p. 215).*

## C.1. Materials

### C.1.1. Chemical and biological materials

Deionised water was obtained from a MilliQ Millipore system. α,ω dicarboxy terminated polyNIPAM ($M_w$ = 4,600 g/mol or $M_w$ = 22,000 g/mol) were purchased from Polymer Source Inc. Butan-1-ol, bovine serum albumin, Brij C2, Brij C20, chloroform (HPLC grade, stabilized with ethanol), cholesterol, cyclohexane (anhydrous), dimethyl sulfoxide (anhydrous), ethylene diamine, FITC-labeled dextran (10,000 g/mol), fluorescein isothiocyanate (isomer mixture), fluorescein sodium salt, heavy water (except for NMR), hexane-1,6-diamine, hexane-1,6-diol, methanol (spectrophotometric grade), nile red, ovalbumin, phosphate buffered saline 10× concentrate, rhodamine B (laser grade), Sephacryl 300-HR, Sephacryl 400-HR, Sephacryl 500-HR, sodium chloride, sodium carbonate, sodium dihydrogenophosphate, sodium dodecyl sulfate (SDS), sodium tetraborate (borax), sucrose, trypan blue, 2,4-diisocyanato-1-methylbenzene (also known as toluene diisocyanate, TDI) were purchased from Sigma-Aldrich. 1,2-dioleoyl-*sn*-glycero-3-phosphocholine (DOPC) was purchased from Avanti Polar Lipids, Inc. Calcein (acidic form), Texas Red-labeled bovine serum albumin, Texas Red-labeled neutral dextran (3,000 g/mol) were purchased from life technologies. D-glucose was purchased from Merck KGaA. Hydrochloric acid (0.1 mol/L and 1 mol/L) and sodium hydroxide solution (1 mol/L) were purchased from Merck Millipore. Sulforhodamine 101 (laser grade) was purchased from Acros organics. UCST polymers were provided by Yue Zhao (Université de Sherbrooke, Québec, Canada). Diethyl ether, hydrochloric acid (37 %), sodium hydroxide solution (9.3 mol/L) and sodium iodide were purchased from VWR. Black hole quencher (BHQ-1) was purchased from Biosearch Technologies. Molecular sieve (4 Å) was purchased from Fisher Scientific France. Deuterated solvents for NMR (DMSO-$d_6$, $D_2O$) were purchased from Euriso-top.

### C.1.2. Specific laboratory furnitures

Teflon spacers (Grace Bio-Labs SecureSeal, 1 well, diam. × thickness 9 mm × 0.12 mm) were purchased from Sigma-Aldrich. Glass slides for microscopy and dialysis cassettes (Slide-A-Lyser, 100 µL – 500 µL and 0.5 – 3 mL, MWCO 3,500 g/mol) were purchased from Fisher Scientific France. Syringe filters (PVDF, 0.22 µm, low protein binding) were purchased from Merck-Millipore. Syringe filters (Whatman, cellulose acetate, 1.2 µm) were purchased from VWR. Polystyrene culture dishes with glass bottom, suitable for fluorescence microscopy (35×10 mm, aperture 22 mm) were purchased from Willco Wells.

## C.2. Sample preparation procedures

### C.2.1. Fluorescein isothiocyanate netrin-1 labeling

*Procedure adapted from [302].* A carbonate buffer (pH 9.5, 0.5 mol/L) is prepared by dissolving 14.0 g of anhydrous sodium hydrogenocarbonate and 11.0 g anhydrous sodium carbonate in 500 mL deionized water. 65 µL of a netrin-1 solution in PBS at 1 g/L (0.942 nmol, 1 eq.) was dialyzed against the carbonate buffer for 2 hours at 5 ℃. 0.65 µL of a FITC solution at 5 g/L in anhydrous DMSO (18.8 nmol, 9 eq.) were added to the netrin-1 solution. The reaction mixture was kept 2 hours at room temperature under gentle stirring, protected from light, then dialyzed for one day against PBS at 5 ℃. As the protein solution volume was too small, the gel permeation chromatography step described in the cited reference was not performed.

The concentration of the protein and its degree of labeling was measured by UV-visible spectroscopy. The concentration of the protein was obtained according to the following formula, which eliminates the FITC contribution to the absorbance at 280 nm:

$$C_{\text{Netrin-1}} = \frac{A_{280} - 0.31 \cdot A_{495}}{\varepsilon_{280}} \tag{C.1}$$

where $A_{280}$, $A_{495}$ are the absorbances of the labeled-protein solution at 280 nm and 495 nm respectively, $\varepsilon_{280}$ is the attenuation coefficient of the protein at 280 nm. 0.31 corresponds to the attenuation coefficient ratio of FITC at 280 nm and 495 nm. As no mention of netrin-1 attenuation coefficient was found in the literature, $\varepsilon_{280}$ has been evaluated using a numerical method. Netrin-1 PDB was retrieved from RCSB Protein Databank (ref. 4OVE)[1]. The amino-acid list was fed to ExPASy ProtParam tool [303, 304] to give $\varepsilon_{280}$ = 46,475 L/mol/cm. This value assumes that all cysteins form disulfide bonds, which has been confirmed using Pymol[2] on the PDB file. For mole to mass conversion, the computed molecular weight of netrin-1 was used (48,918.1 g/mol).

[1] `http://www.rcsb.org/pdb/explore/explore.do?structureId=4OVE`
[2] version 1.7.6.0, retrieved from `http://www.pymol.org`

The degree of labeling has been calculated using the relationship:

$$\text{degree of labeling} = \frac{A_{495}}{\varepsilon_{495}(\text{FITC})} \times \frac{1}{C_{\text{Netrin-1}}} \tag{C.2}$$

where $\varepsilon_{495}$(FITC) is the attenuation coefficient of FITC at 495 nm (69,000 L/mol/cm).

## C.2.2. α,ω diamino-terminated poly(NIPAM) synthesis

### α,ω di-NHS terminated poly(NIPAM) synthesis

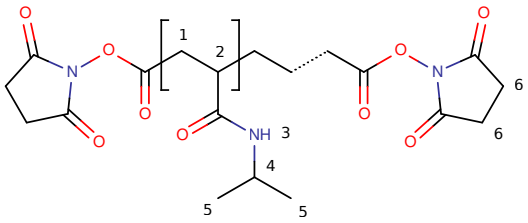


**Figure C.1.** *poly(NIPAM)-NHS$_2$, $M_w$ = 4,794 g/mol.*

Prepared according to [305]. 200 mg of α,ω dicarboxy-teminated poly(NIPAM) (4,600 g/mol, 43.5 µmol, 1 eq.), 15.0 mg of *N*-hydroxysuccinimide (130 µmol, 3 eq.) and 26.9 mg of *N*, *N*'-dicyclohexyl carbodiimide (130 µmol, 3 eq.) were dissolved in 2 mL of anhydrous dichloromethane on ice bath under magnetic stirring. After complete dissolution of the reactants, the ice bath was removed and the stirring was pursued overnight to yield a white suspension. The suspension was poured in dry diethyl ether under magnetic stirring to give a white precipitate isolated by centrifugation. This precipitate was redissolved in anhydrous dichloromethane and precipitated once more in dry diethylether, isolated by centrifugation and dried in vacuo for at least 6 hours. α,ω di-NHS terminated poly(NIPAM) was obtained as a white brittle solid (170 mg, yield 81.6 %). NMR (DMSO-$d_6$): δ=1.07 ppm 6.3 H, (5), δ=1.5 ppm 2.3 H (1), δ=2.0 ppm 1.1 H (2), δ=2.8 ppm 0.17 H (6), δ=3.9 ppm 1.0 H (4), δ=7.2 ppm 1.0 H (3).

### α,ω di-amino terminated poly(NIPAM) synthesis

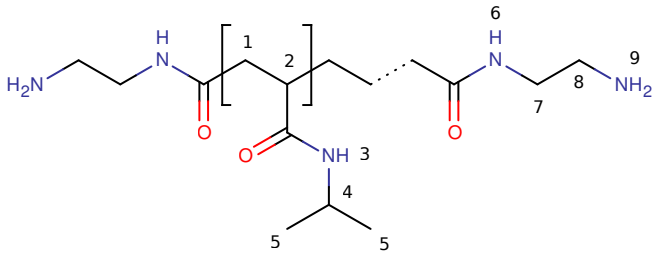


**Figure C.2.** *poly(NIPAM)-(NH₂)₂, $M_w$ = 4,684 g/mol.*

Prepared according to [306]. 28 µl of ethylene diamine (418 µmol, 10 eq.) were added to 5 mL of 50 mmol/L borax buffer. 100 mg of α,ω diamino-terminated poly(NIPAM) (4,794 g/mol, 41.72 µmol in chain ends, 1 eq.) were dissolved in 1 mL of anhydrous DMSO to give an homogeneous colorless solution. This solution was added dropwise to the previous one under magnetic stirring. The reaction was allowed to proceed for two days at room temperature. The obtained solution was dialyzed (Slide-a-Lyser, 0.5-3 mL, MWCO 3500 g/mol) against MilliQ water for 2 days and ice-dried to give a white fluffy solid (78.9 mg, yield 80.8 %). NMR (DMSO-$d_6$): δ=1.05 ppm 6.17 H (5), δ=1.48 ppm 1.84 H (1), δ=1.99 ppm 1.02 H (2), δ=3.87 ppm 1.00 H (4), δ=7.21 ppm 0.97 H (3)+(6). (7), (8) and (9) can't be distinguished from the other signals.

## C.3. Sample characterization

### C.3.1. Dynamic and static light scattering

All light scattering-based experiments were conducted on the same device: a BI-200SM Goniometer System (Brookhaven Instruments Corporation) equipped with a 637 nm LED laser with a variable power output (0 – 30 mW) and a BI-CROSS CORR dual-photomultiplier as the detector. The temperatures of the decaline and the sample were fixed arbitrarily between 10 and 50 °C with a regulated circulating bath (PolyScience). Before any set of measurement, the intensity of light scattered by a sample of filtered decaline was recorded as the reference.

#### General purpose hydrodynamic radii measurements

Correlation functions were acquired at 25 °C, at a fixed angle of 90°, using the BIC Dynamic Light Scattering software. The diaphragm opening was set to 100 µm. Samples were analyzed directly or were diluted in the case of high concentrations to avoid multiple diffusions.

The hydrodynamic radius was extracted from the correlograms by the software using the cumulants, biexponential, CONTIN or NNLS algorithms. The intensity of scattered light was also returned by the software (as a function of time and its mean value).

#### Characterization of nano-emulsions prepared from Tween 80/Span 80 mixtures

We study here the stability of emulsions made of aqueous phase + Span 80/Tween 80 + cyclohexane. The aqueous phase is made of HMDA 100 g/L and fluorescein 1 mmol/L in PBS. The final composition of each sample is 50 µL of the aqueous phase, 50 µL of surfactants and 9.8 mL cyclohexane. First, surfactants are added to the cyclohexane and are emulsified with a vortex mixer for 30 seconds. Then, the aqueous phase is added to the obtained solution, and pre-emulsified for 2 minutes with the vortex mixer. The obtained rough emulsion is submitted to ultra-sounds for 3 minutes, with 20 s on/10 s off cycles, on a water bath kept at 10 °C. The ultra-sounds are generated with a Vibracell VCX750 Ultrasonic Cell Disrupter equipped with the microtip; the power was set to 40 % of the maximal available one.

Immediately after preparation and one day later, the size of the droplets obtained after the ultra-sound emulsification step was assessed by dynamic light scattering. As the emulsions are highly diffusive, an optical density with a value of 1 was introduced in the optical path of the laser before hitting the sample, to reduce the intensity of scattered light and enable the measurement. The obtained correlograms were fitted by the second-order cumulants method. The average diameter, the polydispersity and the intensity of scattered light were extracted.

### C.3.2. UV-visible spectroscopy

#### General-purpose spectrum acquisition

Spectra were recorded either on a single-cell ThermoScientific Evolution array spectrophotomoter, equipped with a Peltier temperature-regulated cell holder or a dual-cell Agilent Cary 300 UV-Visible spectrophotometer, equipped with a Peltier temperature-regulated cell holder (TC 1, Quantum Northwest).

Spectra of UV (365 nm) or blue light (470 nm) irradiated samples were recorded on the ThermoScientific Evolution spectrophotometer. The sample was irradiated directly in the spectrophotometer, using a CoolLED light source (PE-2, Roper Scientific). The light was shone from a light guide to the sample through the top of the quartz cuvette holding the sample. The irradiances reached with this system were 35 mW/cm² with UVs and 92 mW/cm².

#### Measurement of azoTAB relaxation time by UV-Visible spectroscopy

**Data acquisition** A solution of azoTAB at 34 mg/L in deionized water was prepared by the dilution of a concentrated solution, obtained by dissolving the dry surfactant in deionized water. The thermal relaxation experiment was performed on a UV-visible spectrophotometer

(Evolution array, ThermoScientific). The solution was poured into a 3 mL quartz cell and kept at 25 ℃ in a thermostated cell holder, protected from light, during all the experiment. The initial absorbance of the sample at 370 nm was recorded prior illumination, as a all-trans reference. UV light (365 nm, CoolLED PE-2, Roper scientific) was shone on the top of the cell for 3 hours at an irradiance of 35 mW/cm² to convert the surfactant into a predominantly cis population (which was validated by the near zero absorbance at 375-380 nm). Spectra were acquired by 30 ms exposure of the cell to the spectrophotometer beam, at a sampling rate of one spectrum every 20 minutes, for 2 days.

**Data processing** The absorbance at 370 nm was plotted as a function of time. To extract the characteristic relaxation time, the relaxation processes was assumed to be of the first order. Its value ($\tau$) was inferred from the initial slop of the curve ($S_0$), the initial absorbance ($A_0$) and the all-trans absorbance ($A_\infty$) which is the state reached at infinite times. These values are linked together by the following expression:

$$\tau = \frac{A_\infty - A_0}{S_0} \tag{C.3}$$

#### Determination of the UCST by UV-visible spectroscopy

*UV-visible spectroscopy has been used to characterize the turbidity of polymer solutions as a function of the temperature. From the temperature vs. transmittance curve was extracted the UCST.*

A polymer solution at 3 g/L in the studied solvent was prepared at a temperature $T$, above the UCST; in practice, the solution was heated ≈ 10 ℃ above the temperature at which the polymer dissolves. This solution was poured in a quartz cell (500 µL), held in the Peltier cell-holder of a ThermoScientific Evolution array spectrophotometer heated at the same temperature $T$. Spectra were recorded every 5 minutes, while the sample temperature was decreased at 1 ℃ per 5 minutes. The turbidity of the sample was inferred from the transmittance of the sample between 650 nm and 700 nm. The UCST was defined as the temperature reached by the sample when its initial transmittance was reduced by a factor of 2.

### C.3.3. Fluorescence intensity measurements

Emission spectra and time-based fluorescence intensity recordings at fixed wavelengths were recorded on a on a Photon Technology International QuantaMaster QM-1 spectrofluorimeter (PTI, Monmouth Junction, NJ) equipped with a Peltier cell-holder (TLC50, Quantum Northwest, Shoreline, WA). Unless specifically specified, the bandwidth of irradiation and excitation slits was set to 2 nm and the Peltier cell holder was set to 20 ℃. To prevent local photobleaching during long-term acquisitions, the sample was homogenized by magnetic stirring. All acquired data were corrected by the intensity of excitation light.

The fluorimeter has been slightly modified to allow the irradiation of the samples directly inside it. The end of the CoolLED (PE-2, RoperScientific) liquid guide was placed at 1.5 cm of the cuvette on its left side.

Time-resolved data acquisition was performed using the *timebased* mode of the acquisition software (Felix GX).

#### Calcein fluorescence in presence of the azo-polymer

2 mL of a 200 nmol/L calcein solution was poured in a 3 mL quartz cell. The fluorescence intensity of this solution was recorded (excitation wavelength: 495 nm, emission wavelength: 515 nm, acquisition frequency: 1 Hz). To this solution were added 20 µL of a 0.1 g/L UV irradiated (cis) polymer solution, yielding a solution at 198 nmol/L calcein and 0.99 mg/L polymer. The fluorescence intensity of the solution was recorded again. Then, blue light or UV light was shone alternatively on the sample through the light guide for 1 or 5 minutes, and then the fluorescence intensity was recorded for 5 minutes.

### C.3.4. Maximum bubble pressure tensiometer

Maximum bubble pressure measurements were conducted on a BPA-1S tensiometer (SINTERFACE, Germany).

#### Quantification of the SDS concentration in capsules suspensions

The maximum bubble pressure tensiometer can be used to quantify the surfactant concentration in a given solution. This relies on establishing a calibration curve from solutions of known concentrations. The general principle of the technique, as well as a short example are reported in appendix D.1, p. D.1.

**Calibration curves** Reference solutions of SDS in PBS were prepared in the 20 µmol/L – 20 mmol/L range. The surface tension of each sample was acquired for bubble lifetimes ranging from 10 ms to 100 s. Each surface tension vs. lifetime curves has been fitted by the following equation:

$$\gamma(t) = \gamma_0 - K\sqrt{t} \tag{C.4}$$

where $\gamma(t)$ is the surface tension for a lifetime of $t$, $\gamma_0$ is the surface tension of the pure buffer and $K$ a factor proportional to the surfactant concentration. Plotting $K$ vs. the surfactant concentration leads to the calibration curve.

**Concentration determination** To determine the residual concentration of SDS in the capsule suspension, 5 mL of this suspension were introduced in the tensiometer. The surface tension was acquired for bubble lifetimes ranging from 10 ms to 100 s. The surface tension vs. lifetime curve was fitted by equation (C.4), to extract the value of $K$. The concentration of SDS in the sample was inferred from $K$, using the calibration curve established beforehand.

### C.3.5. Other characterizations

#### Evaluation of UCST as a function of solute concentration

500 µL of a solution of the 35 ℃ UCST polymer at 3 g/L in deionized water were introduced in a glass test tube. The temperature of the tube was regulated with a water bath (refrigerated thermostat, polystat 26, Fisher Scientific) and controlled continuously in the sample using a digital thermometer (Traceable 4000, VWR). A defined volume of a concentrated aqueous solution of the studied solute (sucrose 1.38 mol/L, HMDA,HCl 1.72 mol/L or sodium chloride 4.45 mol/L) was added to the solution. After homogenization, the temperature of the sample was decreased degree by degree, until the apparition of a precipitate (assessed with unaided eyes). This temperature was noted, and the sample was heated again (≈ +5 ℃). When the polymer was dissolved, the concentrated solution was added again to the sample, and this process was repeated again. The concentration in polymer at the end of the process was 1.5 g/L. N.B.: each solute was processed separately, on freshly prepared polymer solutions.

The volumes added at each step (for each solutes) are summarized in table C.1.

| $\mathbf{V_{concentrated\ solute}}$ **(µL)** | 0 | 26.3 | 31.0 | 36.5 | 43.0 | 50.9 | 60.4 | 71.8 | 85.8 |
|---|---|---|---|---|---|---|---|---|---|
| $\mathbf{C_{sucrose}}$ **(mol/L)** | 0 | 0.07 | 0.08 | 0.09 | 0.11 | 0.13 | 0.15 | 0.17 | 0.20 |
| $\mathbf{C_{HMDA}}$ **(mol/L)** | 0 | 0.09 | 0.10 | 0.12 | 0.14 | 0.16 | 0.19 | 0.22 | 0.25 |
| $\mathbf{C_{NaCl}}$ **(mol/L)** | 0 | 0.22 | 0.26 | 0.30 | 0.35 | 0.41 | 0.48 | 0.56 | 0.65 |

| $\mathbf{V_{concentrated\ solute}}$ **(µL)** | 103 | 124 | 151 | 185 | 230 | 291 | 375 | 500 |
|---|---|---|---|---|---|---|---|---|
| $\mathbf{C_{sucrose}}$ **(mol/L)** | 0.23 | 0.27 | 0.32 | 0.37 | 0.43 | 0.51 | 0.59 | 0.69 |
| $\mathbf{C_{HMDA}}$ **(mol/L)** | 0.29 | 0.34 | 0.40 | 0.47 | 0.54 | 0.63 | 0.74 | 0.86 |
| $\mathbf{C_{NaCl}}$ **(mol/L)** | 0.76 | 0.89 | 1.03 | 1.20 | 1.40 | 1.64 | 1.91 | 2.23 |

**Table C.1.** *Volumes of concentrated solute solutions (total) added to the polymer solutions, and solute concentration in the whole sample. In the first line of the table is shown the* total *volume of solute in a given step.*

## C.4. Various calculations

### C.4.1. Evaluation of the encapsulated volume fraction in a liposome suspension

For this evaluation, we will consider a liposome made of a lipid bilayer, as shown on figure C.3. The three dimensions are linked together by the relation $D = d + 2 \cdot l$. The area per lipid in the bilayer is noted $A$. The number of lipids per vesicle $N_{ves}$ can be expressed as:

$$N_{ves} = \frac{\pi}{A}\left(D^2 + (D - 2l)^2\right) \tag{C.5}$$

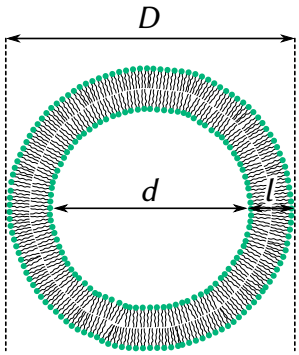


**Figure C.3.** *Schematics of a liposome. $D$ is the diameter of the liposome, $d$ its inner diameter and $l$ the thickness of the lipid bilayer.*

For a suspension of lipid at $C$ g/L, the amount of lipid $N_{\text{lip}}$ in a volume $V_{\text{susp}}$ is equal to:

$$N_{\text{lip}} = \frac{C\mathcal{N}_A V_{\text{susp}}}{M_w} \tag{C.6}$$

where $M_w$ is the molar weight of the lipid. The number of vesicles $n$ in a given volume $V_{\text{susp}}$ is equal to $n = N_{\text{lip}}/N_{\text{ves}}$. The inner volume $V$ of one vesicle is equal to:

$$V = \frac{4}{3}\pi\left(\frac{d}{2}\right)^3 = \frac{4}{3}\pi\left(\frac{D-2l}{2}\right)^3 \tag{C.7}$$

The volume fraction $\varphi$ is therefore given by:

$$\varphi = \frac{nV}{V_{\text{susp}}} = \frac{C\mathcal{N}_A A(D-2\cdot l)^3}{6M_w\left(D^2+(D-2\cdot l)^2\right)} \tag{C.8}$$

and is proportional to $C$.

For a DOPC bilayer, $A \approx 70$ Å², $l \approx 40$ Å [307], $M_w = 786$ g/mol. For 200 nm sized liposomes, with a lipid at 10 g/L, the volume fraction equals to 8 %.

## C.4.2. Evaluation of the characteristic time of release from a porous liposome

These calculations are adapted from reference [228], pages 183–184. A liposome (see figure C.4) is filled with a solution containing molecule whose diffusion coefficient is $D$. The radius of the liposome is $R$ and the thickness of its bilayer $l$; the inner radius will be assimilated to $R$. The concentration of the molecule of interest inside the vesicle is noted $C$. Fick's first law allows to write the following equation:

$$\mathbf{j}(\mathbf{x},t) = -D\,\nabla\, C(\mathbf{x},t) \tag{C.9}$$

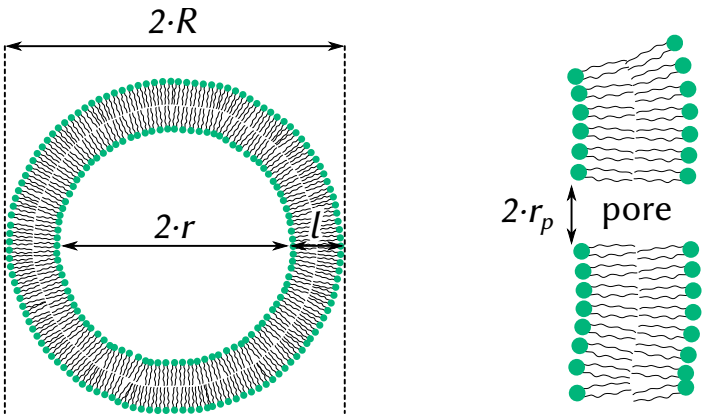


**Figure C.4.** *Schematics of a liposome and a pore in its membrane bilayer. $R$ is the liposome radius, $r$ its inner radius, $l$ the thickness of the membrane and $r_p$ the radius of pore.*

which can be rewritten as

$$\mathbf{j}(t) \sim -\frac{C(t)}{2 \cdot r_p} \tag{C.10}$$

assuming that the largest contribution to the gradient is given by the pore itself, and that the concentration outside the vesicle can be neglected. By definition,

$$\frac{\mathrm{d}N}{\mathrm{d}t}(t) = V\frac{\mathrm{d}C}{\mathrm{d}t}(t) = -4\pi\tilde{r}\,\mathbf{j}(t) \tag{C.11}$$

where $N$ is the amount of molecules inside the vesicle, $V = \frac{4}{3}\pi R^3$ the vesicle volume and $\tilde{r}$ the apparent radius of the pore; $\tilde{r} = r_p - e$, where $e$ is the radius of the entrapped molecule. From equations (C.10) and (C.11), we obtain the following differential equation:

$$\frac{\mathrm{d}C}{\mathrm{d}t}(t) + \frac{3D\tilde{r}^2}{lR^3}C(t) = 0 \tag{C.12}$$

whose solution is exponential, associated with the characteristic decay time $\tau = \frac{lR^3}{3D\tilde{r}^2} = \frac{lR^3}{3D(r_p - e)}$.

For a protein, the associated radius (in nanometers) is given by $e = 0.066\sqrt[3]{M}$, where $M$ is its molar weight in g/mol (see reference [157]). Its diffusivity is given by the Stokes-Einstein law:

$$D = \frac{k_B T}{6\pi\eta e} \tag{C.13}$$

with $T$ = 310 K, $\eta$ = 0.7·10$^{-3}$ Pa·s. A 50 kg/mol protein has a radius of 2.4 nm, which corresponds to a diffusion coefficient of 135 µm²/s. We also consider DOPC vesicles, where $l$ = 40 Å.

The associated characteristic time for a 10 µm vesicle is 21 s, and decrease to 1.4 ms for a 200 nm sized one.

# D. Experimental techniques

## D.1. Maximum bubble pressure tensiometer

The maximum bubble pressure method allows to measure the dynamic surface tension on the air/liquid interface. It is based on the pressure measurement inside a bubble growing in the studied liquid at the extremity of a capillary. This method has been implemented in specific equipments by several companies (Krüss, SInterface, Launda-Brinkmann…) and is used both in the industrial field [308] and in the research field [309, 310] to study various liquids, from fuel mixtures to biological samples.

Maximum bubble pressure is widely used to determine the effect of surfactants on the dynamic surface tension [311, 312]. This technique has been extended to determine the concentration of surfactant in liquids.

### D.1.1. Principle

Air is flowed through a capillary to create bubbles, as depicted on figure D.1. The pressure is recorded as a function of time; as the bubble "grows" (points A & B), its radius diminishes and the pressure increases to reach a maximum (point C). At this point, the radius of the bubble is at its minimum and equals the one of the capillary; the shape of the bubble is a half-sphere. After this point, the radius of the bubble increases and the pressure diminishes until the bubble detaches from the capillary (point E), to give way to another bubble.

The pressure in the bubble is linked to its radius by the Laplace equation:

$$\gamma = \frac{P_C \, R_C}{2} \tag{D.1}$$

where $\gamma$ is the surface tension at the maximum bubble pressure (point C), $P_C$ is the pressure at this point, $R_C$ is the radius of the capillary. However, the value returned by commercial apparatus, like the SInterface BPA-1S maximum bubble pressure tensiometer, is corrected by several factors, taking into account the effect of the capillary size on the surface tension, the effect of the hydrodynamic pressure on the bubble formation, the effect of the liquid viscosity…

#### Effect of surfactants on the dynamic surface tension

Due to their amphiphilic properties, surfactants are known to take interfaces over, which leads to a decrease of the surface tension. The equilibrium state is not reached immediately

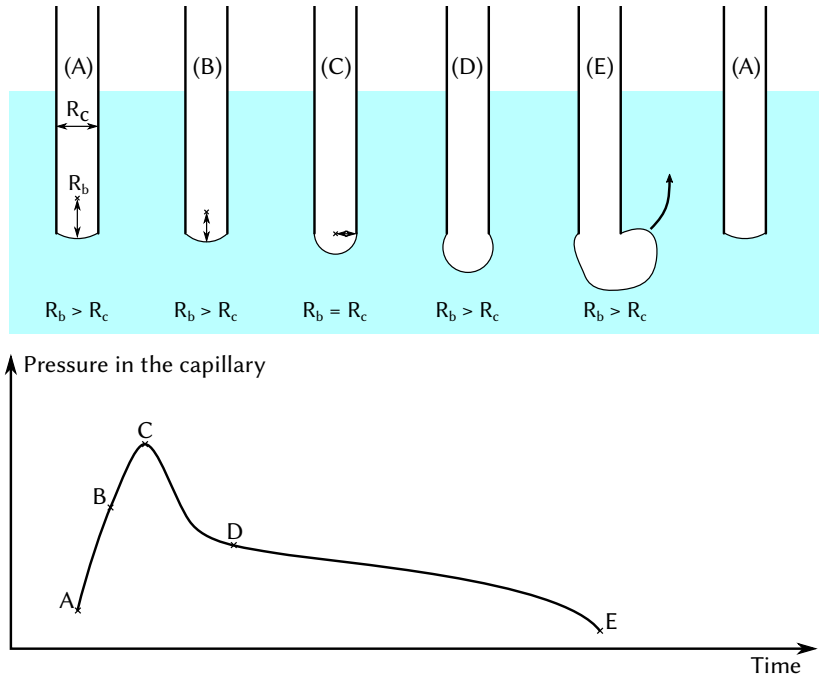


**Figure D.1.** *Upper figure: schematic representing the bubbling process. One cycle is represented (A to E). As the air flows, the volume of the bubble grows. The bubble radius increase up to point C, then decrease until bubble detachment. Lower figure: graph representing the evolution of the pressure in the capillary as a function of time.*

as the molecules, initially dispersed in one phase, need to migrate to the interface. The time evolution of the surface tension can be used to determine the kinetics of surfactant migration/adsorption on the interface. Several models have been proposed to describe the surfactant migration and/or adsorption on the interface [312]. Mechanisms restricted to diffusion can be described by the Ward and Tordai equation:

$$\Gamma(t) = 2\sqrt{\frac{D}{\pi}}\left(c_0\sqrt{t} - \int_0^{\sqrt{t}} c(\tau)\,\mathrm{d}(t-\tau)\right) \tag{D.2}$$

where $\Gamma$ is the surface excess, $c_0$ is the bulk surfactant concentration, $D$ is the diffusion coefficient of the monomeric surfactant, and $c$ is the surfactant concentration near the interface. This equation takes into account the diffusion towards the interface, but also the reverse process, when the interface becomes highly populated. The surface excess is linked to the surface tension by the Gibbs equation:

$$\Gamma = -\frac{1}{nRT}\frac{\mathrm{d}\gamma}{\mathrm{d}\ln c_0} \tag{D.3}$$

where $R$ is the gas constant, $T$ the temperature and $n$ represents the number of species per surfactant molecule: $n = 1$ for neutral surfactants, $n = 2$ for ionic 1:1 surfactants.

### Ward and Tordai equation solution

Ward and Tordai equation (D.2) can't be solved analytically. However, two limit cases can be considered. At short timescales ($t \to 0$), diffusion originating from the surface can be neglected. The solution to this equation in term of surface tension is:

$$\gamma(t)_{t\to 0} = \gamma_0 - 2nRTc_0\sqrt{\frac{Dt}{\pi}} \tag{D.4}$$

where $\gamma_0$ is the surface tension of the solvent. The surface tension is linked to the square root of the time by the *bulk* surfactant concentration $c_0$. This technique can therefore be used to quantify the surfactant concentration in a sample.

Equation (D.2) can also be solved at long time ($t \to \infty$):

$$\gamma(t)_{t\to\infty} = \gamma_{eq} + \frac{nRT\Gamma_{eq}^2}{c_0}\sqrt{\frac{\pi}{4Dt}} \tag{D.5}$$

where $\gamma_{eq}$ is the equilibrium surface tension and $\Gamma_{eq}$ is the equilibrium surface excess. The surface tension is linked to the inverse square root of time by the inverse of the bulk surfactant concentration $c_0$. This approximation also leads to a method to determine the surfactant concentration.

## D.1.2. Determination of surfactant concentration

As mentioned in reference [311], knowing $\gamma(t)$ should be sufficient to determine the surfactant concentration $c_0$. The relation between $c_0$ and $\gamma(t)$ depends only on an apparatus constant characteristic the considered tensiometer. The determination of this constant relies on a video analysis of the bubbling process, which has not been done for our device. Another technique proposed in [308], which relies on a non-linear calibration curve ($c_0$, $\gamma(t)$) for a given $t$. This empirical method does not allow to quantify the surfactant in a wide range of concentrations; the absence of a model to fit the data reduce the robustness of the method.

Here, we use equation (D.4) to draw a linear calibration curve. To illustrate the method, we will focus on SDS solutions in PBS[1] (see table D.1). The dynamic surface tension is measured for each solution using the maximum bubble pressure tensiometer (BPA-1S, SINTERFACE, Germany). The $(t, \gamma(t))$ plot is shown on figure D.2.

The low-concentration curves (up to 0.502 mmol/L) have been fitted by the following equation:

$$\gamma(t) = \gamma_0 - K\sqrt{t} \tag{D.6}$$

with $K = 2nRTc_0\sqrt{D/\pi}$. The fitted curves are shown on figure D.3. For the highest concentrations, only the beginning or the curves have been fitted. Fit results are summarised in table D.2.

| Sample | 1 | 2 | 3 | 4 | 5 | |
|---|---|---|---|---|---|---|
| SDS (mmol/L) | 0.0200 | 0.0320 | 0.0502 | 0.0796 | 0.126 | |
| Sample | 6 | 7 | 8 | 9 | 10 | |
| SDS (mmol/L) | 0.200 | 0.317 | 0.502 | 0.796 | 1.26 | |
| Sample | 11 | 12 | 13 | 14 | 15 | 16 |
| SDS (mmol/L) | 2.00 | 3.17 | 5.02 | 7.96 | 12.6 | 20.0 |

**Table D.1.** *SDS concentration in calibration samples*

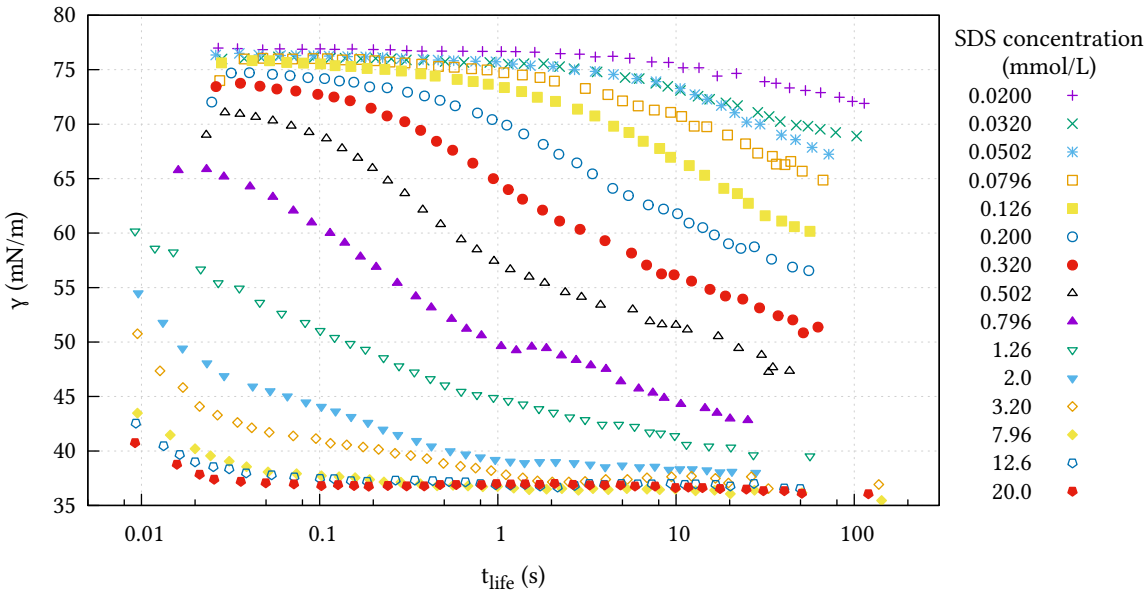


**Figure D.2.** *(bubble lifetime, surface tension) for SDS samples. Its concentration is in the [0.02, 20] mmol/L range.*

The calibration curve is obtained by plotting $K$ as a function of $c_0$. The model implies a linear relationship between these two values. The dataset has been fitted accordingly with the equation $K = A \cdot c_0$, as shown on figure D.4.

To determine the concentration of SDS in an unknown solution, it is only needed to measure the dynamic pressure on the same time range and to fit the beginning of the curve by equation (D.6). $c_0$ can then be extracted from $K$ and the previously determined $A$ by the relation $c_0 = K/A$. As SDS is sensitive to ionic strength, the buffer should be the same for the calibration and the measurement.

[1] Another example is shown with Tween 80 in the Material and Methods, section C.3.4, page 199.

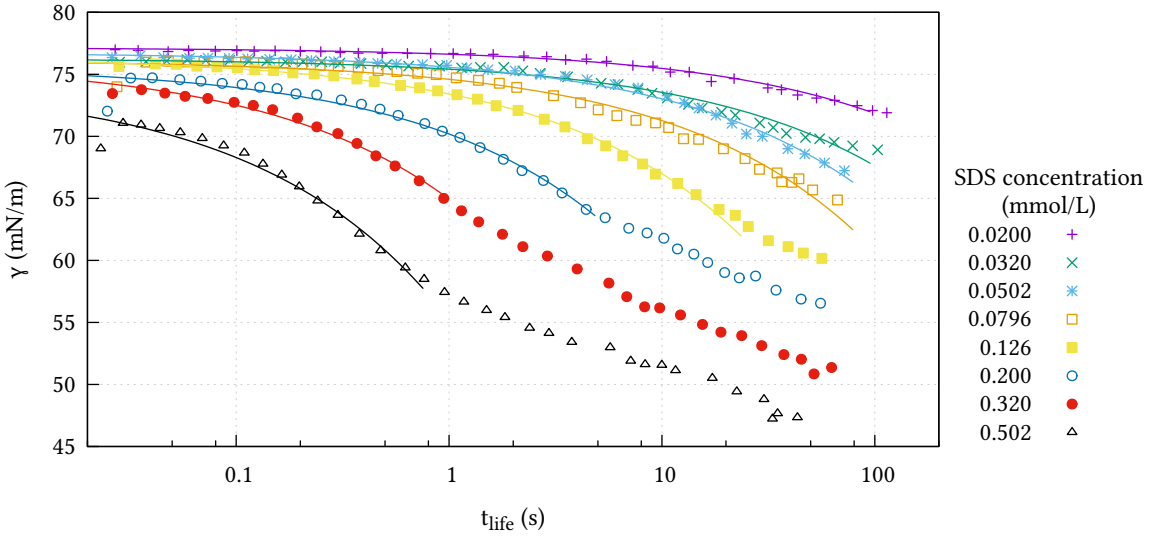


**Figure D.3.** *Dynamic surface tension of SDS solutions fitted by equation* (D.6).

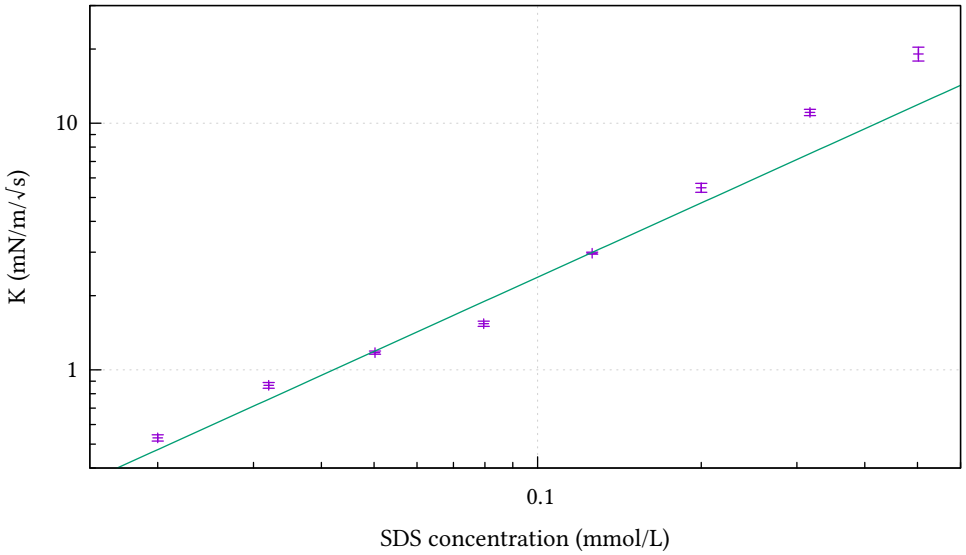


**Figure D.4.** *SDS calibration curve. The points are fitted by the equation* $K = A \cdot c_0$ *with* $A$ *as the fit parameter.* $A = (23.8 \pm 1.0)\ L{\cdot}mN/m/\sqrt{s}/mmol$.

| SDS conc (mmol/L) | K | stddev(K) | $\gamma_0$ | stddev($\gamma_0$) |
|---|---|---|---|---|
| 0.02 | 0.530 | 0.016 | 77.150 | 0.084 |
| 0.032 | 0.866 | 0.023 | 76.279 | 0.089 |
| 0.0502 | 1.175 | 0.017 | 76.744 | 0.058 |
| 0.0796 | 1.538 | 0.037 | 76.13 | 0.12 |
| 0.126 | 2.972 | 0.028 | 76.385 | 0.049 |
| 0.2 | 5.48 | 0.23 | 75.66 | 0.22 |
| 0.317 | 11.06 | 0.32 | 76.00 | 0.17 |
| 0.502 | 19.1 | 1.2 | 74.33 | 0.49 |

**Table D.2.** *Fit parameters of surface tension curves by equation* $K = Ac_0$.

# E. Preparation and characterization of liposomes

## E.1. Sample preparation procedures

### E.1.1. Liposome suspensions preparation

*Liposomes were prepared according to literature by the film hydration/extrusion method [106]. The procedure exposed below in a* general one. Lipid *stands for any kind of lipid or polymer used to build the vesicles. In this work, combinations of DOPC, cholesterol, azoTAB or azobenzene-grafted polymer have been used.*

A film of lipids (750 µg) was prepared in a glass crystallizer by evaporating a solution of these lipids in chloroform/methanol under a flux of nitrogen. Film drying was pursued under vacuum for at least 4 hours. The dried film was hydrated with the aqueous medium (750 µL) and suspended roughly in the aqueous medium with the flow of a plastic pipette. The hydration was pursed under sonication for 10 minutes, to yield a suspension at 1 g/L in lipids. This mixture was submitted to three cycles of freeze/thaw (freezing in liquid nitrogen followed by melting in a water bath at 50 °C) and was finally extruded by filtering it three times on a syringe filter (PVDF, 0.22 µm, Millipore).

### E.1.2. Liposome purification by GPC

The bottom of a 3 mL plastic syringe was stuffed with hydrophilic cotton and filled with about 2 mL of Sephacryl 500-HR. The gel was allowed to sediment for a few minutes and was washed with 40 mL of the aqueous medium (PBS, unless specifically stated). The dead volume of the column was evaluated by following the elution of 100 µL of a dextran blue solution ($M_w$ = 2,000 kg/mol). 200 µL of the vesicle suspension were deposited on the column and eluted with the aqueous medium. 100 µL fractions were collected. *The presence of liposomes in the fractions can't be determined with unaided eyes and has been inferred from systematic DLS measurements, cf. section E.2.1 below.*

# E.2. Sample characterizations

## E.2.1. Systematic size and concentration characterization

The concentration and the size of the vesicles were measured by DLS. The general procedure is presented section C.3.1, page 196. Samples were analyzed as-is, without dilution or further preparation.

## E.2.2. AzoTAB-mediated dissolution of liposomes

### "Low lipid concentration" protocol

Vesicles were prepared as described above in section E.1.1 *Liposome suspensions preparation*, on 750 µg DOPC and with 750 µL deionized water as the aqueous medium. After extrusion, the suspension was centrifuged for 10 minutes at 14,000 g; the pellet was eliminated to yield a suspension of vesicles at approximately 1 g/L.

Trans azoTAB stock solutions were prepared from dry powder and deionized water, at 10 g/L and 1 g/L. A fraction of both solutions was submitted to UV light irradiation (365 nm, 35 mW/cm²) for 4 hours to yield cis-azoTAB stock solutions.

The samples made of azoTAB and liposomes were prepared as follows. In a DLS quartz cell were added deionized water and 50 µL of the liposome suspension. After homogeneization, a defined volume of the cis or trans azoTAB stock solution was added ; the sample was homogeneized again and immediately characterized by DLS to extract the scattered light intensity and their hydrodynamic diameter (cf. appendix C.3.1, p. 196). The samples were allowed to incubate at room temperature for 24 hours, then they were processed again by DLS. The volumes of deionized water and of stock azoTAB solutions used to prepare the samples are reported in table E.1.

| **Final azoTAB concentration (g/L)** | 0.0 | 0.2 | 0.4 | 0.6 | 0.8 | 1.0 | 2.0 | 4.0 |
|---|---|---|---|---|---|---|---|---|
| **azoTAB stock solution** | – | 1 g/L | 1 g/L | 1 g/L | 1 g/L | 10 g/L | 10 g/L | 10 g/L |
| $\mathbf{V_{azoTAB\ stock\ solution}}$ **(µL)** | – | 100 | 200 | 300 | 400 | 50 | 100 | 200 |
| $\mathbf{V_{Deionized\ water}}$ **(µL)** | 450 | 350 | 250 | 150 | 50 | 400 | 350 | 250 |

**Table E.1.** *Sample composition.*

### "High lipid concentration" protocol

A film of DOPC was prepared in a glass crystallizer by evaporating a solution of these lipids in chloroform/methanol under a flux of nitrogen. Film drying was pursued under vacuum for at least 4 hours. The dried film was hydrated with a 20 g/L trans azoTAB solution and

sonicated for ~ 10 min. The samples were allowed to rest for 24 hours at room temperature before use.

The samples were characterized by DLS (cf. C.3.1, p. 196). Light was shone on the sample from the top of the DLS cell, through a light guide. This enabled to irradiate the sample with blue light (470 nm, 91 mW/cm²) or UV light (365 nm, 35 mW/cm²).

### Determination of azoTAB-mediated liposome dissolution kinetics

Vesicles were prepared as described above in section E.1.1 *Liposome suspensions preparation*, on 300 µg DOPC and with 300 µL deionized water or 300 µL NaCl 150 mM as the aqueous medium. After extrusion, the suspension was centrifuged for 10 minutes at 14,000 g; the pellet was eliminated to yield a suspension of vesicles at approximately 1 g/L. A solution of cis azoTAB (8.4 g/L, deionized water), was obtained by irradiating a 8.4 g/L azoTAB solution under UV light (365 nm, 35 mW/cm²) for several hours.

The samples "without NaCl" were obtained from mixing 15 µL of the liposome suspension (film hydrated with deionized water), deionized water and the cis-azoTAB solution (in this order) The samples "150 mmol/L NaCl" were obtained from mixing deionized water, 8.8 µL NaCl 4 mM, the cis-azoTAB solution and 15 µL of the liposome suspension (film hydrated with 150 mM NaCl solution). The volumes of cis-azoTAB solution and deionized water are reported table E.2.

| **Buffer** | **Deionized water** | | | **150 mmol/L NaCl** | | |
|---|---|---|---|---|---|---|
| **Final azoTAB concentration (g/L)** | 0.34 | 0.50 | 1.26 | 0.34 | 0.50 | 1.26 |
| $\mathbf{V_{cis\text{-}azoTAB\ 8.4\ g/L}}$ **(µL)** | 10.0 | 15.0 | 37.5 | 10.0 | 15.0 | 37.5 |
| **Deionized water** | 225 | 220 | 198 | 216 | 211 | 189 |

**Table E.2.** *Sample compositions.*

Immediately after mixing, 200 µL of the samples were transferred into a DLS quartz cell. The hydrodynamic diameter and the intensity of scattered light were measured by DLS (cf. C.3.1, p. 196). The sample was then shone continuously with blue light (470 nm, 92 mW/cm²), from the top of the DLS cell, using a CoolLED (PE-2, Roper Scientific) light source. The hydrodynamic diameter and the intensity of scattered light were measured every 5 minutes for 14 hours.

### Light-sensitivity assessment of azoTAB-loaded liposomes

Liposomes were prepared as reported above in section E.1.1, on 250 µg DOPC. The lipid film was hydrated with 250 µL of a cis-azoTAB solution, at 1.0 g/L, 1.5 g/L, 2.0 g/L or 5.0 g/L. The cis-azoTAB solutions were obtained by irradiating the trans ones with UV light (365 nm, 35 mW/cm²) for at least 15 minutes. The presence of liposomes in each samples was inferred from DLS measurements on raw samples.

The samples containing liposomes were purified by GPC to remove unbound surfactant molecules (cf. section E.1.2). The fraction with the highest concentration in ≈ 200 nm vesicles was determined by DLS.

These fractions were then poured in a DLS quartz cell ; the hydrodynamic diameter and the intensity of scattered light was recorded. The studied sample was then shone continuously with blue light (470 nm, 92 mW/cm²), from the top of the DLS cell, using a CoolLED (PE-2, Roper Scientific) light source. The hydrodynamic diameter and the intensity of scattered light were measured every 5 minutes for 14 hours.

## E.2.3. Characterization of the release from azo polymer-sensitized liposomes

### Preparation of calcein-loaded and azo polymer-sensitized liposomes

A film of lipids (DOPC, azo polymer and possibly cholesterol, 750 µg total) was prepared in a glass crystallizer by evaporating a solution of these lipids in chloroform/methanol under a flux of nitrogen. Film drying was pursued under vacuum for at least 4 hours. The dried film was hydrated with 750 µL of a 25 mmol/L calcein solution in PBS, and suspended roughly in it with the flow of a micropipette. The hydration was pursed under sonication for 10 minutes, to yield a suspension at 1 g/L in lipids. This mixture was submitted to three cycles of freeze/thaw (freezing in liquid nitrogen followed by melting in a water bath at 40 °C) and was finally extruded by filtering it three times on a syringe filter (PVDF, 0.22 µm, Millipore).

The lipid+polymer suspension was placed in a watchglass and precisely weighed. To convert the azobenzene into a predominant cis configuration, the suspension was placed under UV light (365 nm, 10 mW/cm², CoolLED, PE-2, Roper Scientific) for 1 hour. The sample was weighed again and the evaporated water was replaced. The liposomes were then purified by GPC, to remove the outer calcein, as shown in section E.1.2 below.

*N.B.: To prevent the thermal relaxation of the cis azobenzenes, the fractions obtained after purification were kept in a dark room and placed periodically under UV light.*

### Sample selection

After purification, the fractions were analyzed by DLS to assess the presence of liposomes as reported below. The presence of loaded calcein was characterized by forcing the release with Triton X-100. This procedure is explained below. The samples selected for the release study were those with a correct hydrodynamic diameter (≈ 200 nm) and the highest increase of fluorescence during the forced release test.

### Forced release test

A 3 mL quartz cuvette was filled with 2 mL of the elution buffer and 20 µL of the studied liposome suspension (at ≈ 1 g/L in lipids). The fluorescence intensity of the sample was recorded for about 60 seconds, at a frequency of 1 Hz. The excitation wavelength was set

to 495 nm and the emission one to 515 nm. The complete description of the fluorimeter used is reported in appendix C.3.3, p. 198. The recording was stopped and 20 µL of a Triton X-100 solution in deionized water (100 g/L, 160 mmol/L) were introduced in the cuvette. The fluorescence intensity recording was resumed after sample homogenization, and pursued for 60 seconds.

**Remark:** *Triton X-100 is able to dissolve almost instantaneously the membrane of the liposomes [218], as soon as there is more Triton X-100 molecules than lipids in the sample. In this assay, its final concentration is 1.6 mmol/L. The concentration in lipids is roughly 10 mg/L (≈ 13 µmol/L of DOPC). The Triton X-100:lipid ratio is ≈ 120, which ensures that all the vesicles are dissolved.*

### Release experiment

The fluorescence intensity was recorded with the device described in appendix C.3.3, p. 198. The excitation wavelength was set to 495 nm, the emission one to 515 nm, the acquisition frequency to 1 Hz. To prevent a local photobleaching of the sample by the excitation source, the sample was continuously homogeneized by magnetic stirring.

The studied was prepared as follows: a 3 mL quartz cuvette was filled with 2 mL of the sample buffer and 20 µL of the studied sample. The fluorescence of this sample was recorded for about 1 minute. To prevent any damages caused to the detector by the high intensity irradiation, the emission shutter was closed and the recording was paused. The sample was irradiated at 470 nm (14 mW/cm$^2$) through the liquid guide, for the given time (1 or 5 minutes). Immediately after shutting down the light source, the emission shutter was reopened and the recording resumed for at least 30 minutes. At the end of the experiment, the recording was paused again, and 20 µL of a Triton X-100 solution at 100 g/L in water was added to the sample. The sample was let to homogeneize for several seconds and the recording was resumed for 30–60 seconds.

### Data processing

Fluorescence intensity vs. time plots were analyzed as is, without pre-processing.

# F. Preparation and characterization of polymer capsules

## F.1. Millimeter-sized capsules

### F.1.1. General procedures

*The preparation procedure is mostly the same for the capsules made from polyNIPAM or UCST polymers. The only difference resides in the temperatures of all the phases. The temperature of the aqueous phase – from which the capsules are made – will be noted $T_{aq}$, the temperature of the oil phase $T_{oil}$ and the temperature of the redispersion medium $T_{redisp}$. When the capsule is submitted to a temperature ramp, the temperature at the beginning of the ramp is noted $T_{start}$, the one at the end of the ramp $T_{end}$.*

#### Capsule preparation

*The exact composition of the aqueous phase depends on the considered sample. It will be referred only to* the aqueous phase *below, its composition will be exposed on an assay-basis, in the next section.*

The aqueous phase is brought to temperature $T_{\mathrm{aq}}$ and introduced in a microsyringe (Hamilton, 25 µL) kept at the same temperature. 20 mL dry cyclohexane (molecular sieve dried) are poured in a clean and dry glass vial, and brought to $T_{\mathrm{oil}}$ with a water bath. 71 µL TDI (340 µmol) are added cautiously on the bottom of the vial, to ensure that the TDI concentration is almost zero in the upper layers of the cyclohexane. A 1 µL drop is created with the microsyringe and quickly immersed in the upper layer of the cyclohexane. The drop is kept that way 2–5 seconds, then the microsyringe is removed from the cyclohexane. The drop does not cross the oil/air interface and falls at the bottom of the vial. ≈ 12 drop are created per vial this way. This system is kept at $T_{\mathrm{oil}}$ overnight. This preparation procedure is summarized in figure F.1 (polyNIPAM example).

The capsules are then transferred to the redispersion medium (PBS, unless specifically stated). A glass tube is filled with 1 mL of the redispersion aqueous medium and 500 µL cyclohexane. Two drops of a Tween 80-saturated cyclohexane solution are then added. The capsules – still in the reaction vial – and this tube are brought to $T_{\mathrm{redisp}}$. One capsule is transferred from the reaction vial to the cyclohexane layer in the glass tube with a glass pipette. The capsule spontaneously falls to the bottom of the aqueous phase. If the capsule is stuck at the oil/water interface, two drops of the Tween 80-saturated cyclohexane solution

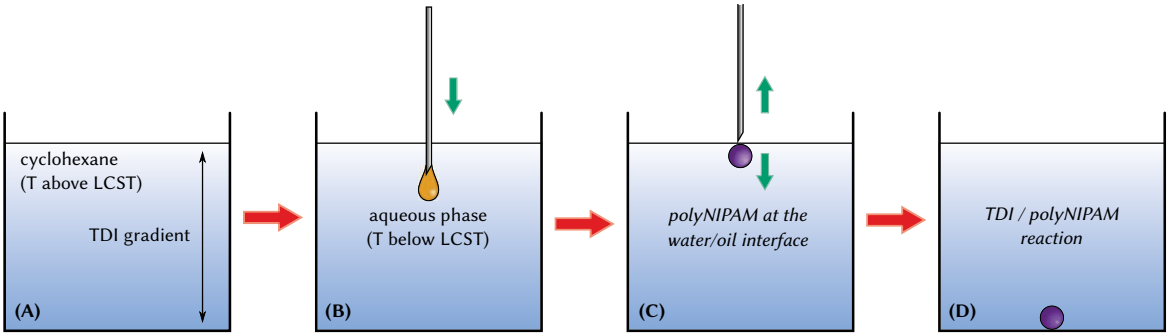


**Figure F.1.** *Synthesis of the capsule in the oil phase. (A) a gradient of TDI concentration is created in cyclohexane, at a temperature above the LCST. Under these conditions, the concentration in TDI at the top of the cyclohexane is considered null. (B) a drop of the aqueous phase is introduced in the oil with a microsyringe. The syringe and its content are at a temperature below the LCST, allowing the solution to flow through the needle. (C) as the oil is at a temperature above the LCST, the polyNIPAM inside the drop precipitates and goes to the water/oil interface. As the drop was kept in the higher levels of cyclohexane, where no TDI can be found, no reaction occurred yet. (D) the drop is made to fall at the bottom of the cyclohexane, were the membrane is synthesized.*

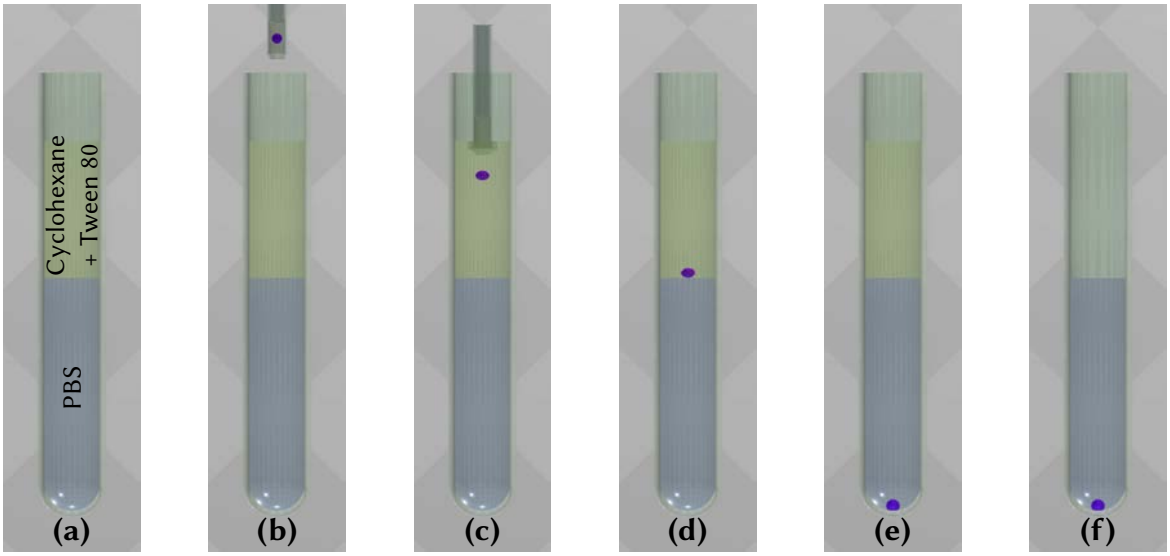


**Figure F.2.** *Capsule transfer from oil phase to aqueous phase.* (a) *a glass tube filled with PBS and cyclohexane + 2 drop of Tween 80-saturated cyclohexane.* (b) *the capsule is transferred into the tube with a glass pipette.* (c) *due to its high density the capsule falls towards the cyclohexane/PBS interface,* (d), (e) *and crosses it spontaneously due to the Tween 80 added in the oil phase.* (f) *after removing the cyclohexane, the capsule can be transferred elsewhere with a glass pipette.*

can be added to ease the crossing. Each capsule is processed the same way in a freshly prepared glass tube. This procedure is shown in figure F.2.

### Capsule characterization by microscopy

**Experimental device** The experimental device used to characterize the capsules is composed of an inverted microscope (Leica DM-IRE2), capable of epifluorescence and phase contrast illuminations. Pictures were recorded with a µEye UI-3250CP (IDS, Stemmer Imaging). The temperature of the sample was regulated using a Peltier microscope stage (Linkam 100-LI3 Peltier stage, Linkam PE-94 controller). On this plate was mounted a fluorescence-grade Petri dish (glass bottom, 35 mm diam.), modified with a raised glass slide (25 mm diam.), as shown on figure F.3. The temperature in the Petri dish – near the studied sample – is recorded using a probed thermometer (Traceable 4000, VWR). Prior to the introduction of the capsule, this Petri dish is filled with ≈ 5 mL of the redispersion medium and heated to $\sim T_{\text{start}}$ with the Peltier plate.

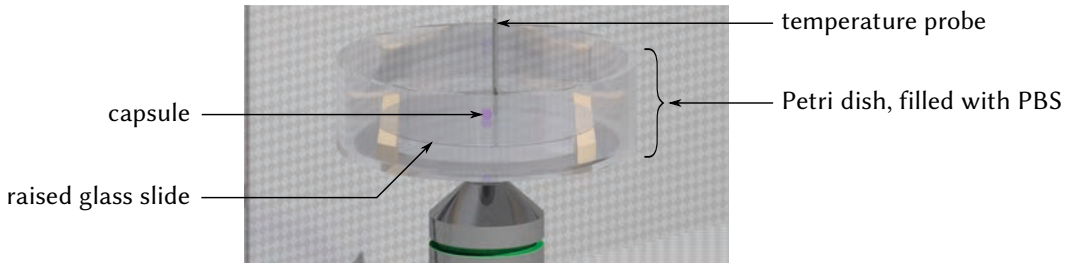


**Figure F.3.** *Schematic representation of the microscope-based setup used to characterize the capsules. The capsules is placed in the PBS filled Petri dish, whose temperature is controlled with a Peltier microscope plate (not represented). If required, the capsule can be elevated with a glass slide, as shown in the picture. The temperature near the capsule was measured with a temperature probe.*

One capsule is studied at a time. The capsule is transferred the Petri dish, on the raised slide, with a glass pipette. Unless specifically stated, the capsule is submitted to a temperature ramp, from $T_{\text{start}}$ to $T_{\text{end}}$. The heating or cooling rate was set to 10 °C/min. N.B.: due to the inertia of the system, the rate achieved in the Petri dish was in the 5–7 °C/min. range.

**Data recording** Fluorescence pictures were taken at regular intervals: first every 5 seconds for 100 seconds (200 pictures), then every 30 seconds for 900 seconds (30 pictures).

**Data processing** Fluorescence pictures were analyzed using FiJi (an ImageJ distribution). After the experiment, the ground level of the camera was recorded at the same exposure time (30 pictures, averaged with ImageJ). A picture of an homogeneous fluorescent object was also taken to correct the inhomogeneities of the illumination field. In this case, the homogeneous object was a solution of Rhodamine 123 in glycerol at 0.1 µmol/L, between 2 glass slides sealed with a 120 µm thick Teflon spacer. Each picture in the dataset were processed in this way:

1. the ground level of the camera is removed by subtracting the adequate picture;
2. the inhomogeneity of the epifluorescence illumination is corrected by dividing the picture stack pixel-wise with the picture of the homogeneous object.

The fluorescence intensity was measured by outlining the capsule with the *threshold* tool and summing the value of each pixel inside this outline with the *measure* tool.

## F.1.2. Assays description

### HMDA millimeter-sized capsules

Capsules were prepared according to section F.1.1. The compositions of the aqueous phases used to build the capsules are reported in the table below. All the preparation steps were performed at room temperature.

| Sample | Aqueous phase composition |
|---|---|
| **10 mg/L** | 10 mg/L HMDA (96 µmol/L), 0.63 mol/L sucrose, PBS |
| **100 mg/L** | 100 mg/L HMDA (0.96 mmol/L), 0.63 mol/L sucrose, PBS |
| **1 g/L** | 10 mg/L HMDA (9.6 mmol/L), 0.63 mol/L sucrose, PBS |
| **10 g/L** | 10 mg/L HMDA (96 mmol/L), 0.63 mol/L sucrose, PBS |
| **100 g/L** | 10 mg/L HMDA (0.96 mol/L), 0.63 mol/L sucrose, PBS |

The transfer protocol was developed with capsules made from the aqueous phases reported below:

| Sample | Aqueous phase composition |
|---|---|
| **"Sucrose"** | 10 mg/L HMDA (96 mmol/L), 0.63 mol/L sucrose in PBS |
| **"NaCl"** | 10 mg/L HMDA (96 mmol/L), 2.22 mol/L sucrose in PBS |

### Evaluation of the effect of sucrose and NaCl on polyNIPAM capsules

Capsules were prepared according to section F.1.1. The compositions of the aqueous phases used to build the capsules are reported in the table below.

| Sample | Aqueous phase composition |
|---|---|
| **"Sucrose"** | 10 g/L α,ω diamino-terminated polyNIPAM (4600 g/mol), 0.63 mol/L sucrose in PBS |
| **"NaCl"** | 10 g/L α,ω diamino-terminated polyNIPAM (4600 g/mol), 2.22 mol/L sucrose in PBS |

The processing temperatures are reported below:

| Sample | $T_{aq}$ | $T_{oil}$ | $T_{redisp}$ | $T_{start}$ | $T_{end}$ |
|---|---|---|---|---|---|
| **"Sucrose"** | 5 °C | RT | 50 °C | 50 °C | 15 °C |
| **"NaCl"** | ≈ 0 °C | RT | 50 °C | 50 °C | 15 °C |

### Characterization of polyNIPAM capsule integrity as a function of the temperature

Capsules were prepared according to section F.1.1, from an aqueous phase made of 10 g/L α,ω-diamino terminated polyNIPAM (4600 g/mol) and 0.63 mol/L sucrose in PBS. The capsules were characterized as reported in section F.1.1. Phase contrast pictures were taken, instead of fluorescence ones. The processing temperatures are reported below:

| $T_{aq}$ | $T_{oil}$ | $T_{redisp}$ | $T_{start}$ | $T_{end}$ |
|---|---|---|---|---|
| 5 °C | RT | 50 °C | 50 °C | 15 °C |

### polyNIPAM capsules release tests

Capsules were prepared according to section F.1.1. The aqueous phases were made of 10 g/L α,ω-diamino terminated polyNIPAM (4600 g/mol), 0.63 mol/L sucrose and a fluorescence probe, in PBS. The characteristics of the fluorescence probe and its concentration are reported below:

| **Encapsulated molecules** | **Molecule concentrations** |
|---|---|
| Sulforhodamine 101 | 50 µmol/L |
| Dextran-TexasRed (3 kg/mol) | 50 mg/L |
| Dextran-FITC (10 kg/mol) | 250 mg/L |
| BSA-TexasRed (66 kg/mol) | 1 g/L |
| Netrin-FITC (68 kg/mol) | 60 mg/L |
| Netrin-FITC (68 kg/mol) and BSA | Netrin-FITC: 60 mg/L, BSA: 1.92 g/L |
| Antibody-FITC (150 kg/mol) | 67 mg/L |

The capsules were characterized as reported in section F.1.1. The processing temperatures are reported below:

| $T_{aq}$ | $T_{oil}$ | $T_{redisp}$ | $T_{start}$ | $T_{end}$ |
|---|---|---|---|---|
| 5 °C | RT | 50 °C | 50 °C | 15 °C |

### Reactive polyNIPAM+HMDA capsule release tests

Capsules were prepared according to section F.1.1. The aqueous phases were made of HMDA, α,ω-diamino terminated polyNIPAM (4600 g/mol), HMDA, 0.63 mmol/L sucrose and sulforhodamine 101 (50 µmol/L) in PBS. Capsules were transferred in PBS or in PBS supplemented with 0.64 mmol/L glucose. PolyNIPAM and HMDA concentrations and the presence of glucose in the redispersion medium is shown below:

| Sample name | $C_{polyNIPAM}$ (g/L) | $C_{HMDA}$ (g/L) | Glucose in redispersion medium |
|---|---|---|---|
| **5 %** | 0.5 | 9.5 | Yes |
| **10 %** | 1.0 | 9.0 | Yes |
| **25 %** | 2.5 | 7.5 | Yes |
| **50 %** | 5.0 | 5.0 | No |

The capsules were characterized in the redispersion medium, as reported in section F.1.1. The processing temperatures are reported below:

| $T_{aq}$ | $T_{oil}$ | $T_{redisp}$ | $T_{start}$ | $T_{end}$ |
|---|---|---|---|---|
| 5 °C | RT | 50 °C | 50 °C | 15 °C |

### Unreactive polyNIPAM+HMDA capsule release tests

Capsules were prepared according to section F.1.1. The aqueous phases were made of HMDA, α,ω-diamino terminated polyNIPAM (4600 g/mol), HMDA, 0.63 mmol/L sucrose and Dextran-TexasRed (3,000 g/mol, 50 mg/L) in PBS. Capsules were transferred in PBS or in PBS supplemented with 0.64 mmol/L glucose. PolyNIPAM and HMDA concentrations are reported below:

| **Sample name** | 5 % | 10 % | 25 % | 80 % | 90 % | 95 % | 100 % |
|---|---|---|---|---|---|---|---|
| **$C_{polyNIPAM}$ (g/L)** | 0.5 | 1.0 | 2.5 | 8.0 | 9.0 | 9.5 | 10.0 |
| **$C_{HMDA}$ (g/L)** | 9.5 | 9.0 | 7.5 | 2.0 | 1.0 | 0.5 | 0.0 |

The capsules were characterized as reported in section F.1.1. The processing temperatures are reported below:

| $T_{aq}$ | $T_{oil}$ | $T_{redisp}$ | $T_{start}$ | $T_{end}$ |
|---|---|---|---|---|
| 5 °C | RT | 50 °C | 50 °C | 15 °C |

### Determination of the working UCST+albumin composition

Capsules were prepared according to section F.1.1. All the procedure was conducted at room temperature. The aqueous phases were made of albumin (BSA or ovalbumin), dextran-TexasRed (3000 g/mol) and an additive (sucrose or heavy water) in PBS. The composition of each phase is reported below:

| Albumin | $C_{albumin}$ | Additive | $C_{additive}$ | Fluorescent probe | $C_{probe}$ |
|---|---|---|---|---|---|
| Ovalbumin | 10 g/L | Sucrose | 20 % w. | Dextran Texas Red | 100 mg/L |
| Ovalbumin | 100 g/L | $D_2O$ | 71.7 % vol. | Dextran Texas Red | 10 mg/L |
| BSA | 10 g/L | Sucrose | 20 % w. | Dextran Texas Red | 100 mg/L |
| BSA | 100 g/L | $D_2O$ | 71.7 % vol. | Dextran Texas Red | 10 mg/L |

The capsules were characterized as reported in section F.1.1. Only a few pictures were taken; the capsules were not submitted to the temperature ramp.

### UCST polymer-based capsules: choice of the fluorophore

Capsules were prepared according to section F.1.1. The aqueous phases were made of ovalbumin, the 43 °C UCST polymer, 71.7 % vol. $D_2O$ and a fluorescent probe in PBS. The composition of each phase is reported below:

| Dye | $C_{dye}$ | $C_{ovalbumin}$ (g/L) | $C_{UCST\ polymer\ (43\,°C)}$ (g/L) |
|---|---|---|---|
| BSA-FITC | 167 mg/L | 80 | 20 |
| Calcein | 10 µmol/L | 80 | 20 |
| Dextran-TexasRed (3,000 g/mol | 10 mg/L | 100 | 10 |

The capsules were characterized as reported in section F.1.1. The processing temperatures are reported below:

| Sample | $T_{aq}$ | $T_{oil}$ | $T_{redisp}$ | $T_{start}$ | $T_{end}$ |
|---|---|---|---|---|---|
| BSA-FITC | 55 °C | RT | RT | 55 °C | |
| Calcein | 55 °C | RT | 15 °C | 55 °C | |
| Dextran-TexasRed | 55 °C | RT | 15 °C | 70 °C | |

### Temperature-sensitivity of UCST:ovalbumin capsules

Capsules were prepared according to section F.1.1. The aqueous phases were made of ovalbumin, the 43 °C UCST polymer, 71.7 % vol. $D_2O$ and 10 µmol/L calcein in PBS. The composition of each phase is reported below:

| Sample name | 0 % | 10 % | 20 % | 30 % | 50 % | 70 % | 80 % | 90 % | 100 % |
|---|---|---|---|---|---|---|---|---|---|
| $C_{UCST\ polymer\ 43\ °C}$ (g/L) | 0 | 10 | 20 | 30 | 50 | 70 | 80 | 90 | 100 |
| $C_{Ovalbumin}$ (g/L) | 100 | 90 | 80 | 70 | 50 | 30 | 20 | 10 | 0 |

The capsules were characterized as reported in section F.1.1. The burst was inferred from the evolution of the shape of the capsule, not on the fluorescence intensity in the capsule. The processing temperatures are reported below:

| $T_{aq}$ | $T_{oil}$ | $T_{redisp}$ | $T_{start}$ | $T_{end}$ |
|---|---|---|---|---|
| 55 °C | RT | RT | 15 °C | 50 °C |

### Determination of the burst temperature of UCST:ovalbumin capsules

Capsules were prepared according to section F.1.1. The aqueous phases were made of ovalbumin, a UCST polymer, 71.7 % vol. $D_2O$ and a fluorescent reporter in PBS. The composition of each phase is reported below:

| Sample | $C_{polymer}$ (g/L) | $C_{Ovalbumin}$ (g/L) | Fluorescent probe | $C_{Probe}$ |
|---|---|---|---|---|
| **90 % 43 °C UCST polymer/10 % ovalbumin** | 90 | 10 | calcein | 10 µmol/L |
| **80 % 43 °C UCST polymer/20 % ovalbumin** | 80 | 20 | BSA-FITC | 10 mg/L |
| **90 % 35 °C UCST polymer/10 % ovalbumin** | 90 | 10 | BSA-TexasRed | 10 mg/L |

The capsules were characterized as reported in section F.1.1. The burst was inferred from the evolution of the shape of the capsule, not on the fluorescence intensity in the capsule. The processing temperatures are reported below:

| Sample | $T_{aq}$ | $T_{oil}$ | $T_{redisp}$ | $T_{start}$ | $T_{end}$ |
|---|---|---|---|---|---|
| **90 % 43 °C UCST polymer/10 % ovalbumin** | 55 °C | RT | RT | 15 °C | 55 °C |
| **80 % 43 °C UCST polymer/20 % ovalbumin** | 55 °C | RT | RT | 15 °C | 55 °C |
| **90 % 35 °C UCST polymer/10 % ovalbumin** | 50 °C | RT | 10 °C | 10 °C | 55 °C |

# F.2. Nanometer-sized capsules

## F.2.1. HMDA-based capsules

### Capsule synthesis

In 9.8 mL of anhydrous cyclohexane were added 50 µL of a Span 80/Tween 80 mixture. The surfactants were dissolved with a vortex mixer for 30 seconds, to yield a translucent or transparent homogeneous solution, depending of the Span/Tween ratio. To this solution were added 50 µL of an aqueous phase made of 100 g/L of HMDA in PBS. The biphasic mixture is pre-emulsified with a vortex mixer for 2 minutes, to yield a milky emulsion. This emulsion was submitted to ultrasounds (Vibracell VCX750 Ultrasonic Cell Disrupter, equipped with a microtip, 40 % power) 20 s on/10 s off cycles for 3 minutes, in a 10 °C water bath. This yield a translucent emulsion, of which 1 mL where reserved for DLS measurements. The 9 mL left were placed under magnetic stirring in a water bath (10 °C); 1.5 TDI equivalents per monomer molecules were added in 3.6 mL anhydrous cyclohexane, then poured dropwise in the heated emulsion. The reaction was allowed to proceed for at least 3 hours.

The Span:Tween volumes used are reported below:

| Span:Tween vol. ratio | 100:0 | 90:10 | 80:20 | 70:30 | 60:40 | 50:50 |
|---|---|---|---|---|---|---|
| $V_{Span\ 80}$ (µL) | 50 | 45 | 40 | 35 | 30 | 25 |
| $V_{Tween\ 80}$ (µL) | 0 | 5 | 10 | 15 | 20 | 25 |

#### Transfer of the capsules in the aqueous phase

1 mL of a suspension of capsules in the oil were transferred dropwise in a solution of SDS at 5.77 g/L (20 mmol/L) in PBS, under vigorous magnetic stirring, to yield a milky emulsion. This emulsion was then submitted to ultrasounds (Vibracell with microtip, 40 % power) for 1 minute, 10 s on/5 s off cycles. The mixture was heated at 70 °C for 30 minutes under magnetic stirring to remove the cyclohexane. The obtained suspension was filtered on cellulose acetate (1.2 µm) prior to DLS measurements.

#### Characterization of hydrodynamic diameters

The crude emulsion and the suspension of capsules in SDS were processed without dilution, as reported in appendix *C.3.1 General purpose hydrodynamic radii measurements*, p. 196.

### F.2.2. Synthesis and characterization of polyNIPAM capsules

#### Capsules synthesis

In 9.8 mL of anhydrous cyclohexane were added 30 µL Span 80 and 20 µL Tween 80. The surfactants were dissolved with a vortex mixer for 30 seconds, to yield a translucent homogeneous solution. To this solution were added 50 µL of an aqueous phase made of α,ω diamino-terminated polyNIPAM and HMDA (cf. table below). The biphasic mixture is cooled at 10 °C with a water bath, and then pre-emulsified with a vortex mixer for 2 minutes, to yield a milky emulsion. This emulsion was submitted to ultrasounds (Vibracell VCX750 Ultrasonic Cell Disrupter, equipped with a microtip, 40 % power) 20 s on/10 s off cycles for 3 minutes, in a 10 °C water bath. This yield a translucent emulsion, of whom 1 mL where reserved for DLS measurements. The 9 mL left were placed in a water bath at 40 °C under magnetic stirring; 1.5 TDI equivalents per monomer molecules were added in 3.6 mL anhydrous cyclohexane, then poured dropwise in the heated emulsion. The reaction was left to proceed for at least 3 hours.

| Sample | $C_{polyNIPAM}$ (g/L) | $C_{HMDA}$ (g/L) |
|---|---|---|
| **polyNIPAM 100 %** | 100 | 0 |
| **polyNIPAM 50 %/HMDA 50 %** | 50 | 50 |

All the next steps were performed at 50 °C. 1 mL of a suspension of capsules in the oil were transferred dropwise in a solution of SDS at 5.77 g/L (20 mmol/L) in PBS, under vigorous magnetic stirring, to yield a milky emulsion. This emulsion was then submitted to ultrasounds (Vibracell with microtip, 40 % power) for 1 minute, 10 s on/5 s off cycles. The mixture was heated at 70 °C for 30 minutes under magnetic stirring to remove the cyclohexane. The obtained suspensions were filtered on cellulose acetate (1.2 µm) prior to DLS measurements.

### Capsules characterization

The hydrodynamic radius and the intensity of scattered light was obtained by DLS (cf. appendix C.3.1, p. 196), at 50 ℃ immediately after filtration. The temperature of the sample was decreased to 20 ℃ (RT, t = 0); 15 minutes after, these measurements were repeated. The sample was kept at room temperature for 8 days. The hydrodynamic diameter and the intensity of scattered light were measured at t = 24 h and t = 8 days.

## F.2.3. Determination of the temperature of release with the calcein+cobalt assay

### Capsule synthesis

In 9.8 mL of anhydrous cyclohexane were added 30 µL Span 80 and 20 µL Tween 80. The surfactants were dissolved with a vortex mixer for 30 seconds, to yield a translucent homogeneous solution. To this solution were added 50 µL of an aqueous phase made of 80 g/L α,ω diamino-terminated polyNIPAM, 20 g/L HMDA, 3.2 µmol/L calcein sodium salt and 7.7 µmol/L cobalt(II) chloride. The biphasic mixture is cooled at 10 ℃ with a water bath, then pre-emulsified with a vortex mixer for 2 minutes, to yield a milky emulsion. This emulsion was submitted to ultrasounds (Vibracell VCX750 Ultrasonic Cell Disrupter, equipped with a microtip, 40 % power) 20 s on/10 s off cycles for 3 minutes, in a 10 ℃ water bath. This yield a translucent emulsion, of whom 1 mL where reserved for DLS measurements. The 9 mL left were placed in a water bath at 40 ℃ under magnetic stirring; 3.6 mL of a solution of TDI at 16.14 mmol/L in cyclohexane ($5.8{\cdot}10^{-8}$ mol, 1.5 eq. with regard of HMDA) were added to the emulsion under moderate magnetic stirring (700 rpm). The reaction was left to proceed for at least 3 hours.

The suspensions of capsules in the oil phase were centrifuged for 2 minutes at 3,000 rpm. To prevent the dissolution of the membrane, the temperature was kept above 40 ℃ by heating the centrifuge rotor in warm water (70 ℃) for 5–10 minutes prior the centrifuge step. Immediately at the end of the centrifugation, the supernatant was discarded and replaced by 1 mL cyclohexane at 40 ℃.

All the suspension of capsules in the oil was transferred dropwise in a solution of SDS at 5.77 g/L (20 mmol/L) in PBS, under vigorous magnetic stirring, to yield a milky emulsion. This emulsion was then submitted to ultrasounds (Vibracell with microtip, 40 % power) for 1 minute, 10 s on/5 s off cycles. The mixture was heated at 70 ℃ for 30 minutes under magnetic stirring to remove the cyclohexane. It was then kept at 40 ℃ in closed vials before any characterization step, still under magnetic stirring.

### Release characterization

**Experimental device** The release was assessed by fluorescence measurements, in the device reported in appendix C.3.3. The fluorimeter was equipped with a custom LED based illumination system. A cyan emitting LED (490 nm, Rebel, Philips) was collimated

with a lens and filtered at 488 ± 10 nm. The LED was driven using a Thorlabs DC4100 set to deliver a current of 50 mA, which allows to irradiate the sample only when required. The fluorescence signal was recorded at 526 nm; all the excitation slits were set to 4 nm bandwidth. To avoid photobleaching during acquisition, the sample was homogenized with a magnetic stirrer, and the fluorescence intensity was only recorded for 4.5 seconds each 30 seconds. The recording of fluorescence intensity was performed during all the release experiment, at a frequency of 10 Hz. The temperature of the sample was recorded manually, using a K thermocouple based thermometer. The sample was submitted to a decreasing ramp of temperature, from 42 ℃ to 5 ℃, at 0.9 ℃/min.

**Sample preparation** 30 µL of the suspension of capsules in SDS were added to 2.7 mL of a solution of EDTA (10 mmol/L) in PBS and introduced in a quartz cuvette.

**Data processing** The fluorescence intensity was corrected from the influence of the temperature, using a reference fluorescence curve obtained from a solution of calcein (100 nmol/L) in PBS, submitted to the same decreasing ramp of temperature.

## F.2.4. Morphological study by cryo electronic microscopy

### Samples preparation

In 9.8 mL of anhydrous cyclohexane were added 30 µL Span 80 and 20 µL Tween 80. The surfactants were dissolved with a vortex mixer for 30 seconds, to yield a translucent homogeneous solution. To this solution were added 50 µL of an aqueous phase made of α,ω diamino-terminated polyNIPAM and HMDA (cf. table below). The biphasic mixture is cooled at 10 ℃ with a water bath, then pre-emulsified with a vortex mixer for 2 minutes, to yield a milky emulsion. This emulsion was submitted to ultrasounds (Vibracell VCX750 Ultrasonic Cell Disrupter, equipped with a microtip, 40 % power) 20 s on/10 s off cycles for 3 minutes, in a 10 ℃ water bath. This yield a translucent emulsion, of whom 1 mL where reserved for DLS measurements. The 9 mL left were placed in a water bath at 40 ℃ under magnetic stirring; 1.5 TDI equivalents per monomer molecules were added in 3.6 mL anhydrous cyclohexane, then poured dropwise in the heated emulsion. The reaction was left to proceed for at least 3 hours.

| Sample | $C_{polyNIPAM}$ (g/L) | $C_{HMDA}$ (g/L) |
|---|---|---|
| **HMDA 100 %** | 0 | 100 |
| **polyNIPAM 50 %/HMDA 50 %** | 50 | 50 |

The suspensions of capsules in the oil phase were centrifuged for 2 minutes at 3,000 rpm. To prevent the dissolution of the membrane, the temperature was kept above 40 ℃ by heating the centrifuge rotor in warm water (70 ℃) for 5–10 minutes prior the centrifuge

step. Immediately at the end of the centrifugation, the supernatant was discarded and replaced by 1 mL cyclohexane at 40 ℃.

All the suspension of capsules in the oil was transferred dropwise in a solution of SDS at 5.77 g/L (20 mmol/L) in PBS, under vigorous magnetic stirring, to yield a milky emulsion. This emulsion was then submitted to ultrasounds (Vibracell with microtip, 40 % power) for 1 minute, 10 s on/5 s off cycles. The mixture was heated at 70 ℃ for 30 minutes under magnetic stirring to remove the cyclohexane. It was then kept at 40 ℃ in closed vials before any characterization step, still under magnetic stirring.

The SDS was then removed from the samples by gel permeation chromatography. A 10 mL syringe was filled with Sephacryl 400 HR and equilibrated with 100 mL PBS at 50 ℃. Immediately after was added 1 mL of the capsules suspended in SDS, and eluted with PBS at 50 ℃. 1 mL fractions were collected on a water bath at 40 ℃. The absence of SDS in the collected fractions was assessed with the maximum bubble pressure tensiometer method (see appendix *C.3.4 Quantification of the SDS concentration in capsules suspensions*, p. 199).

## F.2.5. TexasRed fluorescence in presence of albumin

A solution was prepared from dextran Texas Red (3,000 g/mol, 100 mg/L), ovalbumin (100 g/L) and 71.7 % vol. $D_2O$ in PBS. 8 µL of this solution were sealed between two glass slides, using an adhesive Teflon spacer (120 µm thick). This slide was put in the petri Dish used to characterize the capsules (see figure F.3, p. 217), in place of the raised glass slide; the dish was filled with deionized water.

The fluorescence of the sample was recorded with the epifluorescence microscope, every 5 seconds for 30,000 s. The temperature of the sample was recorded using the probe plunged into the external water. The sample was submitted to increasing and decreasing ramp of temperature, cycled alternatively every hour. The slope of the ramps was 10 ℃/min, from 15 ℃ to 50 ℃; the temperature at the end of the ramp was sustained until the next cycle began.

# G. Quantitative and real-time FRAP measurements

We aim to develop an encapsulation system able to release its content quickly, within one second after stimulation. Our system should be able to encapsulate and release water-soluble molecule of various molecular weight, from small molecules like drugs or fluorescent dyes to bigger ones, like proteins. These objects may or may not be ionized. Techniques relying on the release of a specific object, like the one based on conductivity assessment [313] or on calcein release [249, 250, 314, 315] may not be relevant. The behavior of macromolecules can differ from calcein or ions, at least by their size difference.

However, "free" molecules and encapsulated ones can be distinguished by their diffusivity. The "free" molecules have a diffusivity in the range of 100 µm²/s, while the encapsulated ones have the diffusivity of the vehicle. For 200 nm capsules, the diffusivity will be in the range of 2 µm²/s. These values can be inferred from their radius by the Stokes-Einstein law:

$$\mathrm{D} = \frac{k_\mathrm{B} T}{6\pi\eta R} \tag{G.1}$$

where D is the diffusivity of the species, $k_\mathrm{B}$ the Boltzmann constant, $T$ the temperature, $\eta$ the viscosity of the medium and $R$ the radius of the species. We choose here $\eta_{\mathrm{PBS}} = 10^{-3}$ Pa·s and $T = 293$ K (20 ℃).

Several techniques exists to determine the diffusivity of fluorescent labeled molecules, amongst them FCS and FRAP. FCS experiments give access to both the diffusivity and the concentration of dye in the medium [316, 317]. While it is non invasive, this technique requires acquisition times incompatible with the kinetics of release: 10 minutes to 1 hour of acquisition are required [318, 319], while the capsules are expected to release their content in less than one second. FRAP is mainly used to determine the isotropic [320] or anisotropic [321–324] diffusivity of molecules. The duration of experiments is dependent of the acquisition system speed, the size of the bleached area and the diffusivity of the studied species. With current systems, it is possible to acquire the data of a FRAP experiment in less than one minute. While literature on using FRAP to determine kinetics constants is somewhat abundant, nothing could be found on concentration measurements of fluorescent molecules. In this appendix, we present a FRAP-based technique coupled to a Fourier transform analysis of the data to determine either the diffusivity or the concentration of a given species.

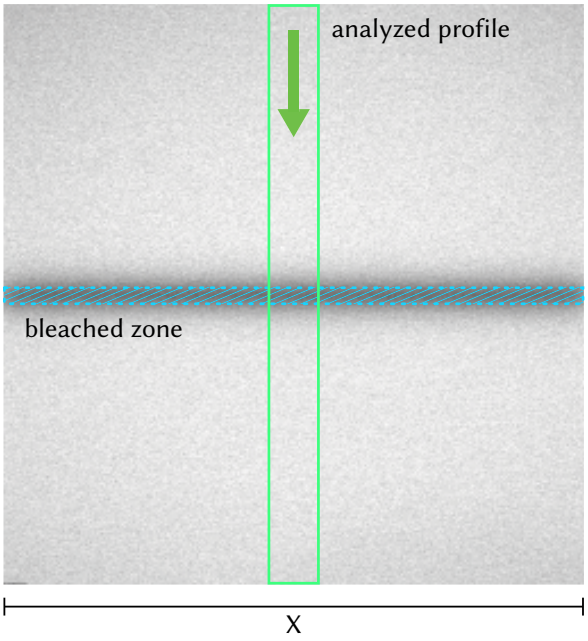


**Figure G.1.** *A fluorescent sample viewed on a confocal microscope. The bleached zone is hatched in blue. The profile of fluorescence intensity is recorded along the direction of the green arrow.*

## G.1. System description

The bleaching of sample is usually done using a laser. Confocal microscopes are convenient tools to perform FRAP experiments, as the reading laser can also be used to bleach the sample. After bleaching, the concentration of fluorescent molecule will homogenize, according to the second Fick's law:

$$\frac{\partial \mathrm{C}}{\partial t}(\mathbf{x}, t) - \mathrm{D}\Delta\,\mathrm{C}(\mathbf{x}, t) = 0 \tag{G.2}$$

where $\mathrm{C}$ is the concentration of the fluorescent molecule and $D$ its diffusivity. In our case, the bleaching pattern is an horizontal line, as shown on figure G.1. The light intensity profile of the laser is gaussian, which is responsible for the gaussian profile of the fluorescence intensity in an orthogonal direction of the bleaching one. If the bleached line is long enough, the system can be considered as unidimensional. This approximation can be made if the size of the bleached line is longer than the characteristic size of the diffusion process, which is given here by the width of the gaussian and the diffusivity of the considered species. To simplify the problem, we will consider an infinite long line bleach, giving a gaussian profile of fluorescence intensity on an orthogonal direction to the line bleach.

# G.2. Theory

## G.2.1. The ideal system: an infinite picture

In a unidimensional configuration, equation (G.2) can be simplified as follow:

$$\frac{\partial \mathrm{C}}{\partial t}(x,t) - \mathrm{D}\frac{\partial^2 \mathrm{C}(x,t)}{\partial x^2} = 0 \tag{G.3}$$

As the initial distribution of fluorescent molecules is gaussian, the solution of (G.3) is the following:

$$\mathrm{C}(x,t) = n_0 - \frac{n}{\sqrt{2\pi(2\mathrm{D}t+\sigma_0^2)}}\,\mathrm{e}^{-\frac{x^2}{2(2\mathrm{D}t+\sigma_0^2)}} \tag{G.4}$$

where $\sigma_0$ is the characteristic width of the gaussian at the time origin, $n$ is related to the amount of fluorophores along the studied profile. The fluorescence intensity measured by the confocal microscope is linked to the concentration by a linear relation, and depends on the quantum yield of the molecule and the intensity of excitation light. This intensity, noted I, verifies:

$$\frac{\partial \mathrm{I}}{\partial t}(x,t) - \mathrm{D}\frac{\partial^2 \mathrm{I}(x,t)}{\partial x^2} = 0 \tag{G.5}$$

$$\mathrm{I}(x,t) = K_0 - \frac{K}{\sqrt{2\pi(2\mathrm{D}t+\sigma_0^2)}}\,\mathrm{e}^{-\frac{x^2}{2(2\mathrm{D}t+\sigma_0^2)}} \tag{G.6}$$

$K$ being proportional to $n$ from equation (G.4). To simplify the analysis, we will deal only with the time-dependent part of this expression. From now, the intensity will be expressed as:

$$\mathrm{I}(x,t) = \frac{K}{\sqrt{2\pi(2\mathrm{D}t+\sigma_0^2)}}\,\mathrm{e}^{-\frac{x^2}{2(2\mathrm{D}t+\sigma_0^2)}} \tag{G.7}$$

In our case, we have at least two species, the free fluorophore called $A_{\text{free}}$ and the fluorophore entrapped in the capsules, called $A_{\text{capsule}}$. Their respective diffusion coefficients are $D_{\text{free}}$ and $D_{\text{capsule}}$. A part of the fluorophores may also adsorb on the observation chamber surface, leading to a third population with a diffusivity almost equal to 0. To get the concentration of the free dye, two problems arise. We need to fit the fluorescence profiles by two or three gaussians, for different acquisition time, as shown on equation (G.4). $D$ and $\sigma_0$ are known or can be measured prior the release experiment. However, the robustness of bi- or tri-gaussian fits is questionable. The second problem concerns the reproducibility of the bleaching and imaging conditions. As the concentration is directly inferred from the fluorescence intensity, the imaging conditions must be exactly the same, for example the position of the observation chamber along the $z$ axis. Due to partial bleaching of the fluorescent molecules and the presence of a possible

To simplify the data processing procedure and to address the aforementioned problems, we propose to consider the diffusion system in the Fourier space, but only for the spatial variables. In this case, equation (G.3) becomes:

$$\frac{\partial \hat{\mathrm{I}}}{\partial t}(q,t) + \mathrm{D}q^2\hat{\mathrm{I}}(q,t) = 0 \tag{G.8}$$

where $q$ is the spatial pulsation and $\hat{\mathrm{I}}$ is the Fourier transform of the fluorescence intensity profile. The solution of this first-order differential equation is:

$$\hat{\mathrm{I}}(q,t) = \hat{\mathrm{I}}(q,0)\,\mathrm{e}^{-\mathrm{D}q^2t} \tag{G.9}$$

This solution is remarkable: the time evolution of $\hat{\mathrm{I}}$ is exponential and does not depend on the initial shape of fluorescence intensity. To get the diffusivity of the considered species, only one exponential fit is required. The accuracy of the result can be improved by fitting $\hat{\mathrm{I}}$ for several values of $q$. In our system, the initial profile of fluorescence intensity is gaussian (cf. equation (G.7)). Its Fourier transform is the following:

$$\hat{\mathrm{I}}(q,t) = K\,\mathrm{e}^{-q^2\left(\mathrm{D}t+\frac{\sigma_0^2}{2}\right)} \tag{G.10}$$

The pre-exponential factor is $K$ which enables to measure the concentration of the fluorescent species. In our case, as presented page 227, the difference of diffusivity between the free dye and the encapsulated one is so large (a factor of 50) that the concentration of one can be considered constant when the other varies. This method should be sufficient to follow the evolution of the concentration as a function of time. However, as explained before, the quantification of the concentration requires reproducible illumination, bleaching and recording conditions. To overcome this issue, we propose to add to the solution a free dye serving as a reference. This dye must have comparable spectral characteristics as the released dye, but not the same diffusivity. Ideally, to distinguish them on the Fourier transform of the fluorescence intensity profile, we need $\mathrm{D}_{\text{free}} = 5\mathrm{D}_{\text{reference}}$, or the opposite. We have now

$$\frac{\mathrm{C}_{\text{free}}}{\mathrm{C}_{\text{reference}}} \propto \frac{K_{\text{free}}}{K_{\text{reference}}} \tag{G.11}$$

independently of the experimental conditions due to the internal reference. The proportionality factor can be measured in a calibration measurement.

## G.2.2. Effect of the size of the recorded picture

To take the Fourier transform of the fluorescent intensity, an infinite picture is needed, as suggested by the definition of this transform:

$$\hat{\mathrm{I}}(q,t) = \int_{\mathbb{R}} \mathrm{I}(x,t)\,\mathrm{e}^{-iqx}\,\mathrm{d}x \tag{G.12}$$

This definition remains true if a finite picture of I is taken, as long as its value outside the picture is zero. Unfortunately, this never happens with gaussian function. $X$ being the size of the recorded picture (see picture G.1), equation (G.12) becomes:

$$\hat{\mathrm{I}}_{\text{picture}}(q,t) = \int_{-\frac{X}{2}}^{\frac{X}{2}} \mathrm{I}(x,t)\,\mathrm{e}^{-iqx}\,\mathrm{d}x \tag{G.13}$$

whose analytical expression in the case of an initial gaussian profile (eq. (G.7)) is:

$$\hat{\mathrm{I}}_{\text{picture}}(q,t) = K\,\mathrm{e}^{-q^2\left(\mathrm{D}t+\frac{\sigma_0^2}{2}\right)} \cdot \mathrm{Re}\left(\mathrm{erf}\left(\frac{X + i2q(2\mathrm{D}t+\sigma_0^2)}{2\sqrt{2(2\mathrm{D}t+\sigma_0^2)}}\right)\right) \tag{G.14}$$

$$= \hat{\mathrm{I}}(q,t) \cdot \mathrm{Re}\left(\mathrm{erf}\left(\frac{X + i2q(2\mathrm{D}t+\sigma_0^2)}{2\sqrt{2(2\mathrm{D}t+\sigma_0^2)}}\right)\right) \tag{G.15}$$

which differs from (G.10) by the error function. The influence of this function will be evaluated in the next part.

## G.3. System implementation

### G.3.1. Setup description

To confirm the equation (G.11), we considered a system made of fluorescein and FITC-labeled dextran in PBS medium. Their diffusion coefficients differs by a factor of 4.4 (see table G.1). Fluorescein concentration was fixed to 5 µmol/L, to serve as internal reference. The concentration of FITC-dextran was chosen between 12.5 and 1000 mg/L (see table G.2), to act as the released dye. For each measurement, 8 µL of the studied mixture were placed between a microscope slide and a coverslip sealed with 120 µm thick spacer. The samples were bleached and viewer using a Zeiss LSM 510 confocal microscope, using full power of the 488 nm line of the argon laser (30 mW). Bleaching was conducted for 10 seconds. Pictures were recorded with a 2 seconds interval, for 7 minutes, with a resolution of 512×512 through a 20× PlanaFluor objective. The parameter set is summarized in table G.1.

### G.3.2. Data analysis

To eliminate the effect of the non-homogeneous illumination of the sample on the recorded data, each picture was normalized by the picture of a homogeneous fluorescent sample taken in the same experimental conditions. The fluorescence intensity profiles were extracted in the orthogonal direction of the bleach. To reduce the acquisition noise, the width of the profile was set to 8 pixels. The Fourier transform of the profiles was the calculated, and

| Parameter | Value |
|---|---|
| $D_{\text{fluorescein}}$ | 350 µm²/s |
| $D_{\text{dextran}}$ | 80 µm²/s |
| $\sigma_0$ | $\sim$ 50 µm²/s |
| $q$ | 4,430 m$^{-1}$ – 13,290 m$^{-1}$ |
| $X$ (picture size) | 1.5 mm |
| Picture resolution | 512×512 |

**Table G.1.** *Experimental parameters for the quantitative FRAP experiment*

| Batch number | 1 | 2 | 3 | 4 | 5 | 6 |
|---|---|---|---|---|---|---|
| Dextran concentration (mg/L) | 12.5 | 25 | 50 | 100 | 150 | 200 |
| Batch number | 7 | 8 | 9 | 10 | 11 | 12 |
| Dextran concentration (mg/L) | 250 | 300 | 400 | 600 | 800 | 1000 |

**Table G.2.** *FITC-dextran concentrations used for the calibration procedure*

the decay of the Fourier transform was plotted as a function of time, for several values of $q$. The data normalization, extraction and transformation were implemented as a set of C libraries, to do the analysis in real time. As the intensity profile is a discrete signal, only discrete values of $q$ are available: they in the range $(k2\pi/X)_{k\in[0,\text{pixel number}]}$. The plots were then fitted using the following equation:

$$y = y_0 + A_{\text{fluorescein}}\, \mathrm{e}^{-D_{\text{fluorescein}} q^2 t} + A_{\text{dextran}}\, \mathrm{e}^{-D_{\text{dextran}} q^2 t} \tag{G.16}$$

where the free fitting parameters were $y_0$, $A_{\text{fluorescein}}$ and $A_{\text{dextran}}$. The relation (G.11) was verified by plotting $\frac{A_{\text{dextran}}}{A_{\text{fluorescein}}}$ as a function of $\frac{C_{\text{dextran}}}{C_{\text{fluorescein}}}$, cf. picture G.2. The linear relationship is verified successfully over more than one decade.

### G.3.3. Error function effect

As explained in part G.2.2, page 231, the contribution of erf to the Fourier transform decay may no be negligible. $\mathrm{Re}\,\mathrm{erf}\,\frac{X+i2q(2Dt+\sigma_0^2)}{2\sqrt{2(2Dt+\sigma_0^2)}}$ is plotted as a function of time, using the parameters in table G.1, for the FITC-labeled dextran and $q = 2 \cdot 4430\,\text{m}^{-1}$ (2nd order). As seen on figure G.1 for $X$ = 1.5 mm, the value of the error function moves away from 1 above 200 s. The maximal error in this configuration is less than 4 percent, which seems reasonable. A simple way to drastically reduce erf impact is to increase the picture size. Increasing the picture size from 1.5 mm to 2 mm decreases the error from 4 % to 0.8 %, with a picture size of of 2.5 mm the maximal error is as low as $2{\cdot}10^{-5}$.

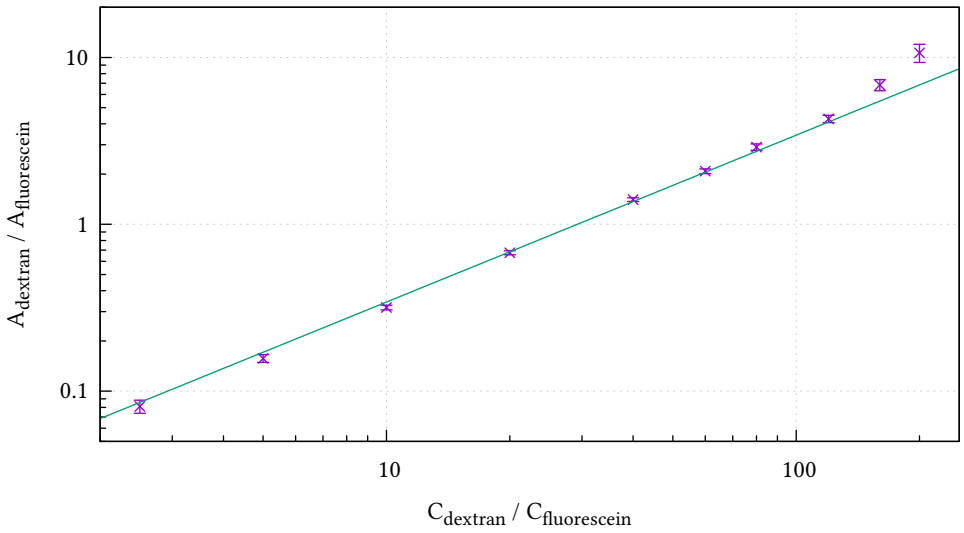


**Figure G.2.** *Plot of concentration ratios vs preexponential factor ratios. Preexponential factors were obtained by fitting the decay for q = 2·4430 m⁻¹, also known as the second order. Points were fitted by the equation $y = Ax$. $A$ = 3.422 ± 0.075.*

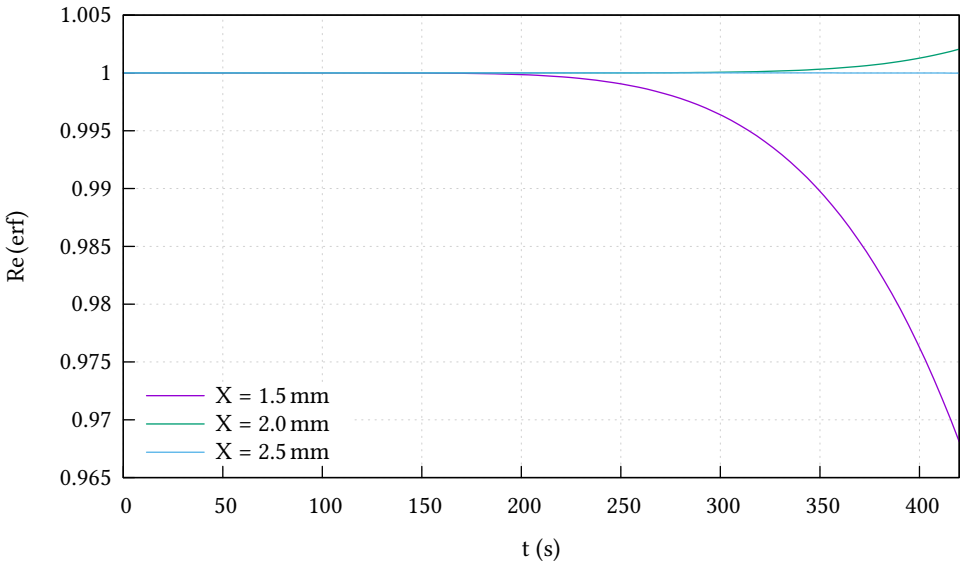


**Figure G.3.** *Value of the real part of the error function, for the FITC-dextran, $q = 2 \cdot 4430\ m^{-1}$. The other parameters are taken from table G.1.*

# Bibliography


(1) Nowak, M.; Machate, A.; Yu, S. R.; Gupta, M.; Brand, M. Interpretation of the FGF8 morphogen gradient is regulated by endocytic trafficking. *Nature cell biology* **2011**, *13*, 153–158 (cit. on p. 3).

(2) Thompson, A. W.; Pujic, Z.; Richards, L. J.; Goodhill, G. J. Cyclic nucleotide-dependent switching of mammalian axon guidance depends on gradient steepness. *Molecular and Cellular Neuroscience* **2011**, *47*, 45–52 (cit. on pp. 3, 10, 12, 175, 181, 182, 184, 185).

(3) Lohof, A. M.; Quillan, M.; Dan, Y.; Poo, M. Asymmetric modulation of cytosolic cAMP activity induces growth cone turning. *The Journal of neuroscience* **1992**, *12*, 1253–1261 (cit. on pp. 3, 180, 181).

(4) Pujic, Z.; Giacomantonio, C. E.; Unni, D.; Rosoff, W. J.; Goodhill, G. J. Analysis of the growth cone turning assay for studying axon guidance. *Journal of Neuroscience Methods* **2008**, *170*, 220–228 (cit. on pp. 3, 10, 181).

(5) Dupin, I.; Dahan, M.; Studer, V. Investigating Axonal Guidance with Microdevice-Based Approaches. *The Journal of Neuroscience* **2013**, *33*, 17647–17655 (cit. on pp. 3, 6, 10, 17, 181, 187).

(6) Keenan, T. M.; Folch, A. Biomolecular gradients in cell culture systems. *Lab Chip* **2008**, *8*, 34–57 (cit. on pp. 3, 10, 17, 181, 182, 187).

(7) Schönherr, E.; Hausser, H.-J. Extracellular matrix and cytokines: a functional unit. *Journal of Immunology Research* **2000**, *7*, 89–101 (cit. on p. 7).

(8) Yamaguchi, T. P. Heads or tails: Wnts and anterior–posterior patterning. *Current Biology* **2001**, *11*, R713–R724 (cit. on pp. 7, 173).

(9) Arnold, S. J.; Robertson, E. J. Making a commitment: cell lineage allocation and axis patterning in the early mouse embryo. *Nature reviews Molecular cell biology* **2009**, *10*, 91–103 (cit. on pp. 7, 173, 174).

(10) Petersen, C. P.; Reddien, P. W. Wnt Signaling and the Polarity of the Primary Body Axis. *Cell* **2009**, *139*, 1056–1068 (cit. on pp. 7, 173).

(11) De la Torre, J. R.; Höpker, V. H.; Ming, G.-l.; Poo, M.-m.; Tessier-Lavigne, M.; Hemmati-Brivanlou, A.; Holt, C. E. Turning of Retinal Growth Cones in a Netrin-1 Gradient Mediated by the Netrin Receptor DCC. *Neuron* **1997**, *19*, 1211–1224 (cit. on pp. 7, 10, 12, 181).

(12) Guthrie, S.; Lumsden, A. Collagen Gel Coculture of Neural Tissue. *Neuroprotocols* **1994**, *4*, 116–120 (cit. on pp. 8, 179).

(13) Marcos, S.; Backer, S.; Causeret, F.; Tessier-Lavigne, M.; Bloch-Gallego, E. Differential roles of Netrin-1 and its receptor DCC in inferior olivary neuron migration. *Molecular and Cellular Neuroscience* **2009**, *41*, 429–439 (cit. on pp. 8, 175, 179, 180).

(14) Joanne Wang, C.; Li, X.; Lin, B.; Shim, S.; Ming, G.-l.; Levchenko, A. A microfluidics-based turning assay reveals complex growth cone responses to integrated gradients of substrate-bound ECM molecules and diffusible guidance cues. *Lab on a Chip* **2008**, *8*, 227–237 (cit. on pp. 9, 189).

(15) Van der Meer, A. D.; Poot, A. A.; Feijen, J.; Vermes, I. Analyzing shear stress-induced alignment of actin filaments in endothelial cells with a microfluidic assay. *Biomicrofluidics* **2010**, *4* 011103, (cit. on pp. 9, 189).

(16) Irimia, D.; Liu, S.-Y.; Tharp, W. G.; Samadani, A.; Toner, M.; Poznansky, M. C. Microfluidic system for measuring neutrophil migratory responses to fast switches of chemical gradients. *Lab on a Chip* **2006**, *6*, 191–198 (cit. on p. 9).

(17) Morel, M.; Shynkar, V.; Galas, J.-C.; Dupin, I.; Bouzigues, C.; Studer, V.; Dahan, M. Amplification and Temporal Filtering during Gradient Sensing by Nerve Growth Cones Probed with a Microfluidic Assay. *Biophysical Journal* **2012**, *103*, 1648–1656 (cit. on pp. 9, 189).

(18) Keenan, T. M.; Hsu, C.-H.; Folch, A. Microfluidic "jets" for generating steady-state gradients of soluble molecules on open surfaces. *Applied Physics Letters* **2006**, *89* 114103 (cit. on pp. 9, 189).

(19) Bhattacharjee, N.; Li, N.; Keenan, T. M.; Folch, A. A neuron-benign microfluidic gradient generator for studying the response of mammalian neurons towards axon guidance factors. *Integr. Biol.* **2010**, *2*, 669–679 (cit. on pp. 9, 10, 190).

(20) Cimetta, E.; Cannizzaro, C.; James, R.; Biechele, T.; Moon, R. T.; Elvassore, N.; Vunjak-Novakovic, G. Microfluidic device generating stable concentration gradients for long term cell culture: application to Wnt3a regulation of β-catenin signaling. *Lab on a chip* **2010**, *10*, 3277–3283 (cit. on pp. 9, 190).

(21) VanDersarl, J. J.; Xu, A. M.; Melosh, N. A. Rapid spatial and temporal controlled signal delivery over large cell culture areas. *Lab Chip* **2011**, *11*, 3057–3063 (cit. on pp. 9, 10, 191).

(22) Goodhill, G. J. Mathematical guidance for axons. *Trends in Neurosciences* **1998**, *21*, 226–231 (cit. on pp. 11, 172, 180).

(23) Ming, G.-l.; Wong, S. T.; Henley, J.; Yuan, X.-b.; Song, H.-j.; Spitzer, N. C.; Poo, M.-m. Adaptation in the chemotactic guidance of nerve growth cones. *Nature* **2002**, *417*, 411–418 (cit. on pp. 10, 181).

(24) Forbes, E. M.; Thompson, A. W.; Yuan, J.; Goodhill, G. J. Calcium and cAMP Levels Interact to Determine Attraction versus Repulsion in Axon Guidance. *Neuron* **2012**, *74*, 490–503 (cit. on pp. 10, 181).

(25) Ming, G.-l.; Henley, J.; Tessier-Lavigne, M.; Song, H.-j.; Poo, M.-m. Electrical Activity Modulates Growth Cone Guidance by Diffusible Factors. *Neuron* **2001**, *29*, 441–452 (cit. on pp. 10, 171, 181).

(26) Zadeh, A. D.; Seveau, S.; Halbwachs-Mecarelli, L.; Keller, H. Chemotactically-induced redistribution of CD43 as related to polarity and locomotion of human polymorphonuclear leucocytes. *Biology of the Cell* **2003**, *95*, 265–273 (cit. on pp. 10, 12, 180, 181).

(27) Bailly, M.; Condeelis, J. S.; Segall, J. E. Chemoattractant-induced lamellipod extension. *Microscopy Research and Technique* **1998**, *43*, 433–443 (cit. on pp. 10, 12, 181).

(28) Meriane, M.; Tcherkezian, J.; Webber, C. A.; Danek, E. I.; Triki, I.; McFarlane, S.; Bloch-Gallego, E.; Lamarche-Vane, N. Phosphorylation of DCC by Fyn mediates Netrin-1 signaling in growth cone guidance. *The Journal of cell biology* **2004**, *167*, 687–698 (cit. on pp. 10, 181).

(29) Zicha, D.; Dunn, G.; Jones, G. English In *Basic Cell Culture Protocols*, Pollard, J., Walker, J., Eds.; Methods in Molecular Biology™, Vol. 75; Humana Press: 1997, pp 449–457 (cit. on pp. 11, 183).

(30) Abhyankar, V. V.; Toepke, M. W.; Cortesio, C. L.; Lokuta, M. A.; Huttenlocher, A.; Beebe, D. J. A platform for assessing chemotactic migration within a spatiotemporally defined 3D microenvironment. *Lab Chip* **2008**, *8*, 1507–1515 (cit. on pp. 11, 12, 185, 186).

(31) Zigmond, S. H. Ability of polymorphonuclear leukocytes to orient in gradients of chemotactic factors. *The Journal of Cell Biology* **1977**, *75*, 606–616 (cit. on pp. 12, 177, 183).

(32) Moghe, P. V.; Nelson, R. D.; Tranquillo, R. T. Cytokine-stimulated chemotaxis of human neutrophils in a 3-D conjoined fibrin gel assay. *Journal of Immunological Methods* **1995**, *180*, 193–211 (cit. on pp. 12, 177).

(33) Zicha, D.; Dunn, G.; Brown, A. A new direct-viewing chemotaxis chamber. *Journal of Cell Science* **1991**, *99*, 769–775 (cit. on pp. 12, 177, 183, 184).

(34) Rosoff, W. J.; Urbach, J. S.; Esrick, M. A.; McAllister, R. G.; Richards, L. J.; Goodhill, G. J. A new chemotaxis assay shows the extreme sensitivity of axons to molecular gradients. *Nature neuroscience* **2004**, *7*, 678–682 (cit. on pp. 12, 184).

(35) Rosoff, W.; McAllister, R.; Esrick, M.; Goodhill, G.; Urbach, J. Generating controlled molecular gradients in 3D gels. *Biotechnology and Bioengineering* **2005**, *91*, 754–759 (cit. on pp. 12, 184).

(36) Pujic, Z.; Goodhill, G. J. A dual compartment diffusion chamber for studying axonal chemotaxis in 3D collagen. *Journal of Neuroscience Methods* **2013**, *215*, 53–59 (cit. on pp. 12, 185).

(37) Ebendal, T.; Jacobson, C.-O. Tissue explants affecting extension and orientation of axons in cultured chick embryo ganglia. *Experimental Cell Research* **1977**, *105*, 379–387 (cit. on pp. 12, 179).

(38) Phillips, R. J.; Burdick, M. D.; Lutz, M.; Belperio, J. A.; Keane, M. P.; Strieter, R. M. The Stromal Derived Factor–1/CXCL12–CXC Chemokine Receptor 4 Biological Axis in Non–Small Cell Lung Cancer Metastases. *American journal of respiratory and critical care medicine* **2003**, *167*, 1676–1686 (cit. on pp. 12, 177).

(39) Cavnar, S. P.; Ray, P.; Moudgil, P.; Chang, S. L.; Luker, K. E.; Linderman, J. J.; Takayama, S.; Luker, G. D. Microfluidic source-sink model reveals effects of biophysically distinct CXCL12 isoforms in breast cancer chemotaxis. *Integr. Biol.* **2014**, *6*, 564–576 (cit. on pp. 12, 177).

(40) Vicker, M. G.; Lackie, J. M.; Schill, W. Neutrophil leucocyte chemotaxis is not induced by a spatial gradient of chemoattractant. *Journal of cell science* **1986**, *84*, 263–280 (cit. on p. 12).

(41) Albrecht, E.; Petty, H. R. Cellular memory: neutrophil orientation reverses during temporally decreasing chemoattractant concentrations. *Proceedings of the National Academy of Sciences* **1998**, *95*, 5039–5044 (cit. on pp. 12, 177).

(42) Robinson, K. R. The responses of cells to electrical fields: a review. *The Journal of cell biology* **1985**, *101*, 2023–2027 (cit. on p. 17).

(43) Pinato, G.; Lien, L.; D'Este, E.; Torre, V.; Cojoc, D. Neuronal chemotaxis by optically manipulated liposomes. *Journal of the European Optical Society - Rapid publications* **2011**, *6* (cit. on pp. 17, 33, 70).

(44) Pinato, G.; Cojoc, D.; Lien, L.; Ansuini, A.; Ban, J.; D'Este, E.; Torre, V. Less than 5 Netrin-1 molecules initiate attraction but 200 Sema3A molecules are necessary for repulsion. *Scientific Reports* **2012**, *2* (cit. on pp. 17, 33, 70, 175).

(45) Sun, B.; Chiu, D. T. Synthesis, Loading, and Application of Individual Nanocapsules for Probing Single-Cell Signaling. *Langmuir* **2004**, *20*, 4614–4620 (cit. on pp. 17, 62).

(46) Fukushima., D. Denaturation of soybean proteins by organic solvents. *Cereal Chemistry* **1969**, *46*, 156 (cit. on p. 17).

(47) Arakawa, T.; Prestrelski, S. J.; Kenney, W. C.; Carpenter, J. F. Protein Therapeutics Using Recombinant Technology Factors affecting short-term and long-term stabilities of proteins. *Advanced Drug Delivery Reviews* **1993**, *10*, 1–28 (cit. on p. 17).

(48) Seddon, A. M.; Curnow, P.; Booth, P. J. Membrane proteins, lipids and detergents: not just a soap opera. *Biochimica et Biophysica Acta (BBA) - Biomembranes* **2004**, *1666*, 105–117 (cit. on p. 17).

(49) Cao, E.; Chen, Y.; Cui, Z.; Foster, P. R. Effect of freezing and thawing rates on denaturation of proteins in aqueous solutions. *Biotechnology and Bioengineering* **2003**, *82*, 684–690 (cit. on p. 17).

(50) Allen, T. M.; Cullis, P. R. Liposomal drug delivery systems: From concept to clinical applications. *Advanced Drug Delivery Reviews* **2013**, *65*, 36–48 (cit. on pp. 17, 19).

(51) Ganta, S.; Devalapally, H.; Shahiwala, A.; Amiji, M. A review of stimuli-responsive nanocarriers for drug and gene delivery. *Journal of Controlled Release* **2008**, *126*, 187–204 (cit. on p. 17).

(52) Viger, M. L.; Sheng, W.; Doré, K.; Alhasan, A. H.; Carling, C.-J.; Lux, J.; de Gracia Lux, C.; Grossman, M.; Malinow, R.; Almutairi, A. Near-Infrared-Induced Heating of Confined Water in Polymeric Particles for Efficient Payload Release. *ACS Nano* **2014**, *8*, 4815–4826 (cit. on pp. 18, 68).

(53) De Gracia Lux, C.; Almutairi, A. Intramolecular Cyclization for Stimuli-Controlled Depolymerization of Polycaprolactone Particles Leading to Disassembly and Payload Release. *ACS Macro Letters* **2013**, *2*, 432–435 (cit. on p. 18).

(54) De Gracia Lux, C.; Olejniczak, J.; Fomina, N.; Viger, M. L.; Almutairi, A. Intramolecular cyclization assistance for fast degradation of ornithine-based poly(ester amide)s. *Journal of Polymer Science Part A: Polymer Chemistry* **2013** (cit. on p. 18).

(55) Fomina, N.; McFearin, C.; Sermsakdi, M.; Edigin, O.; Almutairi, A. UV and near-IR triggered release from polymeric nanoparticles. *Journal of the American Chemical Society* **2010**, *132*, 9540–9542 (cit. on p. 18).

(56) Huu, V. A. N.; Luo, J.; Zhu, J.; Zhu, J.; Patel, S.; Boone, A.; Mahmoud, E.; McFearin, C.; Olejniczak, J.; de Lux, C. G.; Lux, J.; Fomina, N.; Huynh, M.; Zhang, K.; Almutairi, A. Light-responsive nanoparticle depot to control release of a small molecule angiogenesis inhibitor in the posterior segment of the eye. *Journal of Controlled Release* **2015**, *200*, 71–77 (cit. on p. 18).

(57) Olejniczak, J.; Sankaranarayanan, J.; Viger, M. L.; Almutairi, A. Highest Efficiency Two-Photon Degradable Copolymer for Remote Controlled Release. *ACS Macro Letters* **2013**, *2*, 683–687 (cit. on p. 18).

(58) Viger, M. L.; Grossman, M.; Fomina, N.; Almutairi, A. Low Power Upconverted Near-IR Light for Efficient Polymeric Nanoparticle Degradation and Cargo Release. *Advanced Materials* **2013** (cit. on p. 18).

(59) Shi, D.; Matsusaki, M.; Akashi, M. Photo-tunable protein release from biodegradable nanoparticles composed of cinnamic acid derivatives. *Journal of Controlled Release* **2011**, *149*, 182–189 (cit. on p. 18).

(60) Kress, H.; Park, J.-G.; Mejean, C. O.; Forster, J. D.; Park, J.; Walse, S. S.; Zhang, Y.; Wu, D.; Weiner, O. D.; Fahmy, T. M., et al. Cell stimulation with optically manipulated microsources. *Nature methods* **2009**, *6*, 905–909 (cit. on p. 18).

(61) Bangham, A.; Standish, M.; Watkins, J. Diffusion of univalent ions across the lamellae of swollen phospholipids. *Journal of Molecular Biology* **1965**, *13*, 238–IN27 (cit. on p. 19).

(62) Pandey, V.; Chandran, M. S. Liposome drug delivery. *World Journal of Pharmacy and Pharmaceutical Sciences* **2014** (cit. on p. 19).

(63) Walde, P.; Cosentino, K.; Engel, H.; Stano, P. Giant Vesicles: Preparations and Applications. *ChemBioChem* **2010**, *11*, 848–865 (cit. on pp. 19, 37).

(64) Bittman, R.; Blau, L. Phospholipid-cholesterol interaction. Kinetics of water permeability in liposomes. *Biochemistry* **1972**, *11*, 4831–4839 (cit. on p. 19).

(65) Vemuri, S.; Rhodes, C. Preparation and characterization of liposomes as therapeutic delivery systems: a review. *Pharmaceutica Acta Helvetiae* **1995**, *70*, 95–111 (cit. on pp. 19, 37).

(66) Karatekin, E.; Sandre, O.; Brochard-Wyart, F. Transient pores in vesicles. *Polymer International* **2003**, *52*, 486–493 (cit. on p. 20).

(67) Binder, W. H. Polymer-Induced Transient Pores in Lipid Membranes. *Angewandte Chemie International Edition* **2008**, *47*, 3092–3095 (cit. on p. 20).

(68) Tribet, C.; Vial, F. Flexible macromolecules attached to lipid bilayers: impact on fluidity, curvature, permeability and stability of the membranes. *Soft Matter* **2008**, *4*, 68–81 (cit. on pp. 20, 88).

(69) Fuertes, G.; Giménez, D.; Esteban-Martín, S.; Sánchez-Muñoz, O.; Salgado, J. A lipocentric view of peptide-induced pores., English *European Biophysics Journal* **2011**, *40*, 399–415 (cit. on p. 20).

(70) Pidgeon, C.; Hunt, C. A. Light sensitive liposomes. *Photochemistry and Photobiology* **1983**, *37*, 491–494 (cit. on pp. 21, 22).

(71) Song, X.; Perlstein, J.; Whitten, D. G. Supramolecular Aggregates of Azobenzene Phospholipids and Related Compounds in Bilayer Assemblies and Other Microheterogeneous Media: Structure, Properties, and Photoreactivity1. *Journal of the American Chemical Society* **1997**, *119*, 9144–9159 (cit. on pp. 22, 23).

(72) Bisby, R. H.; Mead, C.; Mitchell, A. C.; Morgan, C. G. Fast Laser-Induced Solute Release from Liposomes Sensitized with Photochromic Lipid: Effects of Temperature, Lipid Host, and Sensitizer Concentration. *Biochemical and Biophysical Research Communications* **1999**, *262*, 406–410 (cit. on pp. 22, 73, 90).

(73) Bisby, R. H.; Mead, C.; Morgan, C. G. Photosensitive liposomes as 'cages' for laser-triggered solute delivery: the effect of bilayer cholesterol on kinetics of solute release. *FEBS Letters* **1999**, *463*, 165–168 (cit. on pp. 22, 23, 100).

(74) Morgan, C. G.; Bisby, R. H.; Johnson, S. A.; Mitchell, A. C. Fast solute release from photosensitive liposomes: an alternative to 'caged' reagents for use in biological systems. *FEBS Letters* **1995**, *375*, 113–116 (cit. on p. 22).

(75) Bisby, R.; Mead, C.; Morgan, C. Wavelength-programmed solute release from photosensitive liposomes. *Biochemical and biophysical research communications* **2000**, *276*, 169–173 (cit. on pp. 22, 23, 73, 100).

(76) Kuiper, J. M.; Engberts, J. B. H-aggregation of azobenzene-substituted amphiphiles in vesicular membranes. *Langmuir* **2004**, *20*, 1152–1160 (cit. on pp. 23, 90).

(77) Bisby, R. H.; Mead, C.; Morgan, C. G. Active Uptake of Drugs into Photosensitive Liposomes and Rapid Release on UV Photolysis. *Photochemistry and Photobiology* **2000**, *72*, 57–61 (cit. on pp. 24, 30, 100).

(78) Kano, K.; Tanaka, Y.; Ogawa, T.; Shimomura, M.; Okahata, Y.; Kunitake, T. Photoresponsive membranes. Regulation of membrane properties by photoreversible cis–trans isomerization of azobenzenes. *Chemistry Letters* **1980**, *9*, 421–424 (cit. on p. 24).

(79) Kano, K.; Tanaka, Y.; Ogawa, T.; Shimomura, M.; Kunitake, T. Photoresponsive artificial membrane. Regulation of membrane permeability of liposomal membrane by photoreversible cis-trans isomerization of azobenzenes. *Photochemistry and Photobiology* **1981**, *34*, 323–329 (cit. on pp. 24, 73).

(80) Cui, Z.-K.; Phoeung, T.; Rousseau, P.-A.; Rydzek, G.; Zhang, Q.; Bazuin, C. G.; Lafleur, M. Nonphospholipid Fluid Liposomes with Switchable Photocontrolled Release. *Langmuir* **2014**, *30*, 10818–10825 (cit. on pp. 24, 25, 73).

(81) Liu, X.; Yang, B.; Wang, Y.; Wang, J. Photoisomerisable cholesterol derivatives as photo-trigger of liposomes: Effect of lipid polarity, temperature, incorporation ratio, and cholesterol. *Biochimica et Biophysica Acta (BBA)-Biomembranes* **2005**, *1720*, 28–34 (cit. on pp. 24, 25).

(82) Lei, Y.; Hurst, J. Photoregulated potassium ion permeation through dihexadecyl phosphate bilayers containing azobenzene and stilbene surfactants. *Langmuir* **1999**, *15*, 3424–3429 (cit. on p. 25).

(83) Kauscher, U.; Samanta, A.; Ravoo, B. J. Photoresponsive vesicle permeability based on intramolecular host-guest inclusion. *Organic & Biomolecular Chemistry* **2014**, *12*, 600–606 (cit. on p. 26).

(84) Liu, J.; Yan, L.; Wang, J.; Li, T.; Zhao, H.; Li, L.; Lincoln, S. F.; Prud'homme, R. K.; Guo, X. Reversible photo-responsive vesicle based on the complexation between an azobenzene containing molecule and α-cyclodextrin., en *RSC Adv.* **2015**, *5*, 32846–32852 (cit. on p. 26).

(85) Khairutdinov, R.; Hurst, J. Photocontrol of ion permeation through bilayer membranes using an amphiphilic spiropyran. *Langmuir* **2001**, *17*, 6881–6886 (cit. on pp. 27, 30).

(86) Ohya, Y.; Okuyama, Y.; Fukunaga, A.; Ouchi, T. Photo-sensitive lipid membrane perturbation by a single chain lipid having terminal spiropyran group. *Supramolecular Science* **1998**, *5*, 21–29 (cit. on p. 27).

(87) Spratt, T.; Bondurant, B.; O'Brien, D. F. Rapid release of liposomal contents upon photoinitiated destabilization with UV exposure. *Biochimica et Biophysica Acta (BBA) - Biomembranes* **2003**, *1611*, 35–43 (cit. on pp. 27–29).

(88) Yavlovich, A.; Singh, A.; Tarasov, S.; Capala, J.; Blumenthal, R.; Puri, A. Design of liposomes containing photopolymerizable phospholipids for triggered release of contents., English *Journal of Thermal Analysis and Calorimetry* **2009**, *98*, 97–104 (cit. on pp. 28, 90).

(89) Bader, H.; Dorn, K.; Hupfer, B.; Ringsdorf, H. English In *Polymer Membranes*, Gordon, M., Ed.; Advances in Polymer Science, Vol. 64; Springer Berlin Heidelberg: 1985, pp 1–62 (cit. on p. 27).

(90) Emmelius, M.; Hörpel, G.; Ringsdorf, H.; Schmidt, B. English In *Polymers in Medicine II*, Chiellini, E., Giusti, P., Migliaresi, C., Nicolais, L., Eds.; Polymer Science and Technology, Vol. 34; Springer US: 1986, pp 313–331 (cit. on p. 27).

(91) Yavlovich, A.; Singh, A.; Blumenthal, R.; Puri, A. A novel class of photo-triggerable liposomes containing DPPC:$DC_{8,9}$PC as vehicles for delivery of doxorubcin to cells. *Biochimica et Biophysica Acta (BBA) - Biomembranes* **2011**, *1808*, 117–126 (cit. on pp. 28, 90).

(92) Paasonen, L.; Laaksonen, T.; Johans, C.; Yliperttula, M.; Kontturi, K.; Urtti, A. Gold nanoparticles enable selective light-induced contents release from liposomes. *Journal of Controlled Release* **2007**, *122*, 86–93 (cit. on pp. 29, 90).

(93) Khoobehi, B.; Char, C. A.; Peyman, G. A.; Schuele, K. M. Study of the mechanisms of laser-induced release of liposome-encapsulated dye. *Lasers in Surgery and Medicine* **1990**, *10*, 303–309 (cit. on p. 29).

(94) Zhang, X.; Luckham, P. F.; Hughes, A. D.; Thom, S.; Xu, X. Y. Development of lysolipid-based thermosensitive liposomes for delivery of high molecular weight proteins. *International Journal of Pharmaceutics* **2011**, *421*, 291–292 (cit. on p. 30).

(95) Forbes, N.; Pallaoro, A.; Reich, N. O.; Zasadzinski, J. A. Rapid, Reversible Release from Thermosensitive Liposomes Triggered by Near-Infra-Red Light. *Particle & Particle Systems Characterization* **2014**, *31*, 1158–1167 (cit. on pp. 30, 31).

(96) Forbes, N.; Shin, J. E.; Ogunyankin, M.; Zasadzinski, J. A. Inside-outside self-assembly of light-activated fast-release liposomes. *Physical Chemistry Chemical Physic* **2015**, *17*, 15569–15578 (cit. on p. 31).

(97) Sebai, S.; Cribier, S.; Karimi, A.; Massotte, D.; Tribet, C. Permeabilization of Lipid Membranes and Cells by a Light-Responsive Copolymer. *Langmuir* **2010**, *26*, 14135–14141 (cit. on pp. 31, 70, 73, 87–89).

(98) Kusumi, A.; Nakahama, S.; Yamaguchi, K. Liposomes That Can Be Disintegrated by Photo-Irradiation. *Chemistry Letters* **1989**, *18*, 433–436 (cit. on pp. 32, 70).

(99) Wan, Y.; Angleson, J. K.; Kutateladze, A. G. Liposomes from Novel Photolabile Phospholipids: Light-Induced Unloading of Small Molecules As Monitored by PFG NMR. *Journal of the American Chemical Society* **2002**, *124*, 5610–5611 (cit. on p. 32).

(100) Li, Z.; Wan, Y.; Kutateladze, A. G. Dithiane-Based Photolabile Amphiphiles: Toward Photolabile Liposomes. *Langmuir* **2003**, *19*, 6381–6391 (cit. on p. 32).

(101) Meulen, D. L. V.; Misra, P.; Michael, J.; Spears, K. G.; Khoka, M. Laser mediated release of dye from liposomes. *Photochemistry and Photobiology* **1992**, *56*, 325–332 (cit. on pp. 33, 34).

(102) Dendramis, K. A.; Allen, P. B.; Reid, P. J.; Chiu, D. T. Spectrally tunable uncaging of biological stimuli from nanocapsules. *Chemical Communications* **2008**, 4795–4797 (cit. on pp. 34, 70).

(103) Dendramis, K. A.; Chiu, D. T. Laser Photolysis of Dye-Sensitized Nanocapsules Occurs via a Photothermal Pathway. *Journal of the American Chemical Society* **2009**, *131*, 16771–16778 (cit. on pp. 34, 70).

(104) Gregersen, K. A. D.; Hill, Z. B.; Gadd, J. C.; Fujimoto, B. S.; Maly, D. J.; Chiu, D. T. Intracellular Delivery of Bioactive Molecules using Light-Addressable Nanocapsules. *ACS Nano* **2010**, *4*, 7603–7611 (cit. on pp. 34, 70).

(105) Huang, C.-H. Phosphatidylcholine vesicles. Formation and physical characteristics. *Biochemistry* **1969**, *8*, 344–352 (cit. on p. 35).

(106) Mayer, L.; Hope, M.; Cullis, P. Vesicles of variable sizes produced by a rapid extrusion procedure. *Biochimica et Biophysica Acta (BBA) - Biomembranes* **1986**, *858*, 161–168 (cit. on pp. 35, 209).

(107) Patil, Y. P.; Jadhav, S. Novel methods for liposome preparation. *Chemistry and Physics of Lipids* **2014**, *177*, 8–18 (cit. on pp. 35, 37).

(108) Xu, X.; Costa, A.; Burgess, D. Protein Encapsulation in Unilamellar Liposomes: High Encapsulation Efficiency and A Novel Technique to Assess Lipid-Protein Interaction. *Pharmaceutical research* **2012**, *29*, 1919–1931 (cit. on p. 35).

(109) Hwang, S. Y.; Kim, H. K.; Choo, J.; Seong, G. H.; Hien, T. B. D.; Lee, E. Effects of operating parameters on the efficiency of liposomal encapsulation of enzymes. *Colloids and Surfaces B: Biointerfaces* **2012**, *94*, 296–303 (cit. on p. 35).

(110) Ollivon, M.; Lesieur, S.; Grabielle-Madelmont, C.; Paternostre, M. Vesicle reconstitution from lipid–detergent mixed micelles. *Biochimica et Biophysica Acta (BBA)-Biomembranes* **2000**, *1508*, 34–50 (cit. on p. 36).

(111) Zhang, L.; Hu, J.; Lu, Z. Preparation of Liposomes with a Controlled Assembly Procedure. *Journal of Colloid and Interface Science* **1997**, *190*, 76–80 (cit. on pp. 36, 37).

(112) Pautot, S.; Frisken, B. J.; Weitz, D. Production of unilamellar vesicles using an inverted emulsion. *Langmuir* **2003**, *19*, 2870–2879 (cit. on p. 37).

(113) Van Swaay, D.; deMello, A. Microfluidic methods for forming liposomes. *Lab Chip* **2013**, *13*, 752–767 (cit. on p. 37).

(114) Batzri, S.; Korn, E. D. Single bilayer liposomes prepared without sonication. *Biochimica et Biophysica Acta (BBA) - Biomembranes* **1973**, *298*, 1015–1019 (cit. on p. 37).

(115) Szoka, F.; Papahadjopoulos, D. Procedure for preparation of liposomes with large internal aqueous space and high capture by reverse-phase evaporation. *Proceedings of the National Academy of Sciences* **1978**, *75*, 4194–4198 (cit. on p. 37).

(116) Meure, L.; Foster, N.; Dehghani, F. Conventional and Dense Gas Techniques for the Production of Liposomes: A Review., English *AAPS PharmSciTech* **2008**, *9*, 798–809 (cit. on p. 37).

(117) Szoka, F.; Papahadjopoulos, D. Comparative Properties and Methods of Preparation of Lipid Vesicles (Liposomes). *Annual Review of Biophysics and Bioengineering* **1980**, *9*, 467–508 (cit. on p. 37).

(118) Arevalo, R. C.; Urbach, J. S.; Blair, D. L. Size-Dependent Rheology of Type-I Collagen Networks. *Biophysical Journal* **2010**, *99*, L65–L67 (cit. on p. 38).

(119) Bandyopadhyay, U.; Das, D.; Banerjee, R. K. Reactive oxygen species: oxidative damage and pathogenesis. *Current science* **1999**, *77*, 658–666 (cit. on p. 40).

(120) Sharma, P.; Jha, A. B.; Dubey, R. S.; Pessarakli, M. Reactive oxygen species, oxidative damage, and antioxidative defense mechanism in plants under stressful conditions. *Journal of Botany* **2012**, *2012* (cit. on p. 40).

(121) Murayama, S.; Kato, M. Photocontrol of Biological Activities of Protein by Means of a Hydrogel. *Analytical chemistry* **2010**, *82*, 2186–2191 (cit. on p. 40).

(122) Murayama, S.; Su, B.; Okabe, K.; Kishimura, A.; Osada, K.; Miura, M.; Funatsu, T.; Kataoka, K.; Kato, M. NanoPARCEL: a method for controlling cellular behavior with external light. *Chemical Communications* **2012**, *48*, 8380–8382 (cit. on p. 40).

(123) Murayama, S.; Ishizuka, F.; Takagi, K.; Inoda, H.; Sano, A.; Santa, T.; Kato, M. Small Mesh Size Hydrogel for Functional Photocontrol of Encapsulated Enzymes and Small Probe Molecules. *Analytical chemistry* **2012**, *84*, 1374–1379 (cit. on pp. 40, 41, 43).

(124) Kato, M. Cell analysis using Photodegradable Nanoparticles. *Journal of Photopolymer Science and Technology* **2013**, *26*, 165–169 (cit. on pp. 40, 70).

(125) Azagarsamy, M.; Alge, D.; Radhakrishnan, S.; Tibbitt, M.; Anseth, K. Photocontrolled Nanoparticles for On-Demand Release of Proteins. *Biomacromolecules* **2012**, *13*, 2216–2224 (cit. on p. 41).

(126) Park, S.; Oh, K. T.; Kwag, D. S.; Lee, U. Y.; Lee, D. J.; Lee, E. S. Photoresponsive hyaluronate nanogel as an anticancer drug carrier. *Polymers for Advanced Technologies* **2013**, *24*, 791–796 (cit. on p. 41).

(127) Klinger, D.; Landfester, K. Dual Stimuli-Responsive Poly(2-hydroxyethyl methacrylate-co-methacrylic acid) Microgels Based on Photo-Cleavable Cross-Linkers: pH-Dependent Swelling and Light-Induced Degradation. *Macromolecules* **2011**, *44*, 9758–9772 (cit. on p. 42).

(128) Klinger, D.; Landfester, K. Enzymatic-and light-degradable hybrid nanogels: Crosslinking of polyacrylamide with acrylate-functionalized Dextrans containing photocleavable linkers. *Journal of Polymer Science Part A: Polymer Chemistry* **2012**, *50*, 1062–1075 (cit. on p. 42).

(129) Kloxin, A. M.; Kasko, A. M.; Salinas, C. N.; Anseth, K. S. Photodegradable Hydrogels for Dynamic Tuning of Physical and Chemical Properties. *Science* **2009**, *324*, 59–63 (cit. on p. 42).

(130) DeForest, C. A.; Anseth, K. S. Cytocompatible click-based hydrogels with dynamically tunable properties through orthogonal photoconjugation and photocleavage reactions. *Nature chemistry* **2011**, *3*, 925–931 (cit. on p. 42).

(131) Holmes, C. P. Model studies for new o-nitrobenzyl photolabile linkers: Substituent effects on the rates of photochemical cleavage. *The Journal of organic chemistry* **1997**, *62*, 2370–2380 (cit. on p. 43).

(132) Brieke, C.; Rohrbach, F.; Gottschalk, A.; Mayer, G.; Heckel, A. Light-controlled tools. *Angewandte Chemie International Edition* **2012**, *51*, 8446–76 (cit. on p. 43).

(133) Lee, H.-M.; Larson, D. R.; Lawrence, D. S. Illuminating the chemistry of life: design, synthesis, and applications of "caged" and related photoresponsive compounds. *ACS chemical biology* **2009**, *4*, 409–427 (cit. on p. 43).

(134) Yu, H.; Li, J.; Wu, D.; Qiu, Z.; Zhang, Y. Chemistry and biological applications of photo-labile organic molecules. *Chemical Society Reviews* **2010**, *39*, 464–473 (cit. on p. 43).

(135) Olejniczak, J.; Carling, C.-J.; Almutairi, A. Photocontrolled release using one-photon absorption of visible or NIR light. *Journal of Controlled Release* **2015** (cit. on p. 43).

(136) Bochet, C. G. Photolabile protecting groups and linkers. *Journal of the Chemical Society, Perkin Transactions 1* **2002**, 125–142 (cit. on p. 43).

(137) Nakayama, K.; Tachikawa, T.; Majima, T. Spatial Control of Protein Binding on Lipid Bimembrane Using Photoeliminative Linker. *Langmuir* **2008**, *24*, 6425–6428 (cit. on p. 43).

(138) Klán, P.; Šolomek, T.; Bochet, C. G.; Blanc, A. l.; Givens, R.; Rubina, M.; Popik, V.; Kostikov, A.; Wirz, J. Photoremovable protecting groups in chemistry and biology: reaction mechanisms and efficacy. *Chemical reviews* **2012**, *113*, 119–191 (cit. on p. 43).

(139) Labruère, R.; Alouane, A.; Le Saux, T.; Aujard, I.; Pelupessy, P.; Gautier, A.; Dubruille, S.; Schmidt, F.; Jullien, L. "Self-Immolative" Spacer for Uncaging with Fluorescence Reporting. *Angewandte Chemie* **2012**, *124*, 9478–9481 (cit. on p. 43).

(140) Zhang, H.-J.; Xin, Y.; Yan, Q.; Zhou, L.-L.; Peng, L.; Yuan, J.-Y. Facile and Efficient Fabrication of Photoresponsive Microgels via Thiol–Michael Addition. *Macromolecular Rapid Communications* **2012**, *33*, 1952–1957 (cit. on p. 44).

(141) Patnaik, S.; Sharma, A. K.; Garg, B.; Gandhi, R.; Gupta, K. Photoregulation of drug release in azo-dextran nanogels. *International Journal of Pharmaceutics* **2007**, *342*, 184–193 (cit. on p. 44).

(142) He, J.; Tong, X.; Zhao, Y. Photoresponsive Nanogels Based on Photocontrollable Cross-Links. *Macromolecules* **2009**, *42*, 4845–4852 (cit. on pp. 44, 45).

(143) Costa, D.; Valente, A. J. M.; Miguel, M. G.; Queiroz, J. Gel Network Photodisruption: A New Strategy for the Codelivery of Plasmid DNA and Drugs. *Langmuir* **2011**, *27*, 13780–13789 (cit. on pp. 45, 70).

(144) Costa, D.; Valente, A. J.; Miguel, M. G.; Lindman, B. Light triggered release of solutes from covalent DNA gels. *Colloids and Surfaces A: Physicochemical and Engineering Aspects* **2011**, *391*, 80–87 (cit. on p. 45).

(145) Costa, D.; Valente, A. J.; Queiroz, J. Plasmid DNA nanogels as photoresponsive materials for multifunctional bio-applications. *Journal of Biotechnology* **2015**, *202*, 98–104 (cit. on p. 46).

(146) Sershen, S.; Westcott, S.; Halas, N.; West, J. Temperature-sensitive polymer–nanoshell composites for photothermally modulated drug delivery. *Journal of Biomedical Materials Research* **2000**, *51*, 293–298 (cit. on pp. 46, 47).

(147) Gorelikov, I.; Field, L. M.; Kumacheva, E. Hybrid Microgels Photoresponsive in the Near-Infrared Spectral Range. *Journal of the American Chemical Society* **2004**, *126*, 15938–15939 (cit. on p. 46).

(148) Das, M.; Sanson, N.; Fava, D.; Kumacheva, E. Microgels loaded with gold nanorods: photothermally triggered volume transitions under physiological conditions. *Langmuir* **2007**, *23*, 196–201 (cit. on pp. 46, 47).

(149) Qin, Y.; Chen, J.; Bi, Y.; Xu, X.; Zhou, H.; Gao, J.; Hu, Y.; Zhao, Y.; Chai, Z. Near-infrared light remote-controlled intracellular anti-cancer drug delivery using thermo/pH sensitive nanovehicle. *Acta Biomaterialia* **2015**, *17*, 201–209 (cit. on p. 47).

(150) Shi, S.; Wang, Q.; Wang, T.; Ren, S.; Gao, Y.; Wang, N. Thermo-, pH-, and Light-Responsive Poly(*N*-isopropylacrylamide-*co*-methacrylic acid)–Au Hybrid Microgels Prepared by the in Situ Reduction Method Based on Au-Thiol Chemistry. *The Journal of Physical Chemistry B* **2014**, *118*, 7177–7186 (cit. on p. 47).

(151) Oishi, M.; Nakamura, T.; Jinji, Y.; Matsuishi, K.; Nagasaki, Y. Multi-stimuli-triggered release of charged dye from smart PEGylated nanogels containing gold nanoparticles to regulate fluorescence signals. *Journal of Materials Chemistry* **2009**, *19*, 5909–5912 (cit. on p. 48).

(152) Oishi, M.; Nagasaki, Y. Synthesis, characterization, and biomedical applications of core–shell-type stimuli-responsive nanogels – Nanogel composed of poly[2-(N,N-diethylamino)ethyl methacrylate] core and PEG tethered chains. *Reactive and Functional Polymers* **2007**, *67*, 1311–1329 (cit. on p. 48).

(153) Jochum, F. D.; Theato, P. Temperature- and light-responsive smart polymer materials. *Chemical Society Reviews* **2013**, *42*, 7468–7483 (cit. on p. 48).

(154) Koetting, M. C.; Peters, J. T.; Steichen, S. D.; Peppas, N. A. Stimulus-responsive hydrogels: Theory, modern advances, and applications. *Materials Science and Engineering: R: Reports* **2015**, *93*, 1–49 (cit. on p. 48).

(155) Oh, J. K.; Drumright, R.; Siegwart, D. J.; Matyjaszewski, K. The development of microgels/nanogels for drug delivery applications. *Progress in Polymer Science* **2008**, *33*, 448–477 (cit. on p. 49).

(156) Roger, T.; Fu, S.; Stocker, R.; Davies, M. J. Biochemistry and pathology of radical-mediated protein oxidation. *Biochemical Journal* **1997**, *324*, 1–18 (cit. on p. 49).

(157) Erickson, H. P. Size and shape of protein molecules at the nanometer level determined by sedimentation, gel filtration, and electron microscopy. *Biological Procedures Online* **2009**, *11*, 32–51 (cit. on pp. 50, 202).

(158) Kim, J.; Lim, H.; Hwang, Y.; Woo, H.; Kim, J.; Char, K. Template-free Uniform-sized Hollow Hydrogel Capsules with Controlled Shell Permeation and Optical Responsiveness. *Langmuir* **2012**, *28*, 11899–11905 (cit. on pp. 50, 66).

(159) De Temmerman, M.; Demeester, J.; De Smedt, S.; Rejman, J. Tailoring layer-by-layer capsules for biomedical applications. *Nanomedicine* **2012**, *7*, 771–788 (cit. on pp. 51, 52, 56).

(160) Tao, X.; Li, J.; Möhwald, H. Self-Assembly, Optical Behavior, and Permeability of a Novel Capsule Based on an Azo Dye and Polyelectrolytes. *Chemistry – A European Journal* **2004**, *10*, 3397–3403 (cit. on p. 52).

(161) Bédard, M.; Skirtach, A. G.; Sukhorukov, G. B. Optically Driven Encapsulation Using Novel Polymeric Hollow Shells Containing an Azobenzene Polymer. *Macromolecular Rapid Communications* **2007**, *28*, 1517–1521 (cit. on pp. 53, 70).

(162) Jung, B.-D.; Hong, J.-D.; Voigt, A.; Leporatti, S.; Dähne, L.; Donath, E.; Möhwald, H. Photochromic hollow shells: photoisomerization of azobenzene polyionene in solution, in multilayer assemblies on planar and spherical surfaces. *Colloids and Surfaces A: Physicochemical and Engineering Aspects* **2002**, *198–200*, 483–489 (cit. on p. 53).

(163) Yi, Q.; Sukhorukov, G. B. UV-induced disruption of microcapsules with azobenzene groups. *Soft matter* **2014**, *10*, 1384–1391 (cit. on pp. 53, 55, 70).

(164) Skirtach, A. G.; Antipov, A. A.; Shchukin, D. G.; Sukhorukov, G. B. Remote Activation of Capsules Containing Ag Nanoparticles and IR Dye by Laser Light. *Langmuir* **2004**, *20*, 6988–6992 (cit. on p. 54).

(165) Radziuk, D.; Shchukin, D. G.; Skirtach, A.; Möhwald, H.; Gleb, S. Synthesis of Silver Nanoparticles for Remote Opening of Polyelectrolyte Microcapsules. *Langmuir* **2007**, *23*, 4612–4617 (cit. on p. 54).

(166) Skirtach, A. G.; Muñoz Javier, A.; Kreft, O.; Köhler, K.; Piera Alberola, A.; Möhwald, H.; Parak, W. J.; Sukhorukov, G. B. Laser-Induced Release of Encapsulated Materials inside Living Cells. *Angewandte Chemie International Edition* **2006**, *45*, 4612–4617 (cit. on pp. 54, 70).

(167) Bédard, M. F.; Braun, D.; Sukhorukov, G. B.; Skirtach, A. G. Toward Self-Assembly of Nanoparticles on Polymeric Microshells: Near-IR Release and Permeability. *ACS Nano* **2008**, *2*, 1807–1816 (cit. on p. 54).

(168) Javier, A. M.; del Pino, P.; Bedard, M. F.; Ho, D.; Skirtach, A. G.; Sukhorukov, G. B.; Plank, C.; Parak, W. J. Photoactivated Release of Cargo from the Cavity of Polyelectrolyte Capsules to the Cytosol of Cells. *Langmuir* **2008**, *24*, 12517–12520 (cit. on p. 54).

(169) Pavlov, A. M.; Sapelkin, A. V.; Huang, X.; P'ng, K. M. Y.; Bushby, A. J.; Sukhorukov, G. B.; Skirtach, A. G. Neuron Cells Uptake of Polymeric Microcapsules and Subsequent Intracellular Release. *Macromolecular Bioscience* **2011**, *11*, 848–854 (cit. on p. 54).

(170) Radt, B.; Smith, T. A.; Caruso, F. Optically Addressable Nanostructured Capsules. *Advanced Materials* **2004**, *16*, 2184–2189 (cit. on pp. 54, 55, 70).

(171) De Koker, S.; Hoogenboom, R.; De Geest, B. G. Polymeric multilayer capsules for drug delivery. *Chemical Society Review* **2012**, *41*, 2867–2884 (cit. on p. 56).

(172) Delcea, M.; Möhwald, H.; Skirtach, A. G. Stimuli-responsive LbL capsules and nanoshells for drug delivery. *Advanced Drug Delivery Reviews* **2011**, *63*, 730–747 (cit. on p. 56).

(173) Sukhorukov, G. B.; Shchukin, D. G.; Dong, W.-F.; Möhwald, H.; Lulevich, V. V.; Vinogradova, O. I. Comparative Analysis of Hollow and Filled Polyelectrolyte Microcapsules Templated on Melamine Formaldehyde and Carbonate Cores. *Macromolecular Chemistry and Physics* **2004**, *205*, 530–535 (cit. on p. 56).

(174) Discher, D. E.; Ahmed, F. Polymersomes. *Annual Review of Biomedical Engineering* **2006**, *8*, 323–341 (cit. on pp. 57, 61).

(175) Tong, X.; Wang, G.; Soldera, A.; Zhao, Y. How Can Azobenzene Block Copolymer Vesicles Be Dissociated and Reformed by Light? *The Journal of Physical Chemistry B* **2005**, *109*, 20281–20287 (cit. on pp. 57, 58).

(176) Mabrouk, E.; Cuvelier, D.; Brochard-Wyart, F.; Nassoy, P.; Li, M.-H. Bursting of sensitive polymersomes induced by curling. *Proceedings of the National Academy of Sciences* **2009**, *106*, 7294–7298 (cit. on pp. 57, 61).

(177) Del Barrio, J.; Oriol, L.; Sánchez, C.; Serrano, J. L.; Cicco, A. D.; Keller, P.; Li, M.-H. Self-Assembly of Linear–Dendritic Diblock Copolymers: From Nanofibers to Polymersomes. *Journal of the American Chemical Society* **2010**, *132*, 3762–3769 (cit. on p. 58).

(178) Lin, Y.-L.; Chang, H.-Y.; Sheng, Y.-J.; Tsao, H.-K. Photoresponsive Polymersomes Formed by Amphiphilic Linear–Dendritic Block Copolymers: Generation-Dependent Aggregation Behavior. *Macromolecules* **2012**, *45*, 7143–7156 (cit. on p. 58).

(179) Hu, X.-Y.; Jia, K.; Cao, Y.; Li, Y.; Qin, S.; Zhou, F.; Lin, C.; Zhang, D.; Wang, L. Dual Photo- and pH-Responsive Supramolecular Nanocarriers Based on Water-Soluble Pillar[6]arene and Different Azobenzene Derivatives for Intracellular Anticancer Drug Delivery. *Chemistry – A European Journal* **2015**, *21*, 1208–1220 (cit. on pp. 58, 61).

(180) Lee, H.-i.; Wu, W.; Oh, J. K.; Mueller, L.; Sherwood, G.; Peteanu, L.; Kowalewski, T.; Matyjaszewski, K. Light-Induced Reversible Formation of Polymeric Micelles. *Angewandte Chemie International Edition* **2007**, *46*, 2453–2457 (cit. on p. 58).

(181) Jiang, Y.; Wang, Y.; Ma, N.; Wang, Z.; Smet, M.; Zhang, X. Reversible Self-Organization of a UV-Responsive PEG-Terminated Malachite Green Derivative: Vesicle Formation and Photoinduced Disassembly. *Langmuir* **2007**, *23*, 4029–4034 (cit. on pp. 58, 59).

(182) Cabane, E.; Malinova, V.; Meier, W. Synthesis of Photocleavable Amphiphilic Block Copolymers: Toward the Design of Photosensitive Nanocarriers. *Macromolecular Chemistry and Physics* **2010**, *211*, 1847–1856 (cit. on pp. 59, 60, 70).

(183) Cabane, E.; Malinova, V.; Menon, S.; Palivan, C.; Meier, W. Photoresponsive polymersomes as smart, triggerable nanocarriers. *Soft Matter* **2011**, *7*, 9167–9176 (cit. on pp. 59, 60, 70).

(184) Katz, J.; Zhong, S.; Ricart, B.; Pochan, D.; Hammer, D.; Burdick, J. Modular synthesis of biodegradable diblock copolymers for designing functional polymersomes. *Journal of the American Chemical Society* **2010**, *132*, 3654–3655 (cit. on p. 60).

(185) Han, D.; Tong, X.; Zhao, Y. Fast photodegradable block copolymer micelles for burst release. *Macromolecules* **2011**, *44*, 437 (cit. on p. 60).

(186) Babin, J.; Pelletier, M.; Lepage, M.; Allard, J.-F.; Morris, D.; Zhao, Y. A New Two-Photon-Sensitive Block Copolymer Nanocarrier. *Angewandte Chemie International Edition* **2009**, *48*, 3329–3332 (cit. on p. 60).

(187) Robbins, G. P.; Jimbo, M.; Swift, J.; Therien, M. J.; Hammer, D. A.; Dmochowski, I. J. Photoinitiated Destruction of Composite Porphyrin–Protein Polymersomes. *Journal of the American Chemical Society* **2009**, *131*, 3872–3874 (cit. on pp. 60, 61).

(188) Kamat, N.; Robbins, G.; Rawson, J.; Therien, M.; Dmochowski, I.; Hammer, D. A generalized system for photoresponsive membrane rupture in polymersomes. *Advanced functional materials* **2010**, *20*, 2588–2596 (cit. on p. 61).

(189) Amstad, E.; Kim, S.-H.; Weitz, D. A. Photo- and Thermoresponsive Polymersomes for Triggered Release. *Angewandte Chemie* **2012**, *124*, 12667–12671 (cit. on p. 61).

(190) Brinkhuis, R. P.; Rutjes, F. P.; van Hest, J. C. Polymeric vesicles in biomedical applications. *Polymer Chemistry* **2011**, *2*, 1449–1462 (cit. on p. 61).

(191) Pawar, P. V.; Gohil, S. V.; Jain, J. P.; Kumar, N. Functionalized polymersomes for biomedical applications. *Polymer Chemistry* **2013**, *4*, 3160–3176 (cit. on p. 61).

(192) Liao, J.; Wang, C.; Wang, Y.; Luo, F.; Qian, Z. Recent advances in formation, properties, and applications of polymersomes. *Current pharmaceutical design* **2012**, *18*, 3432–3441 (cit. on p. 61).

(193) Bédard, M. F.; Geest, B. G. D.; Skirtach, A. G.; Möhwald, H.; Sukhorukov, G. B. Polymeric microcapsules with light responsive properties for encapsulation and release. *Advances in Colloid and Interface Science* **2010**, *158*, 2–14 (cit. on p. 62).

(194) Crespy, D.; Stark, M.; Hoffmann-Richter, C.; Ziener, U.; Landfester, K. Polymeric nanoreactors for hydrophilic reagents synthesized by interfacial polycondensation on miniemulsion droplets. *Macromolecules* **2007**, *40*, 3122–3135 (cit. on pp. 62–64, 113, 133, 147, 150).

(195) Anton, N.; Saulnier, P.; Gaillard, C.; Porcher, E.; Vrignaud, S.; Benoit, J. Aqueous-core lipid nanocapsules for encapsulating fragile hydrophilic and/or lipophilic molecules. *Langmuir* **2009**, *25*, 11413–11419 (cit. on p. 63).

(196) Baier, G.; Musyanovych, A.; Dass, M.; Theisinger, S.; Landfester, K. Cross-Linked Starch Capsules Containing dsDNA Prepared in Inverse Miniemulsion as "Nanoreactors" for Polymerase Chain Reaction. *Biomacromolecules* **2010**, *11*, 960–968 (cit. on pp. 63, 133).

(197) Jagielski, N.; Sharma, S.; Hombach, V.; Mailänder, V.; Rasche, V.; Landfester, K. Nanocapsules synthesized by miniemulsion technique for application as new contrast agent materials. *Macromolecular chemistry and physics* **2007**, *208*, 2229–2241 (cit. on pp. 63, 64, 133, 150).

(198) Siebert, J.; Baier, G.; Landfester, K. Thermal and acid labile polyurethanes as a new class of responsive materials in polymeric nanoparticles and nanocapsules. *Journal of Polymer Science Part A: Polymer Chemistry* **2011**, *50*, 80–88 (cit. on pp. 63–65, 133).

(199) Paiphansiri, U.; Dausend, J.; Musyanovych, A.; Mailänder, V.; Landfester, K. Fluorescent polyurethane nanocapsules prepared via inverse miniemulsion: surface functionalization for use as biocarriers. *Macromolecular bioscience* **2009**, *9*, 575–584 (cit. on pp. 63, 65, 122, 133).

(200) Rosenbauer, E.; Wagner, M.; Musyanovych, A.; Landfester, K. Controlled release from polyurethane nanocapsules via pH-, UV-light-or temperature-induced stimuli. *Macromolecules* **2010**, *43*, 5083–5093 (cit. on pp. 63, 64, 133).

(201) Latnikova, A.; Grigoriev, D.; Möhwald, H.; Shchukin, D. Capsules Made of Cross-Linked Polymers and Liquid Core: Possible Morphologies and Their Estimation on the Basis of Hansen Solubility Parameters. *The Journal of Physical Chemistry C* **2012**, *116*, 8181–8187 (cit. on p. 63).

(202) Herrmann, C.; Crespy, D.; Landfester, K. Synthesis of hydrophilic polyurethane particles in non-aqueous inverse miniemulsions. *Colloid and Polymer Science* **2011**, *289*, 1111 (cit. on p. 63).

(203) Taheri, S.; Baier, G.; Majewski, P.; Barton, M.; Forch, R.; Landfester, K.; Vasilev, K. Synthesis and antibacterial properties of a hybrid of silver-potato starch nanocapsules by miniemulsion/polyaddition polymerization. *Journal of Materials Chemistry B* **2014**, *2*, 1838–1845 (cit. on p. 63).

(204) Yiamsawas, D.; Baier, G.; Thines, E.; Landfester, K.; Wurm, F. R. Biodegradable lignin nanocontainers. *RSC Advances* **2014**, *4*, 11661–11663 (cit. on p. 64).

(205) Piradashvili, K.; Fichter, M.; Mohr, K.; Gehring, S.; Wurm, F. R.; Landfester, K. Biodegradable Protein Nanocontainers. *Biomacromolecules* **2015**, *16*, 815–821 (cit. on pp. 64, 65, 122, 147, 151, 157).

(206) On Bioencapsulation, X. I. W., Ed., Biocompatible polymeric nanocapsules by miniemulsion technique., 2007, pp 4–11 (cit. on p. 65).

(207) Yavuz, M. S.; Cheng, Y.; Chen, J.; Cobley, C. M.; Zhang, Q.; Rycenga, M.; Xie, J.; Kim, C.; Song, K. H.; Schwartz, A. G., et al. Gold nanocages covered by smart polymers for controlled release with near-infrared light. *Nature materials* **2009**, *8*, 935–939 (cit. on pp. 66, 67).

(208) Yuan, X.; Fischer, K.; Schärtl, W. Photocleavable microcapsules built from photoreactive nanospheres. *Langmuir* **2005**, *21*, 9374–9380 (cit. on p. 66).

(209) Niikura, K.; Iyo, N.; Matsuo, Y.; Mitomo, H.; Ijiro, K. Sub-100 nm Gold Nanoparticle Vesicles as a Drug Delivery Carrier enabling Rapid Drug Release upon Light Irradiation. *ACS Applied Materials & Interfaces* **2013**, *5*, 3900–3907 (cit. on p. 67).

(210) Weissleder, R. et al. A clearer vision for in vivo imaging. *Nature biotechnology* **2001**, *19*, 316–316 (cit. on p. 68).

(211) Jariashvili, K.; Madhan, B.; Brodsky, B.; Kuchava, A.; Namicheishvili, L.; Metreveli, N. Uv damage of collagen: Insights from model collagen peptides. *Biopolymers* **2012**, *97*, 189–198 (cit. on p. 68).

(212) Sinha, R. P.; Häder, D.-P. UV-induced DNA damage and repair: a review. *Photochemical & Photobiological Sciences* **2002**, *1*, 225–236 (cit. on p. 68).

(213) Neves-Petersen, M. T.; Gajula, G. P.; Petersen, S., *UV light effects on proteins: from photochemistry to nanomedicine*; INTECH Open Access Publisher: 2012 (cit. on p. 68).

(214) König, K.; Becker, T.; Fischer, P.; Riemann, I.; Halbhuber, K.-J. Pulse-length dependence of cellular response to intense near-infrared laser pulses in multiphoton microscopes. *Optics letters* **1999**, *24*, 113–115 (cit. on p. 68).

(215) Watanabe, W.; Arakawa, N.; Matsunaga, S.; Higashi, T.; Fukui, K.; Isobe, K.; Itoh, K. Femtosecond laser disruption of subcellular organelles in a living cell. *Optics Express* **2004**, *12*, 4203–4213 (cit. on p. 68).

(216) Denton, M. L.; Foltz, M. S.; Estlack, L. E.; Stolarski, D. J.; Noojin, G. D.; Thomas, R. J.; Eikum, D.; Rockwell, B. A. Damage thresholds for exposure to NIR and blue lasers in an in vitro RPE cell system. *Investigative ophthalmology & visual science* **2006**, *47*, 3065–3073 (cit. on p. 68).

(217) Vial, F.; Rabhi, S.; Tribet, C. Association of octyl-modified poly (acrylic acid) onto unilamellar vesicles of lipids and kinetics of vesicle disruption. *Langmuir* **2005**, *21*, 853–862 (cit. on pp. 73, 90, 98).

(218) Lichtenberg, D.; Ahyayauch, H.; Goñi, F. M. The Mechanism of Detergent Solubilization of Lipid Bilayers. *Biophysical journal* **2013**, *105*, 289–299 (cit. on pp. 75, 80, 86, 213).

(219) Chevallier, E.; Mamane, A.; Stone, H.; Tribet, C.; Lequeux, F.; Monteux, C. Pumping-out photo-surfactants from an air–water interface using light. *Soft Matter* **2011**, *7*, 7866–7874 (cit. on p. 76).

(220) Lund, R.; Brun, G.; Chevallier, É.; Narayanan, T.; Tribet, C. Kinetics of Photocontrollable Micelles: light-induced self-assembly and disassembly of azobenzene-based surfactants revealed by TR-SAXS. *Langmuir*, submitted (cit. on p. 76).

(221) López, O.; Cócera, M.; Coderch, L.; Parra, J. L.; Barsukov, L.; de la Maza, A. Octyl glucoside-mediated solubilization and reconstitution of liposomes: structural and kinetic aspects. *The Journal of Physical Chemistry B* **2001**, *105*, 9879–9886 (cit. on pp. 78, 81).

(222) López, O.; Cócera, M.; Pons, R.; Azemar, N.; López-Iglesias, C.; Wehrli, E.; Parra, J. L.; de la Maza, A. Use of a Dynamic Light Scattering Technique To Study the Kinetics of Liposome Solubilization By Triton X-100. *Langmuir* **1999**, *15*, 4678–4681 (cit. on pp. 78, 81).

(223) López, O.; Cócera, M.; Pons, R.; Azemar, N.; De la Maza, A. Kinetic studies of liposome solubilization by sodium dodecyl sulfate based on a dynamic light scattering technique. *Langmuir* **1998**, *14*, 4671–4674 (cit. on pp. 78, 81).

(224) Szymczyk, K.; Jańczuk, B. The adsorption at solution–air interface and volumetric properties of mixtures of cationic and nonionic surfactants. *Colloids and Surfaces A: Physicochemical and Engineering Aspects* **2007**, *293*, 39–50 (cit. on p. 80).

(225) De la Maza, A.; Parra, J. Solubilization of unilamellar liposomes caused by quaternary ammonium surfactants. *Journal of controlled release* **1995**, *37*, 33–42 (cit. on p. 81).

(226) Sebai, S.; Milioni, D.; Walrant, A.; Alves, I.; Sagan, S.; Huin, C.; Auvray, L.; Massotte, D.; Cribier, S.; Tribet, C. Photocontrol of the Translocation of Molecules, Peptides, and Quantum Dots through Cell and Lipid Membranes Doped with Azobenzene Copolymers. *Angewandte Chemie* **2012**, *124*, 2174–2178 (cit. on p. 87).

(227) Marie, E.; Sagan, S.; Cribier, S.; Tribet, C. Amphiphilic Macromolecules on Cell Membranes: From Protective Layers to Controlled Permeabilization. *The Journal of Membrane Biology* **2014**, *247*, 861 (cit. on p. 88).

(228) Vial, F. Perméabilisation contrôlée de membranes lipidiques par des copolymères amphiphiles hydrosolubles stimulables., Ph.D. Thesis, 2007, 248 pp (cit. on pp. 90, 201).

(229) Seuring, J.; Agarwal, S. Polymers with Upper Critical Solution Temperature in Aqueous Solution. *Macromolecular Rapid Communications* **2012**, *33*, 1898–1920 (cit. on p. 107).

(230) Zhang, H.; Tong, X.; Zhao, Y. Diverse Thermoresponsive Behaviors of Uncharged UCST Block Copolymer Micelles in Physiological Medium. *Langmuir* **2014**, *30*, 11433–11441 (cit. on p. 108).

(231) Rosenbauer, E.; Landfester, K.; Musyanovych, A. Surface-Active Monomer as a Stabilizer for Polyurea Nanocapsules Synthesized via Interfacial Polyaddition in Inverse Miniemulsion. *Langmuir* **2009**, *25*, 12084–12091 (cit. on pp. 111, 133, 140, 141).

(232) Liu, L.; Shi, Y.; Liu, C.; Wang, T.; Liu, G.; Zhang, G. Insight into the amplification by methylated urea of the anion specificity of macromolecules. *Soft Matter* **2014**, *10*, 2856–2862 (cit. on pp. 117, 128).

(233) Zhang, Y.; Furyk, S.; Sagle, L. B.; Cho, Y.; Bergbreiter, D. E.; Cremer, P. S. Effects of Hofmeister anions on the LCST of PNIPAM as a function of molecular weight. *The Journal of Physical Chemistry C* **2007**, *111*, 8916–8924 (cit. on pp. 117, 145).

(234) Marras, S. A. E. In *Fluorescent Energy Transfer Nucleic Acid Probes*; Springer: 2006 (cit. on pp. 120, 152).

(235) Zeng, W.; Du, Y.; Xue, Y.; Frisch, H. English In *Physical Properties of Polymers Handbook*, Mark, J., Ed.; Springer New York: 2007, pp 289–303 (cit. on p. 125).

(236) Solans, C.; Izquierdo, P.; Nolla, J.; Azemar, N.; Garcia-Celma, M. Nano-emulsions. *Current Opinion in Colloid & Interface Science* **2005**, *10*, 102–110 (cit. on pp. 131, 132).

(237) Solans, C.; Solé, I. Nano-emulsions: Formation by low-energy methods. *Current Opinion in Colloid & Interface Science* **2012**, *17*, 246–254 (cit. on p. 132).

(238) Tadros, T.; Izquierdo, P.; Esquena, J.; Solans, C. Formation and stability of nano-emulsions. *Advances in colloid and interface science* **2004**, *108-109*, 303–318 (cit. on p. 132).

(239) Gutiérrez, J.; González, C.; Maestro, A.; Solè, I.; Pey, C.; Nolla, J. Nano-emulsions: New applications and optimization of their preparation. *Current Opinion in Colloid & Interface Science* **2008**, *13*, 245–251 (cit. on p. 132).

(240) Fu, Z.; Liu, M.; Xu, J.; Wang, Q.; Fan, Z. Stabilization of water-in-octane nano-emulsion. Part I: Stabilized by mixed surfactant systems. *Fuel* **2010**, *89*, 2838–2843 (cit. on p. 132).

(241) Kaltenbach, M.; Devenish, S. R.; Hollfelder, F. A simple method to evaluate the biochemical compatibility of oil/surfactant mixtures for experiments in microdroplets. *Lab on a Chip* **2012**, *12*, 4185–4192 (cit. on p. 132).

(242) Xiangzhong, C.; Weidong, Z.; Xiying, Z.; Tian, X.; Zhen, L.; Zhijian, Y.; Chunlei, Z.; Xiaowei, H. Synthesis of Spherical (Y, Gd)BO3:Eu3+ Phosphor Using W/O Emulsion System. *Journal of Rare Earths* **2006**, *24*, 719–723 (cit. on p. 132).

(243) Davies, R.; Graham, D. E.; Vincent, B. Water–Cyclohexane–"Span 80"–"Tween 80" Systems: Solution Properties and Water/Oil Emulsion Formation. *Journal of Colloid and Interface Science* **1987**, *116*, 88–99 (cit. on p. 133).

(244) Wu, H.; Ramachandran, C.; Weiner, N. D.; Roessler, B. J. Topical transport of hydrophilic compounds using water-in-oil nanoemulsions. *International Journal of Pharmaceutics* **2001**, *220*, 63–75 (cit. on p. 133).

(245) Porras, M.; Solans, C.; González, C.; Gutiérrez, J. Properties of water-in-oil (W/O) nano-emulsions prepared by a low-energy emulsification method. *Colloids and Surfaces A: Physicochemical and Engineering Aspects* **2008**, *324*, 181–188 (cit. on p. 133).

(246) Porras, M.; Solans, C.; González, C.; Martínez, A.; Guinart, A.; Gutiérrez, J. Studies of formation of W/O nano-emulsions. *Colloids and Surfaces A: Physicochemical and Engineering Aspects* **2004**, *249*, 115–118 (cit. on p. 133).

(247) Forgiarini, A.; Esquena, J.; Gonzalez, C.; Solans, C. Formation of nano-emulsions by low-energy emulsification methods at constant temperature. *Langmuir* **2001**, *17*, 2076–2083 (cit. on pp. 133, 142).

(248) Schoth, A.; Landfester, K.; Muñoz-Espí, R. Surfactant-Free Polyurethane Nanocapsules via Inverse Pickering Miniemulsion. *Langmuir* **2015**, *31*, 3784–3788 (cit. on p. 133).

(249) Laszlo, J. A.; Evans, K. O.; Compton, D. L.; Appell, M. Dihydrolipoyl dioleoylglycerol antioxidant capacity in phospholipid vesicles. *Chemistry and Physics of Lipids* **2012**, *165*, 160–168 (cit. on pp. 138, 227).

(250) Laszlo, J. A.; Evans, K. O.; Vermillion, K. E.; Appell, M. Feruloyl dioleoylglycerol antioxidant capacity in phospholipid vesicles. *Journal of agricultural and food chemistry* **2010**, *58*, 5842–5850 (cit. on pp. 138, 227).

(251) Evans, K. O.; Laszlo, J. A.; Compton, D. L. Carboxyl-terminated PAMAM dendrimer interaction with 1-palmitoyl-2-oleoyl phosphocholine bilayers. *Biochimica et Biophysica Acta (BBA) - Biomembranes* **2014**, *1838*, 445–455 (cit. on p. 138).

(252) Kendall, D. A.; MacDonald, R. C. A fluorescence assay to monitor vesicle fusion and lysis. *Journal of Biological Chemistry* **1982**, *257*, 13892–13895 (cit. on p. 138).

(253) Kato, N.; Sakai, Y.; Takahashi, F. Saccharide Effect on the Deswelling Process of the Thermosensitive Poly(N-isopropylacrylamide) Gel. *Bulletin of the Chemical Society of Japan* **2001**, *74*, 2025–2029 (cit. on p. 145).

(254) Spahr, P.; Edsall, J. T. Amino acid composition of human and bovine serum mercaptalbumins. *Journal of Biological Chemistry* **1964**, *239*, 850–854 (cit. on p. 150).

(255) Weijers, M.; Barneveld, P. A.; Stuart, C.; Martien, A.; Visschers, R. W. Heat-induced denaturation and aggregation of ovalbumin at neutral pH described by irreversible first-order kinetics. *Protein Science* **2003**, *12*, 2693–2703 (cit. on p. 151).

(256) Wu, N.; Veillette, A. Immunology: magnesium in a signalling role. *Nature* **2011**, *475*, 462–463 (cit. on p. 171).

(257) Balgude, A.; Yu, X.; Szymanski, A.; Bellamkonda, R. Agarose gel stiffness determines rate of DRG neurite extension in 3D cultures. *Biomaterials* **2001**, *22*, 1077–1084 (cit. on p. 171).

(258) Solon, J.; Levental, I.; Sengupta, K.; Georges, P. C.; Janmey, P. A. Fibroblast Adaptation and Stiffness Matching to Soft Elastic Substrates. *Biophysical Journal* **2007**, *93*, 4453–4461 (cit. on p. 171).

(259) Zhao, M.; Song, B.; Pu, J.; Wada, T.; Reid, B.; Tai, G.; Wang, F.; Guo, A.; Walczysko, P.; Gu, Y., et al. Electrical signals control wound healing through phosphatidylinositol-3-OH kinase-$\gamma$ and PTEN. *Nature* **2006**, *442*, 457–460 (cit. on p. 171).

(260) Blum, M.; Schweickert, A.; Vick, P.; Wright, C. V.; Danilchik, M. V. Symmetry breakage in the vertebrate embryo: When does it happen and how does it work? *Developmental Biology* **2014**, *393*, 109–123 (cit. on p. 173).

(261) Bloch-Gallego, E.; Causeret, F.; Ezan, F.; Backer, S.; Hidalgo-Sánchez, M. Development of precerebellar nuclei: instructive factors and intracellular mediators in neuronal migration, survival and axon pathfinding. *Brain Research Reviews* **2005**, *49*, 253–266 (cit. on pp. 174, 175).

(262) Höpker, V. H.; Shewan, D.; Tessier-Lavigne, M.; Poo, M.-m.; Holt, C. Growth-cone attraction to netrin-1 is converted to repulsion by laminin-1. *Nature* **1999**, *401*, 69–73 (cit. on p. 175).

(263) Sansom, S. N.; Livesey, F. J. Gradients in the brain: the control of the development of form and function in the cerebral cortex. *Cold Spring Harbor Perspectives in Biology* **2009**, *1*, a002519 (cit. on p. 175).

(264) Liu, A.; Niswander, L. A. Bone morphogenetic protein signalling and vertebrate nervous system development. *Nature Reviews Neuroscience* **2005**, *6*, 945–954 (cit. on p. 175).

(265) Janeway, C. A.; Travers, P.; Walport, M.; Shlomchik, M. J., et al., *Immunobiology: the immune system in health and disease*, 5th; Churchill Livingstone London: 2001; Vol. 2 (cit. on p. 176).

(266) Wu, D. Signaling mechanisms for regulation of chemotaxis. *Cell research* **2005**, *15*, 52–56 (cit. on p. 177).

(267) Foxman, E. F.; Campbell, J. J.; Butcher, E. C. Multistep Navigation and the Combinatorial Control of Leukocyte Chemotaxis. *The Journal of Cell Biology* **1997**, *139*, 1349–1360 (cit. on p. 177).

(268) Haessler, U.; Kalinin, Y.; Swartz, M. A.; Wu, M. An agarose-based microfluidic platform with a gradient buffer for 3D chemotaxis studies. *Biomedical microdevices* **2009**, *11*, 827–835 (cit. on p. 177).

(269) Vasaturo, A.; Caserta, S.; Russo, I.; Preziosi, V.; Ciacci, C.; Guido, S. A Novel Chemotaxis Assay in 3-D Collagen Gels by Time-Lapse Microscopy. *PLoS ONE* **2012**, *7*, e52251 (cit. on pp. 177, 185).

(270) Eccles, S. A. Targeting key steps in metastatic tumour progression. *Current Opinion in Genetics & Development* **2005**, *15*, 77–86 (cit. on p. 177).

(271) Liu, Z.; Klominek, J. Chemotaxis and Chemokinesis of Malignant Mesothelioma Cells to Multiple Growth Factors. *Anticancer Research* **2004**, *24*, 1625–1630 (cit. on p. 177).

(272) Ehtesham, M.; Winston, J. A.; Kabos, P.; Thompson, R. C. CXCR4 expression mediates glioma cell invasiveness. *Oncogene* **2006**, *25*, 2801–2806 (cit. on p. 177).

(273) Lumsden, A.; Davies, A. Earliest sensory nerve fibres are guided to peripheral targets by attractants other than nerve growth factor. *Nature* **1983**, *306*, 786–788 (cit. on p. 179).

(274) Lumsden, A.; Davies, A. M. Chemotropic effect of specific target epithelium in the developing mammalian nervous system. *Nature* **1986**, *323*, 538–539 (cit. on p. 180).

(275) Dazert, S.; Kim, D.; Luo, L.; Aletsee, C.; Garfunkel, S.; Maciag, T.; Baird, A.; Ryan, A. F. Focal delivery of fibroblast growth factor-1 by transfected cells induces spiral ganglion neurite targeting in vitro. *Journal of Cellular Physiology* **1998**, *177*, 123–129 (cit. on p. 180).

(276) Chen, H.; He, Z.; Bagri, A.; Tessier-Lavigne, M. Semaphorin–Neuropilin Interactions Underlying Sympathetic Axon Responses to Class III Semaphorins. *Neuron* **1998**, *21*, 1283–1290 (cit. on p. 180).

(277) Liu, G.; Beggs, H.; Jürgensen, C.; Park, H.-T.; Tang, H.; Gorski, J.; Jones, K. R.; Reichardt, L. F.; Wu, J.; Rao, Y. Netrin requires focal adhesion kinase and Src family kinases for axon outgrowth and attraction. *Nature neuroscience* **2004**, *7*, 1222–1232 (cit. on p. 180).

(278) Goodhill, G. J. Diffusion in Axon Guidance. *European Journal of Neuroscience* **1997**, *9*, 1414–1421 (cit. on p. 180).

(279) Gundersen, R. W.; Barrett, J. N. Characterization of the turning response of dorsal root neurites toward nerve growth factor. *The Journal of Cell Biology* **1980**, *87*, 546–554 (cit. on p. 181).

(280) Boyden, S. The chemotactic effect of mixtures of antibody and antigen on polymorphonuclear leucocytes. *The Journal of experimental medicine* **1962**, *115*, 453–466 (cit. on pp. 182, 183).

(281) Albini, A.; Noonan, D. M. The 'chemoinvasion' assay, 25 years and still going strong: the use of reconstituted basement membranes to study cell invasion and angiogenesis. *Current Opinion in Cell Biology* **2010**, *22*, 677–689 (cit. on p. 182).

(282) Kohyama, T.; Ertl, R. F.; Valenti, V.; Spurzem, J.; Kawamoto, M.; Nakamura, Y.; Veys, T.; Allegra, L.; Romberger, D.; Rennard, S. I. Prostaglandin E2 inhibits fibroblast chemotaxis. *American Journal of Physiology-Lung Cellular and Molecular Physiology* **2001**, *281*, L1257–L1263 (cit. on p. 182).

(283) Hooper, S.; Marshall, J. F.; Sahai, E. In *Regulators and Effectors of Small GTPases: Rho Family*, William E. Balch, C. J. D., Hall, A., Eds.; Methods in Enzymology, Vol. 406; Academic Press: 2006, pp 625–643 (cit. on p. 182).

(284) Breckenridge, M.; Egelhoff, T.; Baskaran, H. A microfluidic imaging chamber for the direct observation of chemotactic transmigration., English *Biomedical Microdevices* **2010**, *12*, 543–553 (cit. on p. 182).

(285) Allen, W. E.; Zicha, D.; Ridley, A. J.; Jones, G. E. A Role for Cdc42 in Macrophage Chemotaxis. *The Journal of Cell Biology* **1998**, *141*, 1147–1157 (cit. on p. 184).

(286) Boland, T.; Xu, T.; Damon, B.; Cui, X. Application of inkjet printing to tissue engineering. *Biotechnology Journal* **2006**, *1*, 910–917 (cit. on p. 185).

(287) Moreno-Arotzena, O.; Mendoza, G.; Cóndor, M.; Rüberg, T.; García-Aznar, J. M. Inducing chemotactic and haptotactic cues in microfluidic devices for three-dimensional in vitro assays. *Biomicrofluidics* **2014**, *8* 064122, (cit. on p. 186).

(288) Millet, L. J.; Gillette, M. U. New perspectives on neuronal development via microfluidic environments. *Trends in Neurosciences* **2012**, *35*, 752–761 (cit. on p. 187).

(289) Chung, B. G.; Choo, J. Microfluidic gradient platforms for controlling cellular behavior. *Electrophoresis* **2010**, *31*, 3014–3027 (cit. on pp. 187, 188).

(290) Dhumpa, R.; Roper, M. G. Temporal gradients in microfluidic systems to probe cellular dynamics: A review. *Analytica Chimica Acta* **2012**, *743*, 9–18 (cit. on p. 187).

(291) Kim, S.; Kim, H. J.; Jeon, N. L. Biological applications of microfluidic gradient devices. *Integrative Biology* **2010**, *2*, 584–603 (cit. on p. 187).

(292) Toh, A. G. G.; Wang, Z. P.; Yang, C.; Nguyen, N.-T. Engineering microfluidic concentration gradient generators for biological applications. *Microfluid Nanofluid* **2013**, *16*, 1–18 (cit. on pp. 187, 188).

(293) Lin, F.; Butcher, E. C. T cell chemotaxis in a simple microfluidic device. *Lab Chip* **2006**, *6*, 1462–1469 (cit. on p. 187).

(294) Halilovic, I.; Wu, J.; Alexander, M.; Lin, F. Neutrophil migration under spatially-varying chemoattractant gradient profiles. *Biomedical microdevices* **2015**, *17*, 1–7 (cit. on p. 187).

(295) Dertinger, S. K. W.; Chiu, D. T.; Jeon, N. L.; Whitesides, G. M. Generation of Gradients Having Complex Shapes Using Microfluidic Networks. *Analytical Chemistry* **2001**, *73*, 1240–1246 (cit. on pp. 187, 188).

(296) Taylor, A. M.; Dieterich, D. C.; Ito, H. T.; Kim, S. A.; Schuman, E. M. Microfluidic Local Perfusion Chambers for the Visualization and Manipulation of Synapses. *Neuron* **2010**, *66*, 57–68 (cit. on p. 188).

(297) Ahmed, D.; Mao, X.; Shi, J.; Juluri, B. K.; Huang, T. J. A millisecond micromixer via single-bubble-based acoustic streaming. *Lab Chip* **2009**, *9*, 2738–2741 (cit. on p. 188).

(298) Hung, P. J.; Lee, P. J.; Sabounchi, P.; Lin, R.; Lee, L. P. Continuous perfusion microfluidic cell culture array for high-throughput cell-based assays. *Biotechnology and Bioengineering* **2005**, *89*, 1–8 (cit. on p. 188).

(299) Wu, H.; Huang, B.; Zare, R. N. Generation of Complex, Static Solution Gradients in Microfluidic Channels. *Journal of the American Chemical Society* **2006**, *128*, 4194–4195 (cit. on p. 190).

(300) Sugiura, S.; Szilagyi, A.; Sumaru, K.; Hattori, K.; Takagi, T.; Filipcsei, G.; Zrinyi, M.; Kanamori, T. On-demand microfluidic control by micropatterned light irradiation of a photoresponsive hydrogel sheet. *Lab on a Chip* **2009**, *9*, 196–198 (cit. on p. 191).

(301) Wang, S.; Choi, M.-S.; Kim, S.-H. Bistable photoswitching in poly(N-isopropylacrylamide) with spironaphthoxazine hydrogel for optical data storage. *Journal of Photochemistry and Photobiology A: Chemistry* **2008**, *198*, 150–155 (cit. on p. 191).

(302) Martin Nicolas, M. Colloidal stability and folding of antibodies in the presence of chaperone-like poly(acrylate) derivatives : role of hydrophobic and electrostatic interactions., Theses, Université Pierre et Marie Curie – Paris VI, 2014 (cit. on p. 194).

(303) Gasteiger, E.; Hoogland, C.; Gattiker, A.; Duvaud, S.; Wilkins, M.; Appel, R.; Bairoch, A. English In *The Proteomics Protocols Handbook*, Walker, J., Ed.; Humana Press: 2005, pp 571–607 (cit. on p. 194).

(304) ExPASy ProtParam tool., `http://web.expasy.org/protparam/` (cit. on p. 194).

(305) Xu, X.; Smith, A. E.; Kirkland, S. E.; McCormick, C. L. Aqueous RAFT Synthesis of pH-Responsive Triblock Copolymer mPEO- PAPMA- PDPAEMA and Formation of Shell Cross-Linked Micelles? *Macromolecules* **2008**, *41*, 8429–8435 (cit. on p. 195).

(306) Van Dongen, S. F. M.; Janvore, J.; van Berkel, S. S.; Marie, E.; Piel, M.; Tribet, C. Reactive protein-repellent surfaces for the straightforward attachment of small molecules up to whole cells. *Chemical Science* **2012**, *3*, 3000–3006 (cit. on p. 196).

(307) Pan, J.; Tristram-Nagle, S.; Kučerka, N.; Nagle, J. F. Temperature dependence of structure, bending rigidity, and bilayer interactions of dioleoylphosphatidylcholine bilayers. *Biophysical journal* **2008**, *94*, 117–124 (cit. on p. 201).

(308) Schümann, D. Controlled cleaning by measuring surfactant concentration: Maintenance of defined concentrations of components, surfactants, and builder ensures optimal results in aqueous cleaning processes. *Metal Finishing* **2009**, *107*, 25–30 (cit. on pp. 203, 205).

(309) Kawakami, K.; Sumitani, C.; Yoshihashi, Y.; Yonemochi, E.; Terada, K. Investigation of the dynamic process during spray-drying to improve aerodynamic performance of inhalation particles. *International Journal of Pharmaceutics* **2010**, *390*, 250–259 (cit. on p. 203).

(310) Dixit, N.; Zeng, D. L.; Kalonia, D. S. Application of maximum bubble pressure surface tensiometer to study protein–surfactant interactions. *International Journal of Pharmaceutics* **2012**, *439*, 317–323 (cit. on p. 203).

(311) Christov, N. C.; Danov, K. D.; Kralchevsky, P. A.; Ananthapadmanabhan, K. P.; Lips, A. Maximum Bubble Pressure Method: Universal Surface Age and Transport Mechanisms in Surfactant Solutions. *Langmuir* **2006**, *22*, 7528–7542 (cit. on pp. 203, 205).

(312) Eastoe, J.; Dalton, J. Dynamic surface tension and adsorption mechanisms of surfactants at the air–water interface. *Advances in Colloid and Interface Science* **2000**, *85*, 103–144 (cit. on pp. 203, 204).

(313) Yaroslavov, A. A.; Sybachin, A. V.; Schrinner, M.; Ballauff, M.; Tsarkova, L.; Kesselman, E.; Schmidt, J.; Talmon, Y.; Menger, F. M. Liposomes remain intact when complexed with polycationic brushes. *Journal of the American Chemical Society* **2010**, *132*, 5948–5949 (cit. on p. 227).

(314) Hrafnsdóttir, S.; Nichols, J. W.; Menon, A. K. Transbilayer movement of fluorescent phospholipids in Bacillus megaterium membrane vesicles. *Biochemistry* **1997**, *36*, 4969–4978 (cit. on p. 227).

(315) Evans, K. O. Room-temperature ionic liquid cations act as short-chain surfactants and disintegrate a phospholipid bilayer. *Colloids and Surfaces A: Physicochemical and Engineering Aspects* **2006**, *274*, 11–17 (cit. on p. 227).

(316) Berland, K.; So, P.; Gratton, E. Two-photon fluorescence correlation spectroscopy: method and application to the intracellular environment. *Biophysical Journal* **1995**, *68*, 694–701 (cit. on p. 227).

(317) Schwille, P.; Haupts, U.; Maiti, S.; Webb, W. W. Molecular dynamics in living cells observed by fluorescence correlation spectroscopy with one-and two-photon excitation. *Biophysical journal* **1999**, *77*, 2251–2265 (cit. on p. 227).

(318) Charier, S.; Meglio, A.; Alcor, D.; Cogné-Laage, E.; Allemand, J.-F.; Jullien, L.; Lemarchand, A. Reactant concentrations from fluorescence correlation spectroscopy with tailored fluorescent probes. An example of local calibration-free pH measurement. *Journal of the American Chemical Society* **2005**, *127*, 15491–15505 (cit. on p. 227).

(319) Pashkovskaya, A.; Kotova, E.; Zorlu, Y.; Dumoulin, F.; Ahsen, V.; Agapov, I.; Antonenko, Y. Light-triggered liposomal release: membrane permeabilization by photodynamic action. *Langmuir* **2009**, *26*, 5726–5733 (cit. on p. 227).

(320) Soumpasis, D. Theoretical analysis of fluorescence photobleaching recovery experiments. *Biophysical Journal* **1983**, *41*, 95–97 (cit. on p. 227).

(321) Smith, B. A.; Clark, W. R.; McConnell, H. M. Anisotropic molecular motion on cell surfaces. *Proceedings of the National Academy of Sciences* **1979**, *76*, 5641–5644 (cit. on p. 227).

(322) Travascio, F.; Zhao, W.; Gu, W. Y. Characterization of Anisotropic Diffusion Tensor of Solute in Tissue by Video-FRAP Imaging Technique. *Annals of Biomedical Engineering* **2009**, *37*, 813 (cit. on p. 227).

(323) Shi, C.; Kuo, J.; Bell, P.; Yao, H. Anisotropic Solute Diffusion Tensor in Porcine TMJ Discs Measured by FRAP with Spatial Fourier Analysis., English *Annals of Biomedical Engineering* **2010**, *38*, 3398–3408 (cit. on p. 227).

(324) Travascio, F.; Gu, W. Y. Simultaneous Measurement of Anisotropic Solute Diffusivity and Binding Reaction Rates in Biological Tissues by FRAP. *Annals of Biomedical Engineering* **2010**, *39*, 53 (cit. on p. 227).

# Abbreviations & acronyms

| | |
|---|---|
| avg | average |
| azo | azobenzene |
| azoTAB | azobenzene-containing surfactant |
| BSA | bovine serum albumin |
| C | concentration |
| CMC | critical micellar concentration |
| cryoTEM | cryo-transmission electron microscopy |
| CTAB | cetyl trimetylammonium bromide |
| CTAC | cetyl trimetylammonium chloride |
| $D_h$ | hydrodynamic diameter |
| DLS | dynamic light scattering |
| DOPC | 1,2-dioleoyl-*sn*-glycero-3-phosphocholine |
| DOPE | 1,2-dioleoyl-*sn*-glycero-3-phosphoethanolamine |
| DPPC | 1,2-dipalmitoyl-*sn*-glycero-3-phosphocholine |
| EDTA | ethylenediamine tetracetate |
| EGF | epidermal growth factor |
| ESI | electronic supplementary information |
| FCS | fluorescence correlation spectroscopy |
| FGF | fibroblast growth factor |
| FITC | fluorescein isothiocyanate |
| fMLP | *N*-formylmethionylleucylphenylalanine |
| FRAP | fluorescence recovery after photobleaching |
| GABA | γ-aminobutyric acid |
| GUV | giant unilamellar vesicle |
| HLB | hydrophilic-lipophilic balance |
| HMDA | hexamethylene diamine |
| $I_{diff}$ | intensity of scattered light |
| kcps | kilcounts per second |
| LbL | layer-by-layer |
| LCST | lower critical solution temperature |
| LUV | large unilamellar vesicle |
| NGF | nerve growth factor |
| OVA | ovalbumin |
| PBS | phosphate saline buffer |

| | |
|---|---|
| PEG | poly(ethylene glycol) |
| rpm | revolutions per minute |
| RT | room temperature |
| SAXS | small-angle X-ray scattering |
| SDS | sodium dodecyl sulfate |
| SR101 | sulforhodamine 101 |
| stddev | standard deviation |
| T | temperature |
| $T_C$ | critical burst or release temperature |
| TDI | toluene diisocyanate |
| TEM | transmission electron microscopy |
| TGF | transforming growth factor |
| TNF | tumor necrosis factor |
| TX100 | Triton X-100 |
| UCST | upper critical solution temperature |

# Abstract

Concentration gradients and local delivery of peptides or proteins play a crucial role in intercellular communication. In vitro, the effects of local activation of cells are studied with constrained or invasive artificial protein sources (pipettes, microfluidics). Milder and remotely-triggered techniques for the release of encapsulated biomolecules are highly in demand. To this aim we developed two classes of capsules able to release macromolecules upon an external stimulation. The first system is based on liposomes sensitized with azobenzene-containing amphiphiles (surfactants or polyelectrolytes) that can open pores in the membrane upon exposure to light. The dissolution time of lipids/surfactants assemblies and rate of release (permeability) under light irradiation has been assessed by dynamic light scattering and fluorescence measurements. The second system is a model of capsules with an aqueous core and a polymer shell, formed by interfacial polyaddition. We showed that inclusion of temperature-responsive chains in the membrane, e.g. polyNIPAM, confers temperature-dependant stability to the capsules; we demonstrated with millimeter-sized capsules loaded with dextran or proteins that this can be used to trigger the release. Using chains with UCST in water, we obtained the first temperature-sensitive capsules able to release their content upon increasing the temperature above a threshold. This represents a promising route to the biocompatible delivery of proteins.



**Keywords:** protein; encapsulation; triggered release; light-sensitive liposomes; temperature-sensitive capsules; UCST/LCST polymers.



# Résumé

Les gradients de concentration de peptides ou de protéines, ou leur relargage localisé, jouent un rôle primordial dans les voies de communication inter-cellulaire. L'activation locale de cellules est étudiée in vitro à l'aide de sources artificielles contraignantes ou invasives de protéines (pipettes, dispositifs microfluidiques). Des méthodes plus douces et moins invasives sont très demandées. À cet effet, nous avons développé deux types de capsules capables de libérer des macromolécules sous l'effet d'une stimulation extérieure. Le premier système emploie des liposomes additionnés d'un amphiphile à azobenzène, tensioactif ou polyélectrolyte, capable de générer des pores à travers la membrane sous l'effet de la lumière. Les temps de dissolution des assemblages lipides/tensioactifs et les cinétiques de relargage (perméabilité) sous irradiation lumineuse ont été étudiées par diffusion dynamique de la lumière et fluorescence. Le second système repose sur des capsules à cœur aqueux et à coque polymère, formées par polyaddition interfaciale. Nous avons montré que l'inclusion de chaînes thermosensibles dans la membrane (polyNIPAM, par ex.) rendait la stabilité de la capsule dépendante de la température. Nous avons démontré sur des capsules millimétriques, chargées avec du dextrane ou des protéines, que cela permettait le contrôle du relargage. L'utilisation de polymère à UCST en milieu aqueux nous a permis d'obtenir les premières capsules thermosensibles capables de libérer leur contenu par élévation de la température au dessus d'une valeur critique. Cela ouvre une voie prometteuse au développement d'un système biocompatible de libération de protéines.



**Mots-clefs :** protéine ; encapsulation ; libération contrôlée ; liposomes photosensibles ; capsules thermosensibles ; polymères à UCST/LCST.